Serotonergic Modulation of Glutamate Release in Layer II of Rat Somatosensory Cortex: Mechanisms and Network Specificity

A thesis submitted for the degree of Doctor of Philosophy of
The Australian National University

Submitted for examination in July 2017

Presented by
Fransiscus Adrian Agahari
PhD Candidate (u5073299)
at The John Curtin School of Medical Research of
The Australian National University

Declaration

This thesis is based on research carried out between September 2011 and November 2016 at the John Curtin School of Medical Research, The Australian National University, Canberra, Australia. All experiments were performed by myself, except for the data presented in sections 4.4.3.1 – 2 regarding the noradrenergic modulation of glutamate release, which was acquired by Drs. Julian Choy and Li Li for their PhD projects in the laboratory. All analyses were performed by myself under the supervision of Dr. Christian Stricker. To the best of my knowledge, the content of this thesis is original and the findings detailed inside are novel.

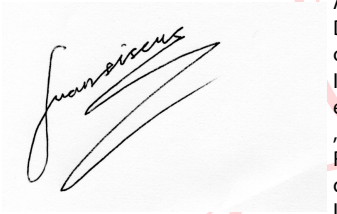

Digitally signed by Fransiscus Adrian Agahari
DN: cn=Fransiscus Adrian Agahari, o=JCSMR - ANU, ou=Eccles Institute of Neuroscience, email=Adrian.Agahari@anu.edu.au, c=AU
Reason: I am the author of this document
Location: Okazaki, Aichi, Japan
Date: 2017.10.23 10:20:07 +09'00'

Fransiscus Adrian Agahari
October 2017

Acknowledgement

I would like to sincerely thank my primary supervisor, Associate Professor Christian Stricker, for teaching, guiding, and mentoring me throughout my PhD research and thesis writing. I am grateful that I was given a chance to undertake a research dealing with synaptic transmission and its neuromodulation in the Neuronal Network Laboratory. I would like to also express my gratitude to my panel members, Professor John Bekkers and Dr. Andrew Delaney, for their constructive inputs and advice so that I could overcome all difficulties in my research. Many thanks to Professor Greg Stuart for his advice in my annual panel meetings, and Dr. Anna Cowan for numerous help throughout my early PhD years.

Special thanks to Drs. Julian Choy and Li Li for providing me with some results from their own work about the noradrenergic modulation, which are used for comparison in my thesis. I also specifically thank Dr. Julian Choy for his help in the technical aspects of patch-clamping and paired-recordings, and also for being a great discussion partner. I really appreciate all the supports from past and present lab members, Ashutosh Mohan, Dr. Mary Ann Go, Le Thuy Van Tran, and Deborah Feakes. Additional thanks to Le Thuy Van Tran and Deborah Feakes for proofreading and commenting on my thesis. I would like to also extend my thank to Garry Rodda for his assistance in making experiments run smoothly, and Dr. Norimitsu Suzuki for valuable advice on how to build my career as a scientist.

I would like to express my deepest gratitude to all my family members. To my father, Daitia Djohan Agahari, my mother, Elizabeth The Soe Hoa, my sister, Fransisca Adelina Agahari, my grandmother, Maria Lim Nyat Ngoe, my aunts, Xaveria The Soe Ping, Theresia The Soe Tjen, and Marceline Lucia Tombokan. I was able to overcome the hardest time in my life during this PhD only because of your everlasting prayers and support. I also thank my sister, who, despite of her business as a medical doctor in Adelaide, still spared her time to proofread my thesis. A very special thank to my deceased grandfather, Stefanus The Ek Tjoe, for always taking good care of myself since I was a small child, even until recently.

Last but not least, I would like to thank the John Curtin School of Medical Research for the scholarship, tuition stipend, and chance given to me. I hope that, through this thesis, I can contribute to a better understanding of brain function.

Abstract

As axons from the raphe nuclei densely innervate the somatosensory cortex, the modulation of transmitter release by serotonin (5-HT) was investigated in pyramidal cells in layer II of rat barrel cortex. The idea was that 5-HT, via presynaptic 5-HT_2 receptors (5-HT_2R) coupled to G_q proteins, activates Ca^{2+} release from stores to increase spontaneous transmitter release.

Addition of 10 µM 5-HT, in the presence of TTX and gabazine, caused a waxing and waning of the instantaneous mEPSC frequency. Specifically, 5-HT increased the frequency by 28 ± 7% within 5 minutes (phase 1). Later, within 5 – 12 minutes, it dropped to below control (-15 ± 3%; phase 2). Thereafter, it resurged back to 27 ± 7% (phase 3). Concomitantly, the mEPSC amplitude remained unaffected.

These changes in spontaneous release were mediated by 5-HT_{2C}R and 5-HT_{2A}R, with the former providing a larger contribution. The downstream signalling was verified by blocking PLCβ, IP_3R, and Ca^{2+} release from stores. The findings were consistent with the activation of a classical G_q cascade. Inhibiting PKC by Gö 6983 rendered the increase sustained, suggesting that a phosphorylation caused the reduction in frequency after reaching an initial peak.

These findings were restricted to a subset of cells (47%), which were subsequently termed responders. No change occurred in non-responders. The two groups differed by the size of the reduction in input resistance (R_{in}) and the change in holding current. For responders, the former was large, but the latter small. In contrast, for non-responders, the former was small, but the latter large.

In connected pairs of pyramidal cells in this layer, 5-HT depressed the EPSC amplitude by 49 ± 3% without significantly altering the paired-pulse ratio. This depression occurred downstream of 5-HT_2R activation. It was caused by Gβγ, because it was blocked by Gβγ-binding peptides (mSIRK/ct-SNAP-25). As Gβγ most likely inhibited voltage-dependent Ca^{2+} channels, limited influx caused the EPSC depression.

Because 5-HT depressed EPSCs in most pairs, specificity in the connectivity between responders and non-responders must exist. In fact, responders were typically post-, whereas non-responders presynaptic. Consistent with this idea, the mEPSC frequency only increased in post-, but not presynaptic cells. Furthermore, postsynaptic cells showed a large drop in R_{in} associated with a small outward current. Conversely,

presynaptic cells showed a small drop in R_{in} together with a considerable hyperpolarization.

My results revealed that, in contrast to the classical tenet of Katz' hypothesis of transmitter release, spontaneous transmitter release increased, whereas evoked release depressed downstream of 5-HT_2R activation. The two mechanisms dissociated at the G_q protein level. Spontaneous release was increased by Ca^{2+} release from stores, whilst evoked release was depressed most likely via inhibition of VDCC by Gβγ. Because of their restriction to responders, these mechanisms would differentially affect the neocortical microcircuitry.

Table of Contents

Table of Figures

Table of Tables

Abbreviations and Symbols

2-APB	2-aminoethoxydiphenyl borate
4F 4PP	4-(4-fluorobenzoyl)-1-(4-phenylbutyl)piperidine
5-HIAA	5-hydroxyindoleatic acid
5-HT	5-hydroxytryptamine
5-HTP	5-hydroxtryptophan
5-HTR	5-hydroxytryptamine receptor(s)
AADC	L-amino acid decarboxylase
ABC	avidin/biotin conjugation
ACSF	artificial cerebrospinal fluid
AHP	afterhyperpolarization
AM	acetoxymethyl ester
AMPA	α-amino-3-hydroxy-5-methyl-4-isoxazolepropionic acid
AP	action potential
AR	adrenergic receptor
ATP	adenosine triphosphate
BAPTA	1,2-bis(o-aminophenoxy)ethane-*N*,*N*,*N*′,*N*′-tetraacetic acid
BDNF	brain-derived neurotrophic factor
cAMP	cyclic adenosine monophosphate
CICR	calcium-induced calcium release
CNS	central nervous system
COM	callosal/commissural neuron
COMT	cathecol-O-methyltransferase
cPDF	cumulative probability density function
CPn	corticopontine-projecting neuron
ct-SNAP-25	C-terminus of synaptosomal-associated protein 25 (peptide)
DA	dopamine
DAG	diacylglycerol
DBH	dopamine-β-hydroxylase
DC	direct current
DMSO	dimethyl sulfoxide
DNQX	6,7-dinitroquinoxaline-2,3-dione
DOB	dimethoxybromoamphetamine
EC_{50}	half maximal effective concentration
EPSC	excitatory postsynaptic current
EPSP	excitatory postsynaptic potential

ER	endoplasmic reticulum
ERK	extracellular signal-regulated kinase
G-protein	guanine nucleotide-binding protein
GABA	γ-aminobutyric acid
Gα	G-protein α subunit
Gβγ	G-protein βγ subunit
GDP	guanosine diphosphate
GIRK	G-protein-coupled inwardly-rectifying potassium (channel)
GPCR	G-protein-coupled receptor
GRK	G-protein-coupled receptor kinase
GTP	guanosine triphosphate
H	action potential height
HEPES	4-(2-hydroxyethyl)-1-piperazineethanesulfonic acid
I_c	capacitive current transient
I_h	hyperpolarization-activated current
I_{hold}	holding current in voltage clamp
IP_3	inositol trisphosphate
IR-DIC	infrared differential interference contrast
KA	kainate
K_i	Inhibitory constant
KS	Kolmogorov-Smirnov
L-DOPA	L-3,4-dihydroxy-l-phenylalamine
LTP	long-term potentiation
LTD	long-term depression
m	quantal content
MAO	monoamine oxidase
MAPK	mitogen-activated protein kinase
mEPSC	miniature excitatory postsynaptic current
mEPSP	miniature excitatory postsynaptic potential
mGluR	metabotropic glutamate receptor
MHPG	3-methoxy-4-hydroxy-phenylglycol
mIPSC	miniature inhibitory postsynaptic current
mIPSP	miniature inhibitory postsynaptic potential
mPFC	medial prefrontal cortex
mSIRK	N-myristoylated SIRKALNILGYPDYD peptide
MW	molecular weight
NA	noradrenaline
NAD	nicotinamide adenine dinucleotide

NET	norepinephrine transporter
NMDA	*N*-methyl-D-aspartate
PB	phosphate buffer
PFC	prefrontal cortex
PIP_2	phosphatidylinositol 4,5-bisphosphate
PKA	protein kinase A
PKC	protein kinase C
PLC	phospholipase C
PPR	paired-pulse ratio
Q	quantal size
RT	action potential rise time
RTK	receptor tyrosine kinase
R_{in}	input resistance
R_s	series resistance
R_{tot}	total cell resistance
S1 cortex	primary somatosensory cortex
SEM	standard error of mean
sEPP	spontaneous end-plate potential
sEPSC	spontaneous excitatory postsynaptic current
sEPSP	spontaneous excitatory postsynaptic potential
SER	smooth endoplasmic reticulum
SERT	serotonin transporter
σ_n	membrane current noise at the baseline of EPSC recording
σ_{noise}	baseline noise standard deviation in mEPSC recording
σ_{wn}	whole-cell noise standard deviation
sIPSC	spontaneous inhibitory postsynaptic current
sIPSP	spontaneous inhibitory postsynaptic potential
SNAP25	synaptosomal-associated protein 25
SNARE	soluble *N*-ethylmaleimide-sensitive factor attachement protein receptor
SSRI	selective serotonin reuptake inhibitor
τ_c	membrane time constant
TBS	Trizma® buffered saline
Tph	tryptophan hydroxylase
TTX	tetrodotoxin
VAMP2	vesicle-associated membrane protein 2
VDCC	voltage dependent calcium channel
vGAT	vesicular GABA transporter

vGluT	vesicular glutamate transporter
V_m	cell's membrane potential
VMA	vanillylmandelic acid
VMAT	vesicular monoamine transporter
V_{rest}	cell's resting membrane potential
V_{rel}	relative difference from resting membrane potential to threshold
V_s	voltage step
V_{thr}	threshold for action potential
W	action potential half-width

1. Introduction

This research project started with the question whether the neuromodulator serotonin (5-HT) is capable of causing calcium (Ca^{2+}) release from presynaptic stores via activation of the classical G_q-protein-mediated signalling cascade, and consequently modulates neurotransmitter release. This question was tested in layer II pyramidal cells of rat somatosensory (S1) cortex, also referred to as barrel cortex. In parts 3 and 4, I will provide the answer to this question for both spontaneous and evoked glutamate release, respectively.

In this introduction, I will start by presenting important concepts related to my field of research. First, I will briefly describe some anatomy and physiology of neocortex, specifically of barrel cortex from the perspective of the whisker-related sensory pathways. Second, I will portray how information transfer between neurons in the neocortex occurs via synaptic transmission. As my research was focused on chemical transmission, the case for electrical transmission will only be introduced superficially. For both spontaneous and evoked transmitter release, the respective dependency on Ca^{2+} from extra- and intracellular sources will be reviewed. Third, I will introduce aspects of 5-HT relating to its synthesis, innervation, release and receptor actions. Additionally, as some of my results will be compared with data when noradrenaline (NA) modulated transmitter release via α_1-adrenoceptors (α_1-AR), which, like 5-HT_2 receptors (5-HT_2R), are also linked to a G_q cascade, these considerations will be extended to also include NA.

1.1. Neocortex and Primary Somatosensory Barrel Cortex

One of the most important functions of the brain, and specifically neocortex, is to process information stemming from different sensory modalities. Proper processing of this information is critical for the generation of an appropriate behavioural output, which could manifest itself as a suitable response to the demands of the environment.

The neocortex consists of the grey matter of the two hemispheres that fill out most of the cranium, specifically its antero-lateral and dorsal parts. It does not include the hippocampus, basal ganglia and the olfactory bulb. In humans, its structure is gyrated, but not so in rodents, where the surface is flat. Based on the information processed, mouse and rat neocortex could be grossly divided into four primary areas (Rash & Grove, 2006; Lodato & Arlotta, 2015). In rostral to caudal order, these are: 1) motor (producing

output to control fine motor behaviours), 2) somatosensory (processing input from the senses like touch and in rodents the whiskers), 3) auditory (sound), and 4) visual cortex (vision). Although these areas each process different kinds of information, the neocortical structure is uniformly composed of six layers (I – VI), with the first layer superficial and VI deepest. Based on the development of the different layers, layer IV, which is called the granular layer, is the first to be established. Layers II and III are also called supragranular, and layers V and VI as infragranular layers; both develop afterwards.

Whilst different layers have a slightly different composition of excitatory and inhibitory neurons, generally, throughout neocortex, ~80% of cells are excitatory neurons, whilst the rest are inhibitory (GABAergic). The somata of excitatory neurons in layers II, III, V, and VI have a pyramidal shape and are referred to as pyramidal cells. A feature of all these excitatory cells is that they show spines along their dendrites (Ramón y Cajal, 1904) and they release the neurotransmitter glutamate (glutamatergic). In layers II and III, these pyramidal cells can be classified into 1) associative projection neurons and 2) commissural projection neurons. The former send their axons to other areas in the ipsilateral hemisphere, including to different layers of the same area. The latter project to the contralateral hemisphere via the *corpus callosum*. In layers V and VI, there are also corticofugal projection neurons that extend their axons to distal target(s) outside the cortex, like spinal cord, thalamus, basal ganglia and cerebellar nuclei (Molyneaux *et al.*, 2007). Besides pyramidal cells, in layer IV, there are two other excitatory cell types, namely spiny stellate and star pyramidal cells (White, 1978).

The inhibitory cells are often referred to as interneurons. The strict definition of an interneuron was that the cell only makes local connections within the same layer or (spinal) segment. However, at the present time, it was realised that in neocortex, these connections can span to multiple layers (Kawaguchi & Kubota, 1996, 1997, 1998; Lodato *et al.*, 2015). They are exclusively inhibitory by releasing the transmitter γ-aminobutyric acid (GABAergic). It is important to notice that the GABAergic interneurons are very diverse (Gupta *et al.*, 2000), and each neocortical layer has a different composition of interneurons (Simons & Woolsey, 1984; Uematsu *et al.*, 2008). A morphological feature of most, but not all these interneurons, is that they have somata that are not pyramidal in shape. In addition, their dendrites are sparsely studded with spines, and often beaded (Keller & White, 1987; Kubota *et al.*, 2011). Large variations in electrophysiological and connection properties of these cells present an immense difficulty in creating a widely accepted systematic classification (DeFelipe *et al.*, 2013). However, in recent years, a simpler classification based on the molecular expression of certain peptides, like parvalbumin and somatostatin, and additionally 5-HT_{3A} receptors, was used to include most types of interneurons (Lee *et al.*, 2010; Kepecs & Fishell, 2014).

The study of neocortical function is often done in the somatosensory cortex of rodents, specifically S1. Its cytoarchitechture is special because “barrel”-like structures are formed in this area. These barrels were initially revealed using either the Nissl or Nissl-Golgi staining methods (Woolsey & Van der Loos, 1970), but they can also be easily distinguished in unstained tissue (as in an experiment where differential interference contrast optics are used to observe brain slices). The barrels form in layer IV, and are characterized by higher density of cells particularly along the “walls” in contrast to the centre parts. The beauty of this S1 barrel cortex is that each barrel receives the input from exactly one whisker in the mystacial part of the rodent face (Welker & Woolsey, 1974). The somatosensory input from a single whisker is processed in the neocortical column associated with the layer IV barrel in its centre (Petersen & Sakmann, 2001).

The afferent pathway from whisker to barrel cortex is as follows. The stimulus-induced whisker motion activates the sensory receptor, which makes contact with the peripheral branch of trigeminal ganglion cell (Birdwell *et al.*, 2007). The central branch of the trigeminal ganglion cells then relays the information as a sequence of action potentials to the trigeminal nucleus in the brain stem (Torvik, 1956; Clarke & Bowsher, 1962). This information is then passed to the thalamus through parallel pathways, namely the lemniscal, the extralemniscal, and the paralemniscal pathways. From the thalamus, the information is relayed to the barrel cortex, mostly in layer IV (Deschenes *et al.*, 2005). Specifically, the lemniscal pathway connects the dorsomedial section of ventroposterior medial nucleus in the thalamus to the corresponding barrel (layer IV). Whisker-induced signals are then relayed from layer IV to II/III, where they are subject to local recurrent excitation or amplification (Douglas & Martin, 2004). From layer II/III, neurons project this information to layer V where the output from the column is generated and relayed to other parts of the brain or subcortical structures (Petersen & Sakmann, 2001). From layer V, there is a forward connection to layer VI, from which cells project back to the thalamus to control the afferent inputs. The intracortical steps are often referred to as columnar processing of the sensory information.

Note that my thesis focusses on how information flow along the intralayer (horizontal) connections between neighbouring pyramidal cells in layer II is modulated by 5-HT. As this information transfer includes synaptic transmission between pyramidal cells, I will proceed to give a short background of the physiology of chemical transmission.

1.2. Physiology of Synaptic Transmission

The transfer of information or “signal relay” from one neuron to another occurs at synapses through a process named synaptic transmission. There are two types of

transmission, electrical and chemical. Both essentially involve specific presynaptic and postsynaptic elements, but fundamentally differ in 1) the physical components at the synapse, 2) the speed of transmission, 3) typically, the directionality of the information transfer, and 4) ontogeny or prevalence period. Here, I will briefly describe the former (electrical) before proceeding to the details of the latter (chemical synaptic transmission).

1.2.1. Electrical Transmission

An electrical synapse takes the form of a gap junction, which is an intercellular ion channel connecting the cytoplasm of two neurons. This channel is formed by two connexons, specifically one each in the pre- and postsynaptic neurons. The connexon itself is typically made up of six subunits called connexins. (Pereda *et al.*, 2013).

Following Ohm's law, the gap junction enables current to flow (ions) through its channel in a manner proportional to the trans-junctional voltage. In this case, information is transferred from one neuron to another neuron almost instantaneously, *i.e*. less than one third of a millisecond. Depending on how the trans-junctional voltage changes due to neuronal activity, current may also flow in the reverse direction, creating the bidirectional and graded characteristics of electrical transmission (Furshpan & Potter, 1959; Connors, 2017).

Electrical synaptic transmission does not only depend on the conductance of the gap junction, but also on the resistance and membrane time constant of the postsynaptic cell. Since most neurons in mammalian brain have large membrane time constants in the order of tens of milliseconds, electrical transmission functions as a low-pass filter (Connors & Long, 2004), which attenuates high frequency signals like action potentials (APs) much stronger than low frequency ones. Therefore, even in the case of strong excitatory activity such as during a burst of APs in the presynaptic cell, the postsynaptic cell could hyperpolarize if there is a large afterhyperpolarization (AHP) following a single AP (Galarreta & Hestrin, 2001). Conversely, if the AHP is small and short, the burst of APs in the presynaptic cell could result in a postsynaptic depolarization (Landisman *et al.*, 2002). These examples illustrate that the electrical synaptic transmission can be both excitatory and inhibitory. Inhibition of the postsynaptic cell through electrical synapses could also normally occur when the presynaptic cell undergoes hyperpolarization (Apostolides & Trussell, 2013).

The functions of gap junction and electrical synaptic transmission include synchronization and phase-locking, generating antiphase firing (Bennett & Zukin, 2004; Gibson *et al.*, 2005; Merriam *et al.*, 2005; Hu & Agmon, 2015), de-synchronization

(Vervaeke *et al.*, 2010), regulating network oscillations (Buhl *et al.*, 2003), reducing whole-cell noise and enhancing signals in neuronal circuits (Medvedev, 2009), and regulating the formation and tuning of microcircuits (Yao *et al.*, 2016).

Using dyes to track coupling between neurons, Connors *et al.* (1983) and Peinado *et al.* (1993) showed that the electrical synapses are commonly expressed in neocortex during an early postnatal period (70% of neurons during P1 – 4). Along with maturation, this type of synapse decreases in number, with less than 20% of neurons showing coupling after P18. Neurons expressing such synapses in adult age are typically interneurons, specifically fast-spiking parvalbumin (Galarreta & Hestrin, 1999, 2002), irregular-spiking (Galarreta *et al.*, 2004), and late-spiking (Chu *et al.*, 2003) interneurons. In contrast, excitatory cells in the neocortex are known to only express these electrical synapses during the first two postnatal weeks (Sutor & Hagerty, 2005). From then on, these pyramidal cells utilize chemical synapses for information transfer. Because my thesis focusses on networks made up of excitatory cells at the age of P15 – 20 in rat, electrical synapses will not be discussed any further. In fact, the definition of synapses or synaptic transmission will solely refer to chemical synapses.

1.2.2. Chemical Transmission

In comparison with electrical synapses, the components of chemical synapses are much more complex. Both, the presynaptic and postsynaptic elements are very different, including their morphology, protein biochemistry, signal generation and relay, and ionic dependency. Here, I will explain these properties in the context of excitatory chemical transmission (glutamatergic transmission) in the neocortex, and then address specifically some points of interest for my PhD research.

Chemical transmission occurs at junctions between a presynaptic nerve terminal, also referred classically as a bouton, and a postsynaptic element, in neocortex typically a spine head on a piece of dendrite. How the signal is generated and then relayed to the postsynaptic cell using these elements can be summarized as follows. Upon a sufficiently large physiological stimulus in the presynaptic cell, an action potential is generated at the end of the axon initial segment (Palmer & Stuart, 2006). The action potential then propagates along the axon down to its nerve terminals. Due to the large change in membrane voltage associated with the AP, the terminal membrane is depolarized by 60 – 100 mV. This depolarization activates high voltage-dependent Ca^{2+} channels (VDCC), which then open causing a short Ca^{2+} influx. This Ca^{2+}, through an interaction with the soluble *N*-ethylmaleimide-sensitive factor attachment protein receptor (SNARE) complex, triggers neurotransmitter-containing synaptic vesicles to quickly fuse with the

presynaptic membrane at the active zone, thus releasing the neurotransmitter into the synaptic cleft. The neurotransmitter diffuses across the synaptic cleft of ~20 – 40 nm (Palay, 1956), and then binds to specific receptor(s) on the spine head on the postsynaptic cell. These receptors, majorly ligand-gated ion channels, then open and let ions flow into the postsynaptic compartment. The activated postsynaptic receptor(s) yield a postsynaptic voltage change that then propagates along the dendrite to the soma to be summed and integrated with other inputs to the dendrites of the postsynaptic cell.

Neurotransmitter release at chemical synapses is dependent on SNARE proteins in concert with a Ca^{2+} sensor like one of the synaptotagmins (reviewed by Sudhof & Rizo, 2011; Sudhof, 2013). The latter senses the Ca^{2+} influx and then triggers the fusion of synaptic vesicles with the presynaptic membrane (reviewed by Sudhof, 2012). Different SNARE proteins have been recognised and classified into two different groups depending on which subcellular membrane compartment their anchors reside to. The first group comprises the v-SNAREs (vesicle). The anchor here is within the vesicular membrane. The second group contains the t-SNAREs (target), which are anchored in the terminal (cytosolic) membrane (for details see Wilhelm *et al.*, 2014).

The classic conception of vesicle fusion states that three different SNARE proteins are essential for fusion competency. These proteins are the v-SNARE synaptobrevin (either isotype 1 or 2) also called vesicle-associated membrane protein 1 or 2 (VAMP1/2), and the two t-SNAREs syntaxin-1, and SNAP-25. In preparation for transmitter release, these SNARE proteins assemble to form a *trans*-SNARE complex, in which four α-helix domains (one from synaptobrevin, one from syntaxin-1, and two from SNAP-25) form a coiled-coil interaction, bringing the two membranes of the vesicle and of the nerve terminal close together like that of a zipper (Hayashi *et al.*, 1994; Hayashi *et al.*, 1995; Sudhof & Rizo, 2011).

When the intracellular Ca^{2+} concentration increases via influx through VDCCs, another vesicle associated protein, synaptotagmin 1, acts as the Ca^{2+} sensor, by binding Ca^{2+} at its two C2 domains (Davletov & Sudhof, 1993; Sutton *et al.*, 1995; Sugita *et al.*, 1996; Ubach *et al.*, 2001; Fernandez-Chacon *et al.*, 2002; Choi *et al.*, 2010; Chen & Jonas, 2017). The binding with Ca^{2+} enables synaptotagmin 1 to remove the fusion “lock” by complexin (another SNARE protein; Tang *et al.*, 2006) and interact with the membrane phospholipid (Zhang *et al.*, 1998; Arac *et al.*, 2006). As the result, a conformational change of the SNARE complex occurs from a *trans*- to *cis*-configuration, merging the two membrane leaflets together with subsequent fusion pore opening and neurotransmitter release. After full fusion has occurred, the *cis*-SNARE complex

dissociates by the ATPase *N*-ethylmaleimide-sensitive factor (NSF; Brunger, 2005; Sudhof & Rizo, 2011).

In the case of excitatory neurotransmission in neocortex, the vesicle contains glutamate. This transmitter binds to two different types of glutamate receptors characterised by their postsynaptic transduction as coined by Eccles and McGeer (1979). The first type consists of ionotropic receptors. The feature here is that all receptors are individually linked to a ligand-gated ion channel, in the case of glutamate, a non-selective cation channel. According to the most specific agonist at each of these receptors, there are three ionotropic groups, namely 1) α-amino-3-hydroxy-5-methyl-isoxazolepropionic acid (AMPA) receptors, 2) *N*-methyl-D-aspartate (NMDA) receptors, and 3) kainate (KA) receptors. All three ionotropic glutamate receptors are widely and abundantly expressed in the neocortex. The second type consists of metabotropic receptors. The feature here is that these receptors are individually coupled to a specific type of G-protein, which produces intracellular signalling cascade that may target or affect ion channel(s). In case of the metabotropic glutamate receptors (mGluRs), they have eight isotypes, which are grouped into three, namely group I – III (Niswender & Conn, 2010).

The three ionotropic receptors have a tetrameric structure. Both, homo- and heterotetramers are found for both AMPA and KA receptors, but only heterotetramers for NMDA receptors. In the case of AMPA receptors, these homo-/heterotetramers are composed of subunits from four different genes, namely $GluA_{1-4}$ (Keinanen *et al.*, 1990; Monyer *et al.*, 1992; Greger *et al.*, 2017). In the case of NMDA receptors, three genes have been found, namely $GluN_{1-3}$ (Monyer *et al.*, 1992; Regan *et al.*, 2015) of which $GluN_2$ has four members. In the case of KA receptors, five genes have been cloned, namely $GluK_{1-5}$ (Bettler *et al.*, 1990; Carta *et al.*, 2014). Although the three receptor groups share a non-specific cation conductance (Na^+, K^+, and in some cases Ca^{2+}), their kinetics and sizes of the respective conductances vary in many aspects.

AMPA receptors have fast kinetics and activate in the range of few hundreds of microseconds. They are responsible for the fast component during synaptic transmission. NMDA receptors are unique because their activation requires the coincidence of 1) glutamate binding to the respective receptor, 2) a depolarization to about -40 mV to relieve the Mg^+ block of the channel at the GluN2 subunits, and 3) the presence of the co-agonist glycine (or alternatively serine; Johnson & Ascher, 1987) bound to either the GluN1 or GluN3 subunit. Note that, under normal physiological conditions, the cerebrospinal fluid (CSF) contains sufficient amount of glycine. The kinetics of these NMDA receptors is typically slow in the range of tens of milliseconds. In contrast to the AMPA receptors, they carry the slow component in synaptic transmission. The KA

receptors share similar mechanisms for activation and desensitization as the AMPA receptors (Mayer, 2006; Perrais *et al.*, 2010). However, KA receptors need extracellular Na^+ for activation, unlike the AMPA receptors which still activate normally in the absence of this ion (Plested *et al.*, 2008). Furthermore, the rate of recovery from glutamate-induced desensitization is much longer (~10 fold) for KA than the AMPA receptors (Bowie & Lange, 2002). The kinetics of the EPSCs mediated by KA receptors, in contrast to those by AMPA receptors, are much slower; *i.e*. they have a longer rise and decay times (Kidd & Isaac, 1999).

As indicated above, the mGluRs are comprised of eight different isotypes classified into three different groups. Group I consists of mGluR1 and mGluR5, which are coupled to G_q-protein. Group II includes mGluR2 and mGluR3, and group III includes mGluR4 and mGluR6-8. All receptors in groups II and III are coupled to $G_{i/o}$-protein. Because mGluR1 and mGluR5 are coupled to the G_q-protein, their activation results in the subsequent activation of phospholipase Cβ (PLCβ), which then hydrolyses phosphatidylinositol 4,5-bisphosphate (PIP_2) to produce inositol trisphosphate (IP_3) and diacylglycerol (DAG). mGluR2 – 4 & 6 – 8 activate the $G_{i/o}$-protein to inhibit adenylyl cyclase, which results in the drop in the intracellular concentration of cyclic adenosine monophosphate (cAMP).

The three groups are expressed widely in neurons and glial (astrocytic) cells in the brain, including the neocortex. Group I mGluR are often expressed postsynaptically, and their activation causes a depolarization of the postsynaptic cell or, more generally, causes an increased membrane excitability (Valenti *et al.*, 2002). However, when expressed presynaptically, they are able to increase neurotransmitter release rate (Park *et al.*, 2004; Choy *et al.*, 2017a). In contrast, group II and III mGluRs are predominantly expressed in presynaptic nerve terminals. Their activation typically inhibits neurotransmitter release (van den Pol *et al.*, 1998; Chen *et al.*, 2002; Doi *et al.*, 2002; Shen & Johnson, 2003; Mateo & Porter, 2007).

1.3. Neurotransmitter Release

The details of neurotransmitter release as described above, are based on widely studied and understood synaptic transmission due to stimuli that evoked AP(s). This process is termed evoked neurotransmitter release. However, there is also neurotransmitter release without or independent of a stimulus. This release is termed spontaneous neurotransmitter release. Many aspects of the spontaneous release are still a matter of debate among neuroscientists. Some contentious examples are 1) whether spontaneous and evoked releases utilize the same SNARE proteins and/or synaptic vesicles, and 2) what the physiological function of the spontaneous release is. Here, I will expand on the

essential aspects of spontaneous glutamate release because a large part of the data presented here deals with its modulation. This will be followed by discussing the Ca^{2+} dependence of glutamate release, as it is an important aspect in this thesis.

1.3.1. Spontaneous Neurotransmitter release

The concept of spontaneous neurotransmitter release was initially introduced by Fatt and Katz (1950). At the frog neuromuscular junction, they observed spontaneously occurring miniature end-plate potentials (mEPPs; representative of acetylcholine release from the presynaptic terminal) without any stimulus. The mEPPs had the following characteristics: 1) The amplitudes were ~1 mV (approximately 100 times smaller than the AP evoked by the stimulus of the muscle nerve). 2) The frequency was 0.1 – 100 Hz, and 3) the mEPPs had a rapid rise of 1 – 2 ms and 4) a slow decay time (half-decay of 3 – 4 ms). 5) The mEPP amplitude was dependent on the extracellular Na^+ concentration, but independent of the extracellular Ca^{2+} concentration. 6) The frequency was independent of both the extracellular Na^+ and Ca^{2+} concentration, but 7) it increased as the temperature or the osmotic pressure of the superfusate increased (Fatt & Katz, 1952).

Similarly, spontaneous synaptic events were also observed in many regions of the central nervous system, specifically in motoneurones of the spinal cord (Brock *et al.*, 1952; Katz & Miledi, 1963; Kuno, 1964; Colomo & Erulkar, 1968; Korn *et al.*, 1987) and in various brain regions, such as hippocampus (Brown *et al.*, 1979; Swann *et al.*, 1990; Strowbridge *et al.*, 1992; Hosokawa *et al.*, 1994) and neocortex (Watanabe & Creutzfeldt, 1966; Pare *et al.*, 1998). In the case of excitatory synapses, they are called spontaneous excitatory postsynaptic potentials or currents (sEPSPs or sEPSCs). The application of the fast Na^+ channel blocker tetrodotoxin (TTX) did not abolish them, indicating that transmitter release is not caused by spontaneous electrogenesis in the axon, *i.e*. locally generated AP(s). To differentiate spontaneous events in the presence of TTX from those without, the former are termed miniature excitatory postsynaptic potentials or currents (mEPSPs or mEPSCs; Katz & Miledi, 1963).

In most regions of the brain, sEPSP/Cs and mEPSP/Cs are typically mediated by both AMPA and NMDA receptors (McBain & Dingledine, 1992; Myme *et al.*, 2003). However, the recording conditions, *i.e*. the presence or lack of extracellular Mg^{2+} and the holding potential, determine whether typical NMDA-mediated sEPSP/Cs or mEPSP/Cs can be observed or not. Hence, the kinetics (average time course) may change accordingly. The frequency and amplitude of these spontaneous events in neocortex differ vastly between cell types and layers, making it hard to capture some general characteristics. Therefore,

I will only present characteristics of mEPSCs in pyramidal cells of layer II in the somatosensory cortex (S1 barrel cortex), as it was the focus of my studies.

A pyramidal cell in layer II of S1 barrel cortex receives approximately 10,000 synaptic inputs, ~70% of which are of intracortical origin (Gruner *et al.*, 1974; Larkman, 1991; DeFelipe & Farinas, 1992). With such a large number of inputs, Simkus and Stricker (2002b) showed that in these cells, obtained from Wistar rats at the age of 12 – 17 days, the average sEPSC frequency *in vitro* was 33 ± 13 Hz with an amplitude of -9.9 ± 2.7 pA. These sEPSCs had an average rise time of 0.7 ± 0.8 ms, and a half-width of 2.1 ± 3.8 ms. In the presence of TTX, the mEPSCs in these cells had an average frequency of 28 ± 24 Hz and amplitude of -10 ± 3 pA. Neither the frequency, amplitude, rise time, nor the half width of sEPSCs and mEPSCs were significantly different from each other. Note that the s/mEPSC frequency might be higher *in vivo*. When using the $GABA_A$ receptor blocker bicuculline and the AMPA receptor antagonist DNQX, no mEPSCs were observed indicating that these mEPSCs were mediated solely by AMPA receptors. The presence of Mg^{2+} in artificial cerebrospinal fluid (ACSF) and a holding potential at -70 mV further strengthened their conclusion. With such a high frequency, recordings of mEPSCs are perfectly suited for the study of the mechanism(s) of spontaneous release and its modulation.

As indicated above, whether the spontaneous glutamate release utilizes the same SNARE proteins as the evoked release remains an open question. In cultured hippocampal neurons of homozygous knockout mice lacking synaptobrevin/VAMP2, the mEPSC frequency decreases to ~15% of control (heterozygous) without any change to the amplitude and rise time, whilst evoked release is absent (Schoch et al., 2001). The complete loss of syntaxin 1A and 1B in mouse hippocampal neurons abolishes both mEPSCs and evoked EPSCs (Vardar et al., 2016). In mature hippocampal cultures from SNAP-25 knockout mice, Ca^{2+}-evoked release is abolished, but a low mEPSC frequency of ~10% of control is still observed (Bronk *et al.*, 2007). These studies make two important points: 1) A large proportion of the spontaneous glutamate release is based on utilising synaptobrevin/VAMP2, syntaxin 1, and SNAP-25, similar to the evoked release. 2) Other SNARE protein(s) may also be involved in the spontaneous release. The first candidate tested was Vti1a, because it is robustly trafficked at synapses without AP firing, and its knockdown reduced the frequency of mEPSCs (Ramirez *et al.*, 2012). Another candidate is VAMP7, because reelin facilitates spontaneous transmitter release by specifically mobilizing VAMP7-containing synaptic vesicles (Bal *et al.*, 2013).

Another debated matter regarding spontaneous transmitter release is the nature and number of different vesicle pools involved. Using a genetically-encoded probe that

contains biotinylated VAMP2, Fredj and Burrone (2009) and Andreae *et al.* (2012) found that synaptic vesicles for spontaneous release belong to the resting pool, vesicles of which are not or poorly mobilized upon neuronal activity. The idea of a "distinct" pool involved in spontaneous release was then rebutted by Hua *et al.* (2010). Because cross-depletion of recycled vesicles occurs for both spontaneous and evoked release, they suggested that the recycling pool was involved in both instances. To the best of my knowledge, there is still no decisive answer to the old question if spontaneous release utilises a different pool of vesicles than evoked. I hope that some of my results may shed some light on some of these ideas (see parts 3, and 4).

In contrast to what Fatt and Katz (1952) reported for sEPPs, spontaneous glutamate release can be affected by extracellular Ca^{2+} concentration ($[Ca^{2+}]_o$). Increasing the $[Ca^{2+}]_o$ increases the rate of release as shown by Katz and Miledi (1963). This may occur via activation of the Ca^{2+}-sensing receptor, which is a highly expressed G-protein-coupled receptor in nerve terminals (Ruat *et al.*, 1995). Consequently, the increased rate becomes independent of Ca^{2+} influx through VDCC (Vyleta & Smith, 2011; Tsintsadze *et al.*, 2017). Similarly, Ca^{2+} from intracellular stores (smooth endoplasmic reticulum) also affects the rate of spontaneous release. Simkus and Stricker (2002a) have shown that either emptying or blocking Ca^{2+} efflux from the presynaptic stores significantly decreased the mEPSC frequency in neocortical layer II pyramidal cells. Furthermore, increasing Ca^{2+} efflux by activating IP_3 via group I mGluR or ryanodine receptors led to a significant increase in the mEPSC frequency.

Such findings led to an important question, *i.e*. if neuromodulatory transmitters other than glutamate, via (presynaptic) G_qPCR, might also be capable of activating presynaptic Ca^{2+} stores. Such transmitters include noradrenaline (NA) acting via α_1-adrenergic receptors (AR) and serotonin (5-HT) via 5-HT_2R. This idea was first tested for α_1-AR (Choy *et al.*, 2017a). Some remaining issues will also be presented in part 4 of this thesis. In summary, NA indeed activated presynaptic α_1-AR and caused Ca^{2+} release from stores seen as a sustained increase in mEPSC frequency. In this context, and to further extend the understanding of neuromodulatory action on spontaneous release in cortex, I studied if 5-HT also modulated the mEPSC frequency through the same or similar mechanism. Consequently, access to store release may be a universal mechanism of altering spontaneous transmitter release in the central nervous system.

It remains a debate what the physiological role of spontaneous transmitter release is. It has been suggested that it may assist numerous essential functions. First, it may serve to maintain the postsynaptic ultrastructure of synapses (spine density and length) (McKinney *et al.*, 1999; Tyler & Pozzo-Miller, 2003). Second, it may regulate long-term

synaptic plasticity by activating postsynaptic mGluR and thereby increase the Ca^{2+} concentration required for the insertion of new AMPA receptors into the postsynaptic density (Jin *et al.*, 2012a; Jin *et al.*, 2012b). Third, it may regulate neuronal excitability and AP firing by directly modulating postsynaptic conductances in the dendritic membranes (Pare *et al.*, 1998; Carter & Regehr, 2002).

1.3.2. Evoked Neurotransmitter Release

In this section, I will describe how evoked transmitter release occurs and its dependency on Ca^{2+}, both from extracellular and intracellular sources.

Very early in the history of intracellular recording, it was recognised that Ca^{2+} played a crucial role in transmitter release (Del Castillo & Katz, 1954a; for review see Katz, 1962). In short, the action potential depolarizes the nerve terminal membrane and in doing so activates VDCC, which then open for Ca^{2+} to flow into the presynaptic terminal. This event then triggers vesicle fusion and subsequent neurotransmitter release. Specifically, in presynaptic nerve terminals of pyramidal cells in neocortex, both N- and P/Q type VDCCs are expressed (Qian & Noebels, 2001; Yu *et al.*, 2010). The amount of release as a function of Ca^{2+} influx is best described via a cooperativity around 4 – 5 (Hill coefficient of 4; Dodge & Rahamimoff, 1967; Wu & Saggau, 1994; Borst & Sakmann, 1996). In fact, Dodge and Rahamimoff (1967) provided an interpretation of this cooperativity as indicating that 4 – 5 Ca^{2+} ions are necessary to bind to the Ca^{2+} sensor for release to occur. Because of this power relationship, it can be estimated that a 12.5% decrease in Ca^{2+} influx for example depresses the EPSC/P amplitude by ~50%.

In contrast to the requirements for extracellular Ca^{2+}, the dependency of evoked release on Ca^{2+} from intracellular stores like the smooth endoplasmic reticulum (SER) has gained much less exposure. Emptage *et al.* (2001) showed that, in boutons of hippocampal pyramidal cells in culture, Ca^{2+}-induced Ca^{2+} release (CICR) from stores augmented the Ca^{2+} transients and paired-pulse facilitation. Further, Liang *et al.* (2002) found that Ca^{2+} transients in mossy fibre terminals in response to a brief train of APs were also augmented by Ca^{2+} from stores. The understanding was expanded by de Juan-Sanz *et al.* (2017) in their recent study, showing that axonal endoplasmic reticulum (ER) acts as a Ca^{2+} buffer during neuronal activity and creates a feedback loop controlling the cytosolic Ca^{2+} via the ER Ca^{2+}-sensing protein STIM1.

Clear evidence of how Ca^{2+} from intracellular stores affects evoked glutamate release raised an intriguing question if neuromodulators utilize the stores in modulating EPSP/C. I addressed this question by extending my research to the modulation of EPSC between

layer II pyramidal pairs by NA and 5-HT, and elucidating the respective mechanisms. The results were rather interesting because they revealed Gβγ subunit-dependent mechanisms targeting different effectors (for details see part 4).

1.4. Neuromodulation

Both the spontaneous and evoked neurotransmitter release could be modulated by different type of neuromodulators, hence, signal or information transferred between neurons is altered accordingly. There are six majorly known neuromodulators, namely acetylcholine, histamine, neuropeptides (*e.g.* oxytocin/hypocretin), dopamine, NA, and 5-HT. Because I mainly investigated serotonergic modulation of glutamate release in S1 barrel cortex layer II pyramidal cells, and provided comparisons with adrenergic modulation in the same region and layer for my PhD thesis, I focus my description on NA and 5-HT among the major neuromodulators.

With the order of NA first, then followed by 5-HT, I explain the most essential aspects of how they run their function as neuromodulators. I start by describing their biosynthesis and degradation processes in the brain respectively. This will be followed by detailed locations of the nuclei of NA- and 5-HT-containing neurons. Subsequently, I will explain to which brain regions the axons of these nuclei project to. Receptors which bind NA (adrenergic receptor; AR) and 5-HT (5-HTR) will be explained from the perspectives of signalling mechanisms and their expression locations. Note that the abbreviation of receptor(s) with R refers to both the singular and the plural. Finally, I describe in general some physiological functions related to the adrenergic and serotonergic modulations.

1.4.1. Noradrenaline

Noradrenaline (NA), in the USA also called norepinephrine, belongs to the group of monoamines. Its structure contains 1) a benzene ring with two attached hydroxyl groups (-OH) located adjacently and 2) an ethylamine side chain with one amine group ($-NH_2$). NA is synthesized in the brain from the amino acid tyrosine. The first step of its biosynthesis, which is also its rate-limiting step (Fitzpatrick, 1991), converts tyrosine via tyrosine hydroxylase into 3,4-dihydroxy-l-phenylalamine (L-DOPA). L-DOPA is then converted in the presence of coenzyme pyridoxal phosphate into dopamine by the aromatic amino acid decarboxylase or DOPA decarboxylase. In noradrenergic neurons (specifically in its synaptic vesicles), dopamine is then converted further into NA by dopamine-β-hydroxylase (DBH), also called dopamine-β-monooxygenase. This step involves a hydroxylation and requires ascorbic acid as electron donor.

NA is released from synaptic vesicles via exocytosis from specific nerve terminals (see below), the axons of which originate in the *locus coeruleus*. Its action is then terminated primarily by reuptake into respective nerve terminals via the Na^+ and Cl^--dependent norepinephrine transporter (NET; Blakely *et al.*, 1994; Bonisch & Bruss, 2006).

NA undergoes degradation by two enzymes, namely monoamine oxidase (MAO) and cathecol-O-methyltransferase (COMT). MAO has two different isozymes called as MAO A and B (Shih, 1991). MAO A is found concentrated in adrenergic (noradrenaline) cells in the *locus coeruleus* (Shih *et al.*, 1999a), and this isozyme catalyses NA oxidative deamination to yield 3,4-dihydroxyphenylglicol and 3,4-dihydroxymandelic acid. COMT then catalyses the chemical reaction in which the methyl group of S-adenosylmethionine is transferred to the 3-position hydroxyl group of both 3,4-dihydroxyphenylglicol and 3,4-dihydroxymandelic acid to yield 3-methoxy-4-hydroxy-phenylglycol (MHPG) and 3-methoxy-4-hydroxy-mandelic acid (vanillylmandelic acid; VMA) respectively. The degradation by these two enzymes can also happen in the reverse order. In this case, NA is initially converted into normetanephrine by COMT, which then undergoes oxidative deamination catalyzed by MAO A to end up with the same final two products of MHPG and VMA.

This cycle of biosynthesis and degradation primarily occurs in noradrenergic cells. In the mammalian brain, noradrenergic cell bodies can be grouped into the *locus coeruleus*, the dorsal medullary group (located close to the dorsal motor nucleus of vagus nerve in the medulla), and the lateral tegmental system (located in the pontine tegmentum and reticular formation of the pons). Among these three groups of nuclei, the *locus coeruleus* is the most important one because its axons widely and diffusely innervate brain. The axons project rostrally (dorsal bundle) to innervate thalamic nuclei and different regions of cortex including the neocortex, hippocampus, the basolateral amygdala, and the septum (Loughlin *et al.*, 1986). Other axons project dorsally to innervate cerebellum (Olson & Fuxe, 1971), and caudally to innervate the spinal cord (Hancock & Fougerousse, 1976; Nygren & Olson, 1977).

NA signals at synapses via AR. Based on their pharmacological profiles and the associated signalling pathways, AR are classified into three different groups. Note that all groups are G-protein-coupled receptors (GPCR). The first group consists of α_1-AR, which are coupled to the G_q-protein. There are three subtypes of α_1-AR: α_{1A}, α_{1B}, and α_{1D}-AR (Bylund *et al.*, 1994; Hieble *et al.*, 1995). In the brain, α_{1A}-AR are expressed in the cerebral cortex (Jones *et al.*, 1986; Parkinson *et al.*, 1988; Papay *et al.*, 2006; Santana *et al.*, 2013), hippocampus (Zilles *et al.*, 1991; Papay *et al.*, 2006), dorsal thalamus, hypothalamus, midbrain, pontine olivary nuclei, trigeminal nuclei, cerebellum

(Jones *et al.*, 1986; Papay *et al.*, 2006), and the *nucleus accumbens* (Mitrano *et al.*, 2012). α_{1B}-AR are also expressed in cerebral cortex, thalamus, dorsal and medullary raphe nuclei (Nicholas *et al.*, 1991). α_{1D}-AR have been found in cerebral cortex, hippocampus, olfactory bulb, the dorsal geniculate and ventral posterolateral nuclei of thalamus (Sadalge *et al.*, 2003). Binding of NA to α_1-AR activates the G_q-protein to cause the activation of PLCβ, which then hydrolyses PIP_2 to produce IP_3 and DAG. The former increases Ca^{2+} release from intracellular stores, whilst the latter may activate protein kinase C (PKC).

The second group consists of α_2-AR, which are coupled to the $G_{i/o}$-protein and inhibit adenylyl cyclase, resulting in a lowering of intracellular cAMP. Activated Gβγ subunits of the $G_{i/o}$-trimer are also capable of activating K^+ channels (Williams *et al.*, 1985) and inhibiting voltage-dependent Ca^{2+} channels (Boehm, 1999; Timmons *et al.*, 2004). Three genes have been found to code for α_2-AR, namely α_{2A}, α_{2B}, and α_{2C}. In brain, the expression of these three subtypes are as follows. α_{2A}-AR are found in the *locus coeruleus*, cerebral cortex, hippocampus, hypothalamus, amygdala, brain stem and septum, α_{2B}-AR in the thalamus and α_{2C}-AR in the cerebral cortex, hippocampus, basal ganglia, olfactory tubercle, and striatum (Scheinin *et al.*, 1994; King *et al.*, 1995; Holmberg *et al.*, 1999).

The third and last group contains the β-AR, which are coupled to the G_s-protein. When NA binds to β-AR, the G_s-protein activates adenylyl cyclase, causing an increase in the intracellular cAMP concentration. There are three different subtypes: β_1, β_2, and β_3. In the brain, β_1-AR are highly expressed in layer I and II of cerebral cortex, cingulate cortex, hippocampus, ventral striatum (the islands of Calleja), and the mediodorsal and ventral nuclei of thalamus. β_2-AR are highly expressed in the molecular layer of cerebellum and the central, paraventricular, and caudal lateral posterior nuclei of thalamus. Both β_1 and β_2-AR are co-expressed to a similar extent in layer IV of cerebral cortex, the *substantia nigra*, olfactory tubercle, medial preoptic nucleus, and the nuclei in the medulla (Rainbow *et al.*, 1984). β_3-AR are expressed in cerebral cortex and hypothalamus (Evans *et al.*, 1999) and the subgranular zone of hippocampus (Jhaveri *et al.*, 2010).

One of the outcomes of AR activation is a change in neuronal excitability and an associated de- or hyperpolarization. As all AR are metabotropic receptors, these outcomes are generated downstream of GPCR activation, mostly with specific channel(s) as targets or effectors. For example, NA can activate α_1-AR to suppress a leak K^+ conductance, and/or β-AR to enhance the hyperpolarization-activated cation current (I_h), resulting in a switch from rhythmic bursting activity to sparse spike firing in the thalamus (Pape & McCormick, 1989; McCormick *et al.*, 1991). NA, via α_2-AR

activation that relieves the tonic inhibition of TREK-2 channels by protein kinase A (PKA), can also cause a hyperpolarization to reduce the excitability of layer II/III pyramidal neurons of entorhinal cortex (Xiao *et al.*, 2009). In addition, the Gβγ subunits of activated α_2-AR can open a G-protein-activated inwardly rectifying K^+ (GIRK) conductance, inducing a hyperpolarization in *locus coeruleus* neurons (Williams *et al.*, 1985). In cortical and hippocampal pyramidal neurons, NA enhances the excitability by suppressing a slow Ca^{2+}-activated K^+ current (I_{AHP}) downstream of β-AR activation (Madison & Nicoll, 1982; Haas & Konnerth, 1983; Foehring *et al.*, 1989; McCormick *et al.*, 1991; Satake *et al.*, 2008).

Another outcome of noradrenergic activity is the modulation in transmitter release. There is ample of evidence in the literature showing that NA modulates both spontaneous (mEPSP/Cs) and evoked transmitter release (EPSP/Cs). Some examples include the following: In layer II/III pyramidal cells of the medial prefrontal cortex (mPFC), NA can increase the mEPSC frequency via activation of presynaptic α_1-AR (Zhang *et al.*, 2013). However, in layer II/III and V pyramidal cells of mPFC and temporal cortex, NA depresses evoked EPSCs (Roychowdhury *et al.*, 2014) via α_1-AR activation (Salgado *et al.*, 2016). In CA3 pyramidal cells of organotypic slice cultures from rat, NA depresses the evoked EPSP amplitude via presynaptic α_1-AR activation (Scanziani *et al.*, 1993). In addition, a recent study in layer II of rat barrel cortex in this laboratory found that NA increases the mEPSC frequency in a subset of pyramidal cells (Choy *et al.*, 2017a), but depresses the EPSC amplitude in all pyramidal pairs recorded from (Choy *et al.*, 2017b; for details see part 4).

By modulating neuronal excitability and/or neurotransmitter release in different regions of brain, NA plays an important role in many physiological brain functions, such as attention and arousal (Mitchell & Weinshenker, 2010). It also affects the consolidation of long-term memory in the amygdala (Clem & Huganir, 2013) and hippocampus (O'Dell *et al.*, 2015; Walling *et al.*, 2016). Furthermore, α_1-AR antagonists are widely used in the treatment of psychotic episodes (Wadenberg *et al.*, 2000; Ma *et al.*, 2006; Lopez-Gil *et al.*, 2010).

1.4.2. Serotonin

1.4.2.1. Biosynthesis and Metabolism of Serotonin

5-HT is also a monoamine, but its synthesis derives from L-tryptophan. Following its initial identification in brain by Twarog and Page (1953), a vast set of studies have been done to further understand its physiological role.

Serotonin is synthesized in the central nervous system from the amino acid L-tryptophan, which is acquired primarily from dietary protein and transported to the brain via blood circulation. Initially, in serotonergic neurons, tryptophan is converted into 5-hydroxtryptophan (5-HTP) by tryptophan hydroxylase (Tph), specifically the Tph2 isoform (Walther *et al.*, 2003). 5-HTP then undergoes decarboxylation, catalysed by an enzyme called aromatic L-amino acid decarboxylase (AADC), to yield the transmitter 5-HT. During this biosynthetic process in two steps, the hydroxylation by Tph2 is the rate-limiting step (Cortes *et al.*, 1993).

Freshly synthesized 5-HT is then stored in synaptic vesicles by vesicular monoamine transporter 2 (VMAT2; Weihe *et al.*, 1994; Peter *et al.*, 1995; Erickson *et al.*, 1996) through an active transport process, in which the cytoplasmic 5-HT is exchanged with vesicular protons. 5-HT is released via exocytosis into the extracellular cerebrospinal fluid where it can bind to its cognate receptors.

Upon release, the mechanism of terminating its activity is via re-uptake by the serotonin transporter (SERT; Rudnick, 2006) into the nerve terminal or the glial cells, again as with NA, via transport along the Na^+ gradient.

Furthermore, 5-HT also undergoes breakdown through oxidative reaction(s), which are also catalysed by MAO, to yield 5-hydroxy-indoleacetaldehyde. As mentioned earlier, there are two isozymes of MAO, namely MAO A and B (Shih, 1991). Whilst 5-HT is preferentially oxidized by MAO A, interestingly serotonergic neurons predominantly contain MAO B, which preferentially oxidizes both phenylethylamine (PEA) and dopamine (DA), but not 5-HT (Shih & Chen, 1999; Shih *et al.*, 1999b, a). The product of oxidation by MAO, is 5-hydroxy-indoleacetaldehyde, which then is oxidized further by the nicotinamide adenine dinucleotide$^+$ (NAD^+)-dependent aldehyde dehydrogenase. The final product is 5-hydroxyindoleatic acid (5-HIAA), which is excreted via the urine.

1.4.2.2. Serotonergic Neurons and Axonal Projections

The biosynthesis process of 5-HT in mammalian brain, as described above, occurs in serotonergic neurons that specifically contain the necessary enzymes. Based on cytoarchitectural criteria, their cell bodies cluster in different nuclei in the mesencephalon, specifically in the set of raphe nuclei (Taber *et al.*, 1960). This set contains nine groups, numbered B_{1-9} (Törk, 1990; Lesch & Waider, 2012). Their details are as the followings: 1) B_1 – raphe pallidus nucleus in the caudal ventrolateral medulla. 2) B_2 – raphe obscurus nucleus. 3) B_3 – raphe magnus nucleus, rostral ventrolateral medulla, and lateral paragigantocellular reticular nucleus. 4) B_4 – raphe obscurus nucleus (dorsolateral part). 5) B_5 – median raphe nucleus (caudal part). 6) B_6 – dorsal

raphe nucleus (caudal part). 7) B_7 – principal dorsal raphe nucleus (rostral part). 8) B_8 – principal median raphe nucleus (rostral main part), caudal linear nucleus, and nucleus *pontis oralis*. 9) B_9 – *Nucleus pontis oralis* in the supralemniscal region (Törk, 1990).

The serotonergic projection to the forebrain originates from the dorsal (B_6 and B_7), median nuclei (B_5 and B_8), and the B_9 group. The median raphe nuclei projects mainly to the hypothalamus, septum, and dorsal hippocampus. In comparison, the dorsal raphe nucleus projects to the striatum, amygdala, and ventral hippocampus. Regarding cerebral cortex, more specifically neocortex, both the median and dorsal raphe nuclei send their projections in an overlapping manner, but topographically organized to target different cortical neurons. One important point to notice is that axon fibres and terminals from the median and dorsal raphe nuclei have different characteristics. The axons that project from the median raphe nuclei (M fibres) are made up of thick and relatively coarse fibres. They have short and thin branches, with large and round boutons. In contrast, the axons from the dorsal raphe nuclei (D fibres) contain very fine fibres. They branch profusely and end with small fusiform boutons (Törk, 1990; Hensler, 2006). As expected based on the respective properties, these serotonergic neurons also differ in 1) electrophysiological characteristics, *i.e*. neurons in the median raphe nuclei have shorter time constants and a larger after-hyperpolarization after an AP, and 2) autoreceptor inhibition, *i.e*. neurons in the dorsal raphe nuclei have a higher efficacy of reacting to 5-HT_{1A}R activation (Beck *et al.*, 2004).

B_1 to B_4 cell groups, which are distributed between the mid-pons and the caudal medulla, send axonal projections to the brainstem and spinal cord. In more detail, B_1 projects to Rexed laminae I and II of the dorsal horn (Bowker *et al.*, 1982; Hylden *et al.*, 1986), B_2 and B_4 to lamina IX of the ventral horn (Bowker *et al.*, 1982; Bowker, 1986), and B_3 to intermediolateral cell column (Loewy & McKellar, 1981).

The nine serotonergic groups are interconnected. Afferent connections link the median and dorsal raphe nuclei, and also the three cell groups of B_9 with B_1 and B_3.

1.4.2.3. Serotonin Receptors

5-HT signals via seven different groups 5-HT receptors (5-HTR), namely 5-HT_{1-7}R. These include a total of 23 subtypes of metabotropic GPCR, and an ionotropic non-specific ligand-gated cation channel, which is comprised of 5 different subunits (Hoyer *et al.*, 1994; Fink & Göthert, 2007; Pytliak *et al.*, 2011). In addition, recently a novel type of 5-HTR called Pr5-HT_8 has been discovered in the larvae of the small white butterfly, *Pieris rapae* (Qi *et al.*, 2014).

The ligand-gated cation channel (5-HT_3R), upon 5-HT binding, allows Na^+, K^+, and Ca^{2+} to permeate through the conducting pore. This channel has a heteropentamer structure, which is formed by 5-HT_{3A-E} receptor subunits. Different genes code for different subunits, with 5-HT_{3C-E} specific to humans. The exact heteropentameric composition(s) between different subunits likely depend on the brain region (Barnes *et al.*, 2009). Regarding the location of 5-HT_3R in the brain, high density expression is found in the nucleus of solitary tract, dorsal motor nucleus of vagus, *area postrema* (Gehlert *et al.*, 1991), amygdala, hippocampus, neocortex, and olfactory bulb where they are typically found on GABAergic interneurons (Koyama *et al.*, 2017). In addition, these receptors are also expressed in the superficial layers of the spinal dorsal horn (Kia *et al.*, 1995).

In contrast, the metabotropic receptors can be summarized as follows. The 5-HT_1R and 5-HT_5R groups are coupled to the $G_{i/o}$ protein, which lowers cAMP. In contrast, the group of 5-HT_2R are coupled to the G_q protein. The groups of 5-HT_4R, 5-HT_6R, and 5-HT_7R are coupled to the G_s protein. Not much is known about Pr5-HT_8, except that it increases the intracellular Ca^{2+} concentration without affecting cAMP levels. The 5-HT_1R and 5-HT_2R above have been assigned solely to their respective "classical" signalling cascades, actuated typically by Gα. Note, however, that more recent researches also indicate non-classical coupling to a different adaptor protein (arrestin) but also to an alternative non-classical G-protein. In addition, there are instances where the signalling may be carried not by Gα but by Gβγ (Choy *et al.*, 2017a; Choy *et al.*, 2017b; see also results).

The group of 5-HT_1R is comprised of 5-HT_{1A}, 5-HT_{1B}, 5-HT_{1D}, 5-HT_{1E}, and 5-HT_{1F}. Note because 5-HT_{1C}R was re-classified as 5-HT_{2C}R based on its structural and signalling mechanism, 5-HT_{1C}R is omitted from the list (Leonhardt *et al.*, 1992). The locations of each subtype, mostly based on binding studies, could be summarized as follows. 5-HT_{1A}R has long been known to be expressed densely on serotonergic neurons in median and dorsal raphe nuclei (Palacios *et al.*, 1983; Pazos *et al.*, 1987), specifically as somatodendritic autoreceptors that receive the negative feedback (Pan *et al.*, 1993). 5-HT_{1A}R is also highly expressed in prefrontal and frontal (Hoyer *et al.*, 1985; Hoyer *et al.*, 1986a), entorhinal cortex (Cheetham *et al.*, 1989; Chalmers & Watson, 1991), hippocampus, and the amygdala. 5-HT_{1B}R (5-HT_{1B} and 5-$HT_{1Dβ}$R prior to nomenclature reassessment by Hartig *et al.*, 1996) is expressed with high density in the basal ganglia (Middlemiss & Hutson, 1990), more specifically in the *substantia nigra* and the *globus pallidus* (Varnäs *et al.*, 2001), both on the presynaptic terminals of serotonergic boutons and the postsynaptic targets. A recent study by Kjaerby *et al.* (2016) shows that this receptor is also expressed on presynaptic terminals in the ventral hippocampus and the contralateral inputs to the medial prefrontal cortex. 5-HT_{1D}R (5-$HT_{1Dα}$R prior to nomenclature reassessment by Hartig *et al.*, 1996) is not only expressed in the basal

ganglia (*globus pallidu*s, ventral pallidum, caudate-putamen, and *substantia nigra*; Bruinvels *et al.*, 1993), but also in the hippocampus and the entorhinal cortex (Lei, 2012). 5-HT_{1E}R is likely absent from mouse and rat brains as the respective gene has not been found (Bai *et al.*, 2004). However, it is expressed in frontal cortex (Leonhardt *et al.*, 1989), caudate, putamen, hippocampus (Lowther *et al.*, 1992), and olfactory bulb (Bai *et al.*, 2004) in brains of humans and guinea pigs. The 5-HT_{1F}R location differs in different species as shown by Lucaites *et al.* (2005). In rat, (among others) it is expressed in layer IV/V of cortex, the CA3 region of the hippocampus, subiculum, *nucleus accumbens*, caudate-putamen, parafasicular nucleus of thalamus, several amygdaloid nuclei, and olfactory bulb. In human brain, the receptor is expressed in neocortical layers 4 and 5 and in the granule cell layer of the cerebellum.

5-HT_2R were classified into three different subtypes, namely 5-HT_{2A}, 5-HT_{2B}, and 5-HT_{2C}. 5-HT_{2A}R is expressed with high density in neocortex (Watts *et al.*, 1994; Hamada *et al.*, 1998; Hall *et al.*, 2000), the claustrum, piriform cortex, olfactory bulb, pontine nuclei, mammillary bodies, red nucleus, cranial motor nuclei (Hamada *et al.*, 1998), caudate-putamen, *nucleus accumbens*, choroid plexus (Watts *et al.*, 1994), hippocampus, thalamus (Hall *et al.*, 2000), and spinal cord (both on motoneurons in ventral horn, and in the intermediolateral nucleus of the thoracic cord; (Maeshima *et al.*, 1998). 5-HT_{2B}R in the brain, based on an immunohistochemistry study by Duxon *et al.* (1997), is found in the lateral septum, dorsal hypothalamus, medial amygdala, and the cerebellum. 5-HT_{2C}R (formerly named as 5-HT_{1C}R) is highly expressed in ventromedial hypothalamus, *globus pallidus*, *substantia nigra*, and choroid plexus (Hoyer *et al.*, 1986b; Pazos *et al.*, 1987; Abramowski *et al.*, 1995), with low to moderate expression in other regions of brain, including neocortex, hippocampus and the cerebellum (Hoyer *et al.*, 1986b; Abramowski *et al.*, 1995). Further details of the expression of 5-HT_1R and 5-HT_2R, including their layer-specific and subcellular compartmentalisation, will be described later in sections 3.1 and 4.1 in relation with physiological functions in neocortex.

Using specific radioligands, 5-HT_4R was found to be expressed with high density in the olfactory tubercle, *substantia nigra*, striatum (Grossman *et al.*, 1993), as well hippocampus (Bonaventure *et al.*, 2000), very likely on the postsynaptic targets of serotonergic terminals.

5-HT_5R is expressed at a high density in the medial habenula, and with moderate densities in neocortex and the olfactory bulb (Waeber *et al.*, 1998). The mRNA of 5-HT_6R is found in hippocampus, striatum, *nucleus accumbens*, and olfactory tubercle (Ruat *et al.*, 1993a). Another study using polyclonal antibody points out the 5-HT_6R expression in hippocampus (CA1 and dentate gyrus), striatum, *nucleus accumbens*, olfactory tubercle

(plexiform layer), in the frontal and enthorinal cortices, and the cerebellum (Gérard *et al.*, 1997). 5-HT_7R is found to be expressed (in the order from most to least abundant) in the hypothalamus, hippocampus (pyramidal cells), cerebral cortex, olfactory bulb, and the olfactory tubercle (Shen *et al.*, 1993; Mengod *et al.*, 1996). Other researchers have pointed out that this receptor is also expressed in the *taenia tecta*, amygdaloid nuclei (Ruat *et al.*, 1993b), and cerebellar Purkinje cells (Geurts *et al.*, 2002).

One distinctive characteristic of 5-HTR is high ligand binding affinity to agonists. In comparison with other neuromodulator receptors that generally have binding affinities or EC_{50} up to few µM, the one for 5-HTR (and EC_{50}) is within a range from a few to tens of nM (K_i for displacement of [^{3}H] ligands with 5-HT for 5-$HT_{1\&2}$R = 3.8-17 nM; Peroutka & Snyder, 1979; see also Barnes & Sharp, 1999; Ray, 2010). Such a high affinity, up to a thousandfold, suggests a potent and highly sensitive ability for neuromodulation.

Describing ascribed physiological role(s) for each 5-HTR subtype is very difficult. This is because of the following reasons: 1) The same 5-HTR subtype can be expressed in many different brain regions, which all are involved in different physiological roles. 2) The receptors are often expressed in an overlapping manner throughout different brain regions. This fact may suggest that, in producing an outcome, different 5-HTR either work *in tandem* or competitively. 3) Although the specific layers and subcellular compartments, where the 5-HTR are expressed, determine their functional impacts, unfortunately the picture remains incomplete. 4) Compared to other seven transmembrane receptors like AR, 5-HTR are involved in a number of unusual signalling combinations like mimicking alternate G-protein (Kaufman *et al.*, 1995) action, usage of non-classical adaptor proteins (Gray *et al.*, 2003), constitutive receptor activity without ligand binding (for review see Berg *et al.*, 2005), receptor transactivation (Grewal *et al.*, 2001), and the activation of elements of mitogen-activated protein kinase (MAPK) signalling pathways (Watts, 1996). Furthermore, they can heterodimerize with various other GPCR, among others the leptin (Tecott *et al.*, 1995; Yadav *et al.*, 2009), growth hormone secretagogue (Schellekens *et al.*, 2013), D_2 (Albizu *et al.*, 2011; Lukasiewicz *et al.*, 2011), melatonin (Kamal *et al.*, 2015), and mGluR2 (Gonzalez-Maeso *et al.*, 2008; Moreno *et al.*, 2012). Because of this vast complexity, I will only introduce function(s) of the respective 5-HTR in very general terms.

5-HT_{1A}R regulates serotonergic neurotransmission by functioning as a somatodendritic autoreceptor on serotonergic neurons (Sharp & Hjorth, 1990). As expected from its expression with high density in prefrontal cortex, agonism of 5-HT_{1A}R has an anxiolytic and antidepressant effect (Charney *et al.*, 1990; Artigas, 2013). 5-HT_{1B}R may be involved

in diseases related to function(s) of the basal ganglia, for example Parkinson's disease (Riahi *et al.*, 2013).

5-HT_{2A}R, which is highly expressed in neocortex, has been linked to higher cognitive functions. Some anti-psychotic drugs are antagonists with high affinity to this receptor (Leysen *et al.*, 1993; Artigas, 2013). 5-HT_{2A}R is also involved in the hallucinogenic action of some drugs (Gonzalez-Maeso *et al.*, 2007). Activation of 5-HT_{2C}R has been linked to hypolocomotion, hypophagia, and anxiety (Koek *et al.*, 1992; Kennett *et al.*, 1994; Kennett *et al.*, 1996).

Because of a high 5-HT_3R expression in the *area postrema*, antagonists of this receptor have been developed to treat nausea and vomiting in patients undergoing chemotherapy. 5-HT_3R has also been linked to some psychiatric disorders (Lucchelli *et al.*, 1995; Eisensamer *et al.*, 2003), including states of anxiety because the deletion of this receptor in mice was anxiolytic (Kelley *et al.*, 2003).

Agonists at 5-HT_4R have been shown to improve cognitive performance (Letty *et al.*, 1997; Marchetti-Gauthier *et al.*, 1997). They also mediate a rapid antidepressant action via desensitization of 5-HT_{1A} autoreceptors (Lucas *et al.*, 2007). Antagonists at 5-HT_6R are also involved in cognitive enhancement (Rosse & Schaffhauser, 2010), but agonists are likely involved in the control of feeding behaviour (Heal *et al.*, 2008). 5-HT_7R regulates circadian rhythms (Edgar *et al.*, 1993) and sleep (Hedlund, 2009), as both the agonist(s) and antagonist(s) of this receptor are capable to alter these conditions. Some studies also name 5-HT_7R as a potential target of anti-depressant action (Wesolowska *et al.*, 2006; Berman *et al.*, 2009).

1.4.2.4. Modulation of Membrane Properties

Similar to other neuromodulators, 5-HT also modulates membrane properties and neuronal excitability. For example, 5-HT causes two opposite effects on the polarization and excitability of layer V pyramidal cells in rat mPFC (Araneda & Andrade, 1991). The first response is a hyperpolarization by 3.3 ± 2.0 mV via 5-HT_{1A}R activation, most likely by opening of G-protein-coupled inwardly-rectifying potassium channel (Andrade & Nicoll, 1987; Lüscher *et al.*, 1997). The second response is an enhancement of the membrane excitability, which consisted of three different components, namely a membrane depolarization by 3.8 ± 2.1 mV, a switch from an AHP to a long-lasting depolarizing afterpotential after a burst of spikes, and a decrease in spike frequency adaptation. This enhancement of excitability is mediated by 5-$HT_{2(A)}$R activation. In some cells, the depolarization is sufficiently large to induce tonic AP firing at a frequency of 2

– 5 Hz (Zhang, 2003). Later, Beique *et al.* (2007) argued that such an increase in excitability most likely accounts for the increase of spontaneous glutamate release.

These responses were investigated further by Avesar and Gulledge (2012), who found that pyramidal cells which show a 5-HT_{1A}R-mediated hyperpolarization and inhibition of firing are corticopontine-projecting neurons (CPns). In contrast, pyramidal cells with a 5-HT_{2A}R-mediated depolarization and an AP frequency increase are callosal/commissural (COM) neurons. In other words, the projection of these neurons indicates how the excitability changes upon exposure to 5-HT. It is worth noting that this projection-dependent specificity is not solely caused by the difference in 5-HTR expression, because 32% of CPns exhibited a 5-HT_{2A}R-mediated excitation in the presence of a 5-HT_{1A}R blocker (Stephens *et al.*, 2014).

Similar to some studies above, Foehring *et al.* (2002) also found that 5-HT produces opposite responses in excitability in a variety of cells from different layers of rat sensorimotor cortex. In layer II, about 50% of pyramidal cells depolarized by 7 ± 1 mV upon exposure to 5-HT, but the remainder hyperpolarized by 5 ± 2 mV. In layer III, however, 90% of pyramidal cells depolarized by 4 ± 1 mV, but only 10% hyperpolarized by about 3 mV. The depolarization was found to be mediated by 5-HT_2R, whilst the hyperpolarization by 5-HT_{1A}R. However, it remained unclear if the projection of the pyramidal cells determined the direction of change in polarization. In this thesis, I provide data showing that a specific change in neuronal membrane property (R_{in}) actually signified if the pyramidal cell, upon superfusion with 5-HT, would show a significant change in the spontaneous rate of glutamate release or not at all. Further, using paired recordings, I show that there is a specific topology within small networks based on the cell's response to 5-HT.

1.4.2.5. Modulation of Neurotransmitter Release

Following on the explanation from above, 5-HTR activation can modulate transmitter release of both, glutamate and GABA. This has been reported in numerous studies undertaken in different brain regions. For example, presynaptic 5-HT_3R activation increases mEPSC frequency in 42% of *area postrema* neurons (Funahashi *et al.*, 2004). In contrast, presynaptic 5-HT_{1B}R activation induces long-term depression of the evoked EPSC amplitude in medium spiny projection neurons at the corticostriatal synapse (Mathur *et al.*, 2011). Similarly, 5-HT decreases the mEPSC frequency and depresses the evoked EPSC amplitude in interneurons and projection neurons in the basolateral amygdala of rat (Rainnie, 1999). Moreover, 5-HT activates presynaptic 5-HT_3R to

transiently increase the mIPSC frequency in immature CA3 pyramidal cells of the rat hippocampus (Choi *et al.*, 2007).

In neocortex results from several studies also confirm that 5-HT modulates spontaneous release (Aghajanian & Marek, 1997; Marek & Aghajanian, 1998; Aghajanian & Marek, 1999; Marek & Aghajanian, 1999; Lambe *et al.*, 2000; Xiang & Prince, 2003). More details in regard to this observation will be given in the introduction of Part 3. Other aspects, including the relevant receptors and knowledge deficit of molecular mechanisms, will also be delineated, followed by how these are addressed in this thesis (see 3.1).

Likewise, in Part 4, I will further introduce the current state of research in regard to the impact of 5-HT on evoked transmitter release (Tanaka & North, 1993; Torres-Escalante *et al.*, 2004; Komlosi *et al.*, 2012; Barre *et al.*, 2016), the receptor(s) involved, what is currently unknown about the molecular mechanisms, and how I think this could be addressed in this thesis.

1.5. Scope of Thesis

As indicated earlier, this thesis was designed to corroborate if 5-HT, downstream of G_q activation, modulates transmitter release via Ca^{2+} release from presynaptic stores. I started by investigating if and how 5-HT modulates spontaneous glutamate release (mEPSCs). As predicted, I found that 5-HT did increase the mEPSC frequency, however, only transiently. This observation was linked to the activation of 5-HT_2R, which classically signals via G_q. Consistent with this type of signalling cascade, blocking either PLCβ, IP_3R and chelating intracellular Ca^{2+} with BAPTA-AM abolished the action of 5-HT on the mEPSC frequency, suggesting that presynaptic stores are the downstream target of 5-HT_2R in causing the mEPSCs frequency increase.

However, this frequency increase was restricted to a specific population of pyramidal cells in layer II, which were termed responders. About half of all pyramidal cells recorded from corresponded to this group (47%). When compared to cells that did not respond upon 5-HT exposure (non-responders), the former showed a larger decrease in input resistance together with (on average) a small outward current, suggesting that the action of 5-HT was not only specific to a particular type of cells, but also within the same type. It also suggests that distinct properties other than the mEPSC frequency were also subject to modulation by 5-HT.

The impact of 5-HT on evoked glutamate release was subsequently assessed in pairs of pyramidal cells obtained in the same layer. I found that, contrary to the expectation that evoked transmitter release may be increased after exposure to 5-HT, EPSCs actually depressed by 49%. Even though subtle changes in the presynaptic APs and the postsynaptic properties were observed, they were unlikely responsible for the depression observed. I discovered that the depression was also caused by 5-HT_2R activation. However, in this case, the signaling was linked to Gβγ as peptides that bind it were able to block the depression. In contrast to the depression seen with noradrenaline in the same cells, there was no increase in the recovery rate from depression during a burst of 20 APs at 50 Hz, and no decrease in the quantal size based on density estimation. These findings suggest that the target of Gβγ was unlikely SNAP-25, as with noradrenaline, but more likely the VDCC involved in transmitter release.

Given that the depression was not restricted to a subset of cells, but was seen in almost all (97%) pairs recorded from, there is potentially specificity in the connectivity and/or the modulation by 5-HT. In fact, responders were mostly identical with postsynaptic, whereas non-responders with the presynaptic pyramidal cells, further strengthening the idea that 5-HT modulates specific elements in the neocortical microcircuits.

This is the first study where, at the level of single cells, the serotonergic modulation of transmitter release together with the corresponding signalling elements have carefully been investigated in neocortical tissue. These findings may have important physiological implications for future work, and also for the application in psychopharmacology context.

2. Methods

2.1. Slicing of Rat Neocortex

Male Wistar rats, aged 15 – 19 days, were decapitated using a small animal guillotine (model 802; NEMI scientific, Medway, MA, USA) as approved by the ANU animal ethics clearances No. A2011/023 and A2014/013. The head was rapidly placed into icy slush (0°C) of artificial cerebrospinal fluid (ACSF; composition see below), which was continuously gassed with 95% O_2 and 5% CO_2 (Carbogen™; BOC Gases Australia Limited, North Ryde, NSW, Australia) to maintain a pH of 7.4. The head was then removed from the beaker, placed on blotting paper and the skin opened along the midline using a scalpel (surgical blade No. 10; Swann-Morton Limited, Sheffield, UK). Using repetitive cutting movements along the midline suture, the cranium was opened up and flipped on the side using the blade of a bent pair of anatomical forceps (4-in-full curved, serrated eye dressing forceps; Medical Supplies and Equipment Co., Katy, Texas, USA). Using the scalpel blade, two cuts of the brain tissue in the area of the olfactory bulbs and one right before the cerebellum were done to block the neocortex out. Then a cut along the midline was performed to separate the left and right hemispheres, which were immediately put into fresh ice-cold and bubbled ACSF.

Each hemisphere was then taken out of the beaker with ice-cold ACSF, the midline cut surface was blotted dry on blotting paper, transferred onto weighing spatula to be placed and glued onto a stainless-steel stage angled forward by 15° using cyanoacrylic glue (Loctite™ 406; Loctite Australia Pty. Ltd, Caringbah, NSW, Australia). After this step, leftover glue around the tissue was carefully blotted dry using the side of the blotting paper. This stage was then mounted within the cutting chamber of a vibrating microtome (Leica VT 1200S; Leica Biosystems GmbH, Nussloch, Germany), containing ice-cold ACSF that was continuously gassed with Carbogen. The cortex was set to face the cutting blade that was angled at 15° to the horizontal plane (Fig. 2.1.1). The vibration movement along the vertical axis of the blade and its holding unit was adjusted every day for every blade to be ≤ 100 nM using the Vibrocheck unit as part of the VT 1200 S.

Using a double-edge stainless steel, Teflon-coated 0.004'' thick razor blade (Personna; American Safety Razor Company, Verona, VA, USA), the height of the lateral pole of each hemisphere was determined and the vertical axis on the slicer zeroed. The blade was then retracted, then lowered by 3.5 mm to reach the starting point of slicing. The slicing process was conducted by advancing the blade at a forward sectioning speed of 0.07 mm/s and a horizontal amplitude of 1.5 mm. The tissues associated with two initial

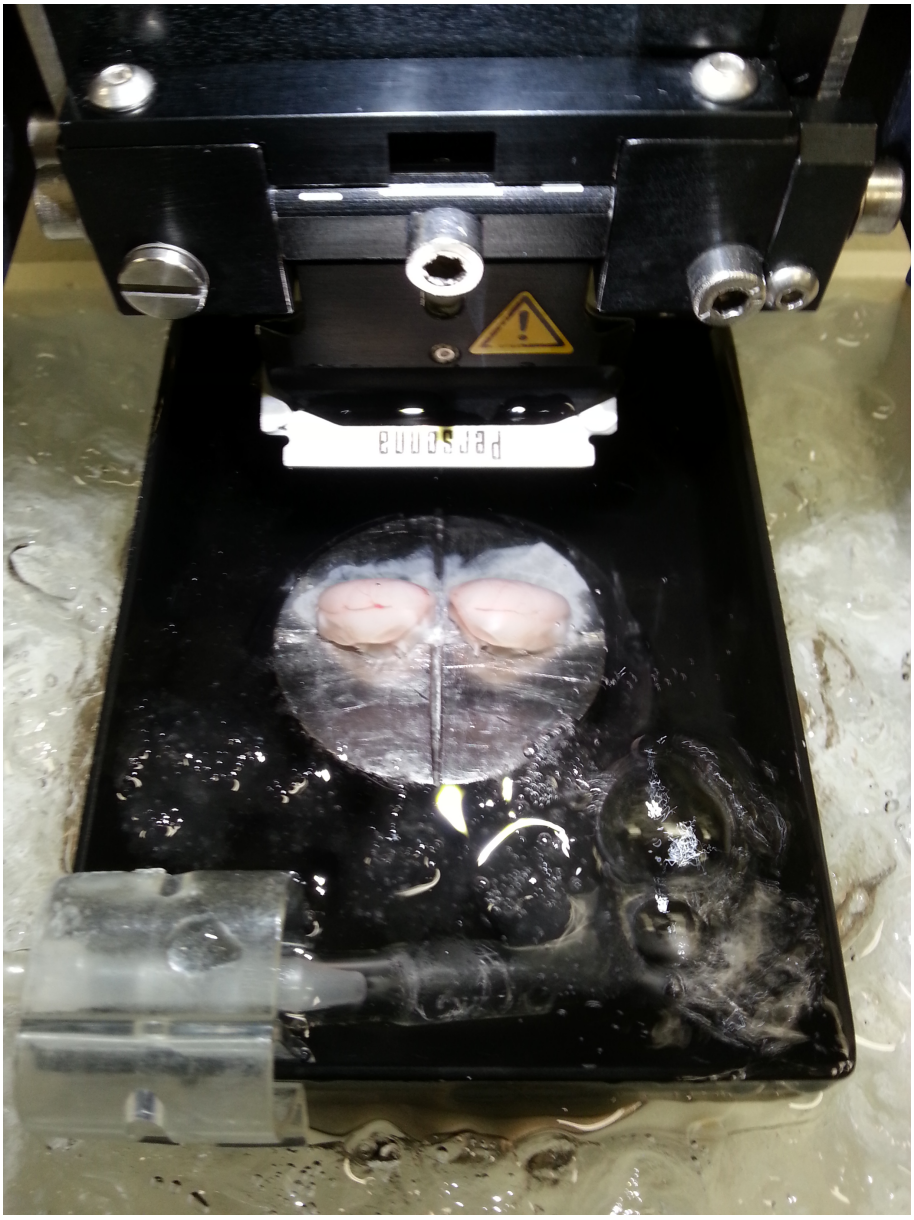

Figure 2.1.1. Mounting of hemispheres on the metal block.
Both hemispheres of rat brain were glued on a stainless-steel stage and mounted in the slicing chamber of the vibrating microtome. The slicing chamber was filled with ice-cold ACSF gassed with 95% O_2 and 5% CO_2.

parasagittal orientation cuts, *i.e*. an initial cut at 3.5 mm and another one at 3.8 mm, were discarded to expose the postero-medial lateral barrel subfield (Woolsey & Van der Loos, 1970; Elston *et al.*, 1997). Subsequently, 6 – 7 slices, each having a thickness of 300 µM, were cut, neocortex and hippocampus separated from the basal ganglia and thalamus using the shaft of a 27G fine needle, and placed in a holding chamber containing Carbogen-gassed ACSF using a transfer pipette (Fig. 2.1.2). The holding chamber was made from a platform of nylon gauze that was mounted roughly halfway up of 250 ml beaker.

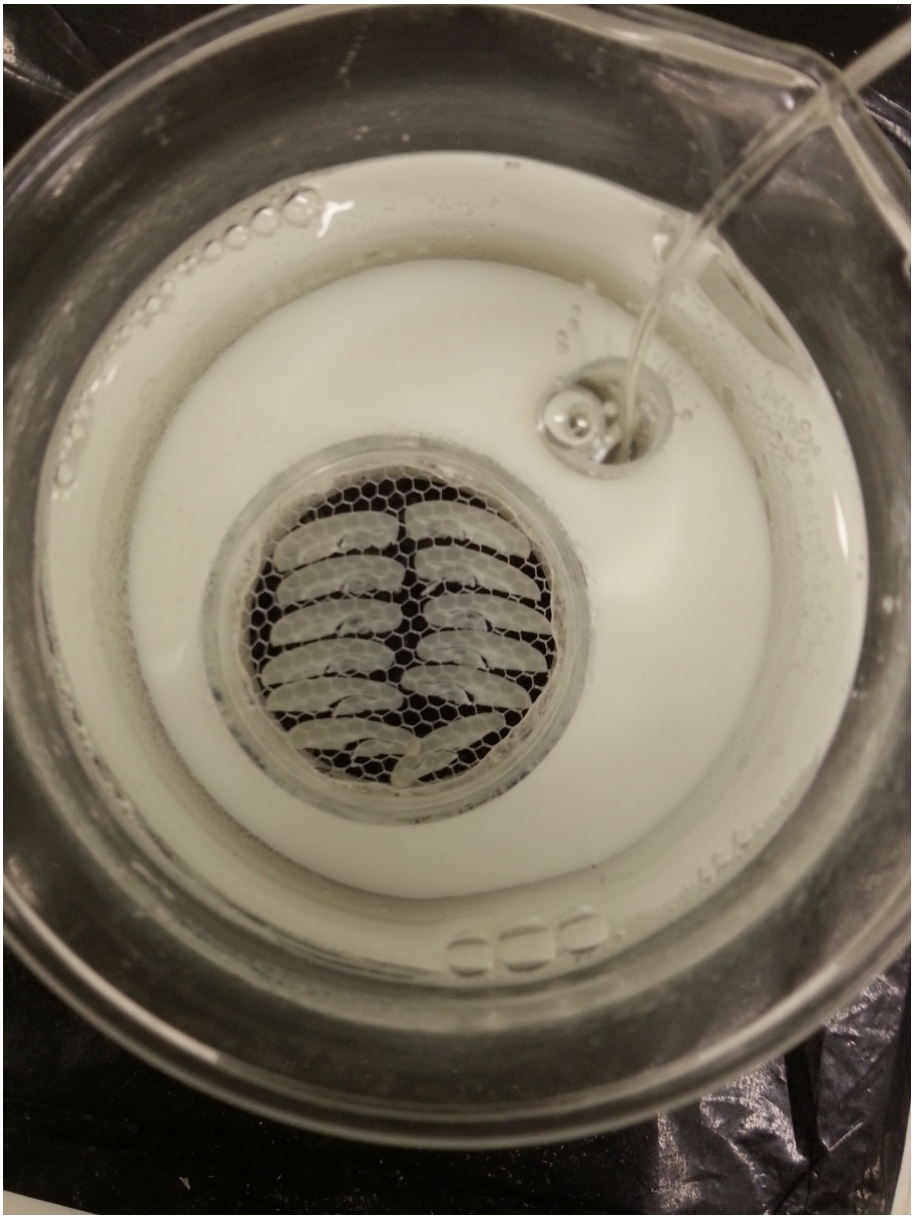

Figure 2.1.2. Layout of slices for incubation.
Parasagittal brain slices on the holding chamber. Six slices were taken from each hemisphere and arranged based on the cutting sequence from top to bottom. The tube entering the chamber provided 95% O_2 and 5% CO_2 (Carbogen^{TM}) gases for buffering while moderately circulate the ACSF.

The holding chamber containing all slices was then put into a water bath set up at 34°C for incubation for at least 30 minutes. After that, the holding chamber was removed from the water bath and subsequently maintained at room temperature until the experiment started.

2.2. Extracellular Solution

The ACSF was made up of (in mM): NaCl, 125; KCl, 2.5; $NaHCO_3$, 25: NaH_2PO_4, 1.25; $CaCl_2$, 2; $MgCl_2$, 1; glucose, 25 (experimental solution) or 10 (slicing solution); gassed with Carbogen to obtain a final pH of 7.4. The osmolality of this ACSF is typically 315 mOsm/kg H_2O. ACSF was prepared fresh daily and kept at 4°C in the refrigerator until the experiment was conducted. Small volume of slicing solution ACSF was kept separately at -20°C in the freezer to produce 12 – 14 ice cubes, which later will be blended with its liquid form to produce ice slush for brain slicing.

2.3. Intracellular Solution

Most electrophysiological recordings were performed in the whole-cell configuration using a K-gluconate-based intracellular solution. This intracellular solution contained (in mM): K-gluconate, 115; KCl, 20; HEPES, 10; phosphocreatine, 10; Mg-ATP, 4; Na-GTP, 0.3; and biocytin 5.4 (0.2% weight/volume). In some experiments, some slightly modified versions of this solution were used. These will be presented and explained in the relevant context. The intracellular solution was aliquoted and kept frozen at -20°C until the experiment was conducted.

2.4. Drugs Used and Their Preparations

All solutions containing drugs were prepared from stock freshly every day.

Tetrodotoxin (TTX; Latoxan L8503, citrate free; MW 319.20), a specific voltage-dependent Na^+ channel blocker, was routinely added to the ACSF used in all recordings of miniature release. A 1000x stock solution (1 mM) was prepared by dissolving 1 mg of TTX in 3.132 ml of 0.1 M citric acid solution, and then kept in the refrigerator. To reach a final concentration of 1 µM, 100 µl of stock solution were added to 99.9 ml of ACSF.

Gabazine (Tocris Bioscience 1262 – SR-95531 hydrobromide; MW 368.23), a specific $GABA_A$ receptor blocker, was routinely added to the ACSF in all experiments. 1000x stock solution (3 mM) was prepared by dissolving 50 mg of gabazine in 45.3 ml of Milli-Q water, and then kept in the refrigerator. To achieve a final concentration of 3 µM, 100 µl of stock solution were added to 99.9 ml of ACSF.

Serotonin (5-HT; Sigma-Aldrich H7752 – creatinine sulphate complex; MW 387.41) was prepared into aliquots of 10 mM stock solution by dissolving 19.37 mg of 5-HT in 5 ml of

0.1 M HCl solution. This stock solution was kept in the -20°C freezer for a maximum time of one month before usage (at -20°C, 5-HT degrades through oxidation at a rate of 3.33 mM per year as shown by ^{1}H NMR; recordings were performed by Dr Laura de la Cruz at the Australian National University Research School of Chemistry). To achieve a final concentration of 10 µM, 100 µl of stock solution were added to 99.9 ml of ACSF. The ACSF containing 5-HT was prepared fresh daily in order to prevent oxidation over time.

α-Methyl-5-HT (Tocris Bioscience 0557 – maleate; MW 310.82), a pan-5-HT$_2$R agonist, was prepared into aliquots of 2 mM stock solution by dissolving 6.22 mg of α-methyl-5-hydroxytryptamine in 10 ml of Milli-Q water. This stock solution was kept in the -20°C freezer for a maximum time of one month before usage. To achieve a final concentration of 20 µM, 1 ml of stock solution was added to 99 ml of ACSF. This experimental solution was prepared fresh daily in order to prevent oxidation of α-methyl-5-HT over time.

Dimethoxybromoamphetamine (DOB; Tocris Bioscience 2863 – hydrochloride; MW 310.62), a selective 5-HT$_2$ receptor agonist, was used under Prohibited Substance Research & Education Program License no. 0020/11 granted by the Government of the Australian Capital Territory. Aliquots of 100 µM stock solution were prepared by dissolving 0.62 mg of DOB in 20 ml of Milli-Q water. The stock solution was kept in the -20°C freezer before usage. Two different concentrations were used in experiments. One concentration was 1 µM, which was achieved by adding 1 ml of stock solution to 99 ml of ACSF. The other concentration was 100 nM, which was achieved by adding 100 µl of stock solution to 99.9 ml of ACSF.

(S)-WAY 100135 (Tocris Bioscience 1253 – dihydrochloride; MW 477.48), a selective 5-HT$_{1A}$ receptor antagonist, was prepared into aliquots of 1 mM stock solution by dissolving 4.78 mg of (S)-WAY 100135 in 10 ml of Milli-Q water. Stock solution was kept in -20°C freezer before further usage. A final concentration of 100 nM was achieved by adding 10 µl of stock solution to 99.99 ml of ACSF.

4F 4PP (Santa Cruz Biotechnology sc-203782 – oxalate; MW 429.49), a selective 5-HT$_{2A}$ receptor antagonist, was prepared into aliquots of 200 µM stock solution by dissolving 0.86 mg of 4F 4PP in 10 ml of dimethyl sulfoxide (DMSO). Stock solution was kept in -20°C freezer before further usage. To achieve a final concentration of 200 nM, 100 µl of stock solution were added to 99.9 ml of ACSF.

RS 102221 (Tocris Bioscience 1050 – hydrochloride; MW 667.1), a selective 5-HT$_{2C}$ receptor antagonist, was prepared into aliquots of 100 µM stock solution by dissolving 0.71 mg of RS 102221 in 10 ml of DMSO. Stock solution was kept in -20°C freezer before

further usage. To achieve a final concentration of 100 nM, 100 µl of stock solution were added to 99.9 ml of ACSF.

Gö 6983 (Selleck Chemicals S2911; MW 442.51), a pan-PKC inhibitor, was prepared into aliquots of 100 µm stock solution by dissolving 0.49 mg of Gö 6983 in 11.073 ml of DMSO. Stock solution was kept in -20°C freezer before further usage. The final experimental concentration was 100 nM. This concentration was achieved by adding 100 µl of stock solution to 99.9 ml of ACSF.

Edelfosine (Tocris Bioscience 3022; MW 523.73), a phospholipase C (PLC) inhibitor, was prepared into aliquots of 3 mM stock solution by dissolving 10 mg of edelfosine in 6.3647 ml of Milli-Q water. The stock solution was kept in -20°C freezer until experimental usage. To get a final concentration of 30 µM, 1 ml of stock solution was added to 99 ml of ACSF.

2-Aminoethoxydiphenylborate (2-APB; Merck Millipore 100065; MW 225.10), an inhibitor of IP_3-induced Ca^{2+} release, was prepared into aliquots of 16 mM stock solution by dissolving 36.02 mg of 2-APB in 10 ml of DMSO. The stock solution was kept in -20°C freezer until experimental usage. To get a final concentration of 16 µM, 100 µl of stock solution were added to 99.9 ml of ACSF.

1,2-Bis(*o*-aminophenoxy)ethane-*N*,*N*,*N*′,*N*′-tetraacetic acid tetrakis(acetoxymethyl ester) (Tocris Bioscience 2787 – BAPTA-AM; MW 764.68), a cell permeable Ca^{2+} chelator, was prepared into stock solution by dissolving 25 mg of BAPTA-AM in 0.981 ml of DMSO, then kept in -20 ºC freezer. For experimental usage, 150 µl of stock solution were added to 850 µl of Milli-Q to acquire 1 ml of 5 mM BAPTA-AM solution, which was subsequently diluted 100 x with 99 ml of ACSF to achieve a final experimental concentration of 50 µM.

Cyclodextrin (Fluka chemical 56332 – 2-hydroxypropyl-β-cyclodextrin; MW = ~1380), a stabilizer of the AM moiety in ACSF, was prepared into aliquots of 70 mM stock solution by dissolving 966 mg of 2-hydroxypropyl-β-cyclodextrin in 10 ml of Milli-Q water. Stock solution was kept in the -20°C freezer before further usage. To achieve a final concentration of 0.7 mM, 1 ml of stock solution was added to 99 ml of ACSF.

Probenecid (Sigma-Aldrich P-8761; MW = 285.36), a facilitator for BAPTA accumulation in the cytoplasm, was prepared into aliquots of 50 mM stock solution by dissolving 142.68 mg of probenecid in 10 ml of 1 M NaOH solution. The stock solution was kept in -20°C freezer until experimental usage. A final concentration of 0.5 mM was achieved by adding 1 ml of stock solution to 99 ml of ACSF.

mSIRK (Merck Millipore 371818; MW 1948.3), a Gβγ-protein selective binding peptide, was used as a solute in the intracellular solution. To achieve a final concentration of 100 µM, 5 mg of mSIRK was firstly dissolved in 103 µl of DMSO then added to 20.497 ml of intracellular solution (described above) to make a total volume of 20.6 ml. This 100 µM mSIRK intracellular solution in 0.5% DMSO was kept in -20°C freezer before further usage. Before recordings were performed, the solution was thawed, mixed with vortex, and sonicated for a minute to give uniform concentration.

2.5. Optical Set-Up (IR-DIC)

Cells were visualized using infrared-differential interference contrast (IR-DIC) optics (Stuart *et al.*, 1993) implemented on a standard Olympus BX51WI (Olympus, Shinjuku, Tokyo, Japan) microscope. The infrared filter used is optimized for transmission at 775 nm and longer. The condenser of this microscope was aligned and optimized to follow Köhler illumination. For imaging, all apertures were fully open. The DIC phase contrast on the microscope was set by a half-plate at the bottom of the condenser such that the neurons were displayed with positive phase; *i.e*. the shape of the somata appeared as convex bodies. The infrared image was displayed on a high-resolution black-and-white video monitor (PVM-145E, Sony, Tokyo, Japan) after being acquired via a camera (VX45; Optronics GmbH, Kehl, Germany) with sensitivity in the IR range, where gain and offset were set on the respective camera controller unit to ~85% and ~50% of full range, respectively.

2.6. Patch Pipettes

Patch electrodes for whole-cell recordings were pulled from borosilicate glass (outer diameter 2 mm, inner diameter 1 mm, length 75 mm; Hilgenberg, Malsfeld, Germany, Art-No. 1807502) using a P-97 type Brown-Flaming-type horizontal puller (Sutter Instruments Co., Novato, CA, USA) using a 3 mm square box platinum filament. The choice of electrode glass rested upon its high dielectric constant compared to similar glasses and wall thickness.

The puller was set up to produce glass electrodes with tip resistances in the range of 3 – 5 MΩ when filled with intracellular solution. This corresponds roughly to an outside tip diameter of 2 – 3 µm as judged on the monitor in DIC. Patch electrodes were produced by utilising a pulling procedure in five steps as described below (table 2.6.1). Electrodes were neither “sylgaarded” nor fire-polished. Typical RAMP values (time at which the

glass reaches a minimum fluidity while stepping up values at 10 units/sec from zero; this value is “typical” for each filament.) of this electrode glass were between 590 – 640.

Table 2.6.1. Program used to pull glass electrode for whole-cell recording.

Whole-cell electrode program (relative to RAMP)				
Step No.	**Heat**	**Pull**	**Velocity**	**Time**
1	Ramp + 10	20	30	180
2	Ramp - 10	15	20	200
3	Ramp - 30	15	20	200
4	Ramp - 60	15	20	200
5	Ramp - 100	10	25	200

Program values used on P-97 Brown-Flaming-type horizontal puller. Values are in arbitrary units set by Sutter. The air pressure was set to 500 units. The air duration at the beginning and end were set to 500 units as well. Electrodes were pulled at a minimum interval of 5 minutes between pulls to minimise the impact of heating up on the electrode tip.

2.7. Recording Setup

The recording chamber was designed by Dr. Christian Stricker and made in the local workshop from Perspex™. It has a circular surface, with two small inlets at its edge for ACSF superfusion pathway, and a rectangular opening at the middle for placing the brain slice (see Fig. 2.7.1). A Mediglass coverslip (24 × 50 mm) was glued to its bottom with a silastic compound (732 RTV Sealant; Dow Corning, Midland, MI, USA) to form a thin base of recording chamber and let light pass through from the bottom.

All the electrophysiological recordings were performed at 36 ± 1°C unless stated otherwise. To maintain this temperature, ACSF was heated before being supplied to the recording chamber using a water jacket around the inflow pipe fed by an external water heater pump (GD 120; Grant Instruments Ltd, Shepreth, Cambridgeshire, UK), which was set to 42 – 44°C. The temperature within the central part of the chamber was measured before each experiment, using a thermistor connected to a multimeter (DMT 1040; Monacor UK Ltd, Buckinghamshire, UK), to make sure that the recording condition was as specified. Otherwise, the temperature in the water jacket was adjusted.

The flow rate of the ACSF was maintained at 3 – 4 ml per min by setting the drip rate to 1-1.2 Hz with an adjustable clamp attached to the initial part of the inflow tube.

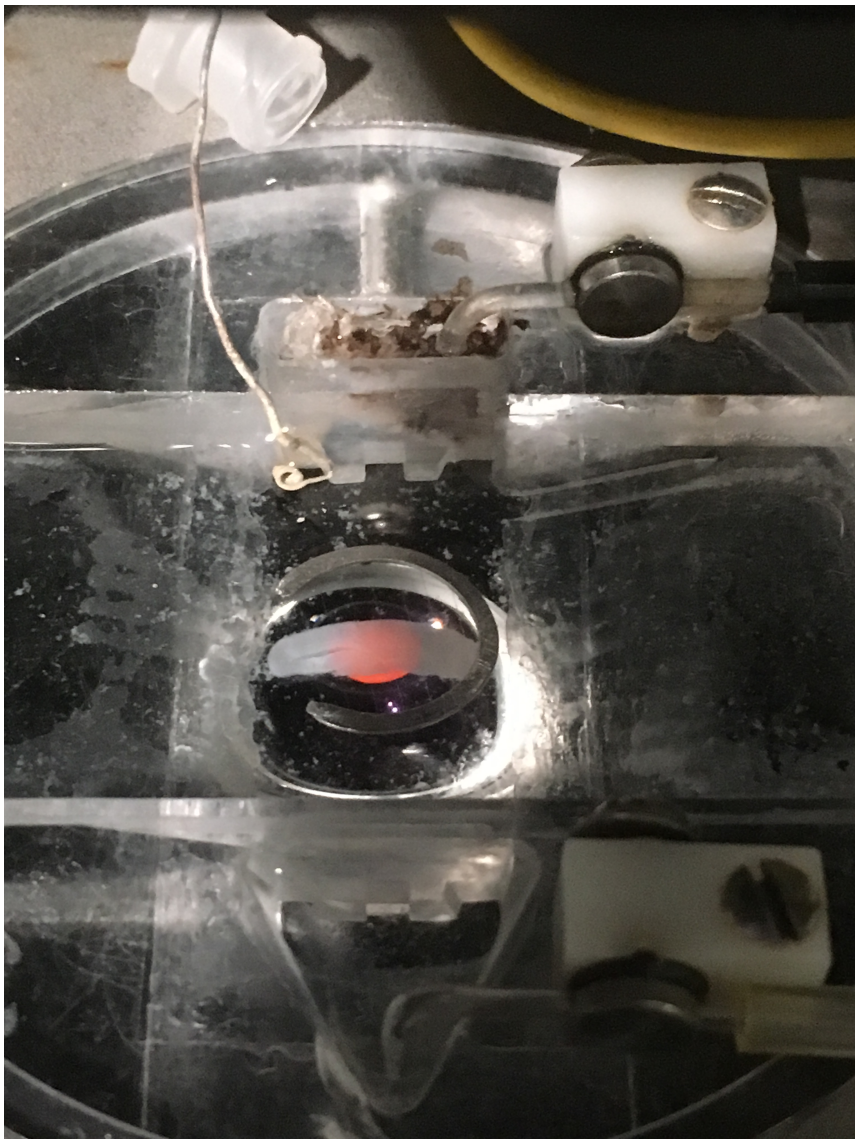

Figure 2.7.3. Position of slices in the recording chamber.
A parasagittal brain slice in the middle compartment of the recording chamber, A harp, made of platinum frame and dental floss, is placed on the slice to prevent any movement due to ACSF flow.

Mechanical disturbances caused by air bubbles emanating from the water jacket were minimised by placing a small roll of nylon gauze at the inflow compartment of the chamber, which was directly in contact with the fluid in the inflow tube. The ACSF entered the recording chamber via the inflow compartment, superfused the brain slice at the centre in a rectangular compartment (see Fig. 2.7.1), and was sucked off in the outflow compartment. The slope of it was angled at ~30° to facilitate the control of the fluid level in the chamber. Continuous outflow was maintained by suction on the angled surface via a fine-tipped, fire-polished glass pipette connected to a Tygon™ (R-3603; Cole-Parmer

Australia New Zealand, Chatswood, NSW, Australia) line attached to the waste reservoirs exposed to a vacuum pump.

The slice containing the barrel cortex was held in place on the bottom of the recording chamber by a platinum ring strung with three threads of silk on top of it. Individual silk threads were untwisted from dental floss (Top Care unwaxed-unflavored dental floss; Topco Associates LLC, Elk Grove Village, IL, USA) and glued at an interval of ~3 mm each using cyanoacrylic glue (Loctite™ 406; Loctite Australia Pty. Ltd, Caringbah, NSW, Australia).

Using the Olympus BX51WI microscope with the 5 times magnifications lens (Olympus MPlan 5x; Olympus, Shinjuku, Tokyo, Japan), layer II of the barrel cortex in the slice was firstly identified. The criteria used are the following: 1) An area of slice that was located roughly above the hippocampus and extending towards the rostral part of the brain. 2) A layer of cells, which was located directly above the thick dark band making up the barrel-like structures (layer IV). And 3) the outermost layer of neocortex with high cell density (adjoining to layer I). In order to choose a target pyramidal neuron, the upper layer II was scanned for small “clumps” of 3 – 6 cells in roughly the same optical plane which were located near the boundary to layer I. Pyramidal cells had a pyramidal-like shape cell body and an apical dendrite that runs towards the layer I in a slightly oblique direction before forming apical tufts. The data set in here did neither contain multipolar nor other interneuron cell types (see *post-hoc* histological verification below).

Two headstages connected to a MultiClamp 700A amplifier (Axon instruments, Molecular Devices, Sunnyvale, CA, USA) were each mounted on MP-225 manipulators (Sutter Instruments, Novato, CA, USA) at an angle of 27° from the horizontal plane. The manipulators were driven with step length size of zero for coarse (visual inspection before making a choice for a cell to be recorded from) and five for fine movement (patching).

2.8. Whole-Cell Recordings

Whole-cell recordings were obtained in the following way. The glass electrode was filled with intracellular solution at its tip, attached to the headstage, and exposed to a constant positive pressure (~3.5 kPa) through a small diameter plastic hose connected to 25 ml syringe and manometer (DM20; Sentinel Systems Gas Detectors, Sorrento, WA, Australia). Under the 40 times magnification lens (Olympus LumPlanFLN 40x; Olympus, Shinjuku, Tokyo, Japan), the tip of the patch electrode was brought down close to the surface of the slice in the ACSF using the micromanipulator. At that stage, the pipette

offset potential was set to zero. Throughout establishing a whole-cell configuration, the electrode tip resistance was gauged by applying a brief 10 mV command potential.

After touching the surface of the slice with the electrode, the tip was lowered down to about the same plane as that of the targeted soma but at a lateral distance of ~40 μM from it. The positive pressure caused a stream of intracellular solution to flow out of the electrode tip, preventing soiling and accumulation of tissue debris at the tip of electrode during the movement within the tissue (Edwards *et al.*, 1989). As the intracellular solution was high in K^+ concentration and, therefore, depolarized cell, the approach towards the target cell was done swiftly. For one last time, the pipette offset was compensated and a negative pressure around -1.5 kPa was pre-set before the pressure valve (type 74.001, Kuhnke, Malente, Germany). In close succession, the electrode tip was quickly horizontally advanced towards the targeted cell. If sufficiently close, a “halo” formed between the electrode tip and the cell surface. At this stage, the pressure valve was flipped to apply the negative pre-set pressure to the electrode. As the result, the cell membrane sealed to the electrode tip more or less immediately. To help the formation of a GΩ seal, the electrode holding potential was hyperpolarized to -70 mV.

When the holding current amplitude reached a value close to 0 pA, indicating a seal resistance in the range of 1 – 2 GΩ, three brief suctions by mouth were applied (around -3, -6, and -9 kPa) to break the membrane inside the electrode tip. The subsequent small opening provided the electrical access to the intracellular compartment in the whole-cell configuration.

2.9. Measurement of Series and Input Resistances

One criterion for the quality of the whole-cell recording in voltage-clamp is that the series resistance (R_s) at the electrode tip should not exceed 20 MΩ (≤ 10% of the value of the input resistance of the cell; see part 3) and does not appreciably change during the duration of the recording (maximum change allowed is ≤ 20% of its initial value). Therefore, R_s was monitored in voltage-clamp at the beginning, in between sequences, and at the end of each recording using a small depolarizing voltage step (V_s) of 0.5 mV for 40 ms. To the decaying phase of the resulting current response, a double exponential transient was fit and extrapolated to the time of onset of the voltage step to obtain the peak amplitude of the capacitive transient without significant contamination by the electrode capacitance. In other words, R_s was estimated from the estimated peak amplitude of the capacitive current transient (I_c) at the onset of the voltage step (t = 0,

when the current is primarily charging the capacitance of the cell, limited by R_s itself) by using the following equation $R_s = V_s / I_c$.

For recordings in current-clamp, the quality was gauged by compensating the bridge circuit using the procedure available in the MultiClamp commander. In this recording configuration, an uncompensated R_s causes a voltage step caused by the current flowing across the uncompensated tip resistor, which can be seen as a voltage-jump at the start or turn-off of the current step.

To assess the quality of recording throughout an entire experiment, monitoring of the input resistance (R_{in}) is also necessary. This was performed in voltage-clamp at a holding potential of -70 mV by using the same V_s of +0.5 mV for 40 ms. The resulting steady state current change at the end of 40 ms served to estimate total resistance (R_{tot}), and R_{in} was calculated as the difference between the R_{tot} and the R_s ($R_{in} = R_{tot} - R_s$). For a recording to be considered sufficiently stable, the R_{in} might only change by ≤ 25 MΩ (13% from pooled average; see part 3) from its initial value. There was no restriction set for pharmacologically induced changes in the R_{in} because it represented physiological changes through opening or closing of certain ion channels.

2.10. Data Acquisition

All data was acquired from layer II pyramidal cells of rat S1 barrel cortex patched in whole-cell configuration, with a sampling frequency of 5 kHz (equals to a sampling interval of 0.2 ms).

Miniature excitatory postsynaptic currents (mEPSCs) were measured in continuous voltage-clamp recordings, with holding potential being set to -70 mV in the MultiClamp commander on a G5 PowerPC (Apple Inc., Cupertino, CA, USA) running OS X 10.4. The typical configuration of the MultiClamp Commander was as follows: 1) output gain was set to 1, 2) the feedback resistor (R_f) to 500 MΩ, 3) the 8-pole built-in Bessel filter to low pass 10 kHz, and 4) the current selection to direct current (DC). Recorded currents or voltages from cells were initially analogue-filtered by a sample-and-hold unit that contained a built-in 10-pole Bessel filter (custom made at JCSMR, ANU, Canberra, Australia). For mEPSC and evoked EPSC, the low-pass cut-off frequency chosen on this unit was typically 1 kHz, whereas for AP it was 10 kHz. The signals were then further amplified, typically by 200 times after removing the respective offset using the sample-and-hold unit. Using an ITC-18 analogue-to digital converter board (Instrutech Corporation, Port Washington, NY, USA), the signals were then converted into a digital

format, which were then stored on the hard disk of the computer using procedures written in IGOR Pro (written by Drs Christian Stricker and Anna Cowan).

During recordings from synaptically connected pyramidal pairs, the presynaptic cell was typically kept in current-clamp, whilst the postsynaptic cell was in voltage-clamp at a holding potential of -70 mV. EPSCs in the postsynaptic cell were evoked every 5 s (0.2 Hz) by injecting a current step into the presynaptic neuron which elicited an AP. Timings were controlled by Master-8 timer (A.M.P.I, Jerusalem, Israel).

2.11. Analysis

Analysis for the modulation of spontaneous release (mEPSC) was performed using Axograph X and custom-built program in IGOR pro version 6, whilst for the modulation of evoked release (EPSC) was performed using only custom-built program in IGOR pro version 6 (WaveMetrics Inc., Portland, OR, USA). Detailed analysis methods will be explained further in the later chapters of 3.3.2 – 3 for mEPSC analysis, and 4.3.4 – 6 for EPSC analysis in pyramidal pairs.

2.12. Junction Potential and Correction

The liquid junction potential was estimated using the equations provided by Barry (1994). Since all experiments were performed at 36 ± 1°C, the value was calculated to be 13.0 mV. The membrane potential values (V_m) were not corrected for the liquid junction potential throughout this thesis.

2.13. Histological Processing of Slices

Neurons were filled with 0.2% biocytin (weight/volume; Toronto Research Chemicals Inc., Toronto, ON, Canada) via the patch solution during recording. After recording, the brain slice containing the recorded neurons was fixed in 4% paraformaldehyde dissolved in 0.1 M phosphate buffer solution (200 mM Na_2HPO_4 and 200 mM NaH_2PO_4 were mixed with certain volume ratio to achieve pH 7.4, and then diluted 1:1 with Milli-Q water), lightly shaken for 30 minutes on a compact rocker (CR300; FINEPCR, Gunpo, Gyeonggi, Korea), and later stored in the refrigerator until further processing. Best results were obtained when processing was done within a week's time; however, in some instances, the time of storage was up to a month.

For histological processing, the slices were firstly washed off the paraformaldehyde solution with 0.1 M phosphate buffer solution several times. Unspecific peroxidases were blocked with hydrogen peroxide (Chem-Supply, Gillman, SA, Australia). They were then incubated in Trizma® solution (pH 7.4, Sigma-Aldrich, Castle-Hill, NSW, Australia) containing 10% volume/volume normal swine serum (Vector Laboratories Inc., Burlingame, CA, USA) in 0.5% v/v *t*-octylhenoxypolyethoxyethanol (triton X-100™; Sigma-Aldrich, Castle-Hill, NSW, Australia) to permeabilise the cell membranes for about 30 minutes. Subsequently, they were incubated in Trizma® + 0.5% v/v triton X-100™ solution containing avidin and biotin-conjugated horseradish peroxidase (Vectastain® ABC Kit; Vector Laboratories Inc., Burlingame, CA, USA) for an hour at room temperature and then stored overnight for at least 12 hours at 2°C in the refrigerator.

The following day, the slices were washed with Trizma® solution and reacted for an hour with 0.1% catechol, 0.05% phenylenediamine, 0.4% di-ammonium-nickel-sulphate-6-hydrate, and 0.6% cobaltous chloride (Sigma Aldrich, Castle-Hill, NSW, Australia) to build-up the redox environment for the next step. One or two drops of 30% hydrogen peroxide were then added to start the chemical redox reaction until staining reached desired level (blackening). The reaction was stopped by repeatedly (at least two times) washing with phosphate buffer solution.

The slices were mounted on glass slides (76.2 × 25.4 mm; Livingstone International Pty Ltd., NSW, Australia), embedded in a watery embedding medium (0.1% Moviol®; Sigma-Aldrich, Castle-Hill, NSW, Australia), covered by coverslips (24 × 24 × 0.15 mm; Knittel Gläser, Braunschweig, Germany) and sealed with nail varnish. Subsequent storage was in the refrigerator.

2.14. Morphological Identification of Cell Types

Cells very firstly identified using a standard laboratory microscope. The cells “filled with” metal precipitates (black) were then imaged on a Zeiss Axioskop 2FS MOT (Carl Zeiss Light Microscope, Göttingen, Germany) at 20x magnification using a Retiga 2000R camera (QImaging, Surrey, BC, Canada) and Neurolucida version 10 (MBF Bioscience, Williston, VT, USA) image acquisition software.

Excitatory pyramidal cells in layer II were identified according to the following criteria: pyramidal or close to cell body shape of about 10 – 25 µm diameter; prominent apical dendrite which elongates via apical tufts to the pial surface in layer I; spiny apical tufts; skirt of basal dendrites; thin axon (if visible) projecting to deeper layers. Cells that did not conform to these criteria were identified as interneurons. Note that my data set might

contain a few layer III pyramidal cells as in some instances, the boundaries were not clear.

Such a layer II pyramidal cell is shown in figure 2.14.1. This cell is identified as originating in layer II because the cell body is located around 215 µm from pia. The shape of the cell body resembles a pyramid, with a diameter of ~15 µm. The apical dendrite is slightly oblique, but elongates to the pial surface, via some spiny apical tufts in layer I. Basal dendrites are distributed more or less symmetrically around the cell body. The axon extends vertically towards deeper layer IV/V.

Most of the layer II pyramidal cells in my data set had apical dendrites at slightly oblique angle to the pia (~20° from vertical). Few cells showed a ~45° obliqueness, but none of the cell showed horizontal or even inverted apical dendrites as described by van Brederode *et al.* (2000).

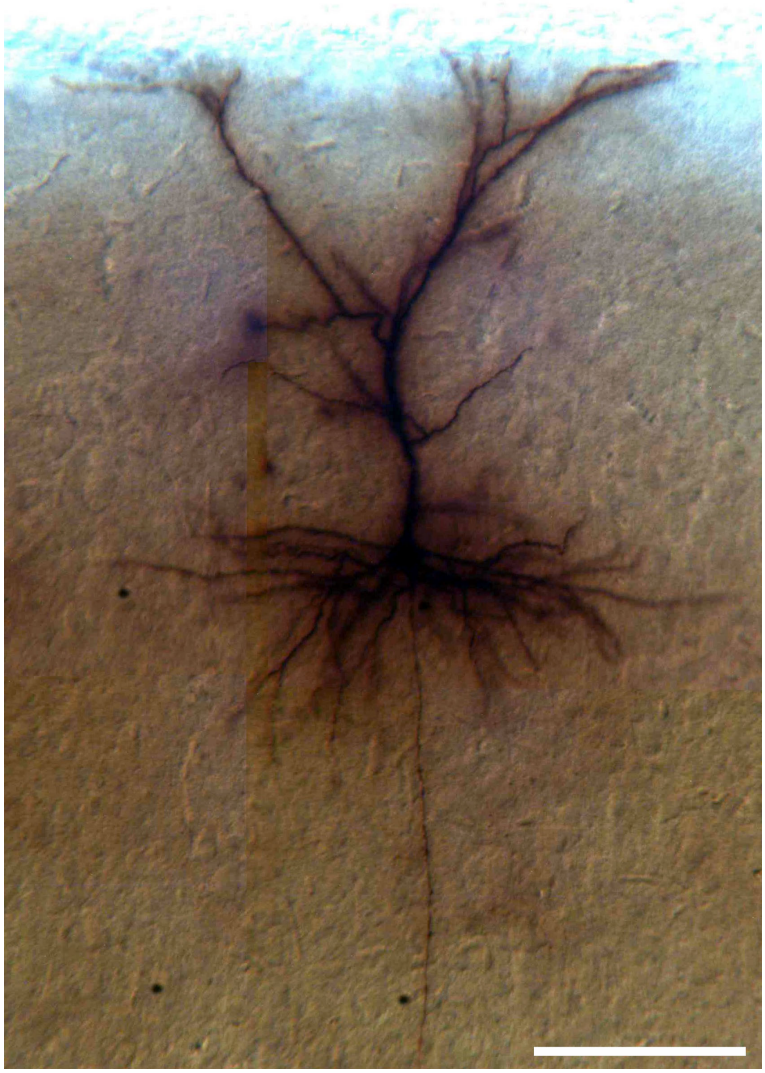

Figure 2.14.1. Morphology of histologically verified layer II pyramidal cell.
A layer II pyramidal cell after *post-hoc* histological processing, showing a pyramidal shaped cell body, apical dendrite and tufts, few oblique, basal dendrites, and thin axon. White scale bar indicates a length of 100 µM.

3. Modulation of Spontaneous Release

3.1. Introduction

In previous research in this laboratory, it was found that both group I metabotropic glutamate receptors (mGluR; Simkus & Stricker, 2002a) and noradrenaline (NA) via α_1-AR (Choy *et al.*, 2017a) were capable of causing Ca^{2+} release from presynaptic stores, which resulted in an increase of mEPSC frequency in layer II pyramidal cells of rat barrel cortex. The common feature of both responses is that in each case, the G-protein-coupled receptor (GPCR) was linked to $G_{q/11}$ (Sternweis & Smrcka, 1992; Exton, 1994).

In the case of NA, it was found that the respective signalling was via PLCβ, as blocking this enzyme with edelfosine prevented the increase in mEPSC frequency. The classical tenet of the associated signalling cascade states that activation of PLCβ results in the hydrolysis of PIP_2 into IP_3 and DAG (Thompson & Dawson, 1964; Gonzales & Crews, 1985; Litosch, 1987; Taylor *et al.*, 1991). Whilst there was no significant evidence for the action of DAG on the mEPSCs recorded, experimental data solidly showed that the signalling molecule IP_3 bound to IP_3 receptors (IP_3R) on stores, which then caused Ca^{2+} release that increased the mEPSC frequency.

This study extends this research effort to 5-HT_2R, as this group of receptors also utilises $G_{q/11}$ as the respective adaptor protein (Baxter *et al.*, 1995; Barnes & Sharp, 1999). The anticipation was that like with NA, the addition of 5-HT to the superfusate would also increase the mEPSC frequency due to the activation of IP_3R on Ca^{2+} stores. In keeping with the previous studies mentioned above, all experiments were performed in the same pyramidal cells in layer II of the rat S1 barrel cortex. Serotonergic nerve terminals from the raphe nuclei are present in this location and layer of cortex (Steinbusch, 1981; Kosofsky & Molliver, 1987; Törk, 1990; Vertes *et al.*, 1999), and 5-HT_2R are also well expressed (Li *et al.*, 2004). Because 5-HT regulates rhythmic whisking (Hattox *et al.*, 2003), such an investigation has likely physiological relevance at least for rodents.

In this context, past studies (Aghajanian & Marek, 1997; Marek & Aghajanian, 1998; Aghajanian & Marek, 1999; Marek & Aghajanian, 1999; Zhou & Hablitz, 1999; Lambe *et al.*, 2000) have provided evidence that 5-HT modulates spontaneous glutamate release in rat prefrontal cortex (PFC). These authors observed that 5-HT in the absence of Na^+ channel blocker TTX significantly increased both the frequency and amplitude of spontaneous excitatory postsynaptic currents (sEPSCs, in contrast to mEPSCs) in layer V pyramidal cells via the activation of 5-HT_{2A}R.

These authors also surmised that the increased sEPSC frequency was the result of enhanced glutamate release from axonal terminals that most likely originated from the midline and intralaminar nuclei of thalamus (Berendse & Groenewegen, 1991; Lambe *et al.*, 2000) and projected to the apical dendrites of layer 5 pyramidal cells. Beique *et al.* (2007), however, argued that the sEPSC frequency increase occurred because a sub-population of PFC pyramidal cells underwent strong excitation after 5-HT_{2A}R activation. In both cases, the authors put the 5-HT_{2A}R at the core of their explanations. However, in none of these studies, the downstream targets of the respective signalling cascade were identified.

Because 5-HT_{2A}R are expressed widely throughout layer II, III, V, and VI of neocortex (Jakab & Goldman-Rakic, 1998), Lambe *et al.* (2000) investigated the serotonergic modulation in different layers of PFC. They found that whilst 87% of layer V pyramidal cells showed a significant increase in sEPSC frequency when 5-HT was applied, in layer II, this increase was restricted to only 25% of pyramidal cells. This finding strongly suggests that there is a difference in regard to the response in at least two sub-populations of pyramidal cells. However, these authors did not provide any further data pertaining to the differential make-up of these two populations. Likewise, Zhou and Hablitz (1999) studied the modulation of both sEPSCs and mEPSCs in frontal and anterior cingulate cortex, broadly including pyramidal neurons from layer II to VI. However, they only presented data in a pooled manner without differentiating between different layers. Consequently, their data was similar to that by Aghajanian and Marek (1997). Some other studies in different regions of neocortex, such as layer II of somatosensory (S1) cortex (Foehring *et al.*, 2002; Torres-Escalante *et al.*, 2004), focused on sIPSCs or evoked transmitter release.

Because most studies just highlighted were done outside of the somatosensory cortex, the question arouse if in barrel cortex the response to 5-HT was qualitatively similar. In addition, the nature of the 5-HTR involved needs characterising together with the downstream targets of this signalling cascade. The findings will be contrasted to those obtained with NA.

3.2. Specific Hypotheses

In analogy to the observations made for NA, I propose to test the following hypotheses for the serotonergic modulation of spontaneous neurotransmitter (glutamate) release in layer II of rat barrel cortex:

1) Serotonin (5-HT) increases the frequency of spontaneous glutamate release, which can be observed as increase in instantaneous mEPSC frequency, but not amplitude.
2) The frequency increase is only observed in a subset of pyramidal cells (responders).
3) This increase is caused by activation of presynaptic 5-$HT_{2A/C}$R coupled to the G_q-protein.
4) Activated 5-$HT_{2A/C}$R produce IP_3 to cause Ca^{2+} release from presynaptic stores, which is observed as an increase in the frequency of mEPSCs.

In this part of my thesis, I characterised some of those missing points mentioned above by concentrating on the serotonergic modulation of spontaneous glutamate release onto pyramidal cells in layer II of young (P15 – 20) rats. I present the data obtained in five sections. First, I characterized their postsynaptic membrane properties like R_{in}, passive membrane, and action potential properties together with the characteristics of sEPSCs and mEPSCs without exposure to 5-HT (3.4.1). I found that the pyramidal cells in this layer had properties indistinguishable from those found in an earlier study (Choy *et al.*, 2017a). Second, I then exposed these cells to 5-HT and observed how this neuromodulator impacted on the parameters just mentioned and specifically on the mEPSCs (and also sEPSCs; 3.4.2). I report that in about 47% of cells recorded from, I saw a transient increase in mEPSC frequency, but not amplitude. Third, based on their responses to 5-HT, I was able to differentiate two populations of pyramidal cells in this layer, subsequently referred to as responders and non-responders (3.4.3). Responders showed a large decrease in R_{in}, whereas non-responders a large hyperpolarizing current. Fourth, using both agonists and antagonists, I determined the subtype of 5-HTR involved in modulating the mEPSC frequency (3.4.4), and identified that, most likely it is 5-HT_{2C}R. Fifth, I then punctually verified the signalling pathway downstream of 5-HT_2R causing the observed transient increase in mEPSC frequency. As predicted for a G_q-mediated signalling cascade and consistent with the hypothesis above, the activation of intracellular Ca^{2+} stores was responsible for the increase in mEPSC frequency (3.4.5).

3.3. Methods and Analyses

3.3.1. mEPSC Recordings

mEPSCs are spontaneously occurring inward currents recorded from the postsynaptic cell in the presence of 1 µM TTX (Na^+ channel blocker) and 3 µM gabazine ($GABA_A$ channel blocker). Each mEPSC originates from the spontaneous release of a glutamate-containing vesicle from the bouton or nerve terminal of the presynaptic cell (Katz & Miledi, 1963).

In the experiments in this thesis, mEPSCs were recorded from pyramidal cells in the upper part of layer II of barrel cortex, which received spontaneous intercortical inputs from many other pyramidal cells (Kisvarday *et al.*, 1986; Elhanany & White, 1990). Once a pyramidal cell was patched in the whole-cell configuration, mEPSCs were recorded in voltage-clamp mode using a continuous recording protocol, with the holding potential set to -70 mV. During the first five minutes of recording in standard ACSF, the stability of the patch and its seal around the electrode and cell were assessed using criteria as follows: 1) series resistance (R_s) remained ≤ 20 MΩ, 2) R_s did not change by more than ± 20% throughout the recording, 3) input resistance (R_{in}) did not change by more than ± 25 MΩ (corresponding to ± 13% of the pooled average as shown later in 3.4.1), and 4) the properties of spontaneous currents including the instantaneous frequencies, amplitudes, and time courses did not change by > 10% over a period of five minutes.

Most experiments were conducted in the following way. The first 5 minutes of the recording served as control period (Fig. 3.4.3B; blue, $t < 0$). Directly following this period, I measured R_s and R_{in} before applying 5-HT or its agonists, respectively. These measurements took ~1 minute, which was the reason of a blank gap between the control period and the start of 5-HT in this mEPSC recording (see Fig. 3.4.3B). At $t = 0$ (red), the superfusion of 5-HT was commenced and the recording of mEPSCs resumed. This was conducted for at least another 15 minutes. For 5-HT, it took less than a minute to reach the recording chamber, and less than another few minutes to exert its full effect.

3.3.2. Template-Matching Algorithm to Detect mEPSCs

Periods of mEPSC recordings were analysed using the template matching algorithm implemented in Axograph™ 4.9 or X (Axograph.com) as described in Clements and Bekkers (1997). This program estimates for each mEPSC its amplitude, the time of the peak, the rise time (10 – 90%, obtained by interpolation) and the half-width (obtained by interpolation) from the fitted scaled template. The procedure is illustrated in Fig. 3.3.1.

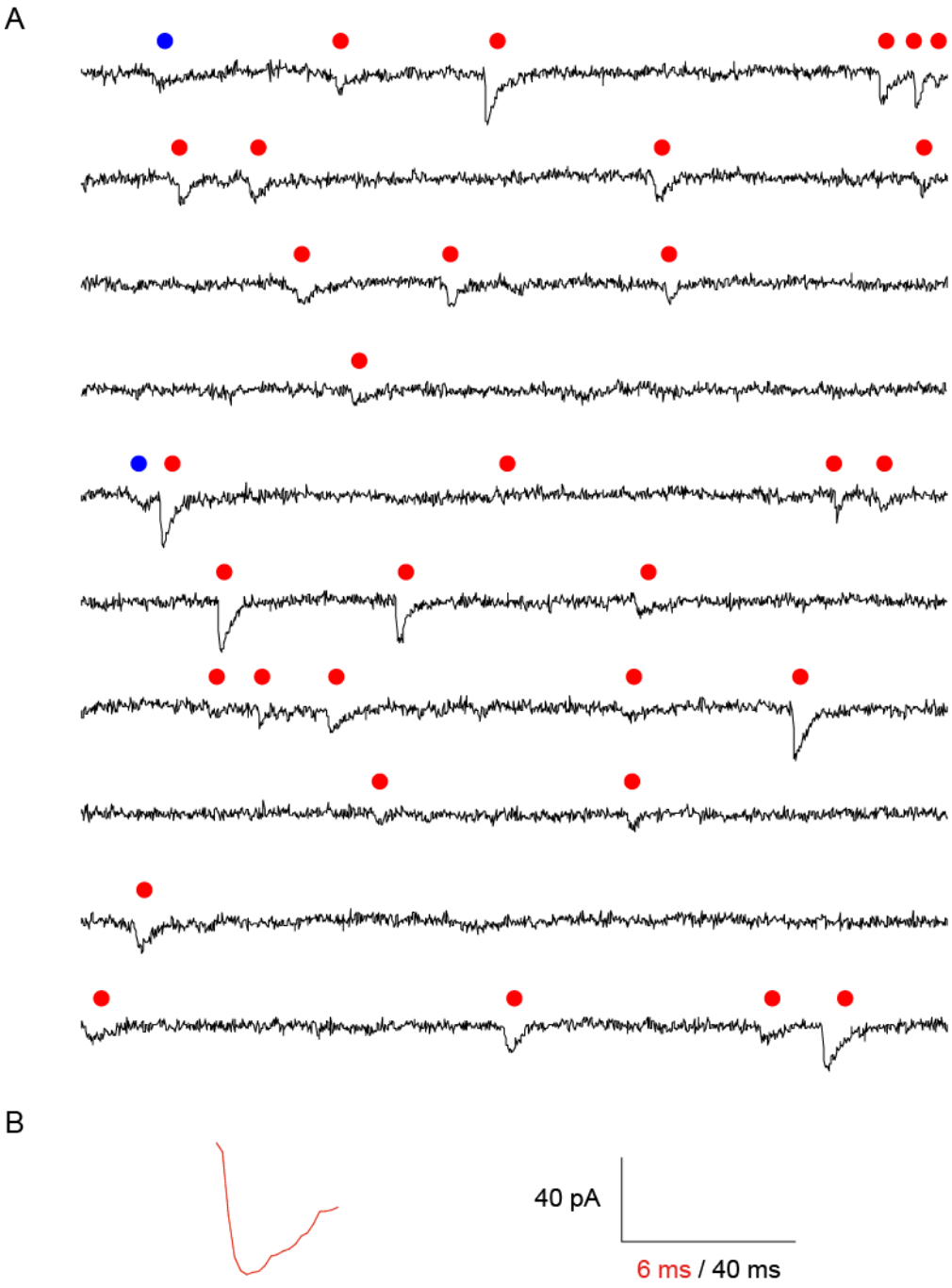

Figure 3.3.1. Detection of mEPSCs using template matching algorithm.
A. Two seconds of a continuous recording segmented into 200 ms periods, each separated vertically from top to bottom. Red dots (●) represent mEPSCs detected by algorithm. Blue dots (●) represented mEPSCs identified visually but not by the algorithm. The total number for visually identified mEPSCs is the sum of red and blue circles. B. Time course of the template used for the detection.

A template was chosen from the mEPSC time courses during the control period based on the following criteria. First, the respective mEPSC must have been free from contamination by other mEPSCs during the rising and early decay phase. Second, its

peak amplitude should be large (as large as possible, typically <-50 pA) to ensure a large signal to noise ratio; *i.e.* the time course is not dominated by the randomness of the recording noise present. Third, the rise time of mEPSC must have been fast (< 1 ms) with the decay time in the range between 5 – 10 ms.

Once an mEPSC had been identified to serve as template (B), the program slid it along the recording to pick up all mEPSC events by optimally scaling the template time course and amplitude and minimising the difference between the scaled template and the recorded time course. When the template fitted the time course well and the criteria of detection were fulfilled, an mEPSC was considered detected.

This template algorithm detected most mEPSCs accurately despite variation in mEPSC kinetics and holding current. However, it also detected false positive mEPSCs, typically small events, which were unlikely different from recording noise. Therefore, such mEPSCs needed elimination and, consequently, the analysis in Axograph™ 4.9 or X was subject to further "thresholding" based on the noise standard deviation (σ_{noise}). The latter corresponded to the point-by-point standard deviation of a chosen stretch of the recording devoid of spontaneous synaptic currents. The data was then subject to a routine in IGOR, during which mEPSCs with amplitudes < $2.5 \cdot \sigma_{noise}$ were removed.

The outcome of a chosen two second recording sequence was then compared with what was identified by a visual detection during the same period (A). Specifically, an mEPSC detected by algorithm and identified visually was considered a match. An mEPSC was considered false negative, if it was detected by eye, but not by the algorithm. In analogy, an mEPSC was considered false positive if it was detected by the algorithm but not visually. Only if the values of false positives and negatives was < 15%, *i.e.* > 85% of mEPSC were matched, the analysis was accepted. If this was not the case, the analysis was repeated with a new template until the above criteria were fulfilled.

Using the template in B, in a recording sequence of two seconds shown in A, the algorithm successfully detected 32 (red) out of 34 visually identified mEPSCs (blue and red). Two mEPSCs that were not detected by the algorithm, but by eye (blue circles), were considered false negatives, corresponding to a fraction of 6% (2/34). Since there were no mEPSC falsely identified by the algorithm, the false positive fraction was 0% (0/34).

3.3.3. Statistical Analyses

In addition to the thresholding function, the custom-made IGOR routine also extracted details of each detected mEPSC, including its amplitude, rise time, half-width and instantaneous frequency as determined by the time between the preceding and the respective mEPSC. Furthermore, the routine also generated histograms and cumulative probability density functions (cPDFs) of the instantaneous mEPSC frequencies and the amplitudes, which were then subject to further statistical analysis.

The cPDFs between the control and periods with pharmacological compounds added (after segmentation into subsets of five minutes each) were then compared and assessed for significance using the Kolmogorov-Smirnov (KS) statistic. Significance was reached if $p_{KS} < 10^{-21}$. This value was set very low because of the very large number of mEPSCs (~20,000 events). It also corresponded to the one also used in Simkus and Stricker (2002b, 2002a), Choy (2011), and Choy *et al.* (2017a).

Depending on the respective outcomes after 5-HT or agonist superfusion, which were based on the level of statistical significance, pyramidal cells were classified into two groups: Cells with a significant increase in mEPSC frequency were named responders, and those without were called non-responders; *i.e.* the frequency change was not different to that observed during the control period.

The probability of observing a certain number of responders and non-responders in different sets of experiments was compared for significance using a chi-squared (χ^2) test. This test performs best with sample sizes in the range of 50 – 100. However, the number of observations for each set of my experiments was typically much smaller (5 – 18). The small counts per category in this case causes the χ^2 value to become small, and correspondingly make the *p* value bigger and less reliable; *i.e.* in this case, the null hypothesis that there was no difference between the two outcomes would be very hard to reject, which unnecessarily penalises the alternative. There is a Yates' correction for small data values, but Haviland (1990) showed that this method is not necessarily better. For this reason, the significance level was set at < 0.10.

Since the instantaneous mEPSC frequency showed a characteristic transient change (see part 3.4.2.1), a one-way repeated measures ANOVA test and a *post-hoc t*-test with Bonferroni correction (Abdi, 2007) were performed to assess significance. As I compared the control with three subsequent phases, an ANOVA of one-way repeated measures was used to test if there was a significant difference ($p_{ANOVA} < 0.05$) between the four different data subsets in the same experiment. For the *post-hoc t*-test with Bonferroni correction, two different data sets in the same experiment were considered significantly

different, if $p_{t\text{-}Bon} < 0.05 / n$, where n is the total number of comparisons in the respective experiment. The number of comparisons was a combination of two out of four different data sets, which was $n = {}_4C_2 = 6$. Therefore, the significance level was set at $p_{t\text{-}Bon} \leq 0.0083$.

For comparing pooled mEPSC amplitudes, a paired *t*-test was used ($p_{pt} \leq 0.05$).

Where appropriate, the numerical values of the rise times and half-widths were used to give insight into the changes in mEPSC time course before and after agonist application. In addition, I averaged all mEPSC time courses from the control and subsequent periods with agonist/antagonist exposure and compared the two by overlaying. The typical length of the time courses was ~5 ms, including a very short baseline, the rising phase, its peak, and a part of the decay phase.

3.3.4. Pharmacological Compounds

All pharmacological compounds were dissolved in ACSF and applied to the slice by the addition to the superfusing solution. All blockers, inhibitors, or antagonists were applied for at least ten minutes prior to the superfusion with 5-HT or agonist. During this time, the solution in the superfusion chamber was fully exchanged and the appropriate concentration reached. 5-HT and the respective agonists were directly added to the superfusate, mostly exerting their full effect within a couple of minutes.

3.3.5. Characterising Passive Membrane and Action Potential Properties

The characterization of the electrophysiological properties of the recorded cells was performed prior to any mEPSC recording (*i.e*. in the presence of standard ACSF) by applying multiple current steps of 500 ms duration in steps of 50 pA starting from -200 pA and ending at 500 pA (see Fig. 3.4.1). The membrane time constant (τ_c) was determined as the time from onset to 63.2% of the maximal voltage deflection by a -200 pA current step. The procedure is illustrated in Fig. 3.3.2. For the hyperpolarizing current step of -200 pA, a single exponential was fitted to the membrane voltage (A). The threshold voltage of the action potential (V_{thr}) was determined as the membrane voltage, at which its first derivative equalled 50 mV/ms (Kole & Stuart, 2008). The action potential amplitude or height (H) was measured as the difference between the peak and V_{thr}. The width of the action potential (W) was measured as the width at half of its height (0.5 H). The relative membrane voltage difference (V_{rel}) was defined as the difference between V_{thr} and the resting membrane potential (V_{rest}; B and C).

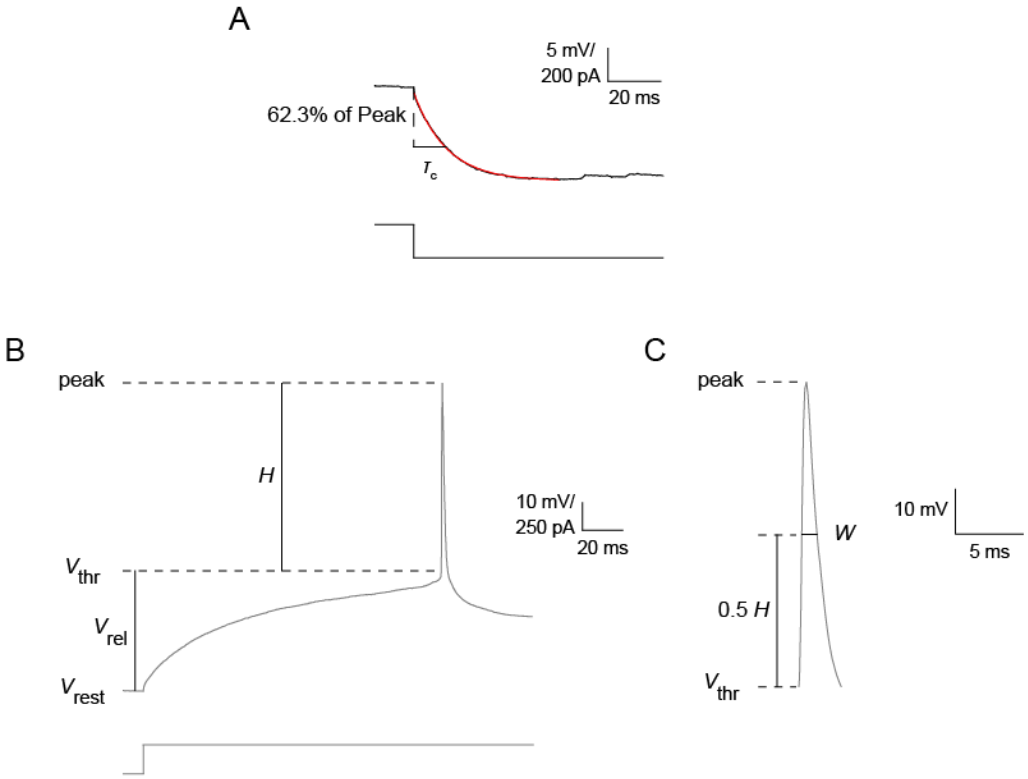

Figure 3.3.2. Estimation of electrophysiological properties.

A. τ_c was determined from the fit of a single exponential (—) to the membrane voltage after injection of a square current pulse of -200 pA. B and C show the determined parameters related to the action potential, including V_{rest}, V_{thr}, V_{rel}, H, and W.

3.4. Results

Results in this part are presented in five sections, 3.4.1 – 3.4.5. First, in 3.4.1, I will characterise the electrophysiological properties, which include the passive properties and the firing pattern of upper layer II pyramidal cells. I will also include the characteristics of mEPSCs and sEPSCs recorded in these pyramidal cells. Second, in 3.4.2, I will provide the basic observation how 5-HT impacted on mEPSCs, including the concentration-response relationship and the respective changes during early postnatal development. Third, in 3.4.3, I will identify some characteristics which differentiate cells with a significant response to 5-HT (responders), from the rest of the cells, which do not show a noticeable change (non-responders). Fourth, in 3.4.4, I will present experiments designed to determine which 5-HT receptor (5-HTR) caused the modulation of mEPSCs. Lastly, in 3.4.5, I will elucidate some of the molecular targets downstream of the respective 5-HTR activation.

Note that all numbers are presented as mean ± standard error of the mean (SEM). Note also that 5-HTR relates to both the singular but also the plural of receptors. The same idea applies to the receptor subtypes, typically indicated by a subscript. For example, 5-HT_{2C}R refers to 5-HT receptor(s) of the subtype 2C.

3.4.1 Electrophysiological Properties and m/sEPSC Characteristics

3.4.1.1. Electrophysiological Properties of Pyramidal Cells

I performed recordings from 198 pyramidal cells in the upper layer II of the barrel cortex. In these experiments, I isolated miniature EPSCs by using tetrodotoxin (TTX) and the $GABA_A$ receptor blocker gabazine. I also performed recordings from 19 other cells, in which spontaneous EPSCs were recovered in the presence of gabazine only, without the addition of TTX. From these recordings, the electrical properties could be determined in 156 cells (72%), which included V_{rest}, the membrane time constant (τ_c), the input resistance (R_{in}), the action potential threshold (V_{thr}), its amplitude referred to as its height (H), width at half-amplitude (W), and the relative voltage difference (V_{rel}) between V_{rest} and V_{thr}.

In this set of 156 pyramidal cells, V_{rest} was on average -76.6 ± 0.3 mV, τ_c 12.7 ± 0.2 ms, R_{in} 187 ± 6 MΩ at a series resistance (R_s) of 12 ± 0 MΩ. The action potential properties were as follows. V_{thr} equalled -38.0 ± 0.3 mV, H 74.0 ± 0.4 mV, W 1.0 ± 0.0 ms, and V_{rel} 38.6 ± 0.4 mV. All pyramidal cells showed a similar firing pattern. In response to a 500 ms long current step larger than rheobase, the pyramidal cells fired action potentials

regularly with only moderate adaptation (Fig. 3.4.1), corresponding to the regular spiking classification by (Connors *et al.*, 1982) and Maravall *et al.* (2004), but contrasting it with a phasic spiking pattern of "immature" layer II pyramidal cells, which only fire action potentials for the first 300 of a 500 ms long stimulus (Lorenzon & Foehring, 1993, 1995; Maravall *et al.*, 2004).

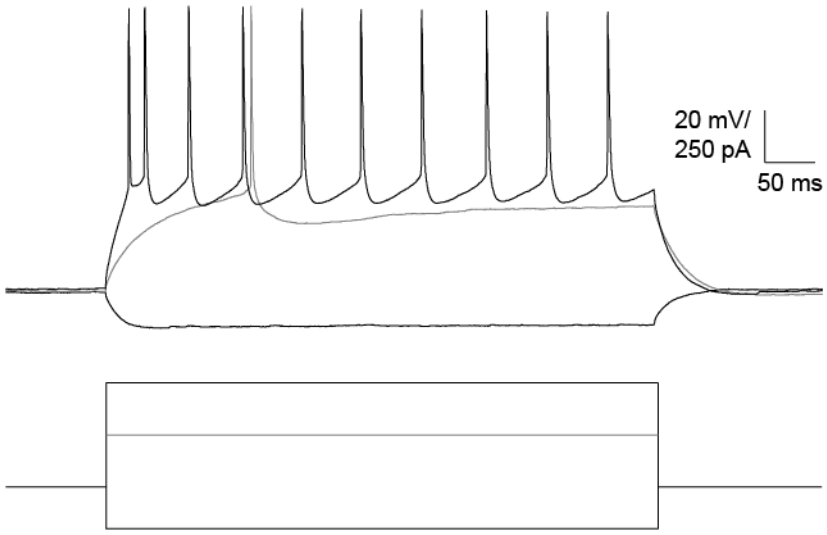

Figure 3.4.1. Firing pattern due to current steps.
Injection of a current step of -200 pA caused a hyperpolarization of 13.2 mV, with a small voltage sag typical of pyramidal cells (bottom). In this case, rheobase was at 250 pA (grey). A current step of 500 pA caused regular spiking at ~20 Hz.

3.4.1.2. Electrophysiological Properties of Spontaneous EPSCs

In the presence of 3 µM gabazine in the superfusate to block $GABA_A$ receptors, I recorded and characterized sEPSCs in 9 pyramidal cells. The point-by-point standard deviation of the noise (σ_{noise}) in these recordings ranged from 1.7 to 2.5 pA, giving an average value of 2.1 ± 0.1 pA. The instantaneous sEPSC frequency ranged from 42 to 82 Hz, with an average value of 56 ± 5 Hz. This is illustrated in Fig. 3.4.2. The average sEPSC amplitude was -11.0 ± 0.4 pA (A), with individual values ranging from -8.8 to -12.7 pA. The average rise time was 0.5 ms, with values ranging from 0.4 to 0.6 ms. The average half-width was 1.4 ms, with values ranging from 1.1 to 1.6 ms. The data for rise times and half-widths are presented without SEM, because were in the range of a few µs, much smaller than the A/D time used in these recordings (200 µs).

In the presence of 1 µM TTX to block voltage-dependent sodium channels, and therefore sodium electrogenesis, together with 3 µM gabazine (as above), I recorded and

characterized mEPSCs in 156 recordings from histologically verified pyramidal cells (B). σ_{noise} in these recordings ranged from 1.3 to 2.4 pA, giving an average value of 1.8 ± 0.1 pA. This value was slightly smaller than the value obtained for sEPSCs (p_t = 0.02), suggesting that blocking sodium channels had a significant impact on the recording noise, which was most likely dominated by perisomatic channels. The instantaneous mEPSC frequency ranged from 23 to 89 Hz, with an average value of 59 ± 1 Hz, not significantly different from those of sEPSC (p_t = 0.64). The mEPSC peak amplitude ranged from -5.4 to -13.7 pA, with an average value of -9.5 ± 0.1 pA. This value was significantly smaller than the sEPSC amplitude (p_t = 0.007), showing that the amplitude was also affected by the block of sodium channels (see Fig. 3.4.2). The mEPSC rise time ranged from 0.4 to 0.7 ms, giving an average value of 0.5 ms, not significantly different from those of the sEPSCs (p_t = 0.058). The half-widths ranged from 0.8 to 2.2 ms, with an average value of 1.6 ms, not significantly different either from those of the sEPSCs (p_t = 0.08).

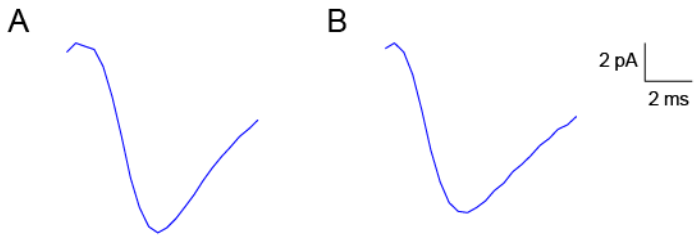

Figure 3.4.2. Time courses of mEPSCs and sEPSCs.
Typical time courses of sEPSC (A) and mEPSC (B) from individual recordings.

3.4.2. 5-HT Transiently Increased mEPSC Frequency But Not Amplitude

In this section, I will describe the effect of 5-HT on both, the mEPSC frequency and amplitude. Specifically, I will present data for pyramidal cells which showed a change in mEPSC frequency to 5-HT (responders), and some that were unresponsive (non-responders). In addition, several control experiments were done to further investigate the nature of this increase in mEPSC frequency. Note that from this point onwards, mEPSC frequency always refers to the instantaneous mEPSC frequency, and the two words are used interchangeably.

3.4.2.1. 5-HT Affects Frequency but Not Amplitude in Responders

First, I checked if 10 µM 5-HT affected the average mEPSC frequency, amplitude, and time course (*i.e*. rise time and half-width). After a control period of at least 5 minutes, upon addition of 10 µM 5-HT to the superfusate, I found that in a preliminary set of experiments, 7 out 15 (47%) pyramidal cells showed transient increases in the mEPSC frequency, without any change to their amplitudes and time courses. Pyramidal cells that showed these transient increase(s) were referred to as responders.

A typical recording from such a responder is shown in Fig. 3.4.3. Recording sequences during the control period and after addition of 5-HT are presented in A0 – 3. The intervals between two subsequent mEPSCs served to calculate the respective instantaneous frequencies, which were then plotted against time (B). For frequencies > 200 Hz, horizontal “banding” may become visible in the respective figures. This arises because the instantaneous frequencies were calculated based on the A/D conversion rate, which was 5 kHz and which gives a time resolution for the intervals of 200 µs.

During the control period (A0) with σ_{noise} of 1.6 pA, 5473 mEPSCs were detected. The average instantaneous mEPSC frequency was 47 ± 1 Hz, the amplitude -8.5 ± 0.1 pA, the rise time and half-width 0.5 and 1.5 ms, respectively. This control recording was considered stable, as all minute averages (blue dots in D) did not deviate by ≥ 15% from the average value (dashed line in D). After this period, the recording was interrupted for a minute (gap before 0) to measure the series (R_s) and input resistances (R_m; 16 and 148 MΩ, respectively).

Compared to the control period, after the addition of 10 µM 5-HT ($t \geq 0$), and for a continuous recording period of 15 minutes, I recovered 23’007 mEPSCs. The average instantaneous frequency increased transiently from 47 ± 1 to 60 ± 2 Hz (A1); *i.e.* by 31 ± 7% within 1 – 2 minutes. This increase is clearly discernible in B, with more dots at higher frequencies preset. In D, these values are plotted as minute averages together with the respective SEM. In F, the respective cPDFs for the mEPSC frequencies during the control and after 5-HT are illustrated. There was a right shift of cPDF around the time indicated by 1 in B addition of 5-HT, indicating that the frequency increased. However, within about 8 minutes after 5-HT addition, the mEPSC frequency had returned to control values (number 2 in B); *i.e.* 45 ± 2 Hz (A2 and D dashed line). The comparison with control was insignificant.

However, the mEPSC frequency did not remain at this value, but subsequently resurged to 74 ± 2 Hz after about 11 minutes (A3, number 3 in B); *i.e.* by 58 ± 5% from the control

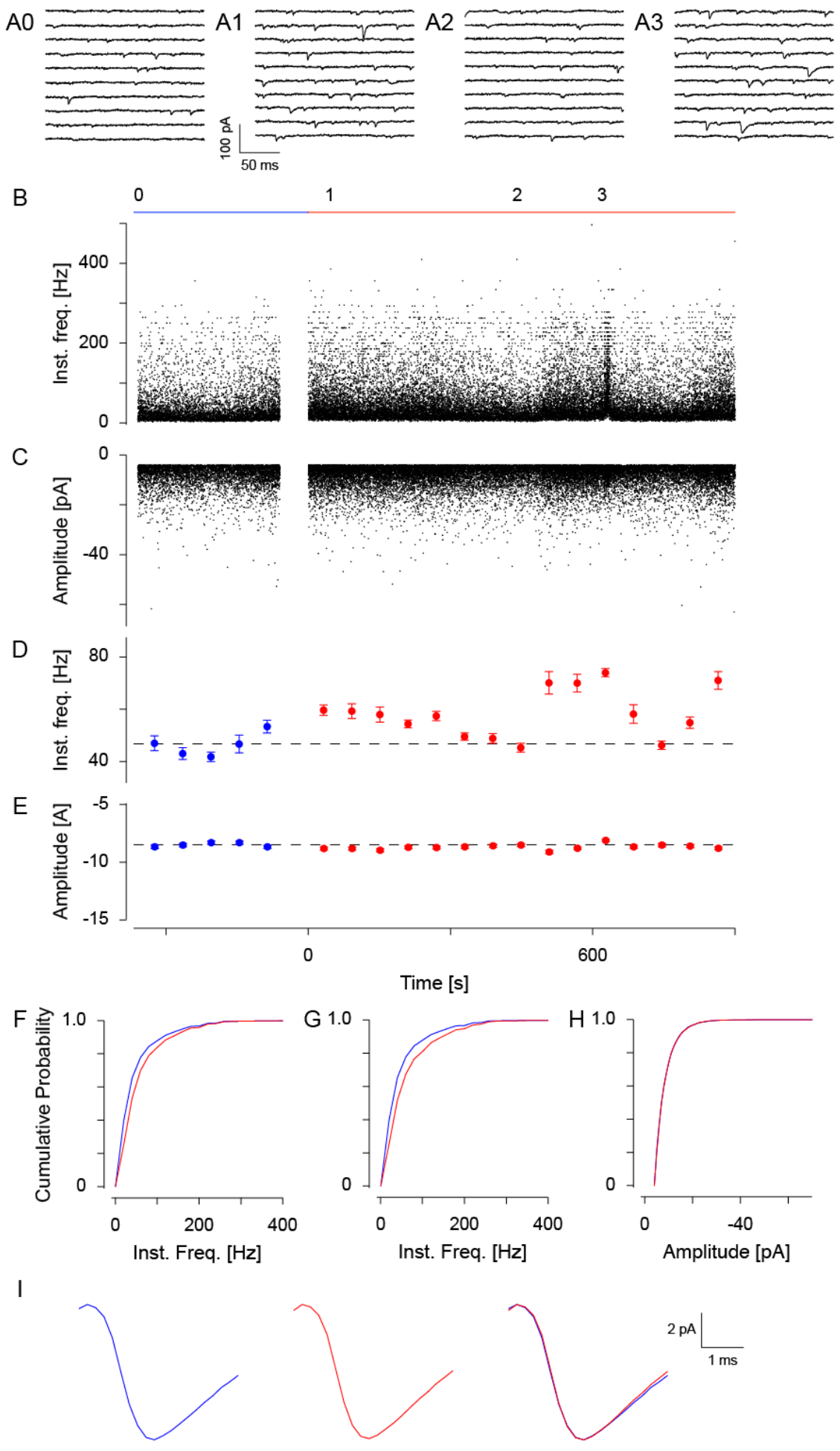
A0
A1
A2
A3
100 pA
50 ms
B
0
1
2
3
Inst. freq. [Hz]
400
200
0
C
Amplitude [pA]
0
-40
D
Inst. freq. [Hz]
80
40
E
Amplitude [A]
-5
-10
-15
0
600
Time [s]
F
Cumulative Probability
1.0
0
0
200
400
Inst. Freq. [Hz]
G
1.0
0
0
200
400
Inst. Freq. [Hz]
H
1.0
0
0
-40
Amplitude [pA]
I
2 pA
1 ms

Figure 3.4.3. mEPSCs frequency increase by 10 µM 5-HT.

Colour code is blue for the data acquired during the control period, red after 5-HT addition. A. Representative periods (2 s) during control (A0) and after addition of 5-HT at different time points (A1 – A3), indicated in B with numbers 0 – 3. B. Time course of all instantaneous mEPSC frequencies during the recording. C. Same as in B but for mEPSC amplitudes. D. Minute averages of the instantaneous mEPSC frequency during the recording. Dashed line indicates the average frequency during control extended for the duration of the whole experiment. E. Same as in D but for mEPSC amplitude. F. cPDFs of the instantaneous mEPSC frequencies during control (0, blue) and the first increase after exposure to 5-HT (1, red). G. Same as in F, except that in this case the comparison was between control and the resurgence (3, red). H. cPDFs of the mEPSC amplitudes during control and after 5-HT. I. The average mEPSC time courses during control (left), after the initial increase (middle) and peak-scaled and overlaid (right).

value (B and D). The comparison of the respective cPDFs during control and this resurgence is shown in G. Similar to the observation in F, there was again a significant right shift. After the resurgence, the frequency again returned back to control values; *i.e.* 45 ± 2 Hz, which, when compared to control, was insignificant.

Overall, during the 15 minutes of recording with 5-HT added to the superfusate, two transient increases in mEPSC frequency were observed, each lasting for about 4 – 5 minutes before returning to control values.

In contrast to the changes in frequency, the amplitude did not show any significant change upon 5-HT exposure (E and H). The mEPSC amplitude during the control period was -8.5 ± 0.1 pA, and remained at -8.4 ± 0.1 pA after 5-HT application. In addition to the comparison of mEPSC amplitudes, the time courses of the two average mEPSCs for the control period and after 5-HT are presented I (left control; middle 5-HT; right overlay). Note that the baselines of the average mEPSCs are not flat due to the fact that many mEPSCs included in this average straddle the decay phase of a preceding mEPSC. The average rise time during the control period was 0.5 and the half-width 1.5 ms. Likewise, there is flattening of the average mEPSC decay phase after about 2.5 ms caused by collisions/superpositions of mEPSCs. For comparison, the two time courses are peak scaled and overlaid (I, right). The graph indicates that there was no appreciable difference between the two time courses. Based on the findings so far, I conclude that the increases in mEPSC frequency were very unlikely caused by variations in mEPSC amplitude seen as a change in frequency, but were most likely caused by a genuine increase in mEPSC frequency. In addition, 5-HT did not have any significant effect on either the amplitude nor the time courses.

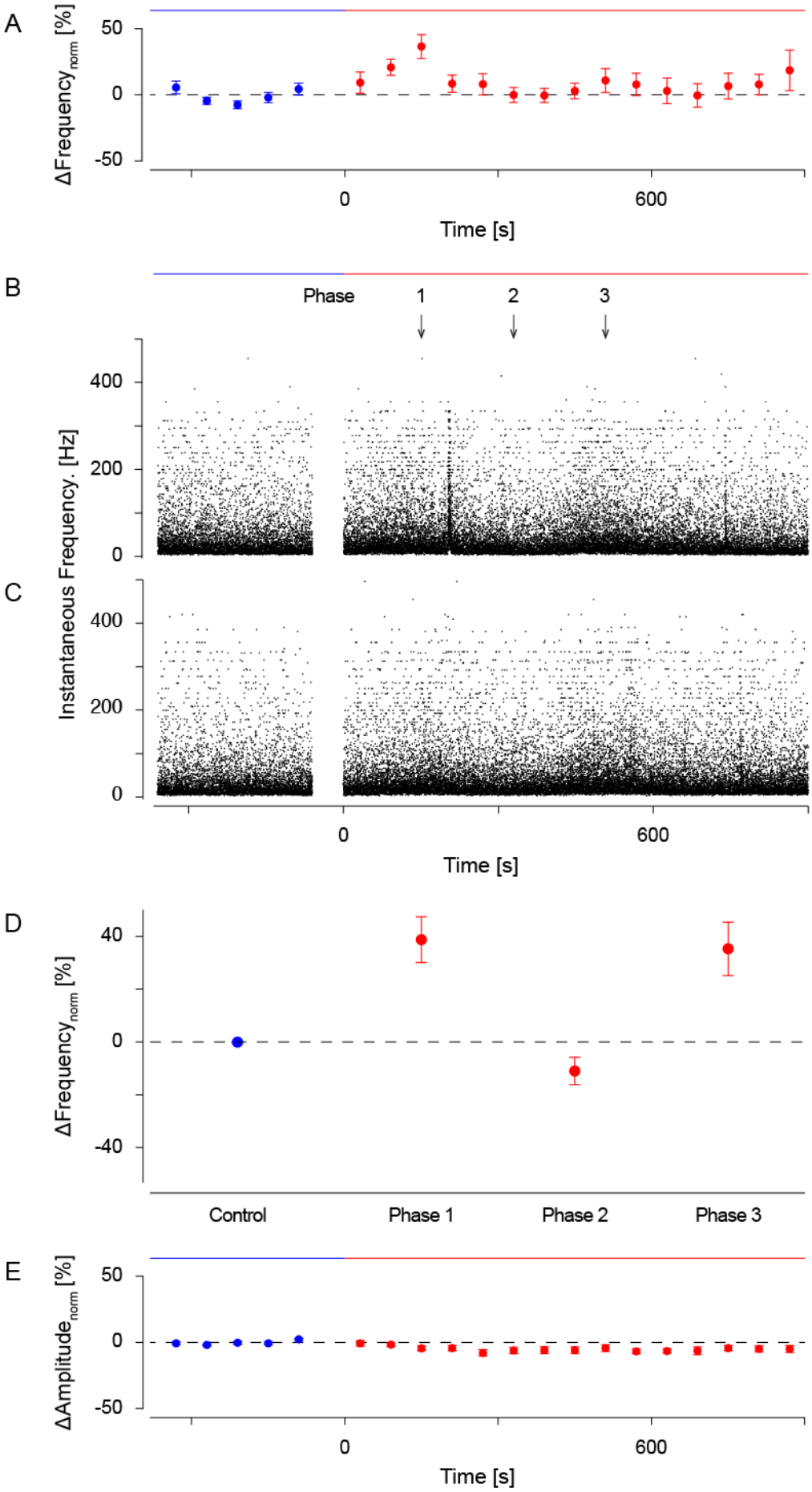
A
ΔFrequency norm [%]
50
0
-50
0
600
Time [s]
B
Phase
1
2
3
400
200
0
C
Instantaneous Frequency. [Hz]
400
200
0
0
600
Time [s]
D
ΔFrequency norm [%]
40
0
-40
Control
Phase 1
Phase 2
Phase 3
E
ΔAmplitude norm [%]
50
0
-50
0
600
Time [s]

Figure 3.4.4. Average mEPSC frequency and amplitude for responders.
Control values normalized to 0%. Same colour code as before. A. Minute averages of the data sets after all 7 recordings were pooled. B. & C. Instantaneous mEPSC frequencies for two simultaneous recordings in the same slice showing that 5-HT affected the mEPSC frequency with identical temporal characteristics. Arrows with numbers indicate when the 3 different phases occurred. D. The average peak frequencies when plotted for the three phases relative to control. E. Minute averages of the average mEPSC amplitudes with the dashed line indicating the average during control.

The average of 7 such responders is illustrated in Fig. 3.4.4. Each point in A represents the average during the respective minute, with the error bar indicating the respective SEM. These minute averages also show an initial increase in mEPSC frequency by 37 ± 10% from 56 ± 5 to 75 ± 5 Hz within ~ 3 minutes after 5-HT addition. Similar to the example given above, the mEPSC frequency had returned to control values within another 4 – 5 minutes. Note that in this average, there was no second increase, even though in all 7 cases significant changes were observed at the individual level. This is due to the fact that the timing of this second increase was variable. This observation is supported by error bars becoming larger with the length of the recording.

Even in cases when data was acquired simultaneously from two cells in the same slice, 5-HT still caused increases in mEPSC frequencies with more or less identical timing. This is illustrated in Figs. 3.4.4B and C, where all individual mEPSC frequencies are shown for both cells. Note that the initial rise, drop and resurgence occurred at a similar time in both recordings (arrows). However, in cells from different slices, the timings were much more variable. A potential explanation may be that 5-HT caused changes in mEPSC frequencies that depended on the state of the slice and its superfusion. Because of this reason, pooling of the minute averages might have been inappropriate. Therefore, I measured the peaks and trough individually and averaged those values. Subsequently, the first mEPSC frequency increase after 5-HT addition is referred to as phase 1 but also as initial increase. The respective value was measured just before the frequency dropped again. Phase 2, also referred to as drop, captures the waning of the frequency to values typically below those during control. The respective value was measured at the minimum during the time course. Phase 3, also referred to as resurgence, includes the (subsequent) second frequency increase. Its value was measured as the maximum during this phase.

Using these conventions, the respective averages of all 7 responders are shown in D. The average mEPSC frequency during the control period was 56 ± 5 Hz, which was normalized to zero for this plot. Upon superfusion with 5-HT, the frequency increased by

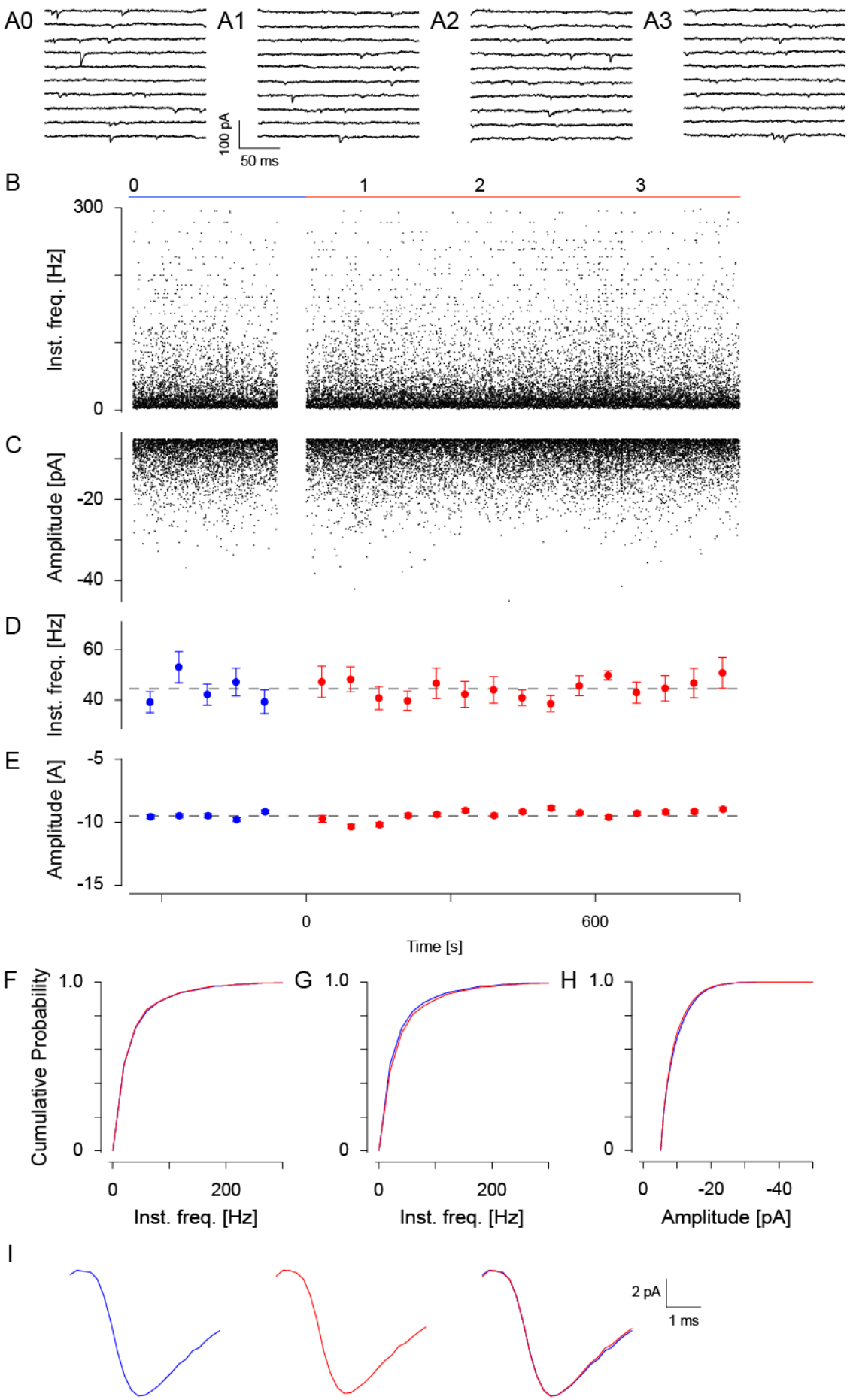
A0
A1
A2
A3
100 pA
50 ms
B
0
1
2
3
300
Inst. freq. [Hz]
0
C
Amplitude [pA]
-20
-40
D
Inst. freq. [Hz]
60
40
E
Amplitude [A]
-5
-10
-15
0
600
Time [s]
F
Cumulative Probability
1.0
0
0
200
Inst. freq. [Hz]
G
1.0
0
0
200
Inst. freq. [Hz]
H
1.0
0
0
-20
-40
Amplitude [pA]
I
2 pA
1 ms

Figure 3.4.5. Non-responder.

A. Recording periods during control (A0), and after the addition of 5-HT (A1 – 3). B. Plot of the instantaneous mEPSC frequencies against time for whole recording period. The numbers 0 – 3 indicate the same times as in Fig. 3.4.3. C. Time course of the individual mEPSC amplitudes throughout the recording. The dashed line indicates the average value during control. D. Minute averages of the mEPSC frequency and amplitude (E) for the duration of the recording. F. cPDFs of mEPSC frequency during control and after 5-HT taken at 1 (B). G. Same as before, but for the period indicated by 3. H. cPDFs of mEPSC amplitude during control (0) and after 5-HT during 3. I. Time courses of average mEPSCs during control (left), after 5-HT (middle) and after peak scaling and overlaying (right).

39 ± 9% during the initial rise within a time window between 1 and 5 minutes (average of 2.7 ± 0.5 min; phase 1). Thereafter, it dropped to -11 ± 5% during phase 2 (5 – 12 min, around an average of 8.3 ± 0.9 min). Lastly, the mEPSC frequency resurged back to 35 ± 10% during phase 3 (9 – 15 min, around an average of 12.3 ± 0.9 min).

The average mEPSC amplitudes for all 7 responders are also shown in E. During control, it was -9.8 ± 0.5 pA, and remained at -9.3 ± 0.4 pA after 5-HT application. This change was insignificant after the pooling of these 7 recordings. In addition, there was also no change in either rise times and half-widths.

3.4.2.2. Impact on Non-Responders

In contrast to what was reported above, I also observed that in the other 8 cells, there was no significant increase in the mEPSC frequency after exposure to 5-HT. These cells will subsequently be referred to as non-responders.

In analogy to the presentation above, an example of such a non-responder is illustrated in Fig. 3.4.5. During the control period, with noise standard deviation of 2.0 pA, an input resistance of 178 MΩ and a series resistance of 17 MΩ, I recovered 4’019 mEPSCs. The respective average instantaneous mEPSC frequency was 45 ± 2 Hz (A0), the amplitude -9.5 ± 0.1 pA, the rise time and half-width 0.6 and 1.5 ms, respectively.

After the addition of 5-HT to the superfusate, the mEPSC frequency in this case remained at 45 ± 2 Hz (A1); *i.e.* it was no different to that observed during control. This remained so throughout the remainder of the recording (A1 – 3) as shown in B and D, both for all individual frequencies and when the minute averages were plotted. Comparisons of cPDFs between the control period and a time window identical to phases 1 and 3 above (F and G, respectively), revealed that there was no change in the frequencies throughout. Similar to the case for the responder above, the mEPSC amplitude did not show any significant change either (C and E). Specifically, the

amplitude during control period was -9.5 ± 0.1 pA, but remained unchanged at -9.2 ± 0.1 pA after exposure to 5-HT. Neither was there a change in the average EPSC time course, rise time nor the half-width (I, right).

In figure 3.4.6, the changes in the minute averages for both mEPSC frequency and amplitude are shown for these 8 cells after normalising the respective control value to 0%. For the 15 minutes of superfusion with 5-HT, neither the frequency nor the amplitude changed. Nor were there any alterations to the average mEPSC time course, rise time and half-width.

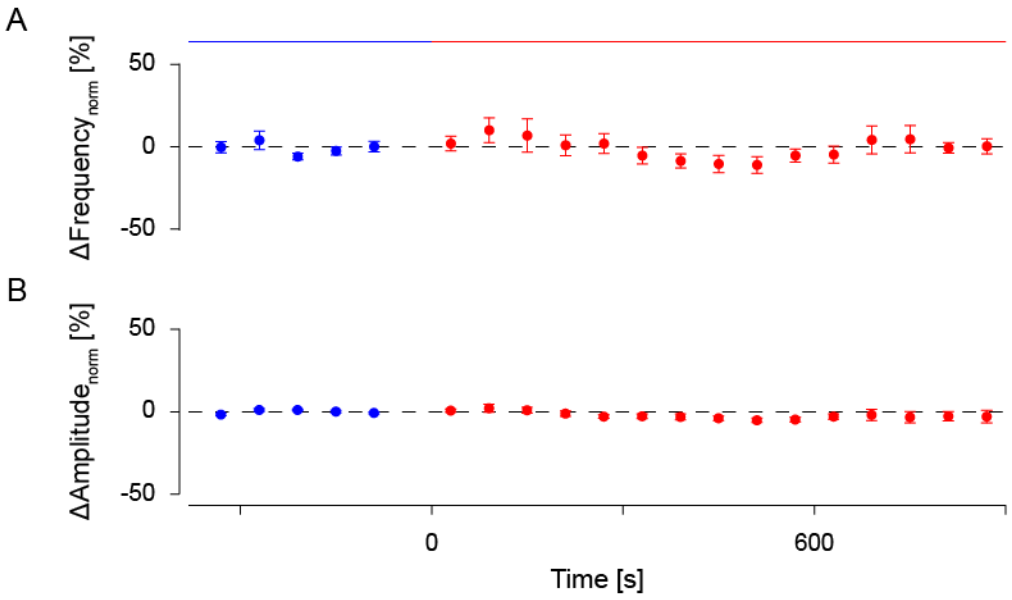

Figure 3.4.6. Average time courses in non-responders.

A. Time courses of the minute averages of the instantaneous mEPSC frequency and amplitude (B) after normalising the control value to 0%.

3.4.2.3. Pooling of Preliminary Data Sets

Because variations in the mEPSC frequency are typically taken as a sign of unstable recording conditions, I wanted to apply more rigorous testing by "diluting" the data in responders with the values obtained from non-responders; *i.e.* by introducing a larger amount of variability at the price of gaining a larger sample size. If under these conditions, significance remained, I would be re-assured that the changes were likely genuine.

Before being able to pool these two data sets, I checked if during control, there were any significant differences in parameters like R_{in}, R_s, mEPSC frequency, amplitude, rise time, and half-width, which may preclude pooling. I found that there were no significant differences between these two groups. Specifically, the differences in R_{in} (202 ± 39 *vs.* 223 ± 31 MΩ; p_t = 0.67), R_s (13 ± 1 *vs.* 12 ± 1 MΩ; p_t = 0.60), the mEPSC frequency (56 ± 4 *vs.* 50 ± 3 Hz; p_t = 0.27), amplitude (-9.8 ± 0.4 *vs.* -10.5 ± 0.6 pA; p_t = 0.43), rise time (0.5 *vs.* 0.5 ms; p_t = 0.69), or half-width (1.3 ± 0.1 *vs.* 1.5 ± 0.1 ms; p_t = 0.18) were all

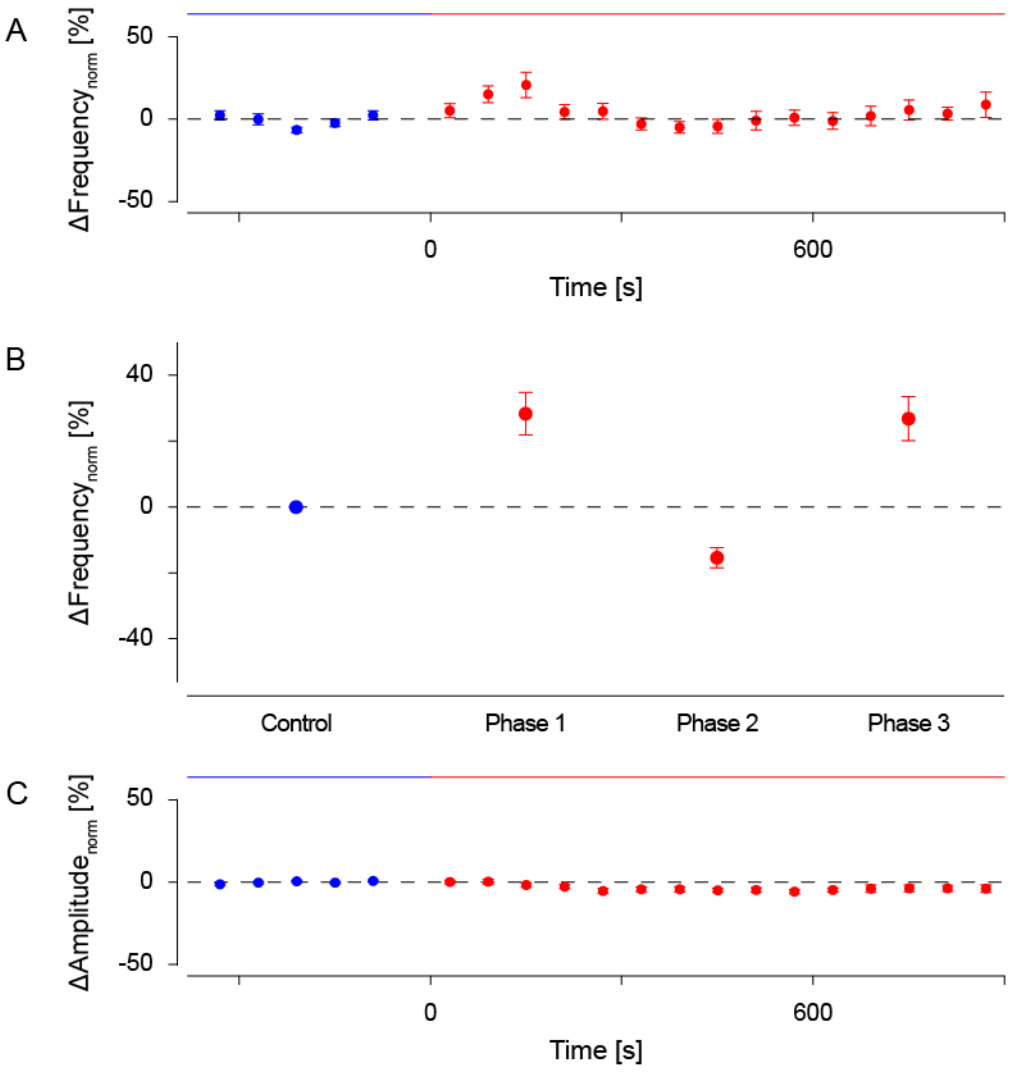

Figure 3.4.7. Pooled data from responders and non-responders.

A. Minute averages of the instantaneous mEPSC frequencies after normalising the control value to 0%. B. Average relative changes in the mEPSC frequencies plotted for the different phases. The dashed line indicates no change. C. Minute averages of the relative change in the mEPSC amplitude.

above the level of significance. Therefore, it was justifiable to pool the data from both preliminary groups. Note, that in 3.4.3, I will later present an analysis of the much larger set of recordings.

After pooling the data from all 15 cells, the respective outcomes are presented in Fig. 3.4.7. In A, the change in the minute averages of the mEPSC frequency are shown after normalising for the control period. As in Fig. 3.4.4A, an initial increase three minutes after the addition of 5-HT still remained, but its value was now only 21 ± 8% (53 ± 3 *vs.* 63 ± 4 Hz). But, and not unlike in Fig. 3.4.4A either, there was no resurgence in the mEPSC frequency. Consequently, I measured the respective peak values during the previously defined phases and averaged those. In the case of non-responders, the values were determined during the third (phase 1), ninth (phase 2) and thirteenth minute (phase 3), respectively.

Table 3.4.1. Peak mEPSC frequencies during different phases.

Phases	Phase 1 1 – 5 min (67 ± 4 Hz)	Phase 2 5 – 12 min (45 ± 3 Hz)	Phase 3 9 – 15 min (68 ± 6 Hz)
Control (53 ± 3 Hz)	+28 ± 7% (10^{-4} **)	-15 ± 3% ($2\cdot10^{-4}$ **)	+27 ± 7% (0.002 *)
Phase 1 1 – 5 min (67 ± 4 Hz)		-32 ± 3% ($1\cdot10^{-7}$ **)	+1 ± 6% (0.41)
Phase 2 5 – 12 min (45 ± 3 Hz)			+51 ± 9% ($9\cdot10^{-5}$ **)

Significance level reached when comparing the different phases within the same group ($p_{ANOVA} = 8\cdot10^{-8}$ **; $n = 15$). Individual comparisons between two phases were further subject to a *t*-test with Bonferroni correction (* $p_{t\text{-}Bon} < 0.008$, ** $p_{t\text{-}Bon} < 0.002$). Phase 1 refers to the initial rise, phase 2 to the intermediate drop and phase 3 to the resurgence. Note that there are differences between all phases except between phases 1 and 3.

This way, the addition of 5-HT still caused detectable changes in the mEPSC frequency ($p_{ANOVA} = 8\cdot10^{-8}$). After normalising the value during control for 0%, the average mEPSC frequency after the addition of 5-HT increased during the initial rise by 28 ± 7% within 1 – 5 minutes (B; 53 ± 3 *vs.* 67 ± 4 Hz; $p_{t\text{-}Bon} = 10^{-4}$; phase 1). The frequency waned again after 5 – 12 minutes by -15 ± 3% when compared to control (45 ± 3 Hz; $p_{t\text{-}Bon} = 2\cdot10^{-4}$;

phase 2), to then resurge back to 27 ± 7% (68 ± 6 Hz; $p_{t\text{-}Bon}$ = 0.002; phase 3). The respective details are given in Table 3.4.1.

On average, the mEPSC amplitude during the control period was -10.2 ± 0.4 pA and remained at -9.7 ± 0.3 pA after 5-HT. When the relative change in the minute average amplitudes was plotted in C, there was no significant difference either. In addition, there was no change either the mEPSC time course, rise time or half-width.

It is reassuring that the differences could also be uncovered with ANOVA in conjunction with a *post-hoc t*-test with Bonferroni correction even when the data sets were pooled. This strengthens the argument that after the addition of 5-HT to the superfusate, the increases in mEPSC frequency are genuine.

With no changes observed for the mEPSC amplitudes, rise times or half-widths, the increases in the instantaneous mEPSC frequency strongly suggest that 5-HT predominantly affects presynaptic targets.

3.4.2.4. Controls for the Transient Nature of the Frequency Increase

Despite the conclusions just reached, I remained concerned whether the transient increases in mEPSC frequency were an artefact of recording or resulted from an inability to track a sustained increase accurately.

I subsequently addressed the possibility of an artefact of recording in 3.4.2.4.1, by performing control recordings without 5-HT over a long period. If in such recordings there were no transient increases, the notion of artefact of recording was unlikely relevant.

To address the alternative that I was not able to track a sustained increase reliably, I performed recordings with 10 µM noradrenaline (NA) in the same way as with 5-HT. NA produced a sustained increase in the mEPSC frequency (Choy, 2011). The respected results will be presented in 3.4.2.4.2. If I was able to reliably track the sustained mEPSC frequency increase with NA, this alternative was ruled out.

3.4.2.4.1. Control Recordings Without 5-HT

To present further evidence that the transient increases in mEPSC frequency by 5-HT were not incurred by simply switching over to a different line feeding the solution, recordings of equal duration were performed, containing a switch-over but without the addition of 5-HT.

Such a recording is presented in Fig. 3.4.8. During a period, equivalent to that of control, the mEPSC frequency was 63 ± 1 Hz (A0, B, and D). This frequency was not different to

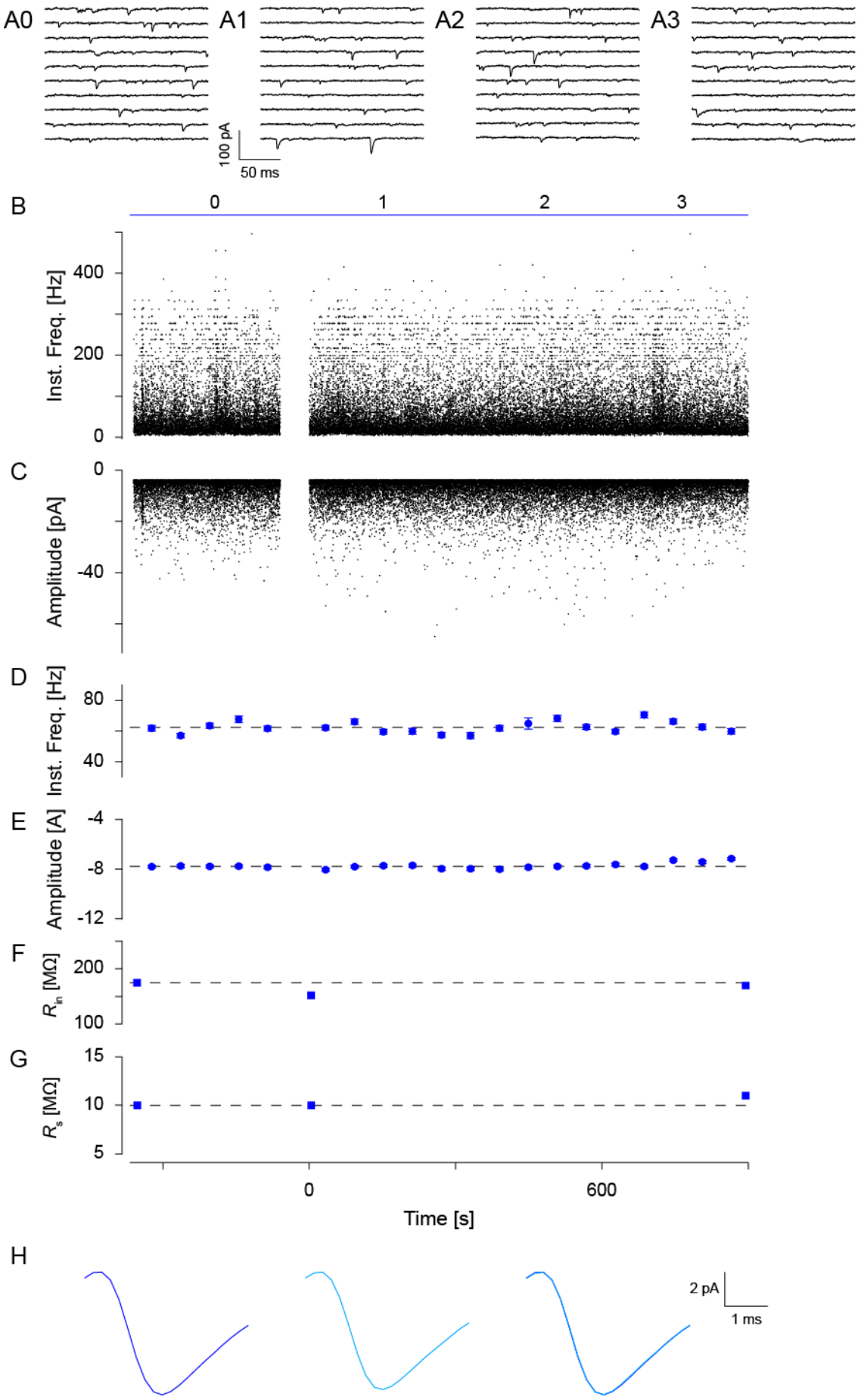
A0
A1
A2
A3
100 pA
50 ms
B
0
1
2
3
Inst. Freq. [Hz]
400
200
0
C
Amplitude [pA]
0
-40
D
Inst. Freq. [Hz]
80
40
E
Amplitude [A]
-4
-8
-12
F
R_{in} [MΩ]
200
100
G
R_s [MΩ]
15
10
5
0
600
Time [s]
H
2 pA
1 ms

Figure 3.4.8. Control recordings without 5-HT.

A. Periods of 2 s containing mEPSCs during the first 5 minutes as control (A0) and at the times indicated in B (A1 – 3). B. Instantaneous mEPSC frequencies plotted against time. Zero indicates the time at which the valve was switched to the solution without 5-HT. C. Same as in B but for the mEPSC amplitudes. D. Minute Averages of the mEPSC frequency and E. amplitude. Dashed lines show the average values during the control period, which was extrapolated to the whole duration of the recording. F. Values of R_{in} and G. R_s measured before, in between, and after the recording. H. Average mEPSC time courses during the control period (left) and the subsequent recording period (middle). The two time courses are shown overlaid on the right after peak scaling.

the one presented above (p_t = 0.67). At t = 0, the perfusion was switched over to another inlet line, but only containing standard ACSF. Thereafter, the recording was resumed for a further 15 minutes. After switching over, the frequency remained at 64 ± 1 Hz, which was not significantly different from control at times equivalent to the phases 1 – 3 (A1 – 3, B). The minute averages of the mEPSC frequency were not different to those of the control period, as shown in D. There was also no change in the mEPSC amplitude (-7.8 ± 0.1 *vs.* -7.5 ± 0.1 pA; C and E). The average mEPSC time course also remained the same (H, right), as was the rise time and half-width (0.5 and 1.4 ms, respectively).

Changes in the mEPSC frequency could also arise if R_s and/or R_{in} changed considerably during the recording. To exclude this possibility, the two parameters were measured at three different time points throughout the recording. The first point was just before the control period, the second right before the change-over, and the third immediately after the final recording period. The respective values for R_s were 10, 10, and 11 MΩ (G) and those for R_{in} 175, 152, and 170 MΩ (F). The values for R_s and R_{in} changed by < 10% throughout the recording and, consequently, would unlikely have significantly affected the mEPSC frequency.

In a set of 6 such recordings, illustrated in Fig. 3.4.9, the mEPSC frequency remained at 51 ± 3 Hz (normalized to 0%; A) and the amplitude at -9.4 ± 0.7 pA (also normalized to 0%; B) without any significant change throughout recordings. The mEPSC time course did not change either, with the rise time remained at 0.6 and the half-width at 1.6 ms. The average values for R_s in these recordings were 13 ± 1 (before), 14 ± 1 (in between), and 15 ± 1 MΩ (after recordings; D). The average values for R_{in} were 231 ± 32 (before), 209 ± 39 (in between), and 252 ± 44 MΩ (after recordings; C).

This set of control recordings indicates that the transient increases in the instantaneous mEPSC frequency after 5-HT superfusion were very unlikely recording artefacts (stability) or caused by time varying changes in either R_s or R_{in}.

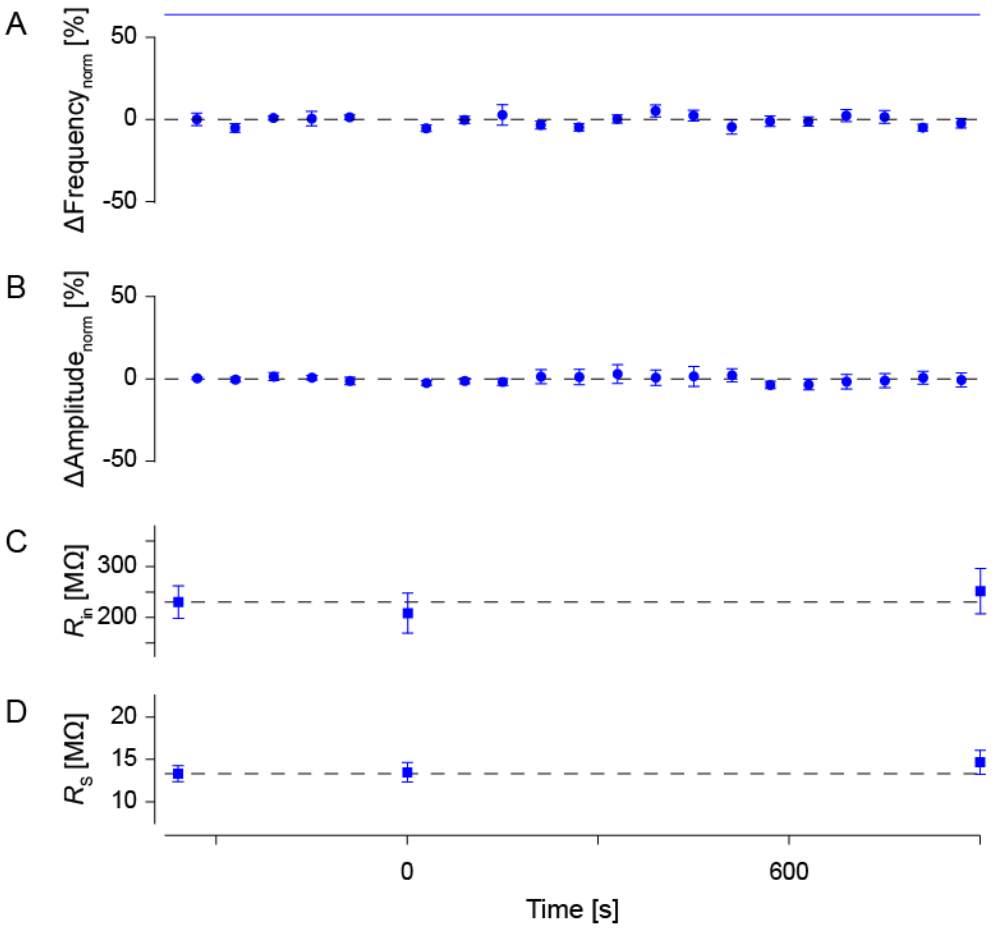

Figure 3.4.9. Minute averages of mEPSC frequency and amplitude.

A. Minute averages of the instantaneous mEPSC frequency and B. amplitude for a data set of 6 recordings. Dashed lines indicate the average values during the control period, which were normalized to 0%. C. Average values for R_{in} and D. R_S taken before, in between and after the recording.

3.4.2.4.2. Sustained Increase in the Presence of NA

A further alternative explanation for the transient nature of spontaneous release may be that with the recording technique used, I could not reliably track a sustained change in the mEPSC frequency over the duration of the recording. To exclude this possibility, I checked if, with my recording set-up and analysis techniques used, I was able to track a sustained increase in mEPSC frequency by NA. From a previous study in this laboratory, I knew that the neuromodulator NA increased the mEPSC frequency in a sustained way throughout the recording period (Choy, 2011; Choy *et al.*, 2017a).

Such a typical recording is presented in Fig. 3.4.10. During the control period, the mEPSC frequency was 53 ± 1 Hz (A0, B, and D). Upon addition of 10 µM NA (t = 0), the frequency increased by 40 ± 5% to 75 ± 2 Hz in a sustained manner (A2 & 3, B, and D). Even during the last minute of recording, the frequency was still 59 ± 1 Hz, significantly above control value (11 ± 3%).

In contrast to the sustained increase in frequency, the mEPSC amplitude did not show a significant change (-6.8 ± 0.1 *vs.* -6.2 ± 0.1 pA; E and H). In addition, the average time courses of mEPSC during control and after addition of NA did not show any significant change either (I), with the average rise time remaining at 0.7 and the half-width at 1.8 ms.

In 4 such experiments, the average frequency during control was not different to the one observed for the data set with 5-HT (p_t = 0.97); in fact, it was the same. Of these 4 cells, a significant increase in the mEPSC frequency after addition of NA was seen in 2 cells. In both cases, it was sustained throughout. The fact that not all cells showed an increase in mEPSC with NA has been observed before (Choy *et al.*, 2017a). This limited set of data suggests that I was also able to track a sustained change in mEPSC frequency reliably, lending further support to the argument that the transient changes observed with 5-HT are indeed genuine.

3.4.2.5. Impact of Different 5-HT Concentrations

An explanation for the existence of responders and non-responders in the preliminary data set could be that 10 µM 5-HT either desensitized the respective receptors in a highly differential manner, or it was not a saturating concentration at these receptors. I addressed these two alternatives by varying the 5-HT concentration. Specifically, I decreased the concentration to 1 µM to see if desensitisation was present, but also increased it to 100 µM to see if the receptors were saturated.

3.4.2.5.1. 1 µM 5-HT

The case for 1 µM 5-HT is presented in Fig. 3.4.11. During the control period (A0, B for t < 0), the frequency was 80 ± 3 Hz, the amplitude -9.9 ± 0.1 pA, the rise time 0.5 ms and the half-width 1.4 ms. After the addition of 1 µM 5-HT to the superfusate, the mEPSC frequency and amplitude remained 71 ± 3 Hz (A1 – 3, B and D) and -9.4 ± 0.1 pA (C and E), respectively. Both changes were insignificant (G and H). In addition, the time courses of the average mEPSC during the control period (I, left) and the last five minutes after addition of 5-HT (I, middle) overlapped with each other (I, right), indicating that there was no change in time course.

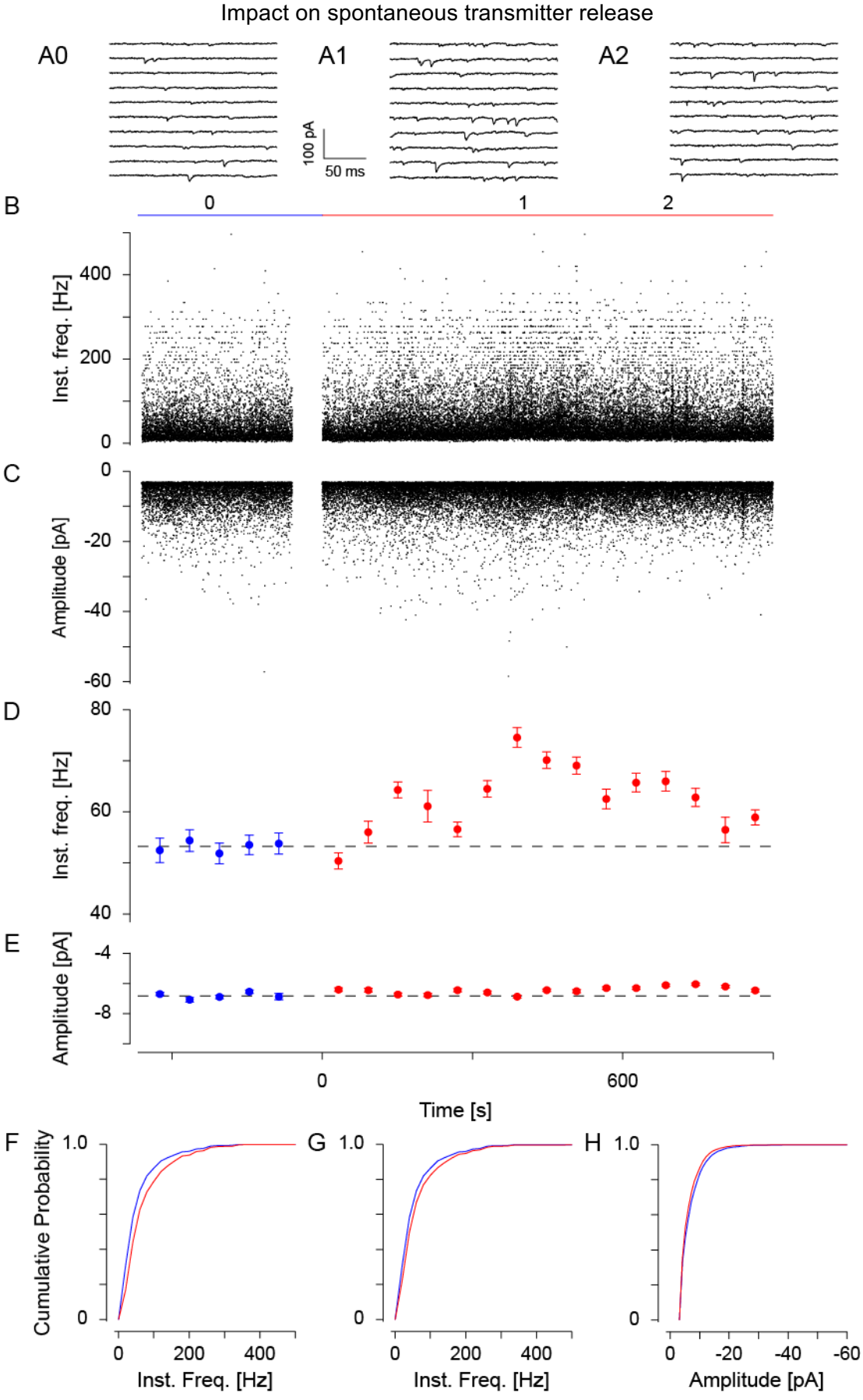
Impact on spontaneous transmitter release
A0
A1
A2
100 pA
50 ms
B
0
1
2
Inst. freq. [Hz]
400
200
0
C
Amplitude [pA]
0
-20
-40
-60
D
Inst. freq. [Hz]
80
60
40
E
Amplitude [pA]
-4
-8
0
600
Time [s]
F
Cumulative Probability
1.0
0
0
200
400
Inst. Freq. [Hz]
G
1.0
0
0
200
400
Inst. Freq. [Hz]
H
1.0
0
0
-20
-40
-60
Amplitude [pA]
I
2 pA
1 ms

Figure 3.4.10. mEPSC frequency increase was sustained with NA.

This figure was made in analogy to Fig. 3.4.3. The legend there also applies here with the exception that instead of 5-HT, 10 µM NA was added to the superfusate, and instead of three, only two recording periods are presented after NA addition.

The time courses of the pooled data for 10 such experiments are presented in Fig. 3.4.12. After exposure to 1 µM 5-HT, no cells showed any increase in the mEPSC frequency. Specifically, the changes in frequency and amplitude (p_t = 0.85) were minimal (A, B, respectively). The average EPSC time courses also remained the same as did rise time and half-width. These values were also not different to those with 10 µM 5-HT. The respective comparisons for the frequency gave a value for p_t of 0.09, 0.85 for amplitude, 0.25 for rise time, and 0.65 for half-width. This indicates that this sample was not biased.

However, the outcome in this sample was different from that with 10 µM 5-HT. Based on a χ^2-test, the two sets were not the same (p_{χ^2} = 0.011), supporting the finding that 1 µM was an insufficient concentration to produce the increase in frequency.

It is also very unlikely that all 10 cells were non-responders. Based on this preliminary sample where 8 out of 15 were non-responders, the chance of having only such cells in the sample is very small; *i.e*. $0.53^{10} \approx 0.002$, strengthening the argument that 1 µM was not high enough.

Compared to 10 µM 5-HT, the rate of desensitisation by 1 µM would be slowed. Therefore, if there were a significant contribution by desensitisation, when the smaller concentration of 1 µM was used, more cells with a frequency increase should have been detected. This was not seen, hence, suggesting that differential desensitisation was a very unlikely explanation for non-responders. This then leaves me to conclude that 1 µM was an insufficient concentration. This conclusion is in agreement with the study by Aghajanian and Marek (1997), which showed that 1 µM 5-HT was insufficient to increase sEPSC frequency in layer V pyramidal cells of neocortex and transitional cortex. One possible explanation for the lack of effect might be the breakdown of 5-HT by MAO A in the slice. I next checked if 100 µM were a saturating concentration.

3.4.2.5.2. 100 µM 5-HT

To address the issue of receptor saturation, an individual case exposed to 100 µM 5-HT is presented in Fig. 3.4.13. Here, the mEPSC frequency was 66 ± 1 Hz during the control period (A0). After the addition of 5-HT, the frequency increased by 55 ± 4% to 103 ± 2

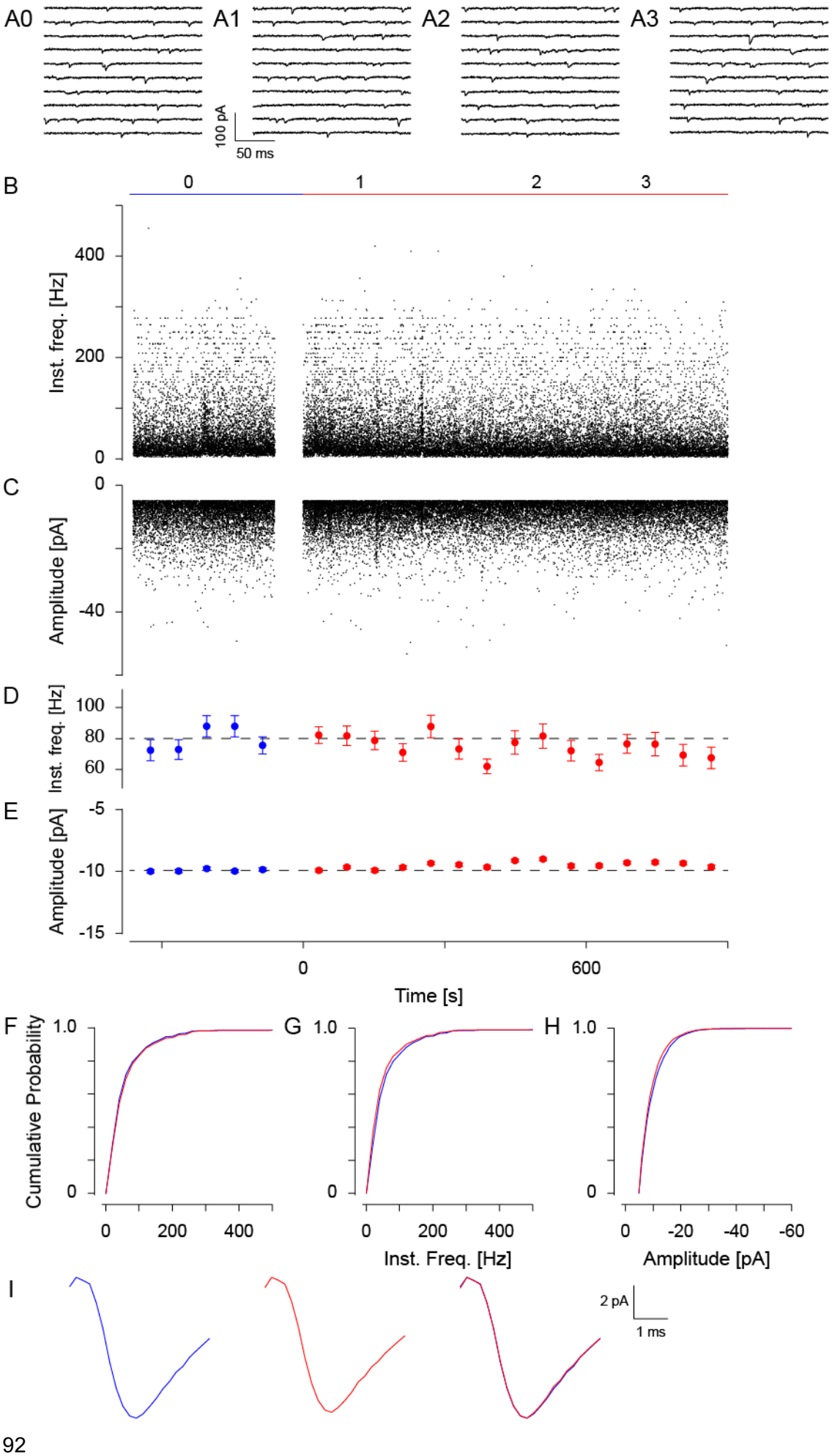
A0
A1
A2
A3
100 pA
50 ms
B
0
1
2
3
Inst. freq. [Hz]
400
200
0
C
Amplitude [pA]
0
-40
D
Inst. freq. [Hz]
100
80
60
E
Amplitude [pA]
-5
-10
-15
0
600
Time [s]
F
Cumulative Probability
1.0
0
0
200
400
G
1.0
0
0
200
400
Inst. Freq. [Hz]
H
1.0
0
0
-20
-40
-60
Amplitude [pA]
I
2 pA
1 ms

Figure 3.4.11. No mEPSC frequency increase with 1 µM 5-HT.

This figure was made in analogy to Fig. 3.4.5. The legend there also applies here with the exception that 1 µM 5-HT was used.

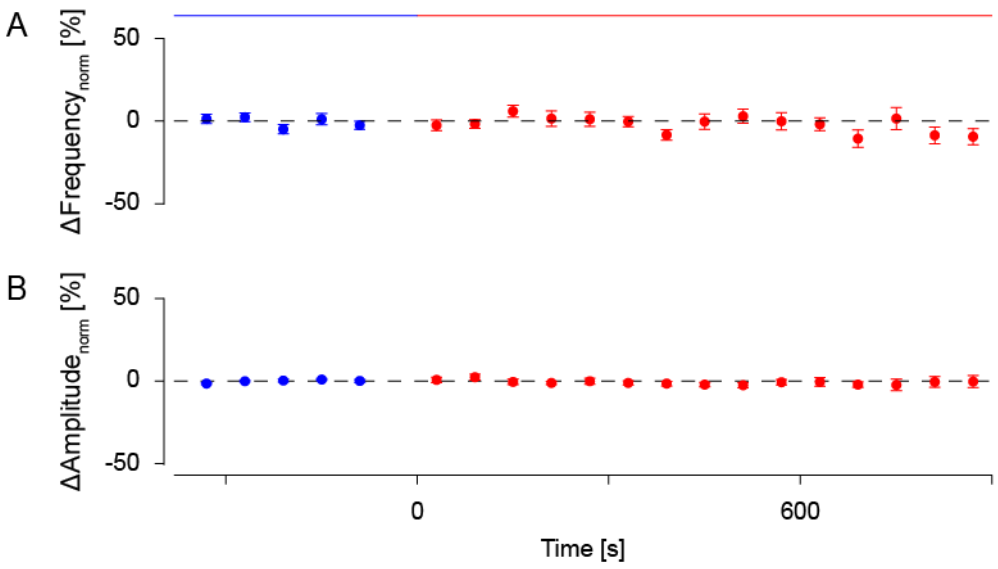

Figure 3.4.12. Outcomes with 1 µM 5-HT.

This figure was made in analogy to 3.4.6. The same legend applies here as well, except that 1 µM 5-HT was used.

Hz within 2 minutes after addition (A1 and F). As before, the initial increase was followed by a drop back to 71 ± 2 Hz after 6 minutes. The mEPSC frequency then resurged by 27 ± 4% back to 84 ± 2 Hz after 12 minutes (A3 and G). Towards the end of this recording, the frequency dropped back to 71 ± 2 Hz again, *i.e.* it approached the value during control but remained significantly different.

However, in this case, there was a decrease in mEPSC amplitude from -8.5 ± 0.1 to -7.8 ± 0.1 pA (E, and H). Despite the smaller amplitude, the average mEPSC time courses did not show any significant change (I, right). In addition, the average rise time and half-width also remained at the control values of 0.6 and 1.6 ms, respectively.

However, I only observed an mEPSC frequency increase in 1 out of the 10 cells studied. In the other 9 cells studied, the average frequency and amplitude together with the rise time and half-width remained at the control value of 66 ± 4 Hz, -10.0 ± 0.5 pA, 0.5 and 1.5 ms, respectively. However, this case illustrates that a lack of receptor saturation was unlikely the cause that gave rise to non-responders.

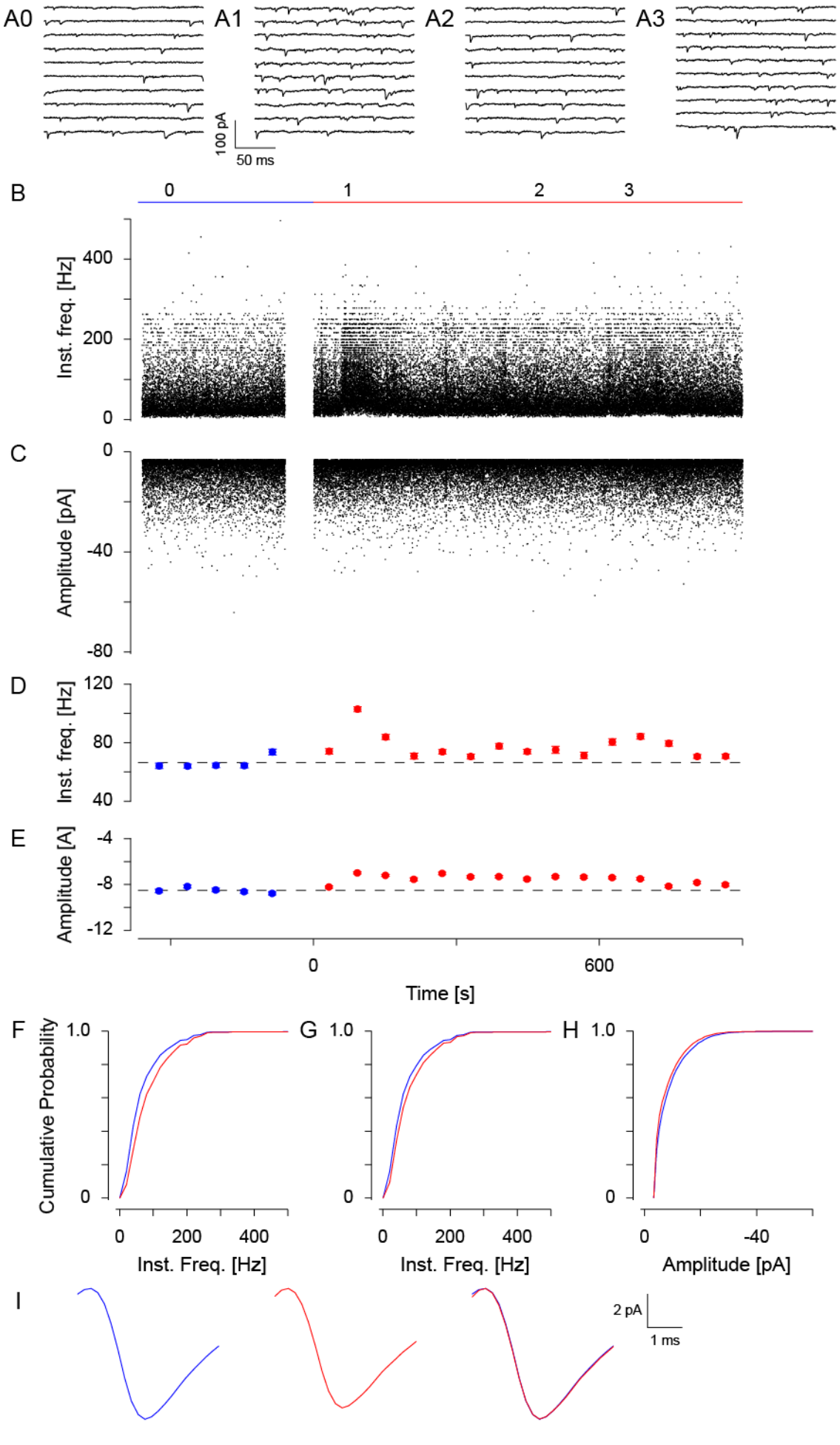
A0
A1
A2
A3
100 pA
50 ms
B
0
1
2
3
Inst. freq. [Hz]
400
200
0
C
Amplitude [pA]
0
-40
-80
D
Inst. freq. [Hz]
120
80
40
E
Amplitude [A]
-4
-8
-12
0
600
Time [s]
F
Cumulative Probability
1.0
0
0
200
400
Inst. Freq. [Hz]
G
1.0
0
0
200
400
Inst. Freq. [Hz]
H
1.0
0
0
-40
Amplitude [pA]
I
2 pA
1 ms

Figure 3.4.13. 100 µM 5-HT increased the mEPSC frequency.

This figure was made in analogy to Fig. 3.4.3. The legend there also applies to this figure except that in this case the exposure was to 100 µM 5-HT.

When the data from all 10 cells was pooled (Fig. 3.4.14), 100 µM 5-HT failed to increase the mEPSC frequency; *i.e*. there were minimal variations in the change in frequency (A), amplitude (B) and time course (not shown).

Based on a χ^2-test, the outcome for this sample was notably different to that seen with 10 µM 5-HT ($p_{\chi^2} = 0.05$). This could have been the case if I obtained a biased sample here. I, therefore, checked if this was the case. I found that the average values for frequency, amplitude, rise time, and half-width were not different from those reported for the set with 10 µM 5-HT. This then suggests that this sample was not biased – and therefore, when cells were exposed to 100 µM 5-HT, mostly no increase in mEPSC frequency was seen. This finding may most likely be explained by the fact that in contrast to 10, 100 µM 5-HT desensitized presynaptic receptors much more powerfully.

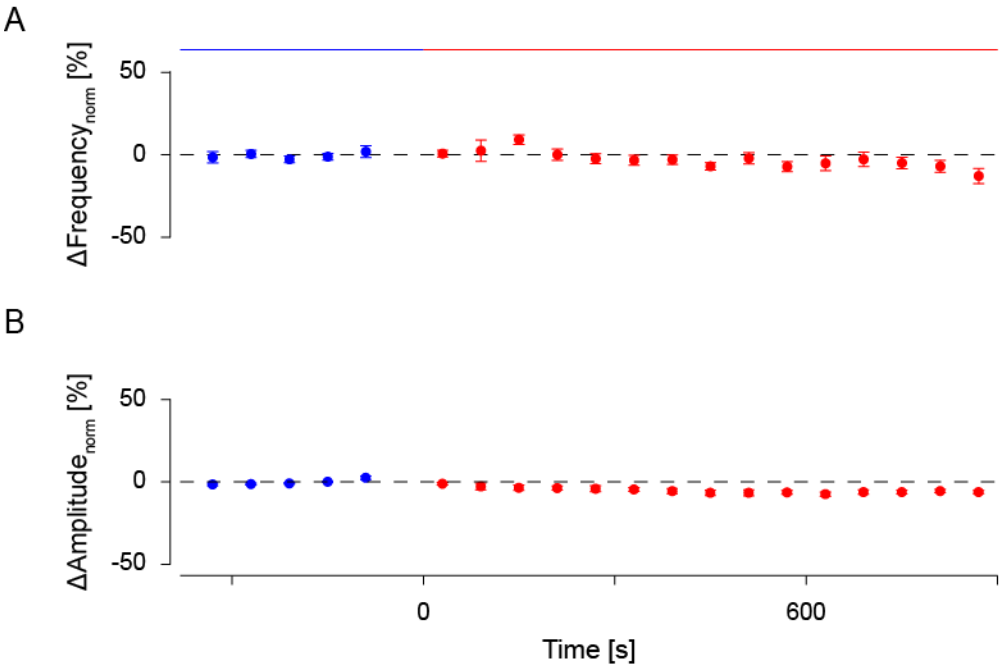

Figure 3.4.14. Pooled data for 100 µM 5-HT.

A. Minute averages of the instantaneous mEPSC frequency and B. amplitude for a data set of 10 recordings with 100 µM 5-HT. Dashed lines indicate the average values during the control period, which were normalized to 0%.

The observations just made suggest the following scenario in regard to the 5-HT concentration: 1 µM was insufficient to produce any increase mEPSC frequency. 10 µM showed the largest change; *i.e*. transient increases in mEPSC frequency occurred for responders. 100 µM, on average, did not show an increase in mEPSC frequency either, but it did result in an increase in just one case. Without wanting to attribute to much weight on this single observation, it may be that at 100 µM, the ratio between responders and non-responders becomes smaller.

3.4.2.6. Age-Dependence of mEPSC Frequency Increases

A further alternative explanation for the fact that 5-HT affected only a subset of cells may be that at the age of the animals used so far (P15 – 19), there is a rapid change in the sensitivity to 5-HT as a consequence of tissue maturation (development). Previous research has shown that the binding affinity of 5-HT to its receptor changes with age (Beique *et al.*, 2004a). Therefore, I checked if the increase in mEPSC frequency changed with age. Specifically, I performed mEPSC recordings in the tissue of animals of different ages: P9 – 12 (young) and P34 – 38 (older). These values were then compared to those of the standard age group (P15 – 19).

3.4.2.6.1. Young Animals (P9 – 12)

In comparison with the values found in the standard age bracket, these cells (n = 8) had a significantly more depolarized V_{rest} (-63.1 ± 1.6 *vs.* -76.6 ± 0.3 mV; $p_t = 10^{-4}$), larger τ_c (20.0 ± 0.9 *vs.* 12.7 ± 0.2 ms; $p_t = 2 \cdot 10^{-4}$), and higher R_{in} (344 ± 49 *vs.* 187 ± 6 mV; p_t = 0.02), but no difference was found in regard to R_s (14 ± 2 *vs.* 12 ± 0 MΩ; p_t = 0.17). For the action potential, H was smaller (66.4 ± 2.0 *vs.* 74.0 ± 0.4 mV; p_t = 0.009) but also V_{rel} (25.8 ± 1.6 *vs.* 38.6 ± 0.4 mV; $p_t = 10^{-4}$). No significant differences were observed for V_{thr} (-37.3 ± 1.1 *vs.* -38.0 ± 0.3 mV; p_t = 0.55) and W (1.1 ± 0.0 *vs.* 1.00 ± 0.01 ms; p_t = 0.051).

Regarding the mEPSC properties, the average instantaneous frequency was significantly smaller in young animals (36 ± 2 *vs.* 59 ± 1 Hz; $p_t = 4 \cdot 10^{-6}$). However, the average amplitude (-10.7 ± 1.3 *vs.* -9.5 ± 0.1 Hz; p_t = 0.39), rise time (0.5 *vs.* 0.5 ms; p_t = 0.91), and half-width (1.5 *vs.* 1.6 ms; p_t = 0.72) were not.

Despite differences in their electrophysiological properties, 10 µM 5-HT caused a similar response to that seen in the standard group. In Fig. 3.4.15, a typical recording from a young rat is presented. V_{rest} in this cell was -63.6 mV, R_{in} 158 MΩ, and R_s 17 MΩ. During the control period (A0), the mEPSC frequency was 42 ± 1 Hz. After the addition of 5-HT, it showed an initial rise by 51 ± 6% within the first minute (A1) to 63 ± 2 Hz (B, D, and F).

After 7 minutes, the frequency had dropped back to 42 ± 2 Hz; *i.e.* to the average during control condition (A2 and D). The frequency then resurged back to 157 ± 8% (107 ± 2 Hz, A3), to then drop again to 33 ± 2 Hz after 15 minutes, which was no different than the control value. This result shows that like in the "standard" tissue (P15 – 19), during the 15-minute recording period with 5-HT application, there were two cycles in which the mEPSC frequency waxed and waned, each lasting for about 3 – 4 minutes.

In this example, the addition of 5-HT also caused mEPSC amplitude to decrease significantly by 25 ± 1% from -8.9 ± 0.1 pA during control to -6.7 ± 0.1 pA after 5-HT (C, E, and H). The decrease occurred gradually within the first five minutes, and then persisted until the end of the recording.

The rise time and half-width of mEPSCs during the control period were 0.7 and 2.1 ms respectively. These values were not affected by addition of 5-HT, as the time course of the average mEPSC remained the same (I, right) throughout recording.

Out of a sample of 8 pyramidal cells studied in young rats, 4 cells showed transient increases after 5-HT application; *i.e.* were responders. Compared to the "standard" age group, this ratio was not significantly different (p_{χ^2} = 0.88).

As done in 3.4.2.3, I averaged the cells of this age group (Fig. 3.4.16, Table 3.4.2). I found that 10 µM 5-HT caused transient increases in the mEPSC frequency (p_{ANOVA} = $2 \cdot 10^{-5}$; A). Specifically, during the control period, the mEPSC frequency was 36 ± 2 Hz. Upon 5-HT exposure, there was an initial rise by 51 ± 9% to 54 ± 5 Hz within 1 – 6 minutes (phase 1; $p_{t\text{-Bon}}$ = 0.001). It then dropped back to 33 ± 3 Hz after 7 – 11 minutes, which was not significantly different from control (phase 2; $p_{t\text{-Bon}}$ = 0.21), different to what was presented for the standard age group, in which the frequency was smaller than control. Subsequently, the frequency resurged back to 86 ± 19% after 8 – 14 minutes (66 ± 8 Hz; phase 3; $p_{t\text{-Bon}}$ = 0.002). This value was no different to that during phase 1 ($p_{t\text{-Bon}}$ = 0.053).

In contrast to the frequency, the mEPSC amplitude significantly decreased after 5-HT exposure in 6 out of 8 cells. These 6 cells comprised 3 responders and non-responders. This indicates that the decrease in amplitude occurred in both, responders and non-responders. Since this significant decrease was only observed in young animals, but not in the "standard" group, a χ^2-test resulted in a highly significant difference (p_{χ^2} = 0.003).

On average, in all 8 cells studied, 10 µM 5-HT caused a significant decrease in mEPSC amplitude by 18 ± 5% from -10.7 ± 1.3 pA to -8.8 ± 1.2 pA (p_{pt} = 0.001; B). This decrease took ~5 minutes to be fully established. However, once established, the decrease was

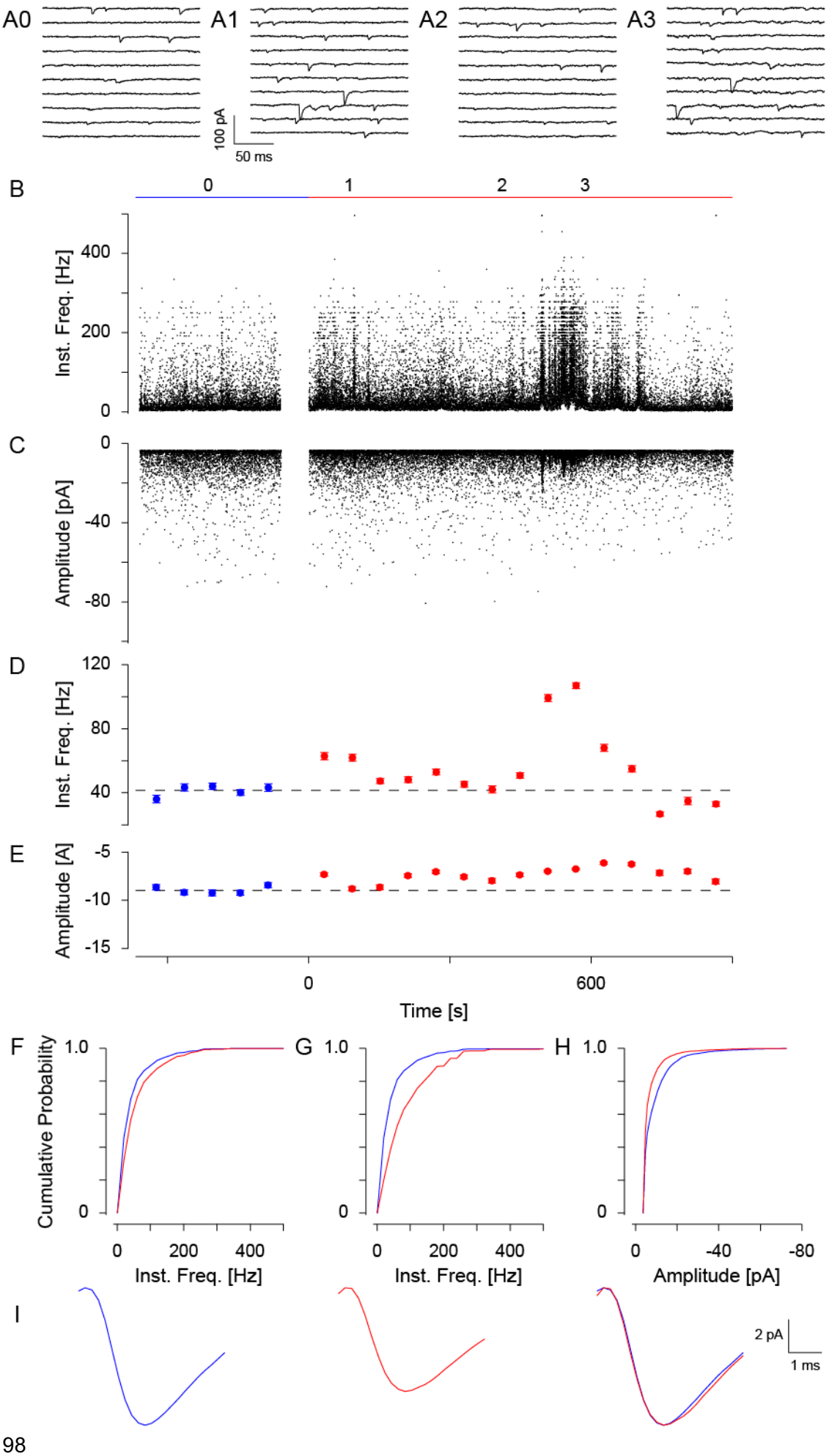
A0
A1
A2
A3
100 pA
50 ms
B
0
1
2
3
Inst. Freq. [Hz]
400
200
0
C
Amplitude [pA]
0
-40
-80
D
Inst. Freq. [Hz]
120
80
40
E
Amplitude [A]
-5
-10
-15
0
600
Time [s]
F
Cumulative Probability
1.0
0
0
200
400
Inst. Freq. [Hz]
G
1.0
0
0
200
400
Inst. Freq. [Hz]
H
1.0
0
0
-40
-80
Amplitude [pA]
I
2 pA
1 ms

Figure 3.4.15. In young animals, the mEPSC frequency increased.

This figure was made in analogy to Fig. 3.4.3. The legend there also applies to this figure except that in this case this cell was from the group of young animals after exposure to 10 µM 5-HT.

sustained for the remainder of the recording. When checked in the individual cells, however, the average time courses of mEPSCs before and after 5-HT remained the same. The average rise time and half-width remained at the control values of 0.5 and 1.5 ms, respectively.

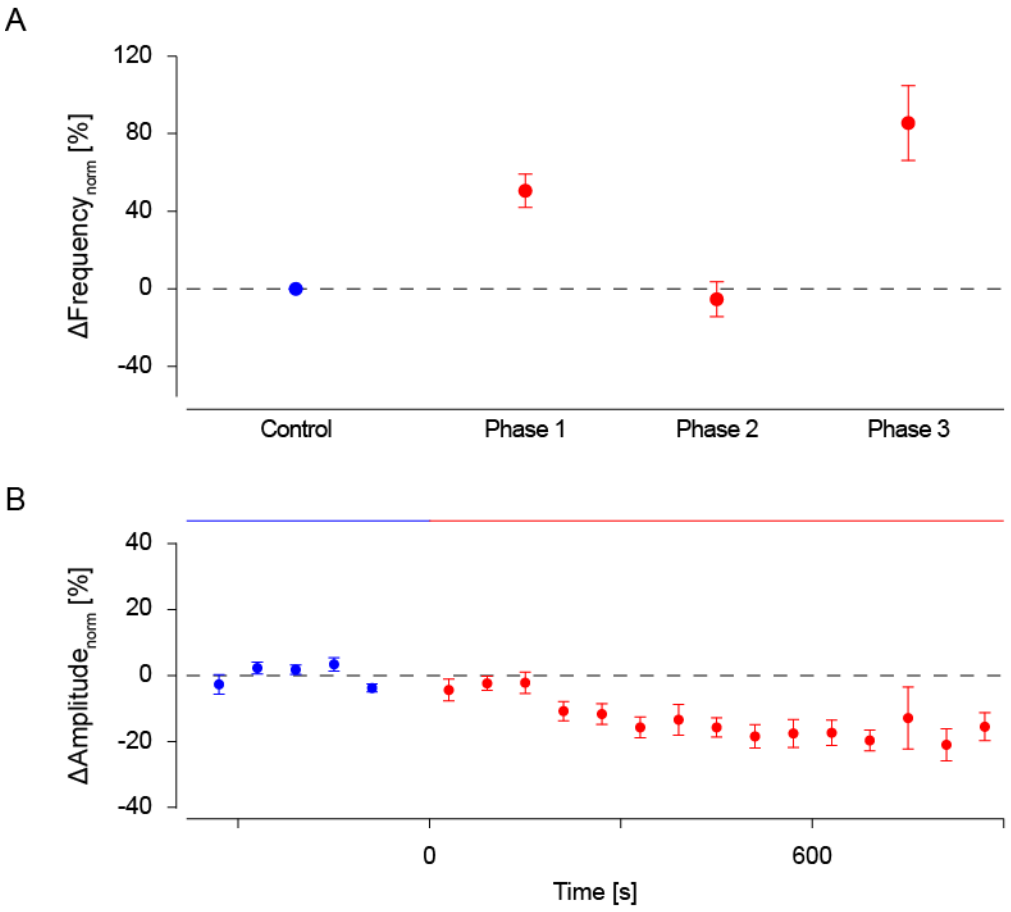

Figure 3.4.16. Pooled data from young animals.

Dashed lines indicate the average values during control period, which were normalized to 0%. A. Average relative changes of peak mEPSC frequencies during the different phases. B. Time course of the minute averages of the mEPSC amplitude throughout the recording.

I conclude that in the set with young animals, and similar to the “standard” age group, 10 µM 5-HT caused the observed increases in mEPSC frequency, but in addition, the amplitude became smaller.

Table 3.4.2. Comparisons of mEPSC frequencies in young animals.

Phases	Phase 1 1 – 6 min (54 ± 5 Hz)	Phase 2 7 – 11 min (33 ± 3 Hz)	Phase 3 8 – 14 min (66 ± 8 Hz)
Control (36 ± 2 Hz)	+51 ± 9% (0.001 **)	-5 ± 9% (0.21)	+86 ± 19% (0.002 *)
Phase 1 1 – 6 min (54 ± 5 Hz)		-36 ± 7% (0.002 *)	+23 ± 12% (0.053)
Phase 2 7 – 11 min (33 ± 3 Hz)			+99 ± 17% ($8 \cdot 10^{-4}$ **)

Significance level reached when comparing the different phases within the same group ($p_{ANOVA} = 2 \cdot 10^{-5}$ **; $n = 8$). Individual comparisons between two phases were further subject to a *t*-test with Bonferroni correction (* $p_{t\text{-}Bon} < 0.008$, ** $p_{t\text{-}Bon} < 0.002$). Phase 1 refers to the initial rise, phase 2 to the intermediate drop and phase 3 to the resurgence. Note that there are differences between all phases except between phases 1 and 3. Most comparisons were significant. There were no differences between control and phase 2, and likewise, between phases 1 and 3.

3.4.2.6.2. Older Animals (P34 – 38)

A typical recording is presented in Fig. 3.4.17, obtained from a cell of a 34 day-old rat. During the control period, the mEPSC frequency was 54 ± 1 Hz, amplitude -6.4 ± 0.1 pA, rise time 0.5 and half-width 1.3 ms. After the addition of 5-HT, both the frequency and the amplitude remained at 52 ± 1 Hz (B, D, F, and G) and -6.0 ± 0.1 pA (C, E, and H), respectively. The time courses of the average mEPSC in control and during last five minutes of 5-HT overlapped with each other (I, right) indicating no change.

Overall, in a set of 6 pyramidal cells from older rats (Fig. 3.4.18), no significant mEPSC frequency increases were detected after addition of 5-HT (A). The change in the average frequency varied around control after normalising to 0% (A). In fact, as there were no responders, this make-up of this set was markedly different from that in the standard group ($p_{\chi^2} = 0.04$).

At this age, the average pooled amplitude also remained at control -6.7 ± 0.3 pA. The values after normalising the control value to 0% are presented in B showing that in relative terms, they varied little around the control value. Likewise, the time course of average mEPSCs also remained unchanged, with an average rise time and half-width of 0.6 and 1.4 ms, respectively.

Comparing the results from the three different age groups, I found that the increases in the mEPSC frequency by 5-HT were most prominent in young animals (phase 1: 51 ± 9 *vs*. 28 ± 7% at standard age; p_t = 0.03; phase 3: 86 ± 19 *vs*. 27 ± 7%; p_t = 0.009), still pronounced in the standard age group, but absent in older animals. The make-up of the sets in regard to responders *vs*. non-responders in the young *vs.* standard sets were not different (p_{χ^2} = 0.88), suggesting that the two groups very unlikely arose as a consequence of a differential effect on 5-HTR affinity during development.

In addition, in 5-HT the mEPSC amplitude became smaller in young animals, but did not change in the other two age groups. This may suggest that the impact of 5-HT on (the dendritic) R_{in} in young animals is larger and therefore more current is lost between the synapse and the somatic recording electrode, making the mEPSC smaller.

3.4.2.7. sEPSC Frequency Not Affected by TTX

Aghajanian and Marek (1997) reported that there was an increase in sEPSC frequency in layer V pyramidal cells of rat prefrontal cortex only if TTX was omitted from the superfusate. This suggests that sodium electrogenesis was involved in the generation of sEPSCs. I, therefore, checked if the frequency increase by 5-HT in my preparation was sensitive to TTX. Therefore, in these recordings, TTX was omitted but gabazine retained in the superfusate. I wondered if this could change the ratio of responders *vs.* non-responders, and if the increase in sEPSC frequency would become sustained?

Recordings of sEPSCs were not without challenges, as each slice underwent epileptiform discharges numerous times. This was to due gabazine blocking $GABA_A$-mediated inhibition. As a consequence, the networks became disinhibited. In voltage-clamp, these epileptic activities were associated with massive inward currents (> -200 pA) that lasted for ~15 seconds. Such periods were easily recognised and excluded from the analysis (small gaps in Fig. 3.4.19). However, such epileptic discharges did not much affect the average sEPSC frequency and amplitude).

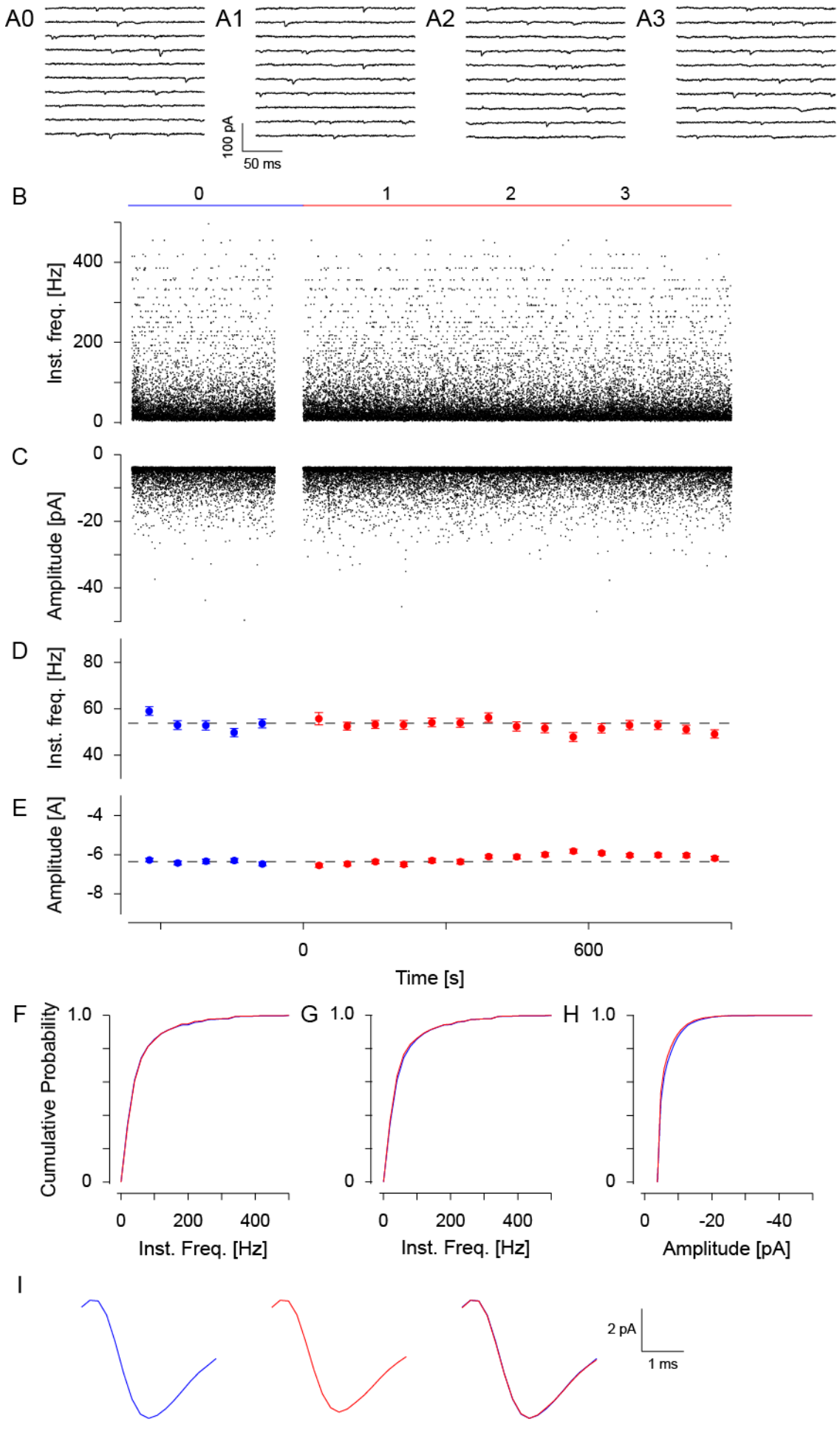
A0
A1
A2
A3
100 pA
50 ms
B
0
1
2
3
Inst. freq. [Hz]
400
200
0
C
Amplitude [pA]
0
-20
-40
D
Inst. freq. [Hz]
80
60
40
E
Amplitude [A]
-4
-6
-8
0
600
Time [s]
F
Cumulative Probability
1.0
0
0
200
400
Inst. Freq. [Hz]
G
1.0
0
0
200
400
Inst. Freq. [Hz]
H
1.0
0
0
-20
-40
Amplitude [pA]
I
2 pA
1 ms

Figure 3.4.17. No frequency increases in older animals.

This figure was made in analogy to Fig. 3.4.3. The legend there also applies to this figure except that in this case this cell was from the group of young animals after exposure to 10 µM 5-HT.

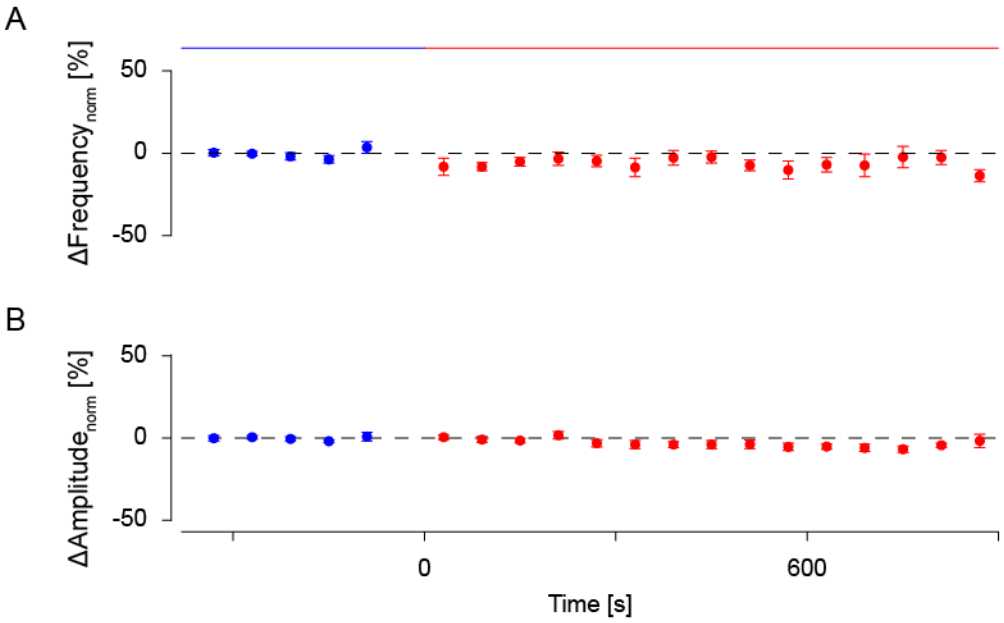

Figure 3.4.18. Pooled data from older animals.

This figure was made in analogy to Fig. 3.4.19. That legend also applies here with the difference that these recordings were obtained in cells from older animals.

In Fig. 3.4.19, data from the only responder is presented. During the control period, the instantaneous sEPSC frequency was 49 ± 2 Hz (A0). After addition of 5-HT, there was an initial rise by 28 ± 8% to 63 ± 3 Hz within 6 minutes (A1, B, D, and F). Compared to control, the frequency then dropped back by 13 ± 11% to 43 ± 5 Hz after 8 minutes (A2). Subsequently, it resurged back by 38 ± 10% from control around 9 minutes (68 ± 4 Hz; A3, B, D, and I). After 15 minutes, the frequency had dropped back to 55 ± 4 Hz. This time course, was very similar to that seen for the mEPSC frequency.

However, the absence of TTX affected the sEPSC amplitude differently than what has been reported (Aghajanian & Marek, 1997). During the control period, the sEPSC amplitude was -9.6 ± 0.1 pA. After 5-HT, the sEPSC amplitude increased by 110 ± 6% to -20.2 ± 0.5 pA within 6 minutes (A1, C, E, and G). The amplitude then decreased back to a value of -9.5 ± 0.2 pA after 8 minutes (A2), which was not different from control.

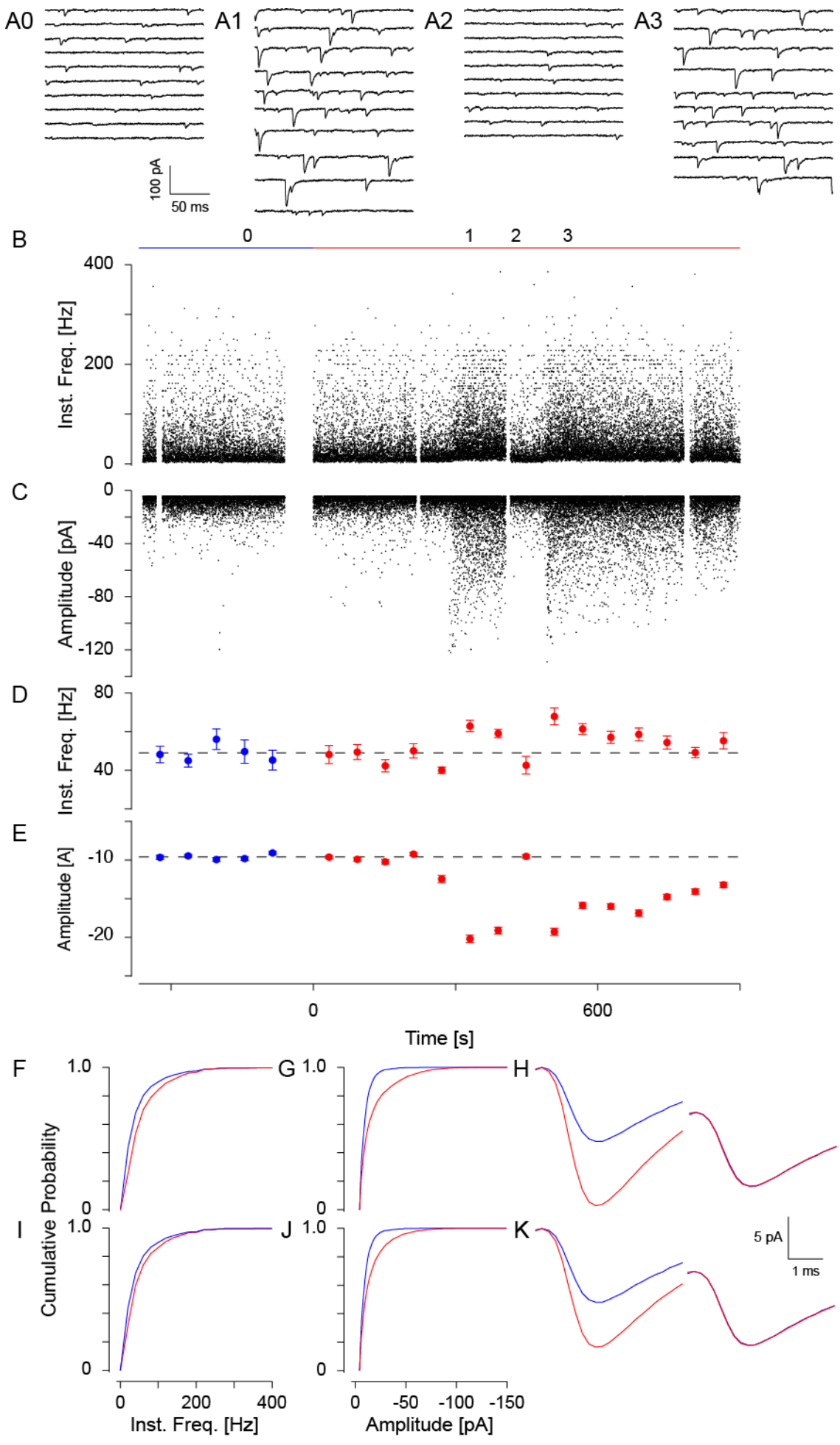
A0
A1
A2
A3
100 pA
50 ms
B
0
1
2
3
Inst. Freq. [Hz]
400
200
0
C
Amplitude [pA]
0
-40
-80
-120
D
Inst. Freq. [Hz]
80
40
E
Amplitude [A]
-10
-20
0
600
Time [s]
F
G
H
Cumulative Probability
1.0
0
I
J
K
0
200
400
Inst. Freq. [Hz]
0
-50
-100
-150
Amplitude [pA]
5 pA
1 ms

Figure 3.4.19. In the absence of TTX, both sEPSC frequency and amplitude increased in 5-HT.

A – E. This part of the figure was done in analogy to Fig. Fig. 3.4.3. The legend there also applies to this part of the figure except that in this case TTX was omitted from the superfusate to obtain sEPSCs. cPDFs of the instantaneous sEPSC frequency (F) and amplitude (G) during control (0) and the first increase (1). H. Time courses of the average sEPSC during control (0) and the first rise (1). The respective amplitudes were peak scaled for the control amplitude and overlaid for comparison. I – K. Same as in F – H, except that in this case, the control (0) was contrasted to the second increase (3).

Thereafter, the amplitude rose again by 101 ± 6% to -19.3 ± 0.5 pA after 9 minutes (A3, C, E, and J). After 15 minutes, the amplitude was still -13.2 ± 0.3 pA. Note that these increases in sEPSC amplitude were much larger than those reported for the frequency.

Despite significant increases in both sEPSC frequency and amplitude, 5-HT did not cause any significant change in the average sEPSC time course throughout the recording. This is indicated in both H and K (right) by the perfect overlay.

Of all 5 pyramidal cells studied, only 1 cell (Fig. 3.4.19) showed increase(s) in the sEPSC frequency after exposure to 5-HT. The ratio of responders *vs.* non-responders was not significantly different from that seen in mEPSC recordings (p_{χ^2} = 0.29). Not unexpectedly, the omission of TTX from superfusate did not influence the ratio of responders and non-responders. The large increases in sEPSC amplitude suggest that there is likely considerable local sodium electrogenesis in the respective presynaptic cells/axons, which may have resulted in synchronised transmitter release. However, neither APs nor spikelets were seen in the somatic (postsynaptic) recordings.

3.4.3. Differences between Responders and Non-Responders

Several lines of experiment (see 3.4.2.5 – 7) were designed to establish what gave rise to the groupings into responders and non-responders. To get further insight and increase the statistical power to the analyses, the data from the different lines of experiment were pooled. Data were pooled from all those experiments in which either 5-HT or a respective agonist was used. However, data from experiments, in which the downstream signalling was pharmacologically blocked, were excluded.

In 3.4.3.1, I will compare the synaptic parameters in both groups. This will be followed by comparisons of the properties of the postsynaptic membrane, the action potential, and firing patterns in 3.4.3.2. In 3.4.3.3, I will present the distinguishing features that

defined responders and non-responders. These characteristics will later be used in the context of evoked transmitter release (see 4.4.5).

3.4.3.1. No Difference in mEPSCs Properties

The pooling resulted in a data set comprising 36 responders and 68 non-responders. During the control period, for each cell, the noise standard deviation (σ_{noise}), average instantaneous mEPSC frequency, its amplitude, rise time, and half-width were determined. Averages of these parameters were then compared between responders and non-responders to see if these could serve as predictor(s) of the subsequent change in mEPSC frequency (Table 3.4.3).

There were no significant differences in any of the synaptic parameters determined. This outcome indicates that both, responders and non-responders, received a similar amount of spontaneous mEPSCs, and that there was no detectable difference in the make-up of the AMPA receptors (AMPAR) involved. As σ_{noise} and R_s were also not different suggests that this grouping did not artefactually arise as a consequence of a systematic bias during the recordings. This lends further support that the respective grouping is genuine.

Table 3.4.3. Synaptic parameters during control.

	Responders (n = 36)	**Non-Responders** (n = 68)	p_t
R_s [MΩ]	13 ± 1	13 ± 1	0.65
σ_{noise} [pA]	1.9 ± 0.1	1.9 ± 0.1	1.00
mEPSC frequency [Hz]	58 ± 2	60 ± 2	0.47
mEPSC amplitude [pA]	-9.3 ± 0.2	-9.8 ± 0.2	0.13
Rise time [ms]	0.5	0.5	0.14
Half-width [ms]	1.5	1.5	0.91

3.4.3.2. No Difference in Postsynaptic Properties

Given that there were no differences in the synaptic parameters investigated, I wondered if some postsynaptic parameters defined these groups. To evaluate this possibility, I determined the electrophysiological postsynaptic properties in this pooled set. These included V_{rest}, τ_c, R_{in}, V_{thr} of the AP, its H, W, and V_{rel} (see 3.3.5 for definition). The average values for both groups are presented in Table 3.4.4 including the respective

significance levels. Interestingly, there were no differences between responders and non-responders in any of the properties analysed.

Table 3.4.4. Passive and AP properties of responders & non-responders.

	Responders (n = 28)	**Non-Responders** (n = 61)	p_t
V_{rest} [mV]	-76.6 ± 0.6	-77.4 ± 0.4	0.29
τ_c [ms]	12.5 ± 0.4	12.8 ± 0.3	0.61
R_{in} [MΩ]	184 ± 14	183 ± 9	0.96
V_{thr} [mV]	-38.4 ± 1.1	-38.2 ± 0.6	0.85
H [mV]	75.5 ± 1.1	73.7 ± 0.8	0.17
W [ms]	1.0	1.0	0.60
V_{rel} [mV]	38.2 ± 1.1	39.2 ± 0.7	0.43

In addition, there was no difference in the firing pattern either (Fig. 3.4.20), with cells belonging to both groups spiking regularly upon a sufficiently large current step as described in 3.4.1.1.

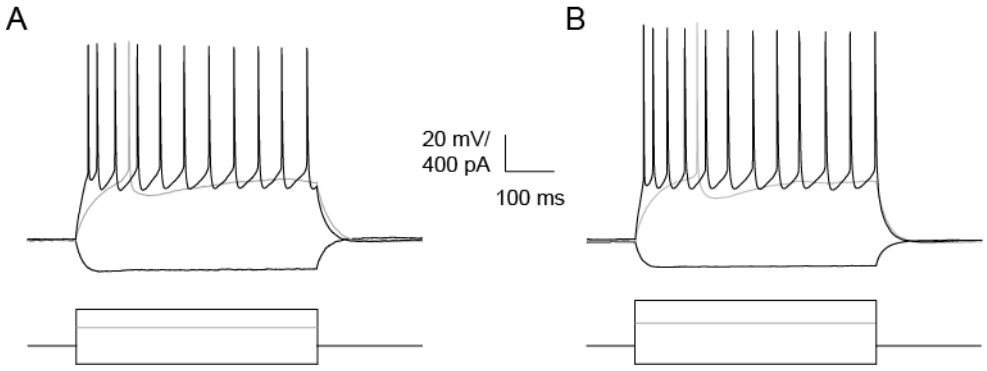

Figure 3.4.20. Firing patterns in responders (A) and non-responders (B).
Responses to a hyper- and two depolarizing current steps. The grey step and respective voltage change is for rheobase.

3.4.3.3. R_{in} Decreased in Both Responders and Non-Responders

Because 1 µM TTX was added to the superfusate to isolate mEPSCs, I was not able to characterize changes in the properties of the action potential and the resulting firing

pattern after the addition of 5-HT. However, I was able to monitor R_{in} throughout the recording. The comparisons of R_{in} and its change after the addition of 5-HT between the two groups are given in Table 3.4.5.

Table 3.4.5. R_{in} in responders *vs.* non-responders.

	R_{in} - Control [MΩ]	R_{in} - 5-HT [MΩ]	ΔR_{in} [MΩ]	p_{pt}
Responders (n = 36)	197 ± 15	141 ± 8	-56 ± 13	10^{-4} **
Non-Responders (n = 67)	191 ± 10	161 ± 7	-30 ± 11	0.004 **

In the pooled data set, 5-HT caused a significant drop in R_{in} in both groups (see also Fig. 3.4.21A later). Specifically, in responders, R_{in} decreased by 56 ± 13 from 197 ± 15 to 141 ± 8 MΩ ($p_{pt} = 10^{-4}$). As indicated, in non-responders, 5-HT also caused a drop in R_{in} by 30 ± 11 from 191 ± 10 to 161 ± 7 MΩ ($p_{pt} = 0.004$). However, in this case, the changes between the two groups were not, but close to significant ($p_t = 0.068$).

A reduction in R_{in} indicates that 5-HT caused the opening of ion channel(s). Previous research has indeed shown that 5-HT can open ion channel(s) which may result either in a de- or hyperpolarization (Andrade & Nicoll, 1987; Araneda & Andrade, 1991; Foehring *et al.*, 2002; Goodfellow *et al.*, 2009).

Because my recordings were made in voltage-clamp at a holding potential of -70 mV, this change in postsynaptic polarisation can be tracked by monitoring the holding current (I_{hold}). A decrease in holding current is caused by a net inward current, whilst an increase corresponds to a net outward current. I, therefore, checked the change in I_{hold} for both responders and non-responders.

Such changes in R_{in} and I_{hold} are illustrated in Fig. 3.4.21. In A, R_{in} is plotted for both responders (black) and non-responders (grey). The values before and after 5-HT application are joined by a dashed line. In B, the change in I_{hold} is presented for a responder. It corresponded to a net inward current of -36.1 pA, which started shortly after 5-HT addition and peaked around 9 minutes. However, not all responders showed a decrease in I_{hold}. Such an example is shown in C, where a small outward current of 18.4 pA is evident, which started 3 minutes after the addition of 5-HT and peaked around 5 minutes. Note that in both instances, the direction of the net in- and outward currents

persisted for the duration after exposure to 5-HT. For responders (n = 25), 10 cells showed a net inward current, whilst the remaining cells were associated with a small net outward current (E). On average, the change in I_{hold} was outward, with an amplitude of 6.3 ± 7.8 pA (F, right).

In contrast, non-responders (n = 51) typically showed a large outward current as shown in D. In this case, an outward current of 45.7 pA started 2 minutes after the addition of 5-HT, and peaked around 4 minutes later. Subsequently, the current gradually became smaller. Again, as above, the direction of the current remained for as long as the cell was exposed to 5-HT. In contrast, there were only 3 that were associated with a small net inward current. The remaining 48 cells showed a net outward current (E). On average, the change in I_{hold} was 34.4 ± 4.2 pA. The change in I_{hold} for non-responders was significantly larger than that for responders (p_t = 0.002; F, right). In addition, when the respective samples were compared using a χ^2-test, the two sets were different ($p_{\chi^2} = 2 \cdot 10^{-4}$), lending further support that the separation into two groups was justified.

To summarise, I found that responders and non-responders differed by the following characteristics. 1) Responders showed larger decrease in R_{in} than non-responders. 2) responders showed a much smaller net outward current, however, there was considerable variability in the current direction. 3) The number of responders showing a net inward current was significantly larger than that for non-responders. These differences will be discussed in more detail in the discussion. Further, in part 4, these characteristics will be further refined in the context of paired recordings to characterise the impact on evoked transmitter release.

3.4.4. 5-HTR Involvement

In this section, I will describe which type of 5-HTR caused the increase(s) in mEPSC frequency. For this purpose, I will present data from experiments using both agonists and antagonists. In addition, I will provide evidence that the transient increase in mEPSC frequency was a consequence of PKC activation, which most likely phosphorylated 5-$HT_{2A/C}$R. Note that the focus here is on the increases in mEPSC frequency, without much addressing the postsynaptic changes reported earlier.

3.4.4.1 5-HT_2R Activation Caused mEPSC Frequency Increase

I hypothesized that the significant transient increases in mEPSC frequency were caused by the activation of 5-HT_2R. I tested this hypothesis by using the pan-5-HT_2R agonist α-methyl-5-HT, which activates 5-HT_{2A} (pK_i = 6.1), 5-HT_{2B} (pK_i = 8.4), 5-HT_{2C}R (pK_i = 7.3)

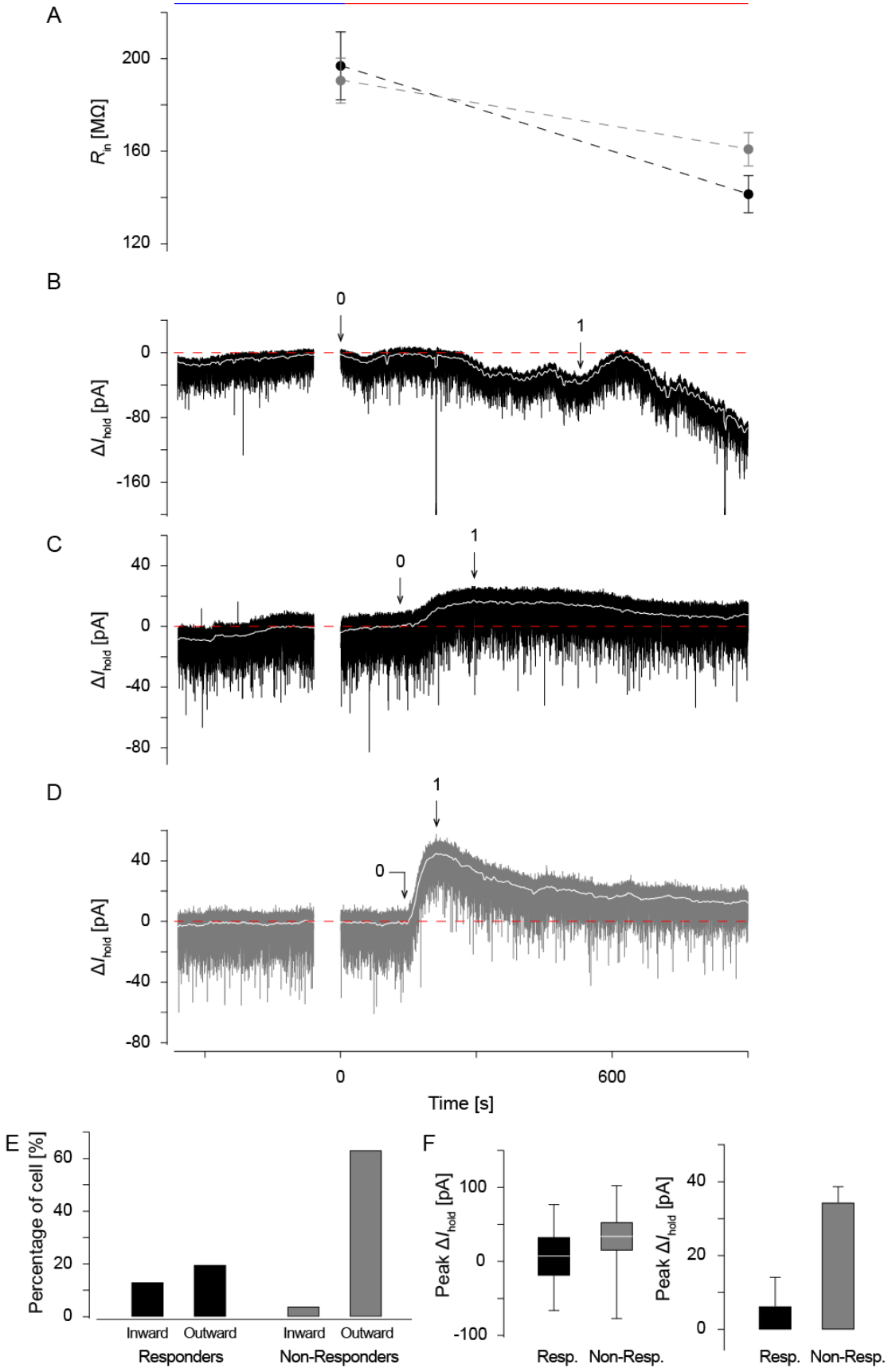
A
200
160
120
R_{in} [MΩ]
B
0
1
0
-80
-160
ΔI_{hold} [pA]
C
0
1
40
0
-40
-80
ΔI_{hold} [pA]
D
1
0
40
0
-40
-80
ΔI_{hold} [pA]
0
600
Time [s]
E
Percentage of cell [%]
60
40
20
0
Inward
Outward
Inward
Outward
Responders
Non-Responders
F
Peak ΔI_{hold} [pA]
100
0
-100
Resp.
Non-Resp.
Peak ΔI_{hold} [pA]
40
20
0
Resp.
Non-Resp.

Figure 3.4.21. Changes in R_{in} and I_{hold} in both groups.
Data from responders are in black, non-responders in grey. A. Values of R_{in} measured before 5-HT exposure and after the recording period plotted against time. Dashed lines join the respective values. B. Time course of the change in I_{hold}. 0 indicates the baseline value, and 1 the peak of the current. C. Time course of I_{hold} in a responder with a small outward current. D. Time course of I_{hold} in a non-responder with a large outward current. E. Make-up of the data set in regard to responders and non-responders showing either a net inward or outward current. F. Box and whisker plot showing the distribution of the peak holding currents for both groups (left), with the average respective current amplitudes (right).

at submicromolar concentrations (Baxter *et al.*, 1995). This agonist has been used in this context before (Zhou & Hablitz, 1999; Beique *et al.*, 2007). In accordance with the study by Zhou and Hablitz (1999), I chose a concentration of 20 µM.

The addition of 20 µM α-methyl-5-HT caused transient increases in the mEPSC frequency in a subset of cells. Fig. 3.4.22 shows an example of a responder. During the control period (A0), the frequency was 52 ± 1 Hz. After α-methyl-5-HT addition, within 2 minutes it increased by 67 ± 5% to 87 ± 2 Hz (A1, B, D, and F). Like for 5-HT, the frequency then dropped back to 48 ± 1 Hz after 8 minutes (A2), which was not different to the control value. Thereafter, it resurged by 108 ± 7% to 108 ± 3 Hz (A3, B, D, and G). This pattern was very similar to what was observed with 10 µM 5-HT.

The average mEPSC amplitude was -7.9 ± 0.1 pA during the control period. With the addition of α-methyl-5-HT, the amplitude gradually decreased by 13 ± 2% to -6.9 ± 0.1 pA (C and E) towards the end of recording. Although this decrease was significant (H), this was not commonly observed. In only 4 (2 responders and 2 non-responders) out of 18 cells was such a significant decrease observed. The average time course of the mEPSC did not change with this agonist either (I, right), as the average rise time remained 0.6 and the half-width 1.8 ms.

In a set of 18 such experiments, the addition of α-methyl-5-HT caused increases in the mEPSC frequency in 6 pyramidal cells. Comparing this result with that using the physiological agonist 5-HT revealed that this set was not significantly different in regard to the number of responders and non-responders (p_{χ^2} = 0.44).

The average values from all 18 cells are presented in Fig. 3.4.23. In A, the respective values are shown for the different phases. I found that α-methyl-5-HT still caused transient increases in the mEPSC frequency ($p_{ANOVA} = 10^{-12}$). During the control period, the average mEPSC frequency was 56 ± 3 Hz. This number served for the subsequent

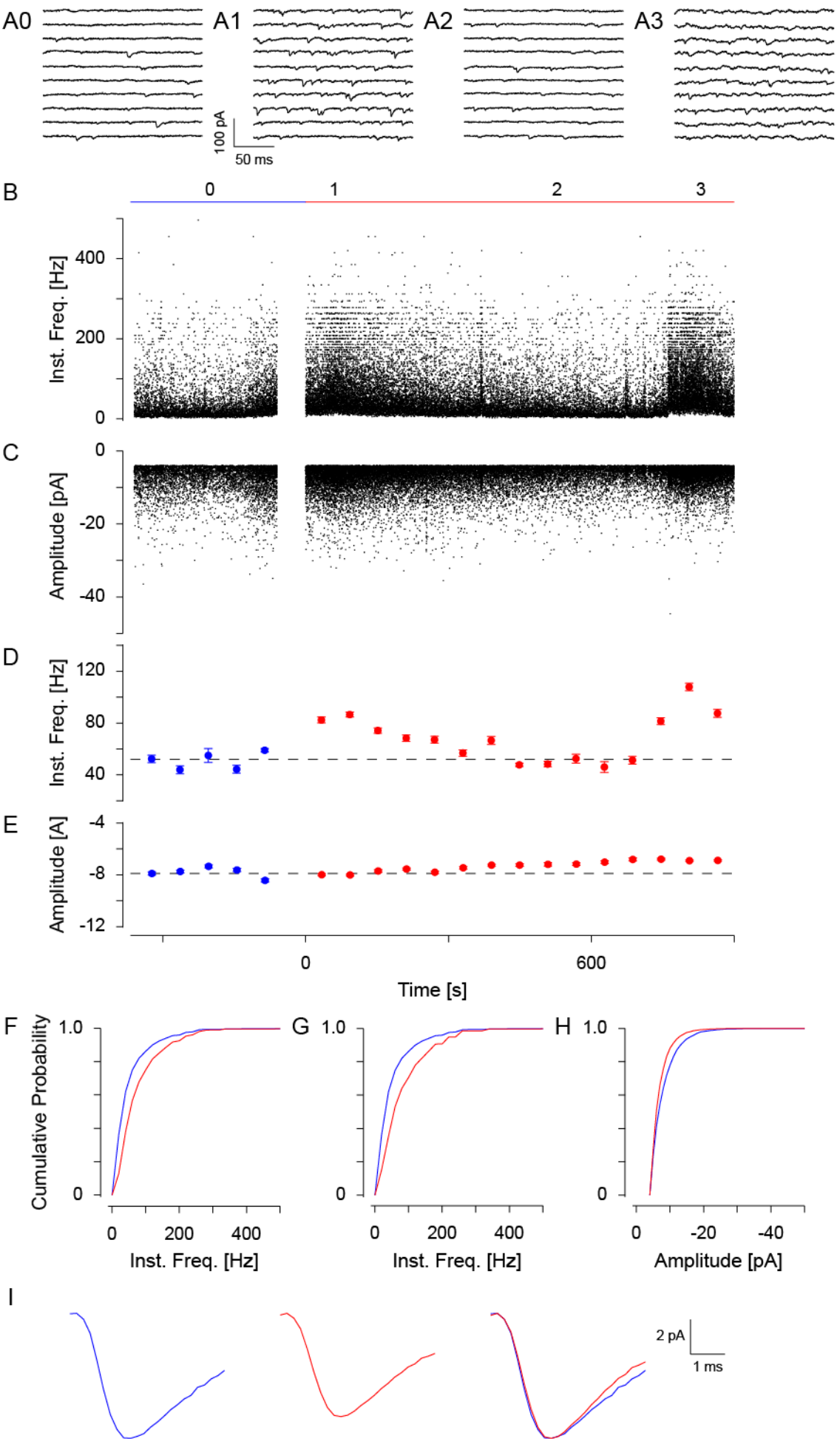
A0
A1
A2
A3
100 pA
50 ms
B
0
1
2
3
Inst. Freq. [Hz]
400
200
0
C
Amplitude [pA]
0
-20
-40
D
Inst. Freq. [Hz]
120
80
40
E
Amplitude [A]
-4
-8
-12
0
600
Time [s]
F
Cumulative Probability
1.0
0
0
200
400
Inst. Freq. [Hz]
G
1.0
0
0
200
400
Inst. Freq. [Hz]
H
1.0
0
0
-20
-40
Amplitude [pA]
I
2 pA
1 ms

Figure 3.4.22. α-Methyl-5-HT mimicked the action of 5-HT.
This figure was made in analogy to Fig. 3.4.3. The legend there also applies to this figure except that in this case this cell exposed to 20 µM α-methyl-5-HT.

normalisation. Upon addition of α-methyl-5-HT, the frequency increased by 21 ± 4% to 68 ± 3 Hz within 1 – 4 minutes (phase 1; $p_{t\text{-}Bon} = 10^{-5}$). It then dropped back by -21 ± 4% to 45 ± 3 Hz after 7 – 11 minutes (phase 2; $p_{t\text{-}Bon} = 2{\cdot}10^{-5}$). Thereafter, the frequency resurged back to 23 ± 7% (68 ± 4 Hz; phase 3; $p_{t\text{-}Bon} = 0.003$). Details of the respective comparisons are given in Table 3.4.6.

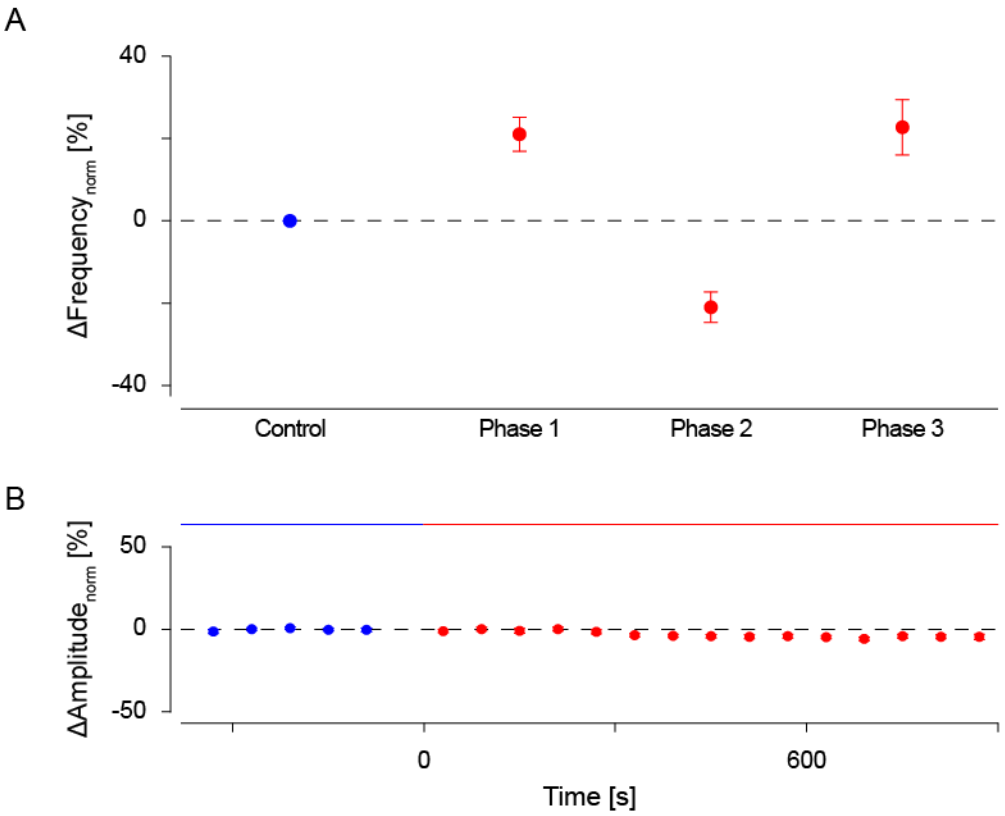

Figure 3.4.23. Pooled data set with α-methyl-5-HT.
This figure was made in analogy to Fig. 3.4.16. The legend there also applies to this figure except that in this case the cells were exposed to 20 µM α-methyl-5-HT.

On average, α-methyl-5-HT did not cause any significant change in the average mEPSC amplitude, as it remained close to the control value of -9.4 ± 0.3 pA (B). In addition, the respective average mEPSC time courses of did not show any significant changes from control either, with both the rise times and half-widths remaining at control values. Again, this is very much as that observed with 5-HT.

To check if the changes in frequency were quantitatively not different from those seen with 5-HT (see 3.4.2.3), I performed comparisons of the respective phases from the two data sets. I found no significant differences (control p_t = 0.33, phase 1 p_t = 0.36, phase 2 p_t = 0.25, and phase 3 p_t = 0.67). This data, showing mimicry of 5-HT's effects by a 5-HT_2R agonist, is consistent with the increases in the instantaneous mEPSC frequency being due to 5-HT_2R activation.

Table 3.4.6. mEPSC frequency increase by α-methyl-5-HT.

Phases	Phase 1 1 – 4 min (68 ± 3 Hz)	Phase 2 7 – 11 min (45 ± 3 Hz)	Phase 3 9 – 15 min (68 ± 4 Hz)
Control (57 ± 3 Hz)	+21 ± 4% (10^{-5} **)	-21 ± 4% ($2\cdot10^{-5}$ **)	+23 ± 7% (0.003*)
Phase 1 1 – 4 min (68 ± 3 Hz)		-34 ± 3 % ($5\cdot10^{-9}$ **)	+1 ± 4% (0.49)
Phase 2 7 – 11 min (45 ± 3 Hz)			+58 ± 9% ($3\cdot10^{-7}$ **)

Significance level reached when comparing the different phases within the same group (p_{ANOVA} = 10^{-12} **; n = 18). Individual comparisons between two phases were further subject to a t-test with Bonferroni correction (* $p_{t\text{-}Bon}$ < 0.008, ** $p_{t\text{-}Bon}$ < 0.002). Phase 1 refers to the initial rise, phase 2 to the intermediate drop and phase 3 to the resurgence. Note that there are significant differences between all phases except between phases 1 and 3.

To strengthen this argument further, I also used another pan-5-HT_2R agonist, namely DOB. Although DOB is classically considered a partial agonist at 5-HT_{2A}R and 5-HT_{2C}R (Arvanov *et al.*, 1999), a more recent study shows that DOB is actually an agonist for all 5-HT_{2A}R, 5-HT_{2B}R and for 5-HT_{2C}R with K_d values of 23.1, 3.9, and 41.5 nM, respectively (Ray, 2010). Because DOB has K_d values of 2550, 940.7, 635.5, and 1427 nM for 5-HT_{1A}R, 5-HT_{1B}R, 5-HT_{1D}R, and 5-HT_{1E}R, respectively (Ray, 2010), I chose a concentration of 1 µM to sufficiently activate 5-HT_2R whilst minimizing and/or avoiding activation of 5-HT_1R.

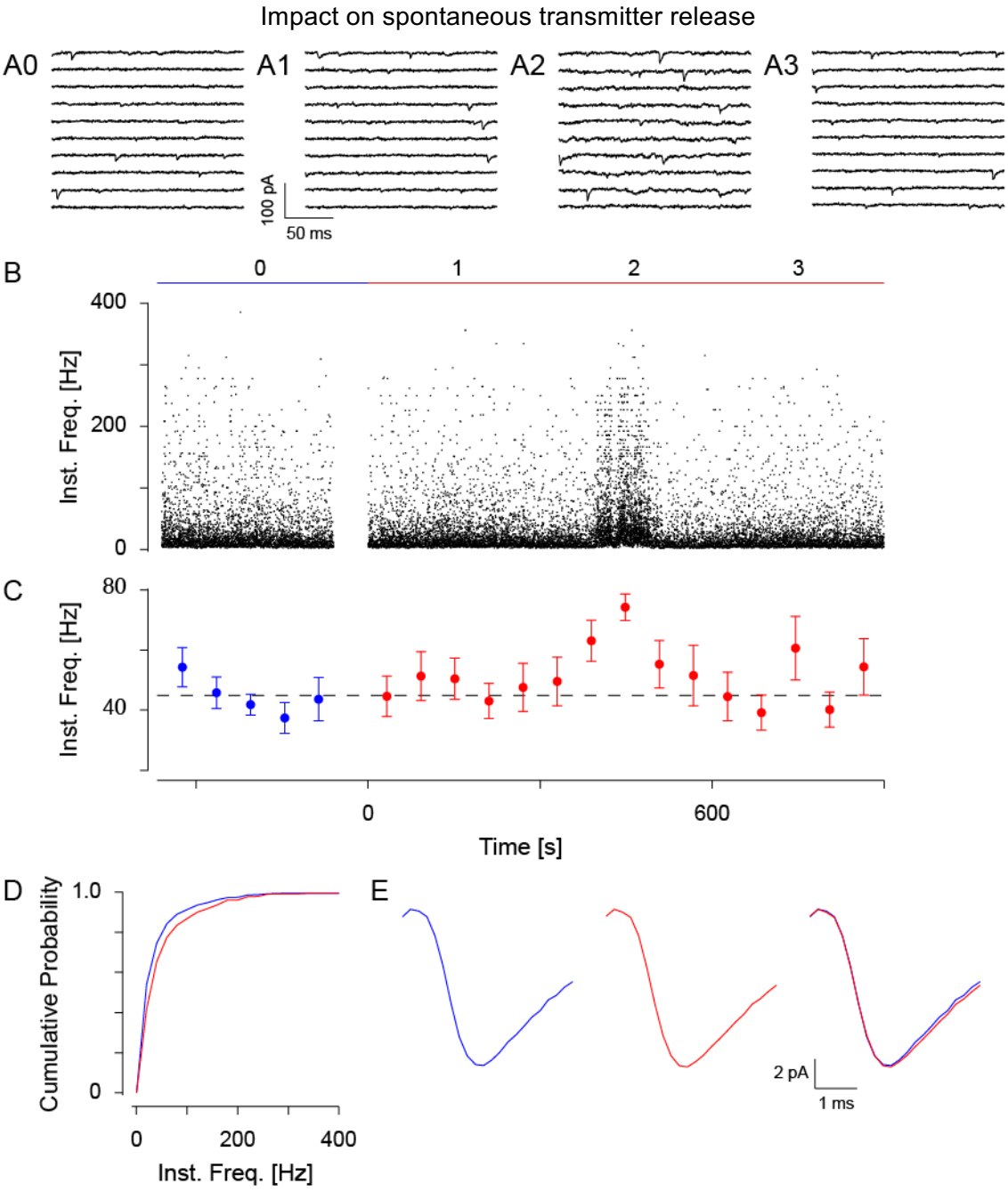

Figure 3.4.24. DOB, another 5-HT$_2$ agonist, increased mEPSC frequency.
This figure was made in analogy to Fig. 3.4.3. except that here the cell was exposed to DOB. In addition, all aspects in regard to mEPSC amplitudes were dropped here (C and E in that figure), and only one set of cPDFs is shown in D. E here corresponds to I in that figure.

In Fig. 3.4.24, the data of a responder exposed to 1 µM DOB is presented. The mEPSC frequency during control period was 45 ± 2 Hz (A0). After DOB was added to the superfusate, the frequency started to rise with a delay of 7 minutes (A1) and increased by 65 ± 12% to 74 ± 4 Hz (B, C, and D). The frequency then gradually decreased back to 45 ± 8 Hz within 11 minutes, which was not different to the control period (A3).

Consequently, in this case, the frequency only increased once, in contrast to what was seen with 5-HT and α-methyl-5-HT.

There was no significant change to the mEPSC amplitude which remained at the control value (11.1 ± 0.1 *vs*. -11.2 ± 0.2 pA). Likewise, the average mEPSC time course did not change either (E, right), with the average rise time and half-width also remaining at the control values (0.5 and 1.6 ms, respectively).

Of the 6 cells exposed to DOB, there were 2 cells, for which an increase in the mEPSC frequency was observed. Again, the outcomes in regard to responders and non-responders were not different to that with 5-HT (p_{χ^2} = 0.58) or α-methyl-5-HT (p_{χ^2} = 1.00).

The two data sets for α-methyl-5-HT and DOB showed that both agonists increased the instantaneous mEPSC frequency. This observation then is consistent with an involvement of 5-HT_2R. Furthermore, as there was no difference between what was observed with 5-HT and α-methyl-5-HT, the latter is a full agonist at 5-HT_2R. Notably, though, the outcomes with DOB were slightly different from those with 5-HT. The respective frequency increase was delayed and observed only once during the length of the recordings. This may suggest that DOB might not cause the same signalling as 5-HT downstream of 5-HT_2R activation.

3.4.4.2. Block of 5-HT_{2A}R with 4F 4PP

As 5-HT_2R activation caused the increases in the mEPSC frequency, the question arises as to which subtype(s) is/are involved. Several studies have identified 5-HT_{2A}R as the subtype that causes the sEPSC frequency increase in layer V pyramidal cell of rat prefrontal cortex (Aghajanian & Marek, 1999; Marek & Aghajanian, 1999; Zhou & Hablitz, 1999; Beique *et al.*, 2007). In addition, there is evidence that 5-HT_{2A}R are expressed presynaptically in the neocortex (Jakab & Goldman-Rakic, 1998), including in layer II of the somatosensory cortex (Lidow *et al.*, 1989). I therefore tested if the mEPSC frequency increases in my preparation were caused by the activation of the 5-HT_{2A}R.

I aimed to selectively block the 5-HT_{2A}R without affecting other 5-HT_2R subtypes. For this purpose, 4F 4PP was added to the superfusate before 5-HT. 4F 4PP is an antagonist with high affinity for the 5-HT_{2A}R (K_i = 5.3 nM), but much lower affinity for the 5-HT_{2C}R (K_i = 620 nM; Herndon *et al.*, 1992). In electrophysiological recordings, the IC_{50} for 4F 4PP at the 5-HT_{2A}R was 84 nM, but 17.14 µM at 5-HT_{2C}R (Acuna-Castillo *et al.*, 2002). Therefore, I chose a concentration of 200 nM for 4F 4PP.

In Fig. 3.4.25, a typical recording is presented. 4F 4PP was added to the superfusate more than 10 minutes before and remained so even when 5-HT was added at t = 0 s. During the control period (*i.e*. with TTX, gabazine, and 4F 4PP present), the mEPSC frequency was 53 ± 2 Hz (A0). After the addition of 5-HT, the frequency increased transiently by 51 ± 13% to 80 ± 6 Hz within the first minute (A1, B, D, and F). After 11 minutes, the frequency had dropped back to control values (51 ± 3 Hz). Thereafter. No significant increases were seen (A2 and G).

The mEPSC amplitude did not show any significant change throughout recording, with it remained at -7.4 ± 0.1 pA (C, E, and H). In addition, there was no change in the time course of the average mEPSC (I), and the average rise time and half-width of mEPSC remained at 0.6 and 1.6 ms, respectively.

Out of a set of 13 cells, despite the presence of 4F 4PP, 6 cells still showed a significant increase after 5-HT addition. In comparison with the data set for 5-HT, the number of responders/non-responders was not different (p_{χ^2} = 0.98). Note that only one transient increase was observed.

Pooling of data from all 13 cells is presented in Fig. 3.4.26. I found that 4F 4PP did not have significant effect on the frequency during control (60 ± 3 *vs.* 53 ± 3; p_t = 0.12) suggesting that it did not have an unwanted effect on the mEPSC frequency. Upon 5-HT exposure and in the presence of 4F 4PP (A), the average frequency increased by 25 ± 4% to 75 ± 4 Hz within 1 – 4 minutes ($p_{pt} = 2 \cdot 10^{-6}$). This transient increase, which lasted for 5 – 6 minutes, was the only significant increase observed throughout the 15 minutes of exposure to 5-HT.

In keeping with previous observations, the average mEPSC amplitude did not show any significant change; it remained at the control value of -9.8 ± 0.4 pA (normalized in B). For each cell, the average time course of the mEPSC remained the same. The average changes for R_{in} and I_{hold} were -62 ± 18 MΩ (p_{pt} = 0.006) and 49.4 ± 9.8 pA ($p_{pt} = 3 \cdot 10^{-4}$) respectively, providing further support that 5-HT could still activate the respective conductance to cause a hyperpolarisation.

I found that blocking 5-HT_{2A}R with 4F 4PP neither altered the ratio of responders and non-responders nor did it affect the peak of the frequency change (28 ± 7 *vs.* 25 ± 4%; p_t = 0.70). I note that only one increase was seen compared to that with 5-HT. Therefore, I conclude that 5-HT_{2A}R have a negligible effect on the initial increase in mEPSC frequency by 5-HT, but may contribute to the later phases of the mEPSC frequency.

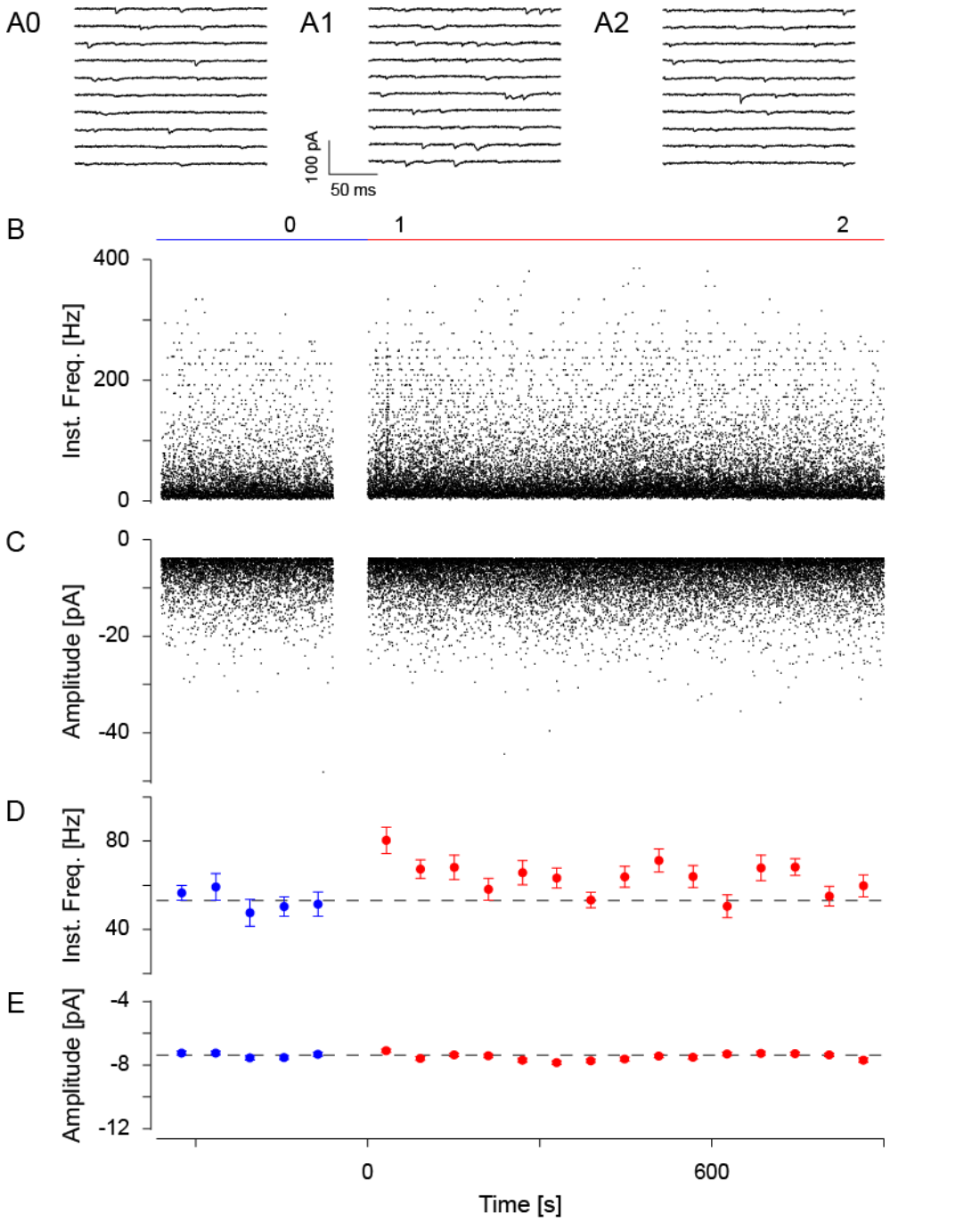
A0
A1
A2
100 pA
50 ms
B
0
1
2
Inst. Freq. [Hz]
400
200
0
C
Amplitude [pA]
0
-20
-40
D
Inst. Freq. [Hz]
80
40
E
Amplitude [pA]
-4
-8
-12
0
600
Time [s]
F
Cumulative Probability
1.0
0
0
200
400
Inst. Freq. [Hz]
G
1.0
0
0
200
400
Inst. Freq. [Hz]
H
1.0
0
0
-20
-40
Amplitude [pA]
I
2 pA
1 ms

Figure 3.4.25. 4F 4PP failed to block the mEPSC frequency increase.
This figure was made in analogy to Fig. 3.4.3. The legend there also applies to this figure except that in this case this cell exposed to 200 nM 4F 4PP before and when 5-HT was added at *t* = 0.

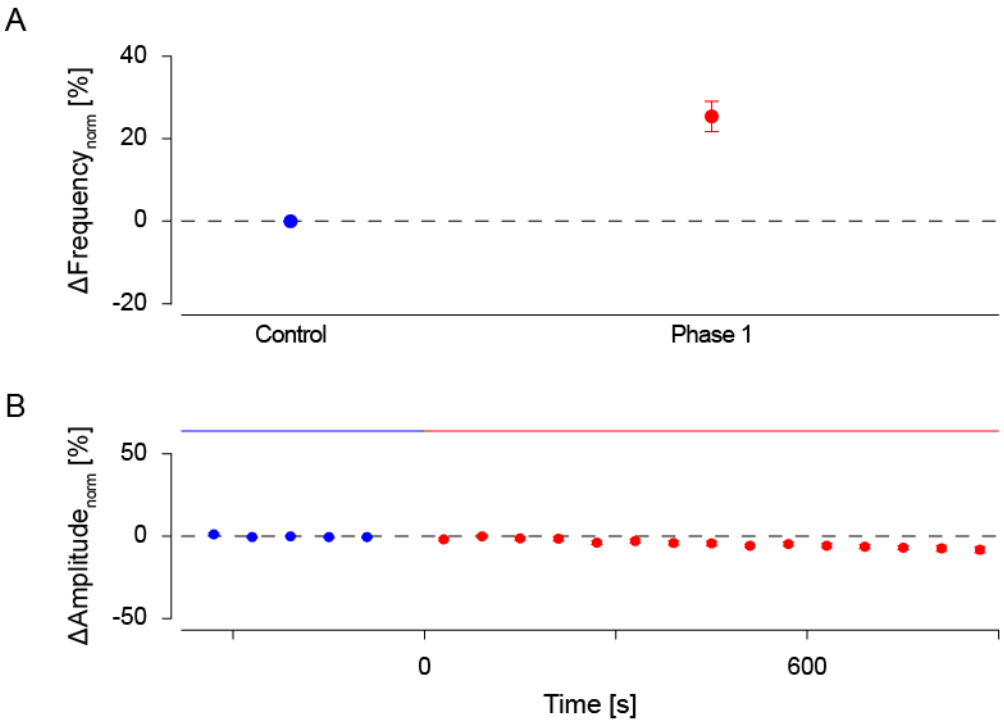

Figure 3.4.26. Pooled data when 5-HT$_{2A}$R were blocked with 4F 4PP.
This figure was made in analogy to Fig. 3.4.16. The legend there also applies to this figure except that in this case the cells were exposed to 200 nM 4F 4PP throughout. At *t* = 0, 10 µM 5-HT was added. Note that there was only one significant increase.

3.4.4.3. Block of 5-HT$_{2C}$R with RS 102221

Regarding the expression of 5-HT$_{2B}$R, its presence in rat brain remains a matter of debate. Although Kursar *et al.* (1994) showed that mRNA of the 5-HT$_{2B}$R was not significantly expressed in rat brain, Duxon *et al.* (1997) showed immunohistochemical evidence of 5-HT$_{2B}$R expression in the rat cerebellum, medial amygdala, lateral septum, and the dorsal hypothalamus. However, to this date, not much evidence has been presented in regard to the expression of 5-HT$_{2B}$R in rat neocortex, especially in the somatosensory cortex. Faint expression may be found on glial cells (Sandén *et al.*, 2000).

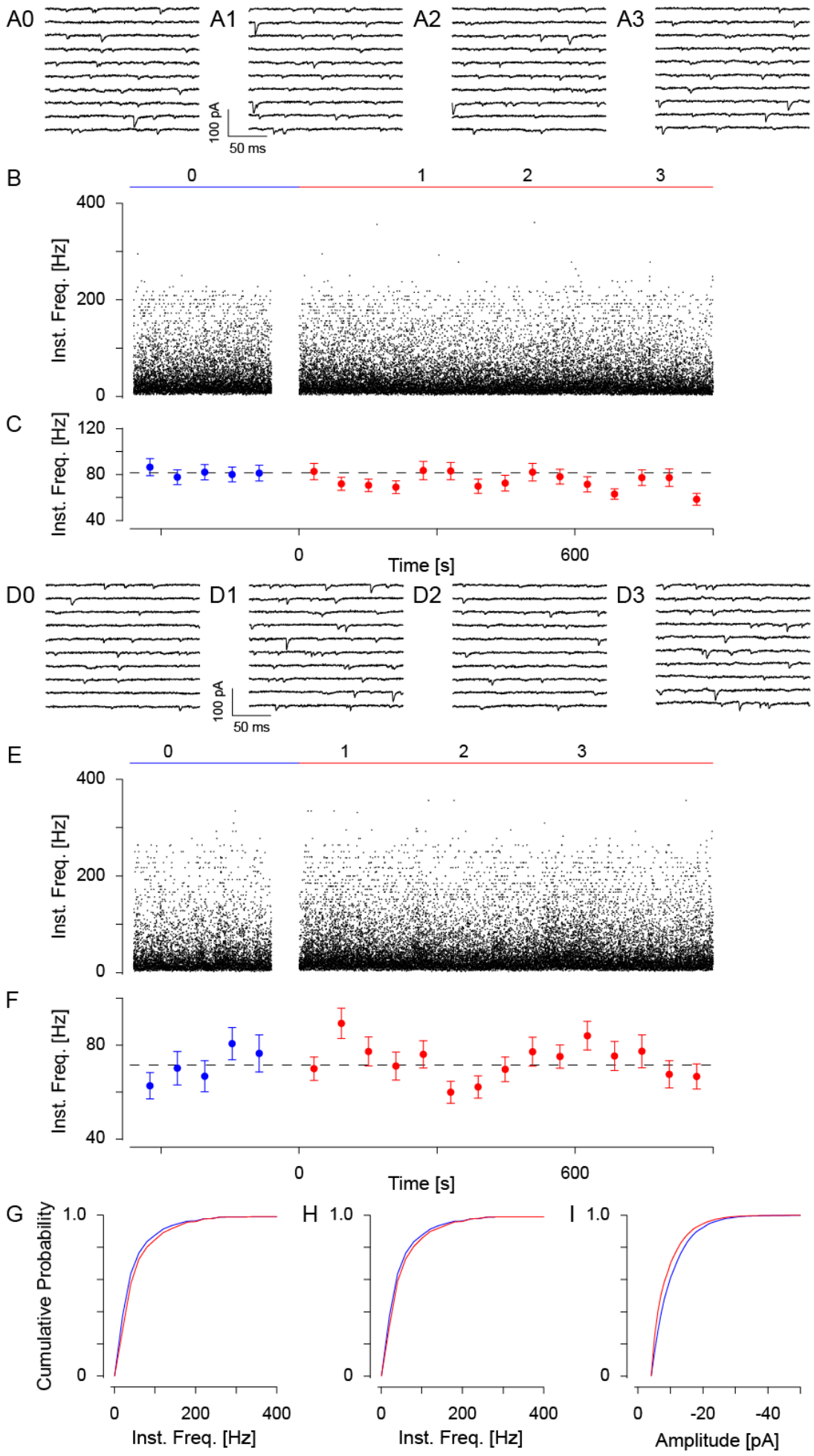
A0
A1
A2
A3
100 pA
50 ms
B
0
1
2
3
400
200
0
Inst. Freq. [Hz]
C
120
80
40
Inst. Freq. [Hz]
0
600
Time [s]
D0
D1
D2
D3
100 pA
50 ms
E
0
1
2
3
400
200
0
Inst. Freq. [Hz]
F
80
40
Inst. Freq. [Hz]
0
600
Time [s]
G
H
I
Cumulative Probability
1.0
0
0
200
400
Inst. Freq. [Hz]
0
-20
-40
Amplitude [pA]

Figure 3.4.27. RS 102221 blocked the mEPSC frequency increase.

A – C for a non-responder; D – G for a responder. A. Representative traces of mEPSCs during the control period (A0) and after addition of 5-HT (A1 – 3) at different time points indicated in B with numbers 0 – 3. B. Time course of all instantaneous mEPSC frequencies. C. Minute averages of the mEPSC frequency. Dashed line indicates the average frequency during the control period. D – I were made in analogy to parts A - C. F. cPDFs of the mEPSC frequencies during control (0) and at point 1. G, H. Same as F, except for comparison with 3 and the last five minutes.

In contrast, the 5-HT_{2C}R (formerly known as 5-HT_{1C}R) is not only highly expressed in the choroid plexus, but also in human and rat cerebral neocortex (Hoyer *et al.*, 1986b; Pazos *et al.*, 1987; Mengod *et al.*, 1990; Abramowski *et al.*, 1995; Nocjar *et al.*, 2015). Hence, the 5-HT_{2C}R is another likely candidate to be tested with an antagonist.

I tested the involvement of the 5-HT_{2C}R using RS 102221, an antagonist having a ~50-fold increased selectivity over 5-HT_{2A}R (Bonhaus *et al.*, 1997). In electrophysiological recordings, the IC_{50} at 5-HT_{2C}R was 32 nM, but 3.01 µM for the 5-HT_{2A}R (Acuna-Castillo *et al.*, 2002). Hence, by choosing a concentration of 100 nM, 5-HT_{2C}R are blocked without much affecting other 5-HT_2R.

In analogy to the experiments presented above (see 3.4.4.2), RS 102221 was added to the superfusate for the duration of the whole experiment, while 5-HT was added at t = 0 s. Out of 9 pyramidal cells studied, I found that 8 failed to show any significant increase in the mEPSC frequency after 5-HT application. In only one, a small but significant transient increase remained (see below). In contrast to the data set with 5-HT, the outcomes in this set of cells was very different (p_{χ^2} = 0.07), suggesting that the increases in mEPSC frequency were caused by 5-HT_{2C}R activation.

In Fig. 3.4.27, a typical recording from a cell without a significant increase in mEPSC frequency is presented. During the control period and in the presence of TTX, gabazine, and RS 102221, the mEPSC frequency was 82 ± 3 Hz (A0). The exposure to 5-HT did not change the mEPSC frequency (A1 – 3, B, and C). Not unexpectedly, the average amplitude, time course, rise time, and half-width did not change either.

For comparison, in D – I, the data from the only cell with a significant increase is illustrated. The mEPSC frequency of the control period was 72 ± 3 Hz (D0). After the addition of 5-HT, a transient increase by 25 ± 10%, to 89 ± 6 Hz was observed within 2 minutes (D1, E, F, and G). The frequency then dropped back to 60 ± 5 Hz after 6 minutes (D2), after which, there was no significant change anymore.

The mEPSC amplitude during the control period was -10.2 ± 0.1 pA. After addition of 5-HT, however, there was a significant decrease to 9.0 ± 0.1 pA (I). The average time courses of mEPSCs during the control period and after 5-HT remained the same.

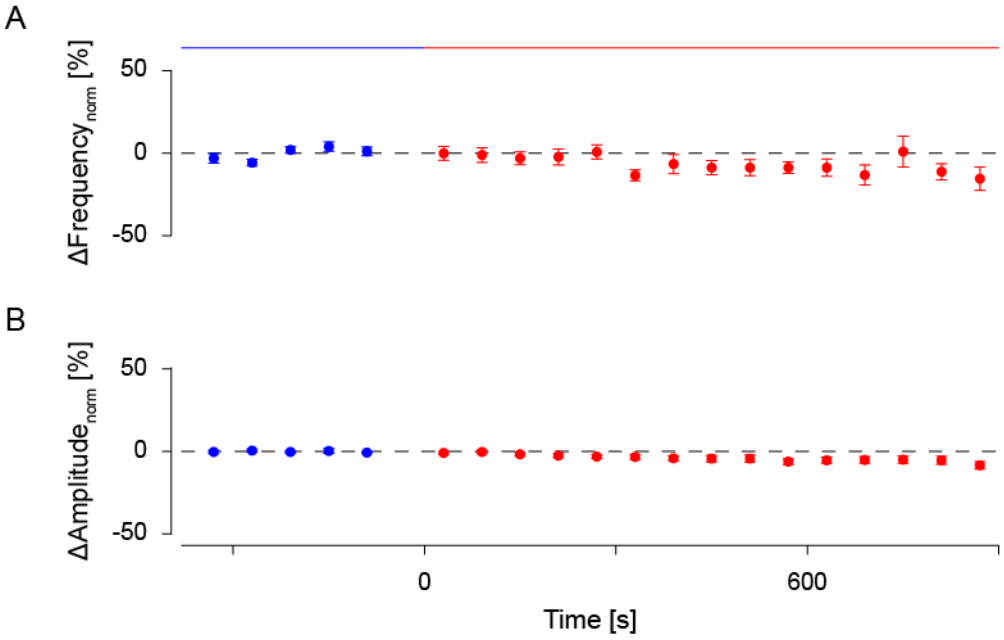

Figure 3.4.28. Pooled data for the experiments with RS 102221.
This figure was made in analogy to Fig. 3.4.16. The legend there also applies to this figure except that here the data were obtained in the continual presence of 100 nM RS 102221 and 5-HT was added at t = 0.

When all data from this type of experiment were pooled (9 cells, Fig. 3.4.28), I found that 10 µM 5-HT failed to cause significant increase in mEPSC frequency when 100 nM RS 102221 was present. This is expected because the majority of the cells did not show any significant change in frequency, and the only increase would hardly render the overall average significant. Specifically, after 5-HT, the average frequency remained unchanged from the control value of 70 ± 4 Hz (A). Note that the average instantaneous mEPSC frequency in the presence of this 5-HT$_{2C}$R antagonist was significantly higher compared to the condition without the antagonist (70 ± 4 *vs.* 53 ± 3 Hz; p_t = 0.007). However, it did not limit the magnitude of the increase by 5-HT in the sole responder. The average amplitude also remained the same throughout (-9.6 ± 0.5 pA; B). The same statement also applies for the average time course of mEPSC. The average changes for R_{in} and I_{hold} were -42 ± 16 MΩ (p_{pt} = 0.03) and 35.3 ± 16.3 pA (p_{pt} = 0.06), respectively.

This data set with RS 102221 shows that blocking 5-HT_{2C}R abolishes the increase in mEPSC frequency in most cells. The small number of cells, in which an increase in frequency remained, however, suggests that there may be a small contribution by 5-HT_{2A}R. In addition, it suggests that waxing and waning of the mEPSC frequency may be caused by an interaction between these two receptors.

3.4.4.4. Block of Both 5-HT_{2A}R and 5-HT_{2C}R

If both receptors were involved in increasing the mEPSC frequency, then their joint block should completely abolish the increase(s) in the mEPSC frequency. I tested this idea by adding both 4F 4PP (200 nM) and RS 102221 (100 nM) to the standard ACSF throughout the recording, and adding 5-HT at t = 0.

A typical such recording is given in Fig. 3.4.29. During control, the instantaneous mEPSC frequency was 55 ± 2 Hz (A0), the amplitude -10.7 ± 0.1 pA, the rise time 0.5 ms, and the half-width 1.5 ms. After the addition of 5-HT, there was no significant change in either the frequency (A1 – 3, B, D, F, and G), amplitude (C, E, and H) or average mEPSC time courses.

The same observation was made for another four cells. However, interestingly, three other cells showed a significant depression of the mEPSC frequency, on average by 39 ± 8 % from 73 ± 2 to 44 ± 6 Hz. This depression occurred around 4 – 5 minutes after 5-HT application and persisted until the end of recording.

Because a non-responder was defined as a cell without a significant mEPSC frequency increase upon exposure to 5-HT, all cells in this set of 8 were non-responders. Hence, the outcome in this set compared to 5-HT was very different (p_{χ^2} = 0.02) indicating that the block of both receptors was responsible for the lack of increase(s) in mEPSC frequency.

The pooled data are presented in Fig. 3.4.30. During the control period, the instantaneous mEPSC frequency was 65 ± 5 Hz (A). Note that this value again was significantly higher than the average frequency without both antagonists (65 ± 5 *vs.* 53 ± 3; p_t = 0.04). After the addition of 5-HT, the frequency dropped by 17 ± 2% to 53 ± 4 Hz ($p_{pt} = 2 \cdot 10^{-4}$). This drop started after 4 minutes, and persisted for the remainder of the recording. The mechanism(s) causing this drop in mEPSC frequency are not fully understood, but some consideration will be provided in the discussion.

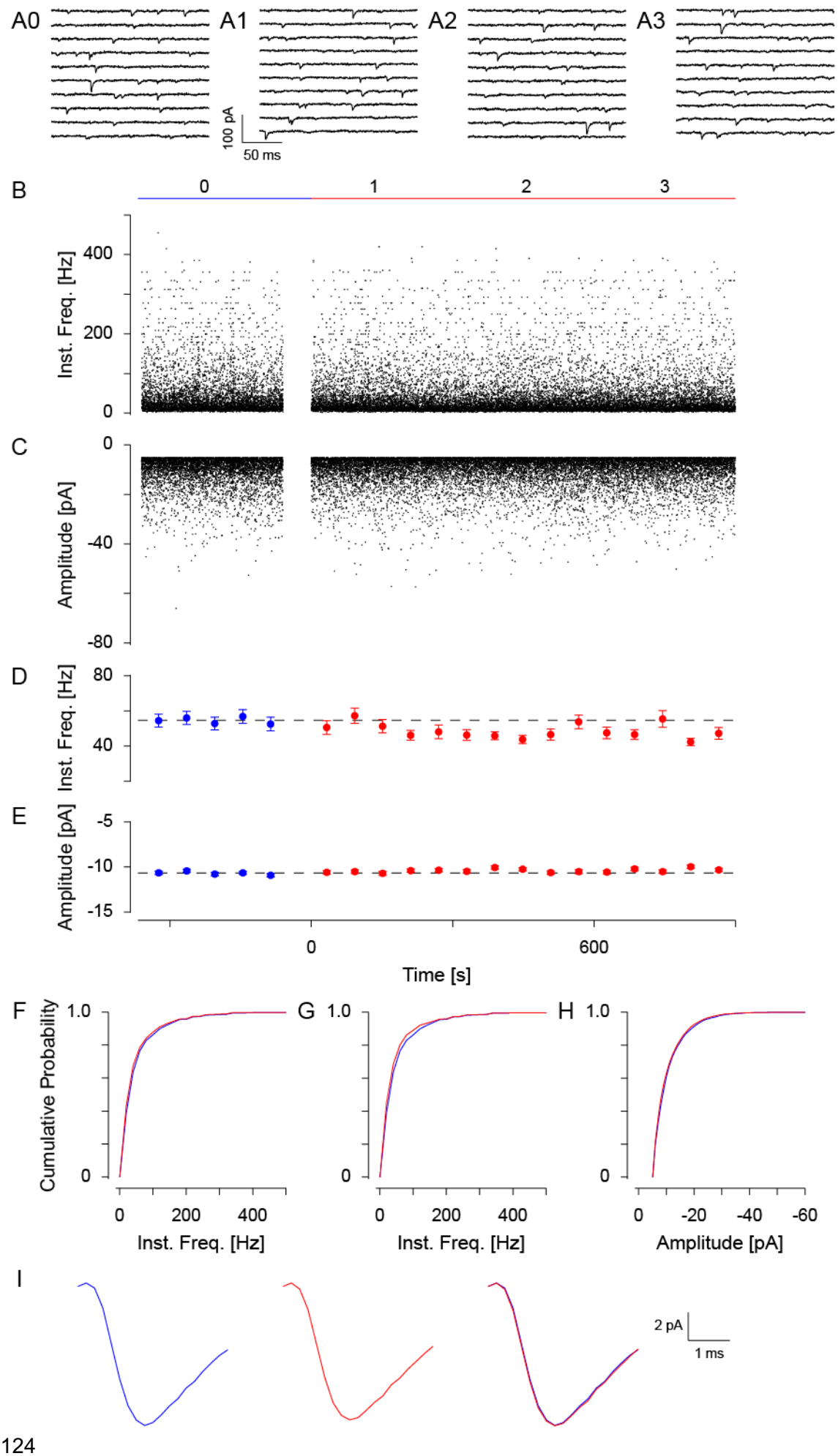
A0
A1
A2
A3
100 pA
50 ms
B
0
1
2
3
Inst. Freq. [Hz]
400
200
0
C
Amplitude [pA]
0
-40
-80
D
Inst. Freq. [Hz]
80
40
E
Amplitude [pA]
-5
-10
-15
0
600
Time [s]
F
G
H
Cumulative Probability
1.0
0
0
200
400
Inst. Freq. [Hz]
0
-20
-40
-60
Amplitude [pA]
I
2 pA
1 ms

Figure 3.4.29. mEPSC increase was blocked with both 4F 4PP and RS 102221.
This figure follows the same logic as the one presented in Fig. 3.4.3. The same legend applies here as well. However, note that both 5-HT_{2A}R antagonist 4F 4PP and 5-HT_{2C}R antagonist RS 102221 were continuously present throughout the recording. 5-HT was added at t = 0.

The average mEPSC amplitude was -10.8 ± 0.7 pA during the control period and -9.9 ± 0.6 pA after 5-HT addition. In B, the time course of the relative amplitude change before and after 5-HT addition is shown. The change was insignificant. The time courses of the average mEPSCs remained the same after 5-HT addition; the rise time remained 0.5 and the half-width 1.5 ms. The average changes for R_{in} and I_{hold} as a consequence of 5-HT addition were -19 ± 26 MΩ (p_{pt} = 0.47) and 32.6 ± 9.1 pA (p_{pt} = 0.009), respectively.

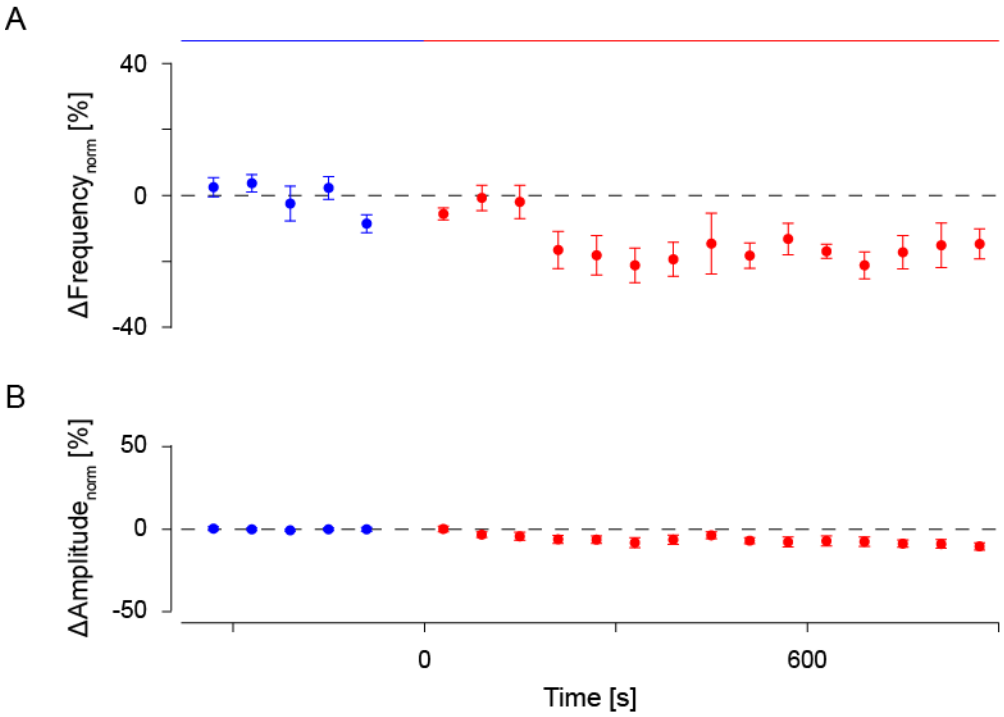

Figure 3.4.30. Pooled data for experiments with 4F 4PP and RS 102221.
This figure was made in analogy to Fig. 3.4.16. The legend there also applies to this figure except that here the data were obtained in the continual presence of both 200 nM 4F 4PP and 100 nM RS 102221 and 5-HT was added at t = 0.

These results strengthen the conclusion made earlier that 5-HT activated both 5-HT_{2A}R and 5-HT_{2C}R, which resulted in the observed transient increases in the instantaneous

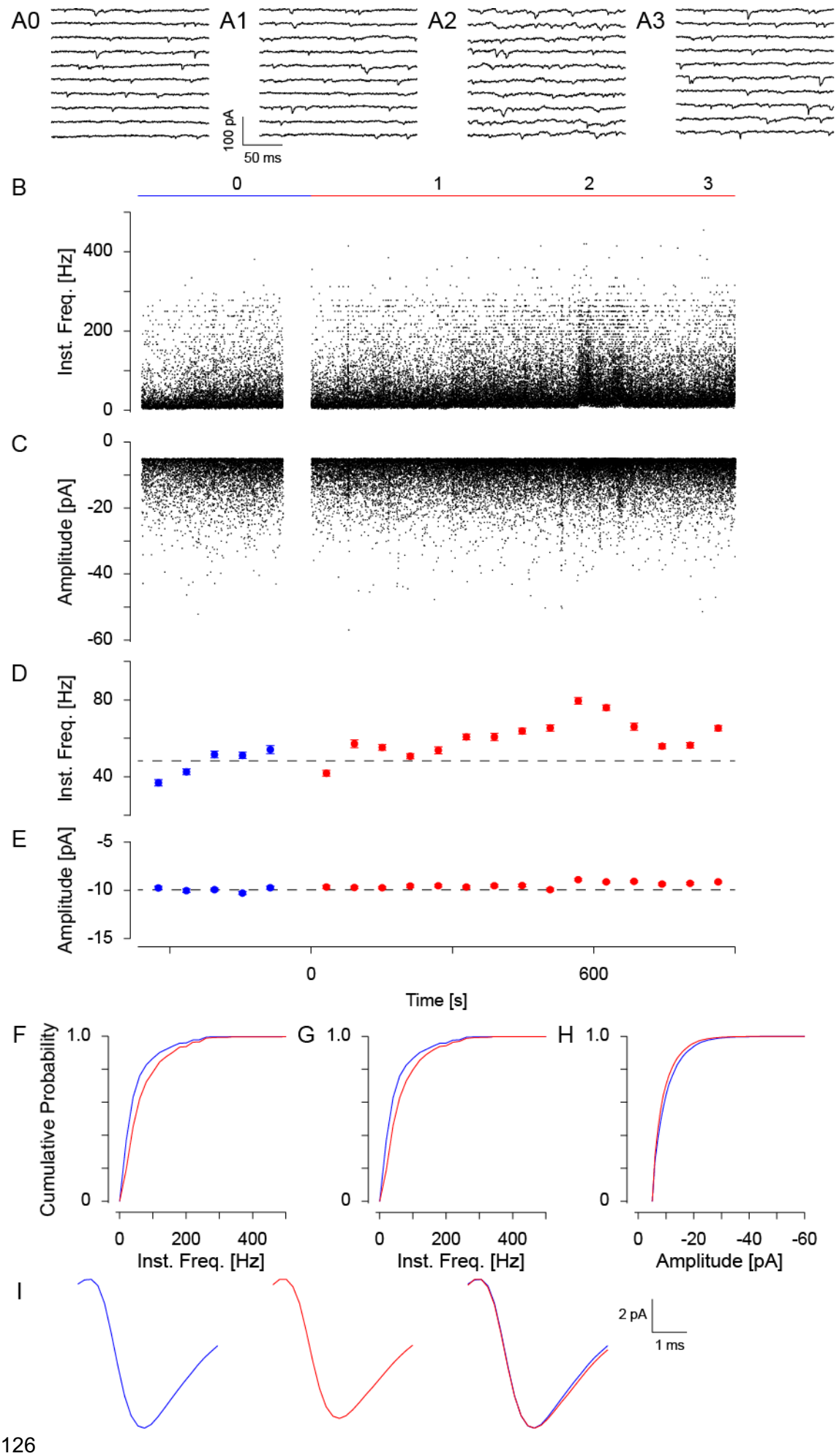
A0
A1
A2
A3
100 pA
50 ms
B
0
1
2
3
Inst. Freq. [Hz]
400
200
0
C
Amplitude [pA]
0
-20
-40
-60
D
Inst. Freq. [Hz]
80
40
E
Amplitude [pA]
-5
-10
-15
0
600
Time [s]
F
G
H
Cumulative Probability
1.0
0
0
200
400
Inst. Freq. [Hz]
-20
-40
-60
Amplitude [pA]
I
2 pA
1 ms

Figure 3.4.31. mEPSC frequency persisted when 5-HT_{1A}R were blocked.
This figure follows the same logic as the one presented in Fig. 3.4.3. The same legend applies here as well. However, note that in this case, (S)-WAY 100135 was continuously present throughout the recording. 5-HT was added at *t* = 0.

mEPSC frequency. This data further indicates that activation of 5-HT_{2C}R contributes much more strongly to the frequency increase than that of 5-HT_{2A}R.

3.4.4.5. No Involvement of 5-HT_{1A}R

So far, the data are consistent with the idea that both 5-HT_{2A}R and 5-HT_{2C}R cause the increases in mEPSC frequency. However, 5-HT_{1A}R are also expressed in the axon initial segment of pyramidal cells (Azmitia *et al.*, 1996; Czyrak *et al.*, 2003), where they may indirectly affect glutamate release by modulating the shape of the AP. To directly test if 5-HT_{1A}R were involved, I performed a set of experiments using the specific antagonist (S)-WAY 100135, which has a high affinity at 5-HT_{1A}R (IC_{50} = 15.5 nM) and is a partial agonist at 5-HT_{1B}R (EC_{50} = 520 nM) and 5-HT_{1D}R (EC_{50} = 25 nM; Davidson *et al.*, 1997).

Using a concentration of 100 nM, all 5-HT_{1A}R are expected to be blocked while the activation of 5-HT_{1B}R and 5-HT_{1D}R is minimised, but 5-HT_{2A}R and 5-HT_{2C}R are not affected. Therefore, I checked if in the presence of (S)-WAY 100135, 5-HT still caused the observed increases in the mEPSC frequency.

Note that these experiments were conducted in the presence of the PKC inhibitor Gö 6983 (100 nM). As will be demonstrated in 3.4.5.1, this PKC inhibitor caused a sustained increase in the mEPSC frequency, but did not have any other observable unwanted effects. The block of PKC should make the outcome of 5-HT_{1A}R activation better discernible if involved in increasing the mEPSC frequency. Consequently, both (S)-WAY 100135 and Gö 6983 were added to the superfusate for the whole duration of the experiment, and 5-HT was added at *t* = 0.

The outcomes of such a typical recording are presented in Fig. 3.4.31. During the control period, the mEPSC frequency was 48 ± 1 Hz (A0). After the addition of 5-HT to the superfusate, the frequency increased by 40 ± 4% to 67 ± 1 Hz (A2, B, D, and F). This increase remained for at least another 10 minutes (A3, B, D, and G). The mEPSC amplitude did not change significantly (-10.0 ± 0.1 *vs*. -9.2 ± 0.1 pA after 5-HT; C, E, H), nor were there any changes to the time courses of the respective mEPSCs (I, right).

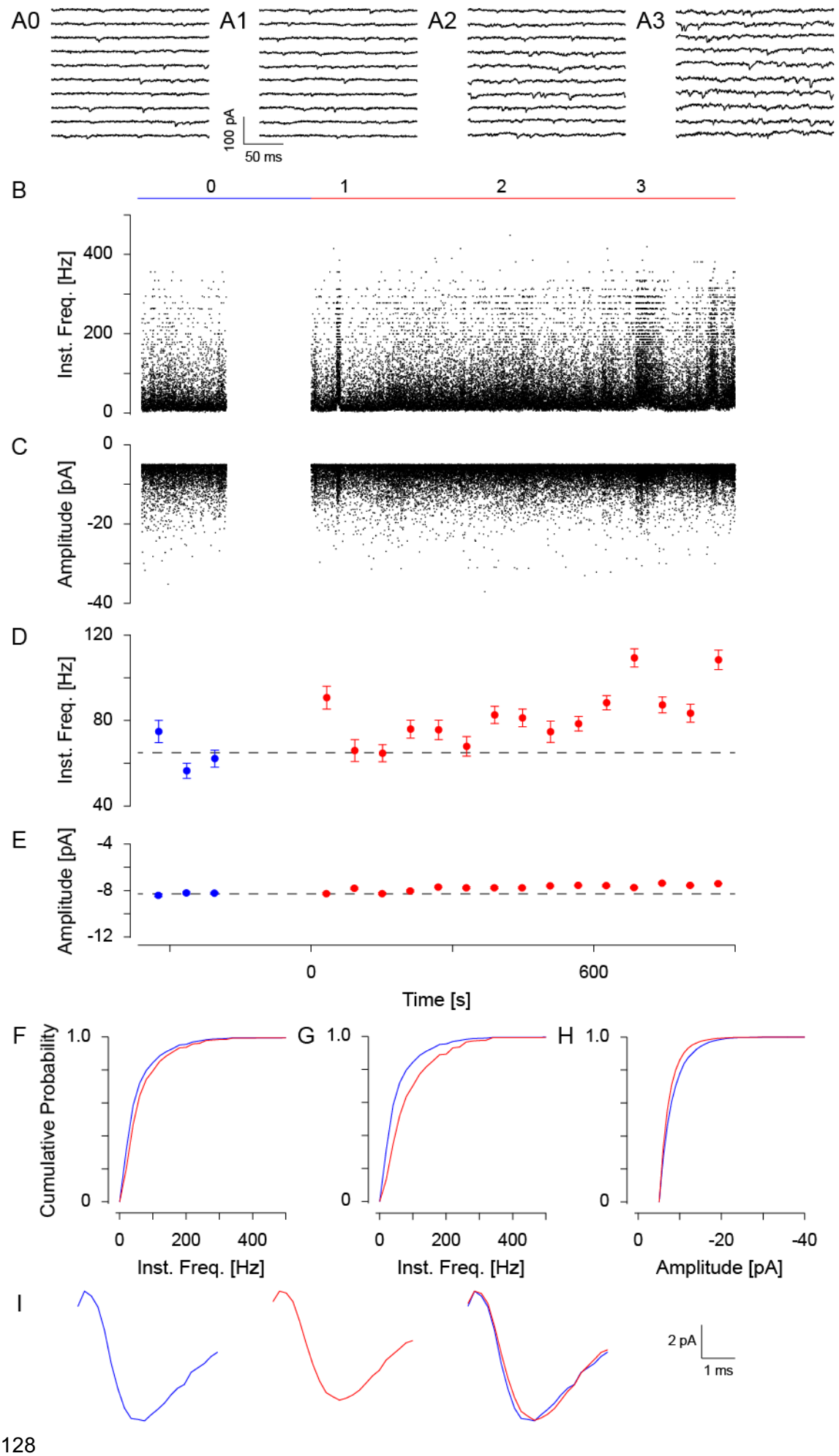
A0
A1
A2
A3
100 pA
50 ms
B
0
1
2
3
Inst. Freq. [Hz]
400
200
0
C
Amplitude [pA]
0
-20
-40
D
Inst. Freq. [Hz]
120
80
40
E
Amplitude [pA]
-4
-8
-12
0
600
Time [s]
F
Cumulative Probability
1.0
0
0
200
400
Inst. Freq. [Hz]
G
1.0
0
0
200
400
Inst. Freq. [Hz]
H
1.0
0
0
-20
-40
Amplitude [pA]
I
2 pA
1 ms

Figure 3.4.32. With PKC blocked, the frequency increase was sustained.
This figure follows the same logic as the one presented in Fig. 3.4.3. The same legend applies here as well. However, note that in this case PKC was blocked by 100 nM Gö 6983 throughout the recording and 5-HT was added at t = 0.

In a set of 5 such experiments, 2 cells showed a sustained significant increase in the mEPSC frequency after 5-HT addition. This percentage of responders was not different from that observed with 5-HT application only (40% *vs.* 47%; p_{χ^2} = 0.80). The average changes for R_{in} was 4 ± 20 MΩ (p_{pt} = 0.50).

These results support the idea that with 5-HT_{1A}R blocked, 5-HT still caused increase(s) in the mEPSC frequency. The data also suggest that the mEPSC frequency increase is independent of 5-HT_{1A}R signalling.

3.4.4.6. Sustained mEPSC Increase with PKC Blocked

Previous studies in HEK cells showed that after prolonged exposure to 5-HT, 5-HT_{2A}R undergo internalization in a protein kinase C (PKC)-dependent way (Bhattacharyya *et al.*, 2002; Raote *et al.*, 2013). If this observation applied here, inhibiting PKC would prevent the internalisation of 5-HT_{2A} and 5-HT_{2C}R, and render the increases in mEPSC frequency from transient into sustained.

For this purpose, PKC was inhibited with Gö 6983 throughout the recording before 10 µM 5-HT was then applied. Gö 6983 is a broad spectrum PKC inhibitor with IC_{50} values of 7, 7, 6, 10, 60, 20000 nM for PKCα, β, γ, δ, ζ, and µ, respectively (Gschwendt *et al.*, 1996). Therefore, by choosing a concentration of 100 nM, most of the PKC isoforms were blocked.

In Fig. 3.4.32, data from such a typical recording are presented. During the control period and in the presence of 100 nM Gö 6983, the mEPSC frequency was 65 ± 3 Hz (A0). After the addition of 5-HT at time zero, the frequency increased by 18 ± 6% to an average value of 77 ± 2 Hz after 7 minutes (A2, B, D, and F). This increase was sustained for the remainder of the recording; *i.e*. the average increase was 51 ± 8% to 98 ± 2 Hz (A3, B, D, and G).

In this example, the mEPSC amplitude during control period was -8.3 ± 0.1 pA. The addition of 5-HT caused a small, but in this case, significant decrease by 10 ± 2% to -7.5 ± 0.1 pA (C, E, and H) by the end of the recording. Significant decreases were only observed in 4 out of 14 cells. Hence, within this population, although a small decrease

was observed in some cell, it remained insignificant (see below). The mEPSC time courses together with the rise time and half-width did not significantly change either (I, right).

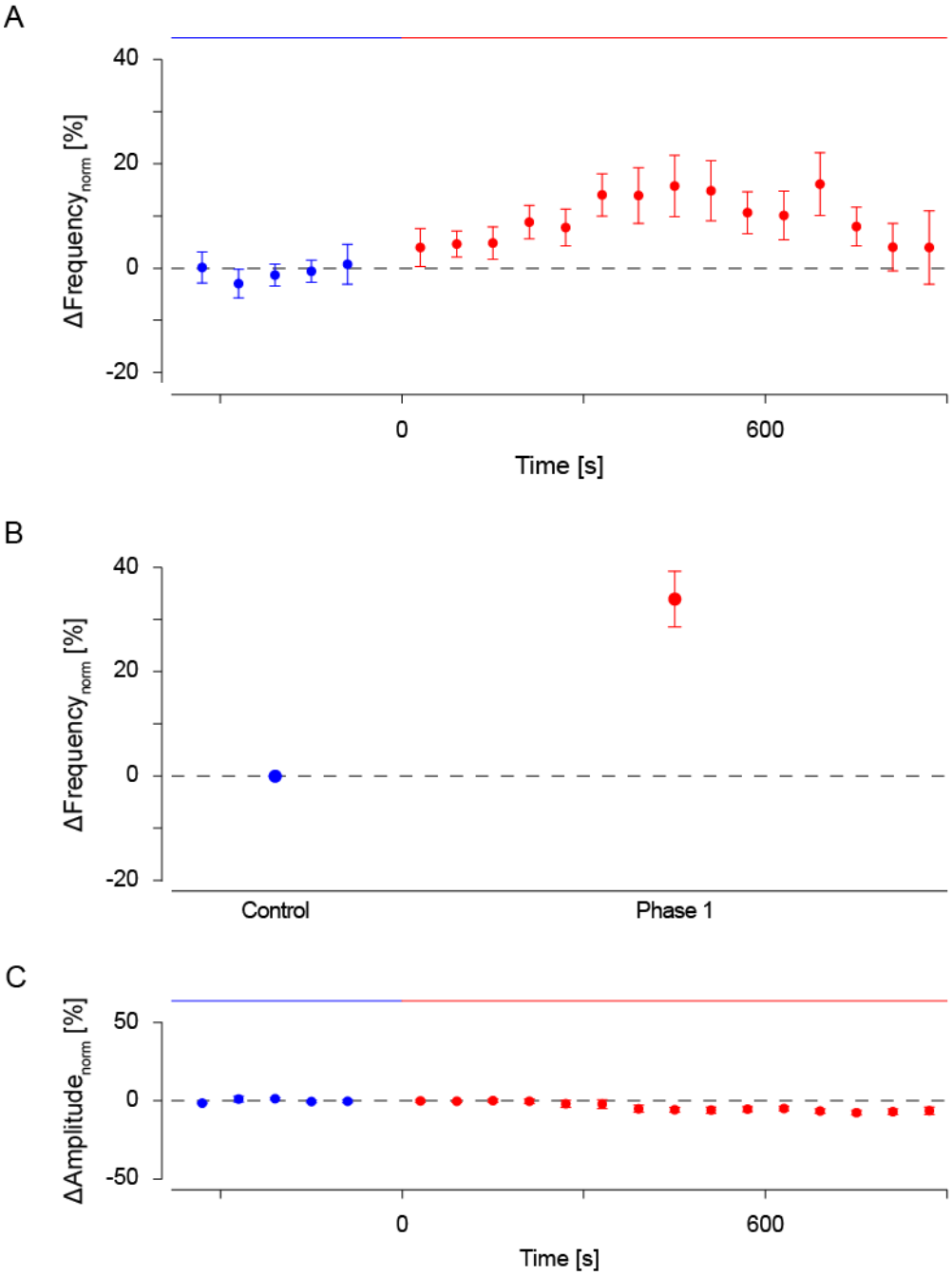

Figure 3.4.33. Pooled data for experiments with PKC block.

A. Time course of the minute averages of the relative change in frequency (normalised for a control value of 0%). B. Average change in mEPSC frequency after aligning for the respective peak values. C. Same as in A but for the changes in mEPSC amplitude.

In a data set of 14 cells, illustrated in Fig. 3.4.33, 7 showed a sustained increase in mEPSC frequency after 5-HT. In comparison to the data set without PKC block, the number of responders/non-responders in this data set was not different (p_{χ^2} = 0.86).

The minute averages of the change in the mEPSC frequency after pooling all 14 cells rose by 16 ± 6% from 61 ± 3 to 72 ± 6 Hz (A). However, this increase was likely an underestimate because in each responder, the rise started at different times. Therefore, I averaged the values after the increase was fully established. For non-responders, the respective value was taken during the seventh minute. During the control period, the average frequency was 61 ± 3 Hz, significantly higher than the value without PKC inhibition (61 ± 3 *vs.* 53 ± 3; p_t = 0.045). After the addition of 5-HT, it increased by 34 ± 5% to 82 ± 6 Hz ($p_{pt} = 6 \cdot 10^{-5}$; B).

The average mEPSC amplitude during control period was -9.4 ± 0.4 pA. This was then used to normalise the amplitude after 5-HT against (C). There was no change in the amplitude. In addition, both the average time course, rise time and half-width also did not change.

This set of data revealed three important points. First, inhibiting PKC rendered transient increases into a single sustained increase. But it did not change the number of responders/non-responders, nor the extent of the increase in the instantaneous mEPSC frequency (p_t = 0.51). Second, the block of PKC increased the frequency during control, indicating that there was tonic PKC activity, which reduced the mEPSC frequency. These data are consistent with the idea above that internalization of 5-HT_{2A}R and/or 5-HT_{2C}R may take place. Third, since both 5-HT_2R and PKC block increased the mEPSC frequency in control by the same amount, suggests that PKC activation is downstream of 5-HT_2R stimulation.

3.4.5. Verifying the Signalling Cascade Downstream of 5-HT_2R Activation

In the following sections 3.4.5.1-3, I will test the involvement of important signalling steps downstream of 5-HT_{2A}R and 5-HT_{2C}R, which caused the increases in the mEPSC frequency. Since both 5-HT_{2A}R and 5-HT_{2C}R are coupled to G_q proteins that classically signal via phospholipase Cβ (PLCβ), I will present data from experiments when PLC was blocked in 3.4.5.1. Further downstream of the signalling cascade, PLC hydrolyses PIP_2 to produce DAG and IP_3. In 3.4.5.2, I will focus on blocking IP_3 receptors (IP_3R). Finally, as IP_3 can cause Ca^{2+} release from intracellular stores that may increase spontaneous

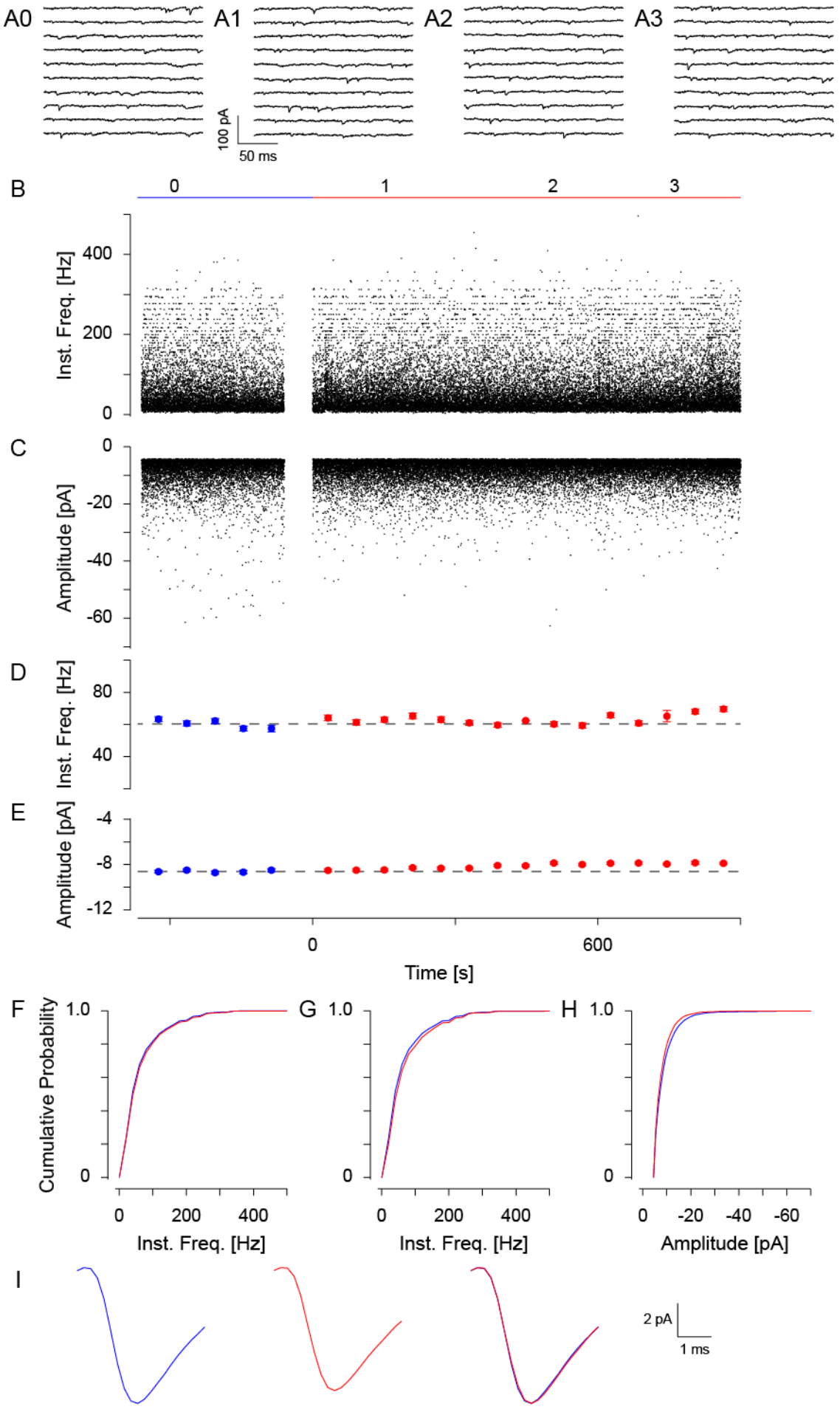
A0
A1
A2
A3
100 pA
50 ms
B
0
1
2
3
Inst. Freq. [Hz]
400
200
0
C
Amplitude [pA]
0
-20
-40
-60
D
Inst. Freq. [Hz]
80
40
E
Amplitude [pA]
-4
-8
-12
0
600
Time [s]
F
Cumulative Probability
1.0
0
0
200
400
Inst. Freq. [Hz]
G
1.0
0
0
200
400
Inst. Freq. [Hz]
H
1.0
0
0
-20
-40
-60
Amplitude [pA]
I
2 pA
1 ms

Figure 3.4.34. Inhibiting PLC with edelfosine.

This figure follows the same logic as the one presented in Fig. 3.4.3. The same legend applies here as well. However, note that in this case, PLC and PKC were blocked by 30 µM edelfosine and 100 nM Gö 6983 throughout and 5-HT was added at *t* = 0.

transmitter release, I performed experiments using BAPTA-AM to chelate intracellular Ca^{2+} in 3.4.5.3. Note that, except for the experiments with BAPTA-AM, in all subsequent experiments, PKC was blocked by Gö 6983 to make the subsequent changes by 5-HT more prominent.

3.4.5.1. Inhibition of Phospholipase C

Agonist binding to 5-HT_{2A}R and 5-HT_{2C}R results in the downstream activation of PLCβ (Shimohama *et al.*, 1998; Watanabe *et al.*, 1998), which marks the first step in the signalling cascade. I tested if inhibiting PLCβ would prevent the observed 5-HT-mediated frequency increases.

For this purpose, PLCβ was inhibited with 30 µM edelfosine (Powis *et al.*, 1992) for at least 10 min prior to the addition of 5-HT. This concentration was chosen in accordance with studies by Horowitz *et al.* (2005) and Choy (2011). Note again that edelfosine was present together with Gö 6983 throughout the experiment (see 3.4.4.6).

A typical recording is shown in Fig. 3.4.34. In this cell, the presence of edelfosine prevented 5-HT from causing any significant increase in the instantaneous mEPSC frequency (B, D, F, and G), as it remained at the control value of 60 ± 1 Hz throughout (A1 – 4). The mEPSC amplitude did not significantly change either (-8.6 ± 0.1 *vs.* 7.9 ± 0.1 pA; C, E and H). In addition, the mEPSC time course during the control period overlapped with that after addition of 5-HT (I, right).

Out of 6 such experiments, I found that 5 cells failed to show an increase in the mEPSC frequency. The remaining cell showed a small increase by 21 ± 3% from 72 ± 1 to 87 ± 2 Hz, which only lasted for four minutes. In comparison to the increase when only Gö 6983 was present (see 3.4.4.6), this increase was much smaller and not sustained, which may indicate an incomplete inhibition of PLC by edelfosine.

It was very unlikely that the 5 cells were all non-responders for the following reasons. 1) The probability of getting 5 non-responders out of 6 cells equals 0.019 ($0.53^5 \cdot (1 - 0.53)$), which unlikely occurred, but cannot be ruled out. 2) In this set of 5, I observed 2 cells with characteristics consistent with those of responders. One cell showed a large decrease in R_{in} by 121 MΩ, accompanied with a small outward current of 16 pA after 5-

HT addition. The other cell showed a decrease in R_{in} by 19 MΩ, which was accompanied by a large inward current of -140 pA. 3) When the properties of these two cells were plotted on the respective distributions of responders, they were in the tail which did not overlap with that for non-responders. Altogether, these considerations indicate that at least two responders were contained in the data set. Consequently, edelfosine prevented the increase in mEPSC frequency.

The pooled data for this set are illustrated in Fig. 3.4.35. The relative changes in the average mEPSC frequency (A) and amplitude (B) were minimal throughout.

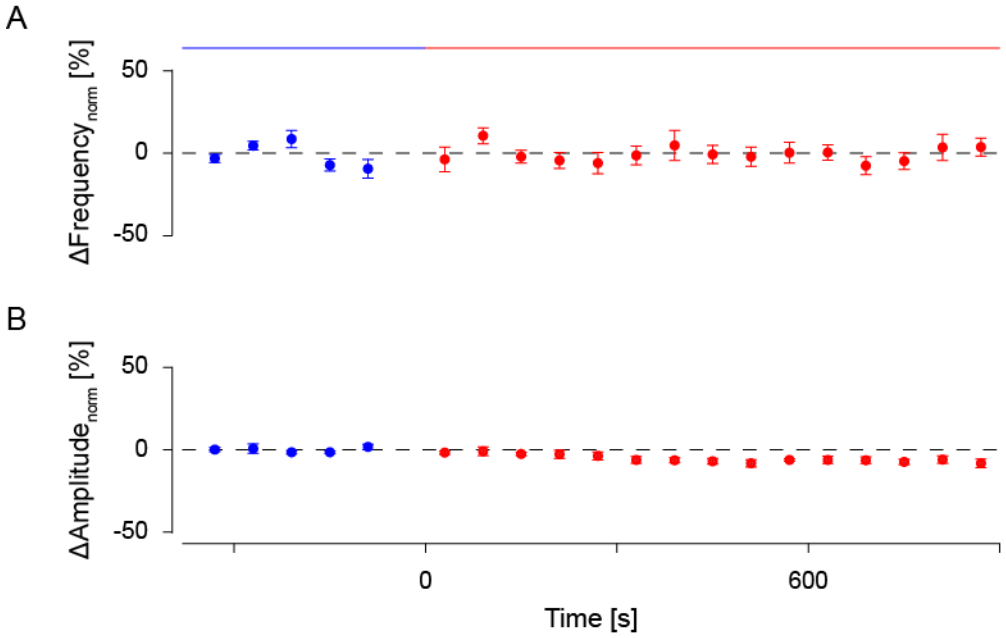

Figure 3.4.35. Pooled data for experiments with edelfosine.
This figure was made in analogy to Fig. 3.4.16. The legend there also applies to this figure except that the data were obtained under the conditions described in the legend above.

This set of data shows that inhibiting PLC with edelfosine prevented 5-HT from causing an increase in the mEPSC frequency downstream of the 5-HT_{2A}R and 5-HT_{2C}R activation. This is consistent with a classical G_q signalling cascade downstream of these receptors.

A further conclusion may be drawn by comparing the outcomes of this experiment with those when the 5-HT_2R were blocked (Fig. 3.4.30A). As indicated above, there was no change in mEPSC frequency, whereas, when the 5-HT_2R were blocked, there was a decrease in mEPSC frequency. This suggests that the decrease in mEPSC frequency

observed in Fig. 3.4.30A most likely occurred as a consequence of a PKC phosphorylation downstream of the respective receptor activation.

3.4.5.2. Block of IP_3R

Activation of PLCβ results in the hydrolysis of PIP_2 to produce DAG and IP_3. As stated in 3.2, I hypothesized that IP_3 binds to its receptor on presynaptic stores, causing Ca^{2+} release to increase the mEPSC frequency. To test this hypothesis, I added the IP_3R blocker 2-APB to the superfusate. In accordance with the previous study by Simkus and Stricker (2002a), I chose a concentration of 16 µM. Be reminded that the PKC inhibitor Gö 6983 (100 nM) was also present throughout the recording.

A typical such recording is shown in Fig. 3.4.36. During the control period, the mEPSC frequency was 54 ± 1 Hz (A0). After exposure to 5-HT, the frequency remained at 54 ± 1 Hz (A1 – 3, B, D, F, and G). There were no significant changes in either the mEPSC amplitude (-7.6 ± 0.1 *vs.* -7.1 ± 0.1 pA; C, E, and H) or its time course (I, right), with the rise time and half-width remaining at 0.6 and 1.9 ms, respectively.

In the presence of 16 µM 2-APB, for all 7 cells studied, 5-HT failed to cause any significant increase in the mEPSC frequency. This outcome was significantly different to the one observed for the set with 5-HT (p_{χ^2} = 0.03).

Pooling the data from all 7 cells (Fig. 3.4.37), the changes in the relative mEPSC frequency (A) or amplitude (B) varied minimally throughout the recording. In addition, in the presence of 2-APB, 5-HT did not have any effect on the time course of average mEPSC, rise time and half-width.

I surmised that people may say that this set was drawn from 7 non-responders, and hence, there is no evidence that 2-APB blocked the 5-HT-induced mEPSC frequency increase. However, this was very unlikely to be the case because of the following reasons. 1) The probability of just having 7 non-responders is small (0.53^7 = 0.011) and therefore unlikely. 2) One cell exhibited the characteristics of a responder (ΔR_{in} of -31 MΩ and an inward current change of -28 pA). In addition, two more showed large decreases in R_{in} (-94 and -97 MΩ) with small outward currents with 5-HT. 3) When the properties of these 3 cells were plotted, their values fell into the respective tails of responders. These considerations suggest that there were at least 3 responders in this set. Consequently, these data do provide evidence that 2-APB blocked the mEPSC frequency increase. In addition, they are also consistent with the idea that a classical signalling cascade gets activated downstream of $5\text{-}HT_2R$ binding.

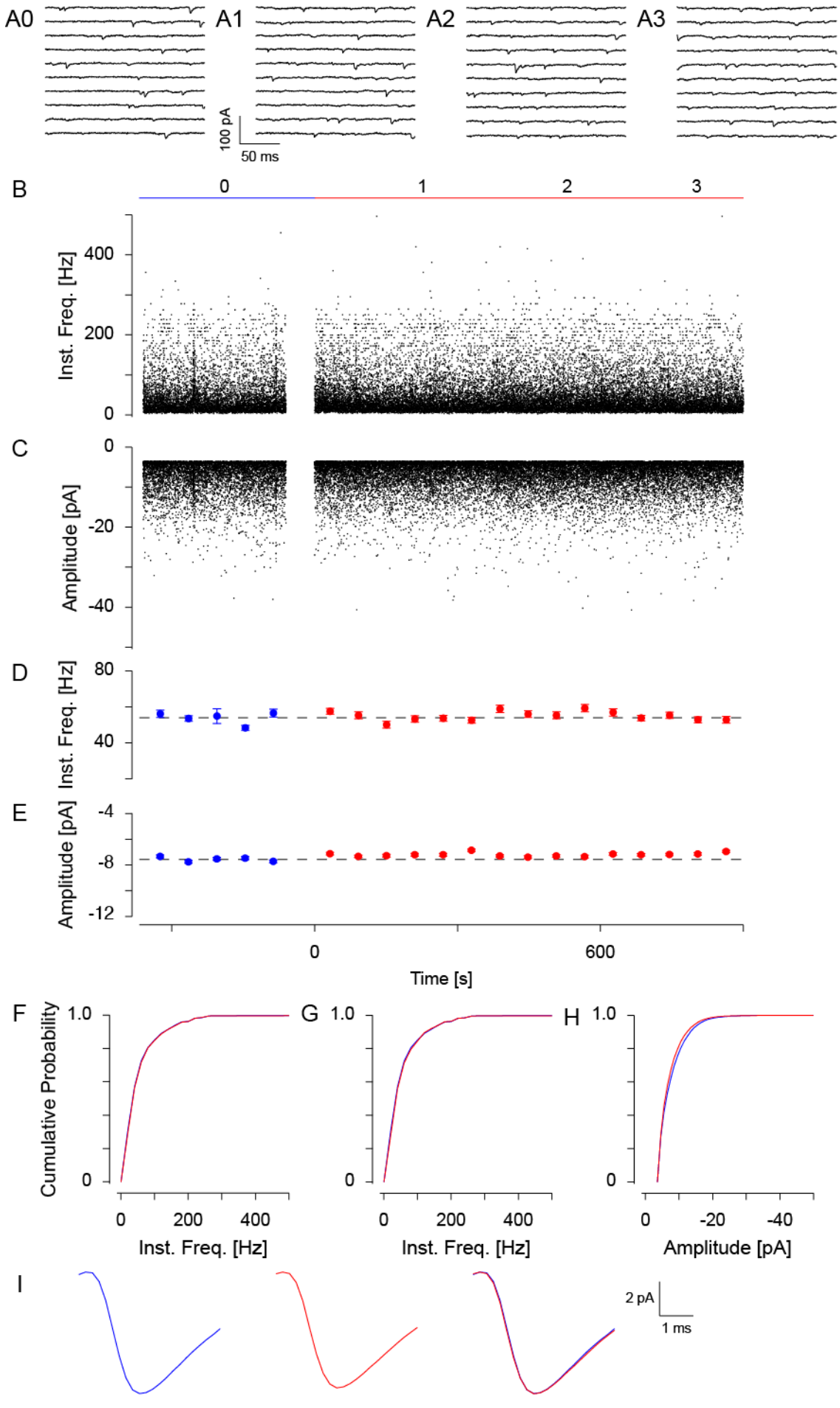
A0
A1
A2
A3
100 pA
50 ms
B
0
1
2
3
Inst. Freq. [Hz]
400
200
0
C
Amplitude [pA]
0
-20
-40
D
Inst. Freq. [Hz]
80
40
E
Amplitude [pA]
-4
-8
-12
0
600
Time [s]
F
G
H
Cumulative Probability
1.0
0
0
200
400
Inst. Freq. [Hz]
-20
-40
Amplitude [pA]
I
2 pA
1 ms

Figure 3.4.36. IP_3R block prevented frequency increase.

This figure follows the same logic as the one presented in Fig. 3.4.3. The same legend applies here as well. However, note that in this case, IP_3R and PKC were blocked by 16 µM 2-APB and 100 nM Gö 6983 throughout the recording and 5-HT was added at t = 0.

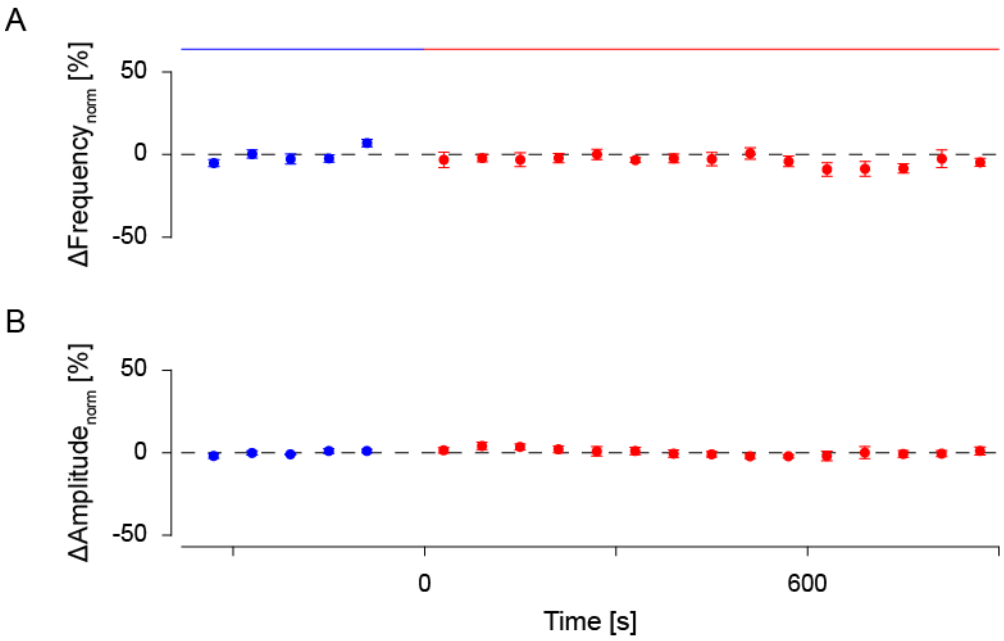

Figure 3.4.37. Pooled data for experiments in which IP_3R were blocked.

This figure was made in analogy to Fig. 3.4.16. The legend there also applies to this figure except that here the data was obtained under the conditions described in the legend above.

3.4.5.3. Chelation of Ca^{2+} Released from Presynaptic Stores

Ca^{2+} released from presynaptic stores may trigger the release of vesicles from the nerve terminal, and may act as the final step in the signalling pathway. I tested this possibility by chelating Ca^{2+} in presynaptic terminals using BAPTA-AM.

BAPTA-AM, at a concentration of 50 µM, was loaded into cells as described by Ouanounou *et al.* (1996). Specifically, this procedure was performed at least 20 minutes prior to the start of the recording. BAPTA-AM was applied in the presence of 0.7 mM cyclodextrin, which stabilized BAPTA-AM in the extracellular solution, and 0.5 mM probenecid, which prevented the transport of BAPTA out of the nerve terminal via organic acid transporters. These three compounds were superfused continuously throughout

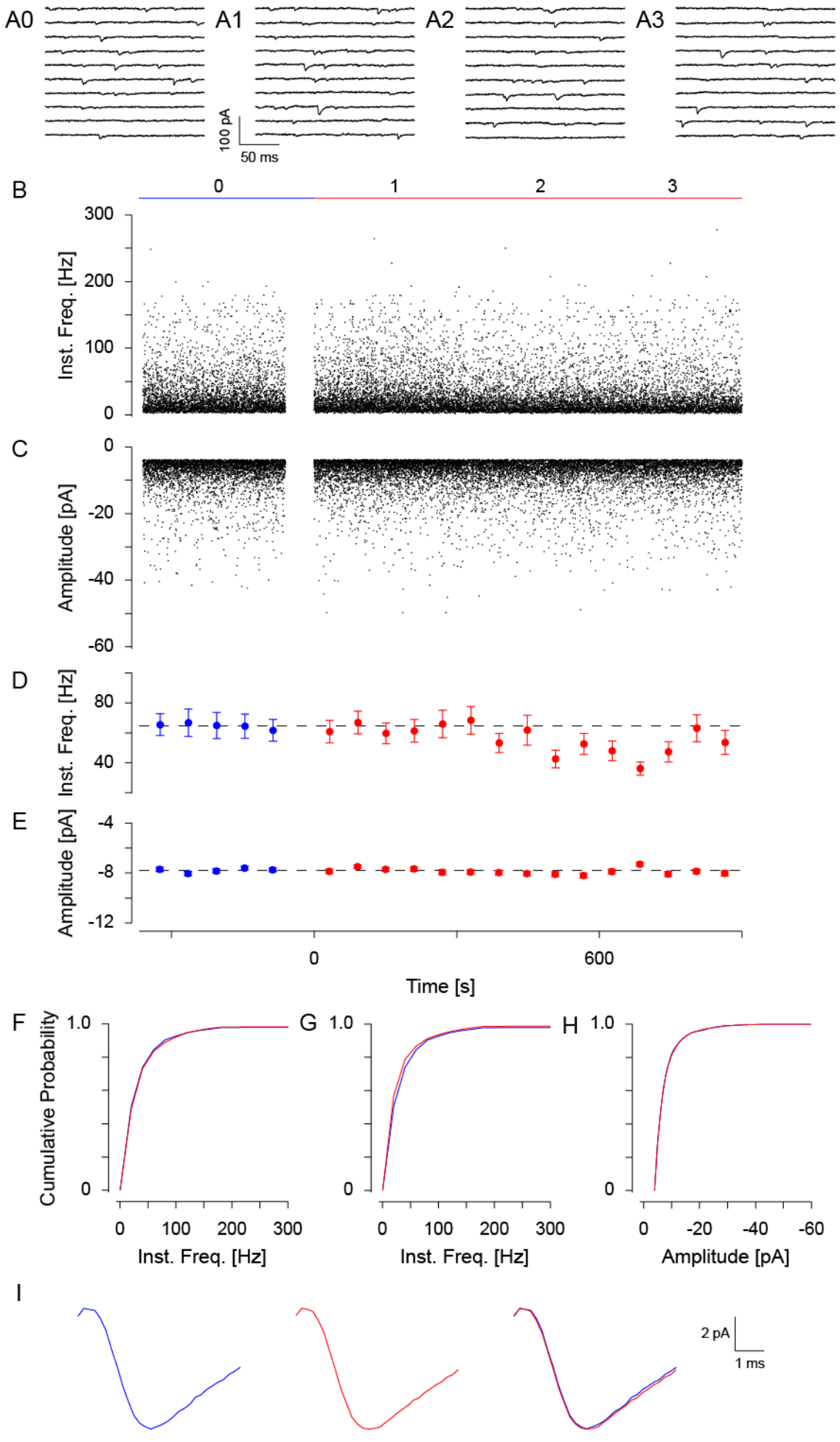
A0
A1
A2
A3
100 pA
50 ms
B
0
1
2
3
Inst. Freq. [Hz]
300
200
100
0
C
Amplitude [pA]
0
-20
-40
-60
D
Inst. Freq. [Hz]
80
40
E
Amplitude [pA]
-4
-8
-12
0
600
Time [s]
F
G
H
Cumulative Probability
1.0
0
0
100
200
300
Inst. Freq. [Hz]
-20
-40
-60
Amplitude [pA]
I
2 pA
1 ms

Figure 3.4.38. Chelation of intracellular Ca^{2+} with BAPTA-AM.

This figure follows the same logic as the one presented in Fig. 3.4.3. The same legend applies here as well. However, note that in this case, Ca^{2+} was chelated after loading 50 µM BAPTA-AM into the nerve terminals. 5-HT was added at t = 0.

recordings. However, because additional 3 compounds were already present in the ACSF, PKC was not blocked in these cases.

Such a recording is shown in Fig. 3.4.38. During the control period, the mEPSC frequency was 65 ± 4 Hz. The subsequent addition of 5-HT did not cause any significant increase in the mEPSC frequency throughout; *i.e.* at the end of the 15-min recording period, the frequency was 54 ± 8 Hz, not significantly different from control (B, D, F, and G). There was also no significant change in either the mEPSC amplitude (-7.8 ± 0.1 *vs.* -7.8 ± 0.1 pA; C, E, and H), time course (I, right), rise time or half-width.

Out of set of 6 such recordings, none showed any significant increase in the mEPSC frequency after 5-HT application. The outcomes of this set when compared to that with 5-HT alone, were very different (p_{χ^2} = 0.04).

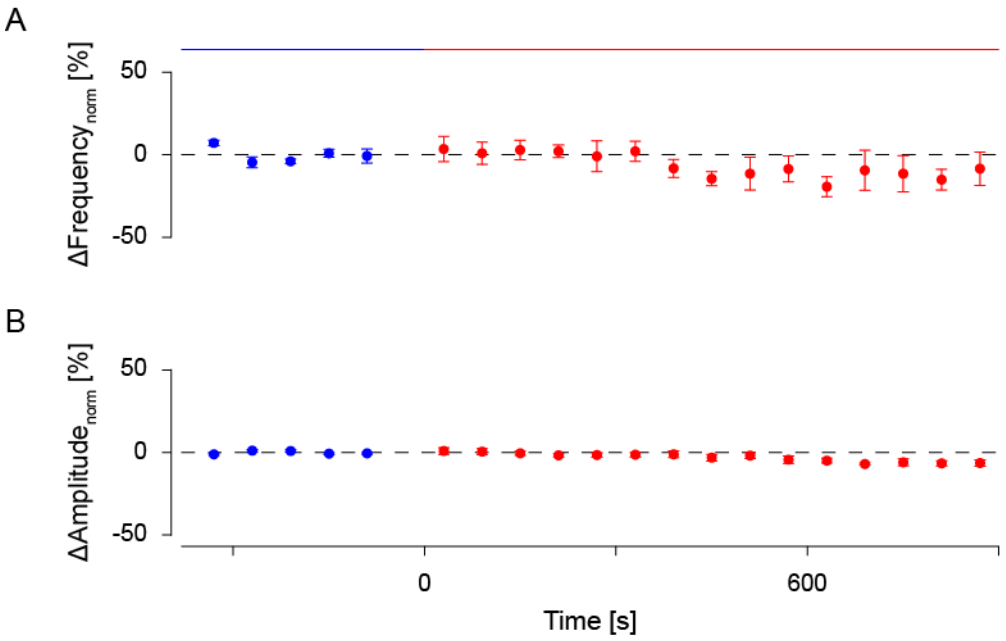

Figure 3.4.39. Pooled data for experiments with BAPTA-AM.

This figure was made in analogy to Fig. 3.4.16. The legend there also applies to this figure except that here the data was obtained under the conditions described in the legend above.

Again, I considered evidence for the presence of responders in this set. The probability of having 6 non-responders in this data set was very low (0.022) and, hence, unlikely. Furthermore, 3 cells showed the characteristics of responders. Specifically, one had an ΔR_{in} of -60 MΩ and a ΔI_{hold} -5 pA, another a ΔR_{in} of -47 MΩ and a ΔI_{hold} 3 pA, and the third a ΔR_{in} of -37 MΩ and a ΔI_{hold} 7 pA. These values were again in the respective tails for responders. Hence, there were at least 3 responders in this set, yet BAPTA-AM prevented the mEPSC frequency increase.

The data for the pooled set is presented in Fig. 3.4.39. After it was normalised for a control value of 0%, the change in both mEPSC frequency (A) and amplitude (B) after exposure to 5-HT was abolished. BAPTA-AM also had no effect on the time course of the mEPSCs, the average rise time and half-width.

From this set of data, I conclude that the increase in mEPSC frequency was most likely caused by Ca^{2+} release from presynaptic stores. In addition, this observation is also consistent with that of a classical signalling cascade downstream of 5-HT_2R activation, congruent with my hypothesis above.

3.5. Discussion

In Part 3 of my thesis, I have investigated how 5-HT modulates spontaneous glutamate release in pyramidal neurons of layer II of rat barrel cortex. I found that in a subset of pyramidal cells (47%) referred to as responders, addition of 10 µM 5-HT to the superfusate increased the mEPSC frequency transiently within the first 5 minutes. It then decreased below control values, but later surged again. The mEPSC frequency increase was not accompanied by a concomitant change in amplitude. Since there was no significant change in either mEPSC amplitude or its time course, the frequency increase by 5-HT is most likely presynaptic. Cells without such a change in mEPSC frequency were subsequently named non-responders. After addition of 5-HT, the most significant difference between these two groups was a much larger decrease of R_{in} in responders than non-responders, suggestive of the opening of (a) larger postsynaptic conductance(s).

The mEPSC frequency increase was predominantly caused by activation of 5-HT_2R, with a larger contribution made by 5-HT_{2C}R than 5-HT_{2A}R. I further verified the signalling pathway downstream of 5-HT_2R activation, and found that inhibiting PLCβ, blocking IP_3R, and chelating intracellular Ca^{2+} all successfully blocked the increase in mEPSC frequency. These results fully support a “classical” signalling cascade whereby PLCβ activation downstream of $G_{q/11}$ hydrolysed PIP_2 to yield DAG and IP_3, the latter of which then bound to IP_3R causing Ca^{2+}release from presynaptic stores seen as an increase in mEPSC frequency. In addition, I found that blocking PKC, which might have been activated downstream of DAG, rendered the transient nature of the mEPSC frequency increase into a sustained one.

3.5.1. Electrophysiological Properties of Pyramidal Cells

Based on a considerable number of pyramidal cells recorded from in layer II, I have been able to characterise some basic electrophysiological properties. Because all cells were histologically verified *post hoc*, I am very confident that this sample consists of a homogeneous population of pyramidal cells, mostly in the upper part of layer II. In agreement with earlier studies in this laboratory (Simkus & Stricker, 2002b, a; Choy, 2011; Choy *et al.*, 2017a; Choy *et al.*, 2017b) and another report in the literature (Feldmeyer *et al.*, 2006), V_{rest} in these cells was quite hyperpolarized. I note that these values were not corrected for a liquid junction potential of 13.0 mV (Barry, 1994) and, therefore, are even more negative. Also in agreement with these studies is the fact that upon a sufficiently large currents step, these cells fire more or less regularly, with the AP threshold typically set at -38 mV.

The characteristics of mEPSCs in these cells are also consistent with earlier studies from this laboratory (Simkus & Stricker, 2002b; Choy *et al.*, 2017a). The mEPSC frequency was typically high, with an average value of 59 ± 1 Hz. Given that this frequency was indifferent from that of sEPSC, *i.e*. was not affected by TTX, it was not generated by spontaneous sodium electrogenesis. However, TTX did have a significant effect on σ_{noise}, which became smaller. This is most likely due to the high density of sodium channels around the soma which may generate a small persistent current at rest. In addition, the mEPSC amplitude became smaller. This is harder to interpret, but a likely explanation is that when the persistent current is removed, electrogenesis by Ca^{2+} and/or NMDA receptors, that may also be present in these axons and cause multivesicular (synchronised) release, is abolished. This would result in a smaller mEPSC amplitude.

3.5.2. Transient Increases in mEPSC Frequency but Not Amplitude

Throughout the different sets of experiments in this part, I have mostly used an agonist concentration of 10 µM in agreement with what Singer *et al.* (1996) have used. I note that in different studies, diverse concentrations were used; in some much less (Lee *et al.*, 2008; Hosford *et al.*, 2014; Nishijo & Momiyama, 2016) and in others much more (Aghajanian & Marek, 1999; Marek & Aghajanian, 1999). However, because the relevant EC_{50} was measured to be ≤ 1 µM (Xu & Chuang, 1987; Singer *et al.*, 1996), the chosen concentration was very likely sufficiently high for receptor activation.

The main finding in this part is that 10 µM 5-HT caused transient increases in mEPSC frequency in a subset of layer II pyramidal cells in the age bracket between P15 and P20, consistent with the hypothesis that downstream of a G_q-mediated signalling cascade, the release of Ca^{2+} from presynaptic stores generates an increased number of mEPSCs. This study shows for the first time that 5-HT causes a specific pattern in the modulation of spontaneous release. Specifically, upon 5-HT activation, and for the typical recording period of 15 minutes, there was a transient increase by 28 ± 7% within the first 4 – 5 minutes, which decayed back to a value below the control level (-15 ± 3%), to then resurge towards the end of the recording (27 ± 7%; see Table 3.4.1).

I provided three lines of evidence that this pattern of mEPSC frequency increase was very unlikely a recording artefact. First, when I instead used 10 µM NA, a sustained increase could be reliably tracked throughout the remainder of the recording period. Second, I also demonstrated that I could reliably track the mEPSC frequency in ACSF over the whole duration of such an experiment without any significant change in frequency, indicating that random variability during the recording is an unlikely explanation for the transient nature of the increase. Third, when PKC was blocked with

Gö 6983, the frequency increase was sustained for the duration of the experiment, suggesting that a PKC-mediated phosphorylation downstream of receptor activation is likely causing the drop in mEPSC frequency (see 3.5.7 below).

In contrast to the mEPSC frequency increase observed with NA (64 ± 7%; n = 42; Choy *et al.*, 2017a), the increase for 5-HT in phase 1 was 28 ± 7%, which was significantly smaller (p_t = 0.001). Despite the involvement of a G_q–linked signalling cascade in both cases (see also below), the smaller response to 5-HT likely reflects the fact that the increase observed was due to an interaction between two processes, one that increased the mEPSC frequency as in the case for NA, and another slower process, which curtailed this increase. In addition, either the relevant 5-HTR or the associated signalling cascade was likely desensitised (see below), also contributing to the smaller increase observed (Roth *et al.*, 1995; Stout *et al.*, 2002).

It is important to point out that the increase observed with 5-HT was not that far above what can reliably be detected with the analysis technique used. The transient nature of the response, and the fact that the frequency increase was only observed in a subset of cells, may have prevented other researchers from observing it. See below for more on the transient nature of this frequency increase.

I found that all throughout the different phases, the mEPSC amplitude did not significantly change. This conclusion was based on the lack of significance between the respective densities (KS statistic), but also from the overall average time courses of mEPSCs as illustrated for example in Fig. 3.4.3I. The lack of change in mEPSC amplitude is similar to that observed for NA (Choy *et al.*, 2017a), but different from the reported small changes by 5-HT_{1B}R or 5-HT_2R (Aghajanian & Marek, 1997; Austgen *et al.*, 2012). However, I note that I cannot rule out small changes to the amplitude that, with the methods used, remained undetectable.

In a limited number of experiments, I observed that the response to 5-HT was developmentally regulated. In contrast to young (P9 – 12) and standard juvenile (P15 – 20), there was no significant increase in the mEPSC frequency in older animals (P34 – 38). However, it needs to be stressed that a small, but undetectable increase may have been present. This observation most likely reflects the postnatal expression of 5-HT_2R, in agreement with a study by Morilak and Ciaranello (1993). They found that the immunoreactivity for 5-HT_2R is high around birth, increases up to P14, but then settles on a smaller adult pattern around P28, indicating that 5-HT_2R remain expressed in the tissue. Despite this observation, it remains unclear why the frequency increase became insignificant in older (P34 – 38) animals. Potential explanations may include a change in receptor heterodimerization (Herrick-Davis *et al.*, 2005; Moutkine *et al.*, 2017), and/or

signal transduction downstream of receptor activation (Knauer *et al.*, 2009; Zhang *et al.*, 2017). As will be discussed below, it is unlikely that this change occurred at the effector level (presynaptic Ca^{2+} stores), but rather at the level of the signalling cascade.

This discussion so far implied that the source of the increased glutamate release was of synaptic (neuronal) origin. However, this tenet is far from established. An alternative explanation may be that the increased glutamate release is of glial, specifically astrocytic origin. In fact, neocortical astrocytes express 5-HT_2R, both the 2A and 2B isoforms (Hirst *et al.*, 1998; Sandén *et al.*, 2000; Xu & Pandey, 2000). In addition, astrocytes are indeed capable of releasing glutamate downstream of Ca^{2+} store activation (Parpura *et al.*, 1994; Pasti *et al.*, 1997; Araque *et al.*, 1998). At this stage, because the experimental proof for an astrocytic involvement is not easy to achieve, this possibility cannot be ruled out. Perhaps, in the near future, via astrocytic expression of designer receptors exclusively activated by designer drugs (DREADD) in neocortex (Urban & Roth, 2015), it may be possible to functionally silence 5-HT_2R on astrocytes and abolish their potential contribution to spontaneous glutamate release.

3.5.3. Impact of 5-HT on Responders *vs.* Non-Responders

Ever since early cellular studies on the function of 5-HT in the central nervous system, it was realised that not all cells uniformly responded to this neuromodulator (North & Uchimura, 1989; Araneda & Andrade, 1991; Larkman & Kelly, 1992; Tanaka & North, 1993; Schmitz *et al.*, 1998; Foehring *et al.*, 2002). It is worth pointing out that in my data set, prior to 5-HT exposure, there were no differences between the two groups of postsynaptic cells, neither in regard to the mEPSC frequency nor the postsynaptic properties (like R_{in}). The groupings into responders and non-responders was simply based on the fact that there was either a significant or no mEPSC frequency increase, respectively. However, when further comparing the data based on this *ad hoc* grouping, also differences in some postsynaptic changes became apparent. Particularly, non-responders showed an insignificant change in mEPSC frequency, typically together with a large outward current associated with a small decrease in R_{in}. Responders, in contrast, showed significant increases in mEPSC frequency, together with, on average, a very small outward current, but in a good number of these cells, an inward current associated with a large reduction in R_{in}.

It is important to point out that this grouping was defined based on the significance level based on the Kolmogorov-Smirnov statistic, the cut-off value of which was notably chosen *ad hoc*. In hindsight, this cut-off was most likely appropriately set, as it

decomposed the data set into two groups, which also showed distinct postsynaptic properties.

It is very unlikely that inadequante space-clamp (Spruston *et al.*, 1993; Williams & Mitchell, 2008) differentially affecting responders and non-responders gave rise to this distinction. First, I could not find that there were systematic differences in the extent of the dendritic tree between the two groups. Second, the fact that in both groups, the mEPSC amplitude and time course remained the same during control and after 5-HT suggests that both groups were similarly affected by space-clamp issues. Third, as both the change in R_{in} and I_{hold} after 5-HT occurred over several minutes (*i.e*. they were slow), the impact of inadequante space-clamp is much smaller than on AMPA mediated mEPSCs. Based on these considerations, I judge the impact to be minimal.

The nature of this distinction is likely associated with the functional expression of the respective 5-HTR on nerve terminals impinging on dendrites of pyramidal cells, from which the recordings were made (see Fig. 3.5.1). A similar distinction was recently made in prefrontal cortex by two different groups (Dembrow *et al.*, 2010; Avesar & Gulledge, 2012), where the expression of the 5-HTR was target specific. In addition, we found a similar grouping when looking at how NA modulated transmitter release (Choy *et al.*, 2017a), although, in this case, the attribution to two groups was less strict.

I reiterate that there was no difference between responders and non-responders in regard to the control mEPSC frequency (58 ± 2 *vs.* 60 ± 2 Hz; p_t = 0.47). Because a large number of nerve terminals onto dendrites in this layer stems from local collaterals (Lübke *et al.*, 2003), a likely scenario could be that the target cells also express 5-HT_2R on their axon terminals, potentially making recurrent contacts back onto themselves (autoreceptors). This could be an explanation for the fact that the increase in mEPSC frequency remained restricted to responders. This possibility is illustrated in Fig. 3.5.1 (scheme 1). An alternative could be that most nerve terminals onto dendrites of layer II pyramidal cells express 5-HT_2R, which in the case of responders are active, but functionally silenced in the case of non-responders (Fig. 3.5.1, scheme 2). This explanation, however, would require some form of “retrograde” message to be delivered to silence the respective nerve terminals. Target cell specific modulation of transmitter release has been described at the crayfish neuromuscular junction (Krause *et al.*, 1998), chick sympathetic ganglion cells (Devay *et al.*, 1999), hippocampus (Scanziani *et al.*, 1996; Scanziani *et al.*, 1998; Toth & McBain, 2000; Koester & Johnston, 2005; Buchanan *et al.*, 2012; Glickfeld *et al.*, 2013), and neocortex (Reyes *et al.*, 1998; Reyes & Sakmann, 1999; Cowan & Stricker, 2004). Admittedly, the difference between the cell types could also lie with the effectors (channels, signalling molecules, *etc*.). However, based on the

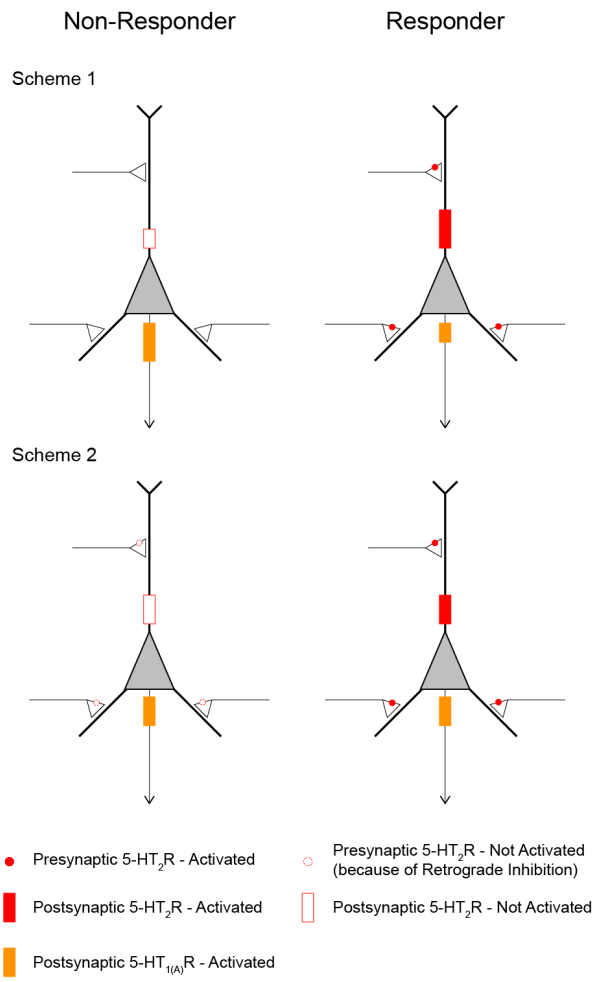

Figure 3.5.1. Schemes generating responders and non-responders.
Two possible schemes depicting the differences between responders and non-responders. In scheme 1, non-responders, which show a large outward current due to the activation of postsynaptic 5-HT_{1A}R, receive synapses, which do not express presynaptic 5-HT_2R. Therefore, 5-HT does not increase the mEPSC frequency. Conversely, responders, which show either a small outward or inward current due to the activation of both postsynaptic 5-HT_{1A}R and 5-HT_2R, receive synapses with functional presynaptic 5-HT_2R. In this case, 5-HT increases the mEPSC frequency. Alternatively, in scheme 2, the postsynaptic properties are the same as in scheme 1. However, in this case, the synapses that project to both groups uniformly express presynaptic 5-HT_2R. But in non-responders, retrograde signalling renders the respective 5-HT_2R non-functional and therefore, there is no mEPSC frequency increase.

available literature, there is little evidence for it. This possibility has therefore not been included in the Fig. 3.5.1. Whilst it is conceivable that the target could functionally curtail transmitter release from nerve terminals, at this stage, I am unable to identify which of

the two illustrated possibilities is at work here. Further points of discussion in regard to this classification will be raised in 4.5.3.

3.5.4. 5-HT Also Affects Postsynaptic Properties

Because 5-HT as the physiological agonist was used in this study, potentially several different 5-HTR could have been activated. Some of the effects showed themselves in the hyperpolarization of the postsynaptic cells upon addition of 5-HT. Specifically, in voltage-clamp (held at -70 mV), responders typically showed a small outward current (hyperpolarizing), with some cells exhibiting a net inward current (depolarizing), but non-responders mostly showed a large outward current (see Figs. 3.4.21 and 3.5.1). In addition, it is worth noting that the reduction in R_{in} was about twice that in responders than non-responders (-56 ± 13 *vs.* -30 ± 11 MΩ, respectively; see Table 3.4.5), indicating that downstream of receptor activation, a much larger conductance was opened in responders.

The fact that in both groups, there were considerable deviations from the typical result, indicates that the underlying conductance change most likely consisted of a mixture of at least two currents, one depolarizing and one hyperpolarizing, with the mixture in responders dominated by an inward and in non-responders by an outward current. The inward current most likely resulted from the activation of postsynaptic 5-HT_2R (Foehring *et al.*, 2002), whilst the outward current from 5-HT_{1A}R (Goodfellow *et al.*, 2009). Given that the outward current for non-responders was larger despite a smaller conductance change, suggests that the driving force on the respective current was larger. With GIRK channels (Lüscher *et al.*, 1997) being the most likely target in this case (as inferred from the lack of hyperpolarization when either of the two Gβγ-binding peptides was present in the presynaptic cells; see also 4.4.4.2 and 3), and given V_{rest} of ~ -78 mV in these cells, a driving force of about 15 mV was behind this current. In contrast, as the conductance change for responders was larger, but the magnitude of the current smaller, suggests that the driving force for the inward current must be significantly smaller than the 15 mV for GIRK channels.

This observation also rules out the possibility that most of this net inward current was caused by the closure of a K^+ conductance as that would have increased R_{in}, which was not observed. This consideration places the apparent reversal potential for this/these conductance/s more positive than -78 mV, likely in the range of about -70 mV. If the depolarizing current were made up of a single type of ion channel, likely candidates could be two pore potassium (K2P) channels (Mathie, 2007; Enyedi & Czirjak, 2010) or voltage- or Ca^{2+}-dependent Cl^- channels like ClC-0 or TMEM16, respectively (Chen &

Hwang, 2008; Zhang *et al.*, 2015). Given that in most instances, the activation of $G\alpha_q$ typically resulted in the inhibition of K2P conductances (Enyedi & Czirjak, 2010), these channels were unlikely involved as an increase in R_{in} should have been observed, inconsistent with my findings. In addition, the two types of Cl^- channels are unlikely involved either, as according to my incomplete knowledge, no link between 5-HT_2R activation and these Cl^- channels has been documented. However, if the underlying current were indeed a mixture of at least two channels with one of them being GIRK, the associated reversal potential for the inward current could likely be considerably more positive than -70 mV, consistent with a current like I_h or another unspecific cation current. In fact, there is evidence that depolarizations can arise downstream of 5-HT_{1A}R activation by shifting the activation curve of I_h to more positive values in motoneurons, thalamic relay neurons and CA1 pyramidal cells (Pape & McCormick, 1989; McCormick & Pape, 1990; Takahashi & Berger, 1990; Larkman & Kelly, 1992; Gasparini & DiFrancesco, 1999). Conversely, in rat prefrontal cortex, a depolarization was reported downstream of 5-HT_2R, while the subtype of this receptor remained undetermined (Araneda & Andrade, 1991), as was the ionic nature of the conductance involved. In the amygdala, a depolarization was observed because of the activation of a TRPC-like current downstream of 5-HT_{2C}R (Yamamoto *et al.*, 2014). From my data set, it is also evident that the depolarization in responders was also downstream of 5-HT_2R, and might have involved both 5-HT_{2A}R and 5-HT_{2C}R, but very unlikely 5-HT_{1A}R. The ionic nature of this depolarizing conductance remains to be elucidated.

3.5.5. 5-HT_2R Activation Causes mEPSC Frequency Increase

I further investigated which 5-HTR caused the mEPSC frequency increase, using both agonists and antagonists. I found that the pan-5-HT_2R agonist α-methyl-5-HT (20 µM; for review see Baxter *et al.*, 1995) mimicked the action of 5-HT, consistent with earlier observations in neocortex (Aghajanian & Marek, 1999; Zhou & Hablitz, 1999; Lambe *et al.*, 2000; Beique *et al.*, 2007) and other locations in the brain (Hori *et al.*, 1996; Rainnie, 1999; Hasuo *et al.*, 2002; Austgen *et al.*, 2012; Sangare *et al.*, 2016). In addition, DOB, another pan-5-HT_2R agonist, also increased the mEPSC frequency, but the pattern of the increase was different from that of 5-HT and α-methyl-5-HT (see below). These observations were further supported by the fact that after 5-HT_{1A}R were blocked with (S)-WAY 100135, I did not find any evidence that these were significantly involved. However, in other preparations, the respective change was attributed to these receptors (Singer *et al.*, 1996; Schmitz *et al.*, 1998; Ding *et al.*, 2013; Hosford *et al.*, 2014).

The involvement of 5-HT_2R was further supported when working with sub-type specific antagonists at 5-HT_{2A}R (4F 4PP) and 5-HT_{2C}R (RS 102221). In fact, with 5-HT_{2A}R

blocked, I observed that there was only one frequency increase. This suggests that 5-HT_{2C}R likely contributed to the initial increase in mEPSC frequency. In contrast, when 5-HT_{2C}R were blocked, the frequency increase(s) were absent in most cells, but in about 11% of them, an early small increase remained detectable; *i.e*. 5-HT_{2A}R contributed a small amount. Given that the increase in mEPSC frequency was fully prevented when both 5-HT_2R were blocked suggests that other 5-HTR like 5-HT_7R are unlikely involved in the modulation of spontaneous release (Beique *et al.*, 2004b; Celada *et al.*, 2013).

The fact that during phase 2, the frequency significantly dropped below that during the control period (-15 ± 3%; see Table 3.4.1), may indicate that there is constitutive 5-HT_2R activation in the absence of 5-HT, which during phase 2 was abolished, most likely due to phosphorylation either of the receptor, the associated G protein subunits or an element in the signalling cascade. In addition, the observation that when both 5-HT_2R and 5-HT_{2C}R were blocked, the control frequency also increased further supports the idea of constitutive receptor activity (see also 3.5.7 below). In fact, there is evidence for such constitutive activity of 5-HT_2R (Harvey, 2003; Berg *et al.*, 2005; Di Giovanni & De Deurwaerdere, 2016), specifically for 5-HT_{2C}R under both *in vivo* and *vitro* conditions (Barker *et al.*, 1994; De Deurwaerdere *et al.*, 2004), but also for 5-HT_{2A}R *in vivo* (Egan *et al.*, 1998). The molecular mechanism for this constitutive activity, *i.e.* activity without agonist binding, is most likely structurally linked to the coupling site of the trimeric G protein to the receptor in the region of the second intracellular loop. If in human 5-HT_{2C}R, via mRNA editing at amino acid positions 156, 158, and 160, the sequence is changed from isoleucine-asparagine-isoleucine (INI) to valine-serine-valine (VSV), the constitutive activity is lost (Niswender *et al.*, 1999). It is unclear, which 5-HT_{2C}R isoform is expressed in my preparation, but a likely candidate is one which shows a high agonist potency for 5-HT, akin to the INI isoform. The extent of constitutive activity (~15%) corresponds roughly to the one reported earlier by Barker *et al.* (1994) and lends credence to the involvement of this potential mechanism.

The transient nature of the mEPSC frequency increases is very unlikely due to a slowly evolving receptor desensitisation (Roth *et al.*, 1995; Stout *et al.*, 2002) because when PKC was blocked, the increase was sustained. However, it is very likely, though, that due to the slow solution exchange during the experiment, which typically took a couple of minutes, the relevant receptors may already have been desensitised at the start of the frequency increase, as 5-HT_2R can do so within this time frame (Stout *et al.*, 2002).

3.5.6. Involvement of 5-HT_{2A}R and 5-HT_{2C}R

It is important to point out that the functional involvement of 5-HT_{2B}R in my preparation is absent or at least insignificant. This is in agreement with an immunohistochemical study in neocortex by Choi and Maroteaux (1996). However, most likely both 5-HT_{2A}R and 5-HT_{2C}R are functionally expressed on presynaptic nerve terminals, with 5-HT_{2C}R making likely a larger contribution to the mEPSC increase than 5-HT_{2A}R.

The two data sets with 5-HT_{2A}R and 5-HT_{2C}R antagonists are best reconciled if the transient nature of the mEPSC frequency increases reflected an interaction downstream of receptor activation (see below). These findings rest upon the co-expression of both receptors either as co-localised homodimers, or potentially as heterodimers, or a combination between homo- and heterodimers. Indeed, there is immunohistochemical evidence that both receptors are co-expressed in neocortex (Pompeiano *et al.*, 1994; Li *et al.*, 2004; Nocjar *et al.*, 2015). Moreover, a recent study in a heterologous expression system suggests that heterodimers between the two receptors can be formed (Moutkine *et al.*, 2017). It was found that under these expression conditions, the downstream signalling remained unaltered. Consequently, I am unable to distinguish which dimers are present in my preparation.

Downstream of 5-HT_{2A}R signalling, bi- and triphasic signalling responses have been seen before (Qvigstad *et al.*, 2005; Zhang *et al.*, 2017). These resulted from the fact that the signalling was not only comprised of the well-known signalling arm, which involves PLCβ activation by $G_{q/11}$ and results in Ca^{2+} release from IP_3R on stores (Streb *et al.*, 1983; Berridge, 1987), but also of alternate signalling. It is well known that 5-HT via 5-HT_{2A}R can also activate the mitogen-activated protein kinase (MAPK), specifically either a member of the extracellular-regulated kinase (ERK) and/or the p38 MAPK pathway (Watts, 1996; Quinn *et al.*, 2002; Kurrasch-Orbaugh *et al.*, 2003; Franklin & Carrasco, 2015; Zhang *et al.*, 2017). The latter typically antagonises the action of the former. In their recent paper, Zhang *et al.* (2017) point out in neurons of *Aplysia* that as a consequence of this interaction between the ERK and p38 MAPK pathways, both of which are activated downstream of the 5-HT_{2A}R activation, multiphasic responses are expected to arise.

In other instances, receptor activation can result in non-classical signalling which, independently of G_q, is transduced via $G_{i/o}$ to activate phospholipase A_2 (PLA_2) to yield arachidonic acid, which then inhibits store release (Berg *et al.*, 1998). Consistent with my observations and extrapolating from such reports, it is likely that the classical signalling downstream of 5-HT_2R is responsible for the initial increase in mEPSC frequency. However, 5-HT_{2A}R with a time delay, either via $G_{i/o}$ or via activation of one

arm of the MAPK pathway (Kurrasch-Orbaugh *et al.*, 2003), inhibited store release and consequently the frequency dropped below the control value. After that, the mEPSC resurged as the inhibition was likely relieved by the other arm of the MAPK pathway. In the future, this idea could be directly tested by using specific MAPK blockers (Zhang *et al.*, 2017).

Because the signalling was independent of G_q and PLCβ in the studies mentioned above, suggests that in the reported context, some 5-HT_{2A}R are likely linked to a non-classical G protein and downstream signalling. If the increase in mEPSC frequency involved the activation of presynaptic Ca^{2+} stores, consistent with G_q signalling, a likely conclusion could be that both classically and non-classically linked 5-HT_{2A}R are present on the respective nerve terminals.

I note that there are potentially other alternative explanations for the different phases. The first considers the surface expression of 5-HT_{2A}R. It has indeed been reported that 5-HT_{2A}R can be internalised in a PKC-dependent way (Bhattacharyya *et al.*, 2002; Gray *et al.*, 2003). Such a scenario is plausible as with PIP_2 hydrolysis by PLCβ, both IP_3 and DAG are produced, the latter of which can result in the activation of PKC (Berridge & Irvine, 1984). The idea then is that after PKC activation (which may take longer as it is further downstream of receptor activation), 5-HT_{2A}R phosphorylation gives rise to internalisation limiting transduction and reducing the mEPSC frequency. These receptors can later be re-inserted into the membrane, but the time taken for this to occur is of the order of 2.5 hours (Gray *et al.*, 2003), much longer than what is reported here for phase 3. Because this resurgence may likely be caused by 5-HT_{2C}R activation, it is possible that 5-HT_{2A}R internalisation during phase 2 may be involved in the decrease in mEPSC frequency.

The second alternate explanation considers receptor desensitisation. It is known that PKC activation can result in 5-HT_{2A}R and 5-HT_{2C}R desensitisation (Boddeke *et al.*, 1993; Berg *et al.*, 2001). I note that in this context, there are other forms of desensitisation associated with the signalling cascade (see below). Nevertheless, it is conceivable that receptor desensitisation may play a role in the second phase, where the mEPSC frequency decreases. However, given that the EPSC depression (see Part 4) did not show a relief with a similar time course to that seen for mEPSCs, the first two possibilities are likely ruled out.

The third alternative rests upon the finding that desensitisation of the 5-HT-mediated response may depend on the downregulation of the G protein transduction. It is known that phosphorylation of the $G\alpha_q$ can downregulate the signalling response (Shi *et al.*, 2007). Functionally, this desensitisation of the signal transduction is indistinguishable

from that of the receptor itself. Because the effect is quite small (~20%) at least in the expression system used, I don't think that this mechanism is significantly at work here.

The fourth alternative is based upon the observation that in a heterologous expression system, the signalling which results in store release is significantly slowed down (~60 seconds) when 5-HT_{2C}R had been subjected to mRNA editing (Price & Sanders-Bush, 2000). A similar slowing has been demonstrated for 5-HT_{2A}R in platelets as a consequence of a receptor polymorphism, where the delay is about 40 seconds (Ozaki *et al.*, 1997). It may well be that in my preparation, most likely downstream of 5-HT_{2C}R, the signalling causing store release is even further delayed, for example via an ancillary protein somewhere in the cascade. This may give rise to a further delay in store release as seen in phase 3. However, given that the delay in my preparation is an order of magnitude longer, I think that such a mechanism was unlikely responsible, as there is no evidence in the literature that such a long delay could have been generated.

The reason why DOB only caused a single transient frequency increase, rather than the two seen with 5-HT, may stem from its biased agonism (Berg *et al.*, 1998), a property commonly shared between different hallucinogens (Gonzalez-Maeso *et al.*, 2007). The concept behind this idea is that depending on which kind of agonist binds to a receptor, downstream signalling can be differentially affected. Since both 5-HT_{2A}R and 5-HT_{2C}R can signal in either a classical or non-classical way, any agonist could show a preference for both ways.

3.5.7. Role of PKC in the mEPSC Frequency Increase

As indicated above, PKC may have played a central role in patterning the 5-HT-mediated mEPSC frequency increases. When PKC was inhibited with 100 nM Gö 6983, the mEPSC frequency increase became sustained for the whole duration of the recording. This observation implies that a critical phosphorylation took place before or during phase 2. I offer two explanations as to how this could arise.

First, as indicated above, PKC itself may be directly involved in the phosphorylation of both 5-HT_{2A}R and 5-HT_{2C}R. In fact, it is known that phosphorylation can result in both receptor internalisation and desensitisation (Boddeke *et al.*, 1993; Berg *et al.*, 2001; Bhattacharyya *et al.*, 2002; Shi *et al.*, 2007). As indicated above, I don't think that there is much evidence for evolving receptor desensitisation during the time of agonist exposure in my preparation. However, it is also known that the MAPK pathway, specifically the ERK pathway, is very sensitive to PKC block (Knauer *et al.*, 2009), as a number of kinases are involved in generating the output from this signalling cascade (for

review see Adams & Sweatt, 2002). I prefer this explanation over receptor desensitisation as it remains consistent with the observations that will be presented in Part 4, specifically the fact that for evoked transmitter release, there is no evidence of receptor desensitisation causing a relief from depression.

In this context, it is important to point out that constitutive 5-HT_2R activity (see above) also has implications for downstream signalling. In fact, it is known that this type of activity leads to increased receptor phosphorylation and consequently a higher degree of desensitisation (Westphal *et al.*, 1995). This may well explain the finding that when 5-HT_{2C}R alone or in combination with 5-HT_{2A}R were blocked, the mEPSC frequency during control rose, suggesting that when the antagonist was bound to the receptor, the constitutive activity was relieved and with it, the downstream signalling that may well have resulted in the phosphorylation of either the receptor or the associated signalling proteins.

Second, an alternative explanation for the pattern in the frequency increases rests upon reports showing that several isoforms of PLCβ are also subject to phosphorylation by PKC (Ryu *et al.*, 1990; Strassheim *et al.*, 1998; Strassheim & Williams, 2000; Yue *et al.*, 2000; Xu *et al.*, 2001). In doing so, the downstream signalling by 5-HT_2R may be curtailed. This explanation would functionally be no different to receptor desensitisation, except that in this case the mechanism of “desensitisation” is at the level of the downstream signalling cascade. Such a mechanism has so far not been identified for 5-HT_2R, and, as a consequence, it is unlikely responsible for the observations made here.

Because it is known that G-protein-coupled receptor kinases (GRKs) are also involved in 5-HT_2R phosphorylation and desensitisation (Sallese *et al.*, 2000), the question arises if Gö 6983 specifically blocked PKC without having an effect on GRKs. However, I have not been able to find any evidence that GRKs could be blocked by this compound. This inhibitor seems to be quite specific for most isoforms of PKC and, consequently, rules phosphorylation by GRK most likely out.

An interesting point, that came to light after all experiments were done, is the fact that both 5-HT_{2C}R and PKC block resulted in the same increase in mEPSC frequency during control, but no such increase was seen when 5-HT_{2A}R were blocked. This is highly suggestive of PKC activation downstream of 5-HT_{2C}R. Future experiments could look into this more specifically.

3.5.8. Verification of Downstream Signalling

The discussion here is intended to punctually verify which signalling cascade is activated by 5-HT_2R to the increase the mEPSC frequency. I note that I did not extensively, but only tested for some crucial steps in the signalling cascade.

Most of the experiments presented in this context were performed with PKC inhibited, just to make sure that the changes associated with receptor activation stood out more and for longer. The classical signalling cascade would involve the activation of PLCβ, the subsequent production of IP_3 and DAG, the activation of IP_3 receptors, and finally Ca^{2+} release from stores.

I note that there was a potential confound in several experiments with blockers of steps in the signaling cascade relating to the complication of responders and nonresponders and possible sampling bias. As for the latter, such experiments cannot provide any insight, the question arises if a sufficient number of responders were in each data set. In most sets of experiment, there were at least 6 – 8 cells. Given that in a randomly obtained set of cells, about half of the cells correspond to responders and non-responders (as in 3.4.2.1), the probability of all cells being of one group only is very small, namely $(0.47)^6$ = 0.01 and $(1 - 0.47)^6$ = 0.02, respectively; or in other words, it was very unlikely that in any of the relevant experiments, there were only non-responders or responders; *i.e*. it was very likely that cells of both groups were contained in the data sets. Nevertheless, this possibility cannot be ruled out. Because of this, I attempted to provide additional evidence by checking if alternative properties like the typical inward current and the size of the change in R_{in} were indicative of responders. Based on these criteria, I found that in each set of experiments, there were at least two to three responders.

3.5.8.1. Involvement of PLCβ

As 5-HT_2R are linked to G_q, signalling downstream of G-protein activation is most likely via one of the four isoforms of PLCβ, namely PLCβ1 – 4. Most of them are expressed in neocortex (Yamada *et al.*, 1991; Shimohama *et al.*, 1998; Watanabe *et al.*, 1998). Certainly, the isoforms PLCβ1 - 3 can be activated by $G\alpha_q$. I note that the same isoforms can also be activated by Gβγ (Exton, 1994; Rhee & Bae, 1997; Rhee, 2001). However, the concentrations required for activation by Gβγ are much higher than for Gα. PLCβ was blocked using 30 µM edelfosine, an ether lipid analogue (Powis *et al.*, 1992; Horowitz *et al.*, 2005). I chose this compound over others like U73122 because the latter showed an unspecific effect on Ca^{2+}-activated cation channels as shown in pancreatic acinar cells (Mogami *et al.*, 1997; Horowitz *et al.*, 2005).

My main finding was that with PLCβ blocked (and in the presence of Gö 6983), in most cells, the mEPSC frequency increase was prevented. I note that in these experiments, I did not test for the effect of edelfosine on its own, as this was tested in a previous study, which reported that there is tonic PLCβ activation in this part of the cortex (Choy, 2011; Choy *et al.*, 2017a). With PLCβ blocked, 5-HT was unable to increase the mEPSC frequency. This finding is consistent with the involvement of a classical G_q-mediated transduction in that PLCβ activation leads to PIP_2 hydrolysis and the production of IP_3 and DAG.

3.5.8.2. IP_3R Activation

In the classical cascade, the production of IP_3 activates IP_3R, leading to Ca^{2+} release from stores. To test this idea, I blocked IP_3R with 16 μM 2-APB. I note that at this concentration, the action of 2-APB was found to be quite specific to IP_3R (Simkus & Stricker, 2002a; Hirst *et al.*, 2008). However, I note that at higher concentrations, which are typically used to block TRP channels (Chinopoulos *et al.*, 2004), the plasmalemmal Ca^{2+}-ATPase (Maruyama *et al.*, 1997), the SERCA pump (Bilmen *et al.*, 2002), store-operated Ca^{2+} channels (Dobrydneva & Blackmore, 2001), and connexins (Bai *et al.*, 2006), 2-APB is unspecific. Consistent with this hypothesis, when the receptors were blocked, again no increase in mEPSC frequency was observed. This outcome is internally consistent with that seen with edelfosine and further supports the idea that 2-APB blocked IP_3R. In accordance with this observation, IP_3R are likely involved in the generation of mEPSCs, consistent with Ca^{2+} store release.

3.5.8.3. Ca^{2+} Release from Stores

Given that in this preparation the generation of mEPSCs is not dependent on random openings of VDCC, but requires intracellular Ca^{2+} release (Simkus & Stricker, 2002a; Choy *et al.*, 2017a), presynaptic chelation by BAPTA-AM should abolish the frequency increase. This was indeed the case as in none of the relevant experiments, an increase in mEPSC frequency was observed. This is again consistent with the idea that 5-HT_2R activation results in the stimulation of the classical G_q-mediated signalling cascade. However, it needs to be stressed that even though this cascade is most likely involved, it does not preclude that DAG may also activate PKC and/or MAPK.

3.5.9. Functional Consequences

5-HT is functionally involved in many different brain states and behaviours like mood, perception, memory, anger, aggression, fear, stress responses, appetite, and sexual

behaviour (Berger *et al.*, 2009). It is also critically implicated in the development of neocortex, and, specifically, in the patterning of barrel cortex (Erzurumlu & Kind, 2001). Furthermore, 5-HTR have been linked to several neuropsychiatric syndromes like depression, schizophrenia, Parkinson's disease, and abnormal mental states like delirium, addiction, psychosis, anxiety and obsessive-compulsive disorders (for review see Chagraoui *et al.*, 2016; Di Giovanni & De Deurwaerdere, 2016). In addition, it has long been known that several antipsychotic drugs like haloperidol and clozapine (neuroleptics) have a pronounced blocking effect on 5-HT_{2A}R with the respective K_i values in the range of 53 and 5.4 nM, respectively (Kroeze *et al.*, 2003). However, it needs to be stressed that such drugs are highly unspecific and are reported to block other receptors as well.

As explained in the introduction, there are seven 5-HTR groups in mammals (Hoyer *et al.*, 1994; Pytliak *et al.*, 2011), with six of them giving rise to some twenty-three G-protein-coupled receptor subtypes. In addition, there is one ionotropic group (5-HT_3R) with five different subunits (5-HT_{3A-E}), not including their alternatively spliced or mRNA edited isoforms. This complexity in 5-HTR expression, in combination with the possibility of receptor heterodimerization or multimerization, and the diverse coupling to various signalling cascades opens up a vast possibility for differential cellular responses. It is not surprising that under such conditions, specific functions and dysfunctions are hard to specifically attribute to specific receptor subtypes.

In this part of my thesis, I have largely concentrated on the effect of 5-HT on spontaneous transmitter release and essentially found that within this context, the significant contributors are predominantly 5-HT_{2C}R with a smaller contribution by 5-HT_{2A}R. Admittedly, whilst both receptors are critically involved in shaping the properties of thalamocortical afferents in layer IV of barrel cortex during development (Erzurumlu & Kind, 2001), their functional role in layer II is much less clear. Given that the impact on mEPSC frequency is not above detectability beyond P28, 5-HT may likely be involved in the developmental fine tuning of specific networks, which certainly contain responders. However, as R_{in} is reduced and GIRK channels are activated in non-responders as well, 5-HT is also involved in tuning of the networks made up of non-responders, but not of their synapses.

Whilst a considerable body of evidence exists for a role of 5-HT in synaptic plasticity in *Aplysia* (Eliot et al., 1993; Alberini et al., 1994; Martin et al., 1997), the situation in mammals is much less clear. At the cellular level, 5-HT has been documented to be involved in some forms of synaptic plasticity, specifically in LTP and LTD in visual cortex, both *in vivo* and *in vitro* (Kojic *et al.*, 2000). Interestingly, both forms of plasticity depend

on the expression of 5-HT_{2C}R. Whilst LTP is typically observed in areas of high receptor expression (blobs in V1), LTD is observed in areas with low expression. As 5-HT_{2C}R are capable of inducing Ca^{2+} release from intracellular stores, it is conceivable that the locally increased Ca^{2+} from stores may serve to lower the threshold for induction of LTP or LTD (Bienenstock *et al.*, 1982). In this context, the triphasic nature of the mEPSC frequency increase may serve as the relevant "patterning" that may ensure efficient induction and expression of the respective long-term plasticity. The issue here is that desensitised receptors/signalling cascade(s) (as in phase 2) may not be able to sufficiently elevate the local Ca^{2+} above the induction threshold for long enough, but upon the resurgence during phase 3, this may become possible.

The outcome of long-term synaptic plasticity is often growth of dendrites and spines (for review see Yuste & Bonhoeffer, 2001). There is evidence that one of the roles of spontaneous transmitter release is that it serves to maintain spines (McKinney *et al.*, 1999). As a consequence, 5-HT could facilitate the formation and maintenance of spines, which has been observed in tissue cultures (Pfister & Goworek, 1978; Chubakov *et al.*, 1986; Yoshida *et al.*, 2011). In addition, 5-HT may exert a trophic effect on neurons in neocortex, potentially similar to that caused by brain-derived neurotropic factor (BDNF) or some other growth factors, which typically signal via receptor tyrosine kinases (RTK). In fact, 5-HT_2R are reported to be able to cause transactivation of RTK, for example of glia-derived neurotrophic factor (Tsuchioka *et al.*, 2008), but also of BDNF (Vaidya *et al.*, 1997). Because constitutive activity is likely involved *in vivo* and a considerable extent of receptor desensitisation (see above) exists with these receptors, the functional outcome of receptor activation may likely be small. However, when 5-HT_2R are blocked by antagonists, the constitutive activity may cease and desensitisation may be relieved. This could result in the functional "re-sensitisation" of these receptors. This is most likely the mechanism at work that may explain the rapid antidepressant effects seen with some 5-HT_2R antagonists (Opal *et al.*, 2014).

A full appreciation of the functional impact of 5-HT on transmitter release is likely linked to a detailed understanding of its impact on evoked release. This will be investigated in the next part, with the idea that if there is a transient increase in spontaneous release, evoked release would be affected in a similar way.

4. Modulation of Evoked Release

4.1. Introduction

In contrast to the considerable number of studies on the serotonergic modulation of spontaneous glutamate release in neocortex, only few studies have investigated the modulation of evoked release in this area of brain (Tanaka & North, 1993; Torres-Escalante *et al.*, 2004; Komlosi *et al.*, 2012; Barre *et al.*, 2016).

Specifically, Tanaka and North (1993) showed that in layer V pyramidal cells of the rat cingulate cortex, 5-HT depressed the EPSP amplitude evoked by extracellular stimulation of either the subcortical white matter or layer V itself. In this study, the receptor causing the depression was identified as 5-HT_{1B}R. Barre *et al.* (2016) showed that at thalamocortical synapses onto layer V pyramidal neurons in the mPFC, activation of presynaptic 5-HT_{2A}R potentiated NMDA receptor-mediated EPSCs. In contrast to these two studies, which focussed largely on synapses formed by extracortical projections, Torres-Escalante *et al.* (2004) stimulated layer V neurons of the rat somatosensory cortex with a bipolar electrode and demonstrated that 5-HT via activation of both 5-HT_1R and 5-HT_2R, altered the release probability at glutamatergic synapses made onto layer II pyramidal cells.

These three studies mentioned remained incomplete because, first, their research method (extracellular stimulation) activated an inhomogeneous set of synapses, and second, whilst the authors determined which 5-HTR were activated, they did not address the downstream molecular targets of modulation.

The use of extracellular stimulation might have resulted in an unspecific stimulation of presynaptic fibres of various origins. The lack of stimulus specificity was partially solved by Komlosi *et al.* (2012), who recorded a limited set of cell pairs in human tissue obtained during surgery. This study provided extremely valuable insights by finding that, in pairs of layer II pyramidal cells, activation of 5-HT_2R caused a depression of unitary EPSPs by more than 50%. Unfortunately, again, they only specified the involvement of 5-HT_2R without elucidating the signalling cascade downstream of its activation.

In analogy with this finding, a previous line of research in this laboratory unveiled that in connected pairs of layer II pyramidal neurons, activation of presynaptic α_1-AR by NA depressed the EPSC amplitude by about two thirds (Choy *et al.*, 2017b). Because there was a dissociation between a concomitant increase in the mEPSC frequency, but a large depression in evoked transmitter release, the mechanism employed by NA was found to

rest upon a Gβγ-mediated inhibition of the release machinery, most likely SNAP-25 (Gerachshenko *et al.*, 2005; Yoon *et al.*, 2007). This mechanism was different from the "classical" signalling cascade downstream of α_1-AR activation which involved spontaneous presynaptic Ca^{2+} store release.

In a further effort to check if similar or different mechanisms were also employed when activating 5-HT_2R, which are also linked to G_q signalling, I examined the impact of 5-HT on evoked glutamate release. In this part of my thesis, I will present data how both NA and 5-HT affected EPSCs recorded in pairs of layer II pyramidal cells in barrel cortex. Subsequently, I will discuss how, downstream of 5-HT_2R activation, an increase in spontaneous release can be reconciled with a large depression of evoked EPSCs.

4.2. Specific Hypotheses

Analogous to the modulation of evoked EPSCs by NA, I propose the following hypotheses for the 5-HT-mediated modulation of evoked EPSCs:

1) 5-HT depresses evoked glutamate release in pairs of pyramidal cells.
2) This depression is caused by activation of presynaptic 5-HT_2R, which are coupled to a G_q signalling cascade.
3) As with NA, downstream of 5-HT_2R activation, the EPSC depression is caused by Gβγ, most likely resulting in the direct inhibition of the SNARE complex.

Consequently, in connected pairs, I first characterized the electrophysiological properties of both pre- and postsynaptic pyramidal cells in layer II of rat barrel cortex. I then assessed the monosynaptic EPSCs between them, including their responses to a paired-pulse stimulus (4.4.1). I found that the electrophysiological and synaptic properties of the pairs of pyramidal cells presented in this thesis were not different to those in the data set with NA, allowing a direct comparison of the two sets. Second, I provide data quantifying the 5-HT mediated changes in both the presynaptic APs and postsynaptic properties, including characterising the respective EPSCs. Furthermore, I performed experiments to determine which 5-HTR were activated to cause this depression (4.4.2). Besides some subtle changes to the APs, I discovered that 5-HT depressed unitary EPSCs by 49 ± 3%. Concomitantly, the presynaptic cells typically hyperpolarized and showed a small drop in R_{in}, whereas the postsynaptic cells showed a variable but small change in holding current, together with a large drop in R_{in}. The depression was mimicked by the 5-HT_2R agonist α-methyl-5-HT. Third, I also present data for the depression caused by NA, and make comparisons between the depression caused by 5-HT and that by NA (Choy *et al.*, 2017a; Choy *et al.*, 2017b; sub-part 4.4.3). I observed that the depression caused by 5-

HT was smaller than that by NA. In addition, the depression by NA was caused by Gβγ as a peptide that "chelates" the dimer subunit was able to prevent the depression. Fourth, I elucidated the signalling downstream of 5-HT_2R activation (4.4.4) and found that as with NA, the depression was also caused by Gβγ. However, in the case of 5-HT but in contrast to NA, there was neither a speed-up in the recovery from the depression (R_{50}) nor a decrease in quantal size. These findings suggest that in contrast to the depression by NA, where Gβγ directly inhibited the SNARE complex, the targets of Gβγ downstream of 5-HT_2R activation were most likely Ca^{2+} channels. In 4.4.5, I then brought together different aspects to reveal that there was specificity in the 5-HT-mediated modulation of transmitter release. Specifically, I found that in my paired recordings, non-responders were typically pre-, but responders postsynaptic. To directly test this specificity, I performed experiments where I was able to confirm this arrangement within the microcircuit in layer II.

4.3. Methods and Analyses

Most aspects in regard to solution and slicing have already been described earlier. Only specific aspects not covered previously will be presented in this part.

4.3.1. Obtaining Paired Recordings

Modulation of evoked release was investigated in paired recordings of layer II pyramidal cells in the somatosensory cortex in rats aged P15 – 19. These cell pairs were connected through glutamatergic synapses made up of predominantly AMPA receptors (Tsumoto *et al.*, 1990). In this section, I will describe in detail how to find connected cell pairs and perform the recordings.

One of the most important aspects in obtaining a successful paired recording is choosing the "optimal" slice in which the connectivity between layer II pyramidal cells is well preserved. With parasagittal slices obtained at a cutting angle of 15° from the midline, the "optimal" slice was typically the 5th slice in brains of these rats; *i.e*. 5.0 – 5.3 mm down from the lateral poles towards the midline cut. In some instances, the 4th slice could also contain connected cell pairs. Once the slice with the best conserved connectivity had been selected and placed into the recording chamber, the temperature of the superfusing ACSF was strictly maintained at 36 ± 1°C, which is within the physiological temperature range. A lower temperature was found to result in a significantly smaller rate of connectivity; *i.e*. connected cell pairs were much harder to find, consistent with an earlier report (Hardingham & Larkman, 1998).

In order to successfully obtain cell pairs, I adhered to the following five criteria. 1) The connectivity between pyramidal cells was best in an area of tissue in which 4 – 5 cells grouped together in very close proximity. I refer to this aggregation as a “nest” of cells. 2) The distance between somata was typically less than 25 µm. 2) Connected cells usually had their somata more or less in the same optical plane as judged with the 40x lens. 4) Both, the apical dendrites and the axon initial segments remained parallel to the optical plane. 5) If two somata were vertically aligned with the top one slightly offset from the bottom one (see also Fig. 4.3.1), the connectivity was greater than if they were horizontally aligned.

If two neurons fulfilled these criteria, both of them were patched in the whole-cell configuration using the same intracellular solution as specified in Part 2, unless stated otherwise.

4.3.2. Recording Conditions

For connected pairs, recordings were performed as follows. Using a MultiClamp 700A, the presynaptic cell was kept in current-clamp with the bridge balance automatically compensated using the MultiClamp Commander. The resting membrane potential (V_{rest}) was then measured and allowed to float freely, except in some cases when it was > -60 mV. In these instances, a constant hyperpolarizing bias current of ~200 pA was delivered to restore a normal V_{rest}. A paired-pulse protocol was employed to elicit two APs at an interval of 50 ms which were evoked by short current steps of 5 ms duration and an amplitude of ~1.8 nA. Such a trial was repeated every 5 s (0.2 Hz) for a minimum of 10 times. The low frequency repetitions were chosen to minimise the induction of long-term depression as described by Feldmeyer *et al.* (2006). The presynaptic membrane potential was sampled at 5 kHz after filtering at 10 kHz using the same sample-and-hold amplifier.

The respective recording arrangements are shown in Fig 4.3.1. The DIC image is presented in A with the two somata of the pyramidal cells patched with two electrodes. The postsynaptic cell was kept in voltage-clamp at a holding potential of -70 mV. The two evoked unitary EPSCs, used to gauge short-term plasticity like depression or facilitation (B), were also sampled at 5 kHz after filtering at 1 kHz. Series resistance (R_s) was monitored continuously by recording the current response to a voltage step of 0.5 mV for 40 ms at the end of every trial. R_s was not compensated as it introduced additional electronic feedback noise into the recording, which negatively affected the signal-to-noise ratio of unitary EPSCs.

Connectivity existed if, after on-line averaging of 10 stimulus trials, two EPSCs above baseline noise and with a delay of < 3 ms to the presynaptic APs were evident (A). The connectivity between two cells was checked in both directions to establish whether it was unidirectional or reciprocal. In cases of the latter, the direction that produced the larger EPSC amplitude was chosen for the subsequent experiment. The control period typically consisted of 300 trials, after which 10 µM 5-HT was added to the superfusate. Subsequently, the recordings were resumed for at least another 300 trials.

To monitor synaptic dynamics, I evoked 20 APs at a frequency of 50 Hz in the presynaptic cell to induce a steady-state EPSC depression. Thereafter, with an interval of 500 ms, I evoked another AP to measure the recovery from steady-state depression (Fuhrmann *et al.*, 2004).

The data were stored on a computer disk using custom-made IGOR Pro procedures.

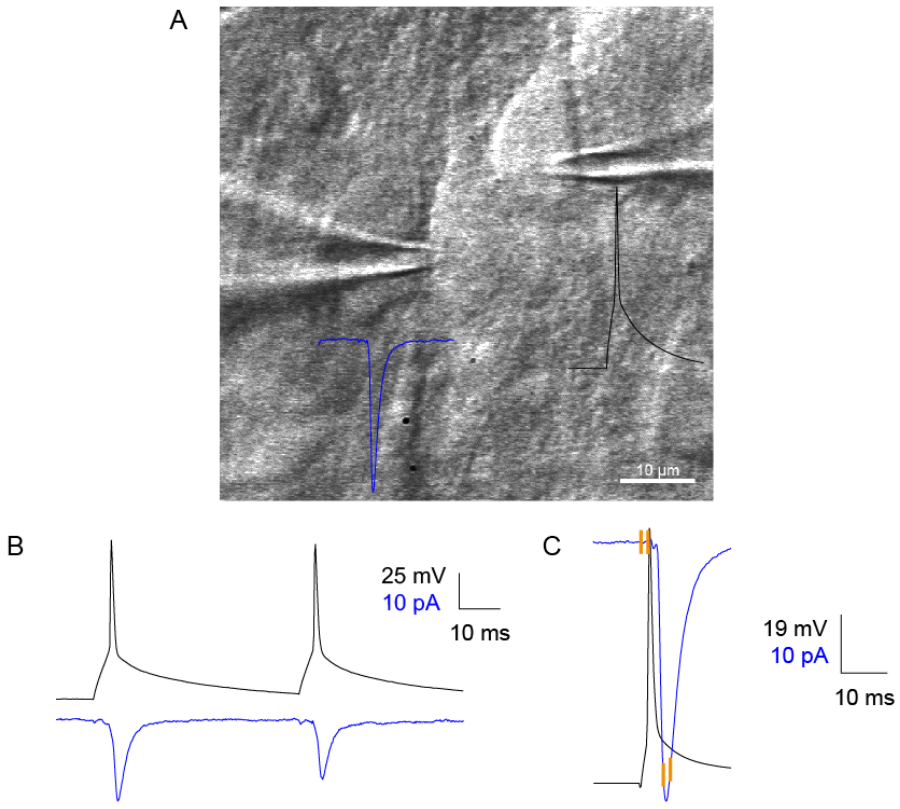

Figure 4.3.1. Paired recordings.

A. DIC image of the two recorded cells in layer II with the tips of the respective patch electrodes visible. Superimposed are the traces of the AP (black) and the postsynaptic EPSC (blue). B. Time courses of the of two elicited APs (50 ms interval; black) and the evoked average EPSCs (blue). C. Overlay of the time courses of the first AP and the respective EPSC indicating the synaptic delay. The two pairs of cursors indicate where and how the amplitude of the EPSC was measured.

4.3.3. Intracellular Solution

In most experiments, the standard intracellular solution as in Part 3 was used. In addition, in some experiments, 100 µM of the commercially available myristoylated Gβγ-binding peptide mSIRK (Goubaeva *et al.*, 2003) was added to the presynaptic patch solution. The addition of this peptide increased the osmolality of the patch solution from 303 to ~310 mOsm/kg H_2O. However, since this value remained lower than the standard osmolality of the ACSF, which was around 320 mOsm, no further dilution was performed. Likewise, the synthesized C-terminal peptide of SNAP-25 (ct-SNAP-25), which also scavenges Gβγ, was added to the presynaptic patch solution in a few experiments. The final concentration of this ct-SNAP-25 was set to 8 mg/ml (= 5.41 mM). Again, no adjustments needed to be made to the patch solution when this peptide was added.

4.3.4. Analysis of EPSCs

Analysis was performed by displaying the AP together with the corresponding EPSC. In order to avoid any contamination by spontaneous EPSCs, each EPSC amplitude was manually examined and measured as the difference between the averages of two time windows, one at the peak (1 ms) and the another before the onset of the EPSC (2 ms baseline; Fig. 4.3.1C). If the baseline or rise-time was contaminated by a spontaneous EPSC, the trial was discarded without replacement. The membrane current noise (σ_n) was then estimated from the population of the differences between the averages of two equivalent time windows along the baseline of the EPSC. These two windows were also chosen such that they did not contain any spontaneous EPSCs either. Note, however, that the whole-cell noise (σ_{wn}) as used in 4.4.5.2 was different to σ_{noise} (as defined in 3.3.2) and σ_n. σ_{wn} represents the point-by-point standard deviation of the membrane current over a large time window (48 ms) and intentionally did not exclude spontaneous EPSCs. It was introduced to capture the impact of spontaneous release. It was measured after the evoked EPSCs had decayed back to baseline, not to be contaminated by asynchronous release (see Fig. 4.4.24). I note that a comparison between σ_{noise} and σ_{wn} could be justified, with the latter always being larger than the former. But this cannot be done with σ_n as the latter was typically about half of either σ_{noise} or σ_{wn}.

The latency from the peak of the AP to that of the EPSC (peak-to-peak latency) was measured during the last minute of the control recording period and during the sixth minute after 5-HT addition, after which 5-HT had certainly reached a constant concentration. The properties of APs were measured as described earlier in 3.3.5. The EPSCs were characterised as follows. The rise time was determined as the time between 10 and 90% of the average peak EPSC amplitude. The half-width was measured as the

width of the EPSC at half of its peak amplitude. The stationarity of EPSCs between two periods (a minute each) was judged by a Student's *t*-test, and considered stationary if $p_t > 0.05$.

4.3.5. Quantification of Synaptic Dynamics

The recovery from short-term depression was quantified as R_{50} based on the following equation

$$R_{50} = \frac{\bar{E}_{Rec} - \bar{E}_1}{\bar{E}_1 - \bar{E}_{SS}},$$

where R_{50} is the recovery at 50 Hz, $\bar{E}_{Rec}$ the average amplitude of the recovery EPSC, $\bar{E}_1$ the average amplitude of the first EPSC, and $\bar{E}_{SS}$ the average amplitude in steady-state depression. $\bar{E}_{SS}$ was calculated as the average of the last four EPSC amplitudes during the 50 Hz train. Note that after a burst of 20 APs, short-term depression was always observed at these synapses; *i.e*. $\bar{E}_{SS} < \bar{E}_1$. As a consequence, the denominator was always positive, and hence, R_{50} was positive if $\bar{E}_{Rec} > \bar{E}_1$. The values of R_{50} during control and 5-HT were then statistically compared using a paired *t*-test. During control condition, the value was typically negative.

4.3.6. Quantal Analysis

Density based quantal analyses of EPSCs were done as described earlier (Stricker *et al.*, 1996a, b; Cowan & Stricker, 2004). In short, after each recording fulfilled the quality criterion of stationarity (*i.e*. having at least 100 – 300 stationary EPSCs evoked during the control period, and approximately an equal number after NA or 5-HT addition), the respective probability density function (PDF) was formed using an optimised Gaussian kernel. To these PDFs, models were first fitted to the null hypothesis (H_0) that these densities could have resulted from a unimodal process (gamma, Weibull, double Gaussian and cubic transform of a Gaussian variable) and, hence, were not created by a multi-modal process. If this H_0 could be rejected, multimodal models of transmission with an increasing number of constraints (complexity) were systematically tested against less complex models. These were a) a quantal model where the normal distributions in the mixture model are separated by a constant increment (*i.e*. quantal size, *Q*); b) a quantal model as in a) but with quantal variance added to the noise variance; c) a quantal model with uniform release probabilities (binomial), with or without quantal variance; and

d) a quantal model with non-uniform release probabilities (compound binomial), with or without quantal variance.

Each of these models of transmission had their parameters adjusted to maximise the likelihood of the fit to the PDF. Once the most appropriate model of transmission was determined, Q, the coefficient of variation of Q (CV_Q) where appropriate, and the quantal content ($m = n * p$ = average EPSC / Q) were calculated. Confidence limits of each parameter were estimated using a balanced bootstrap scheme.

4.3.7. Statistical Analyses

Linear correlations were evaluated using Pearson's correlation test, with r the correlation coefficient, and p_{Pr} the probability under the null hypothesis that there is no correlation.

4.4. Results

The results are presented in five sections, 4.4.1 – 4.4.5. In 4.4.1, I will describe the electrophysiological properties of both the pre- and postsynaptic cells in pyramidal pairs. These include their passive membrane properties, the properties of presynaptic APs, and those of the postsynaptic EPSCs. In 4.4.2, I will describe how 5-HT modulated evoked EPSCs, accompanied with results from experiments that pharmacologically determined which 5-HTR were activated. To get further insight into the molecular mechanism(s), in 4.4.3, I will compare the modulation of the EPSC by 5-HT with that by NA. In 4.4.4, I will present data from experiments designed to determine the signalling pathway downstream of 5-HTR, which caused the EPSC modulation. In addition, I will detail the results of quantal analyses based on density estimation, to unravel the downstream target(s). Finally, in 4.4.5, I will describe how 5-HT affected the "network specificity", and link together the results from Part 3 on spontaneous and from this Part on evoked release.

4.4.1. Properties of Pyramidal Cell Pairs in Layer II

4.4.1.1. Slow Depression Seen in Most Cell Pairs

I obtained recordings from 56 pyramidal cell pairs in layer II of the barrel cortex. The paired-pulse protocol (as described in 4.3.2) was employed in 38 pairs, whilst in the remaining 18 pairs, trains of APs were applied. The characteristics presented in the following two sections 4.4.1.1 and 4.4.1.2 are based solely on the data obtained from the 38 cell pairs studied with the paired-pulse protocol.

A typical result of a paired recording between two pyramidal cells is shown in Fig. 4.4.1. In this pair, the presynaptic cell had an input resistance (R_{in}) of 157 MΩ at V_{rest} of -69.1 mV, and R_s of 19 MΩ. When two square current pulses of 1.2 nA were injected at an interval of 50 ms, two presynaptic APs were elicited (A, top trace). The time delay from the starting point of first current injection to the threshold of the first AP (time to V_{thr}) was 3.1 ms. The threshold of the first AP (V_{thr}) was -43.7 mV. The difference between V_{thr} and V_{rest}, called relative membrane voltage difference (V_{rel}), was 25.4 mV in this case. The height of the first AP (H), measured from V_{thr} to its peak, was 70.3 mV. The time taken from V_{thr} to the peak of AP is called action potential rise time (RT), which in this case was 0.6 ms. The width of this AP at half amplitude (W) was 0.9 ms.

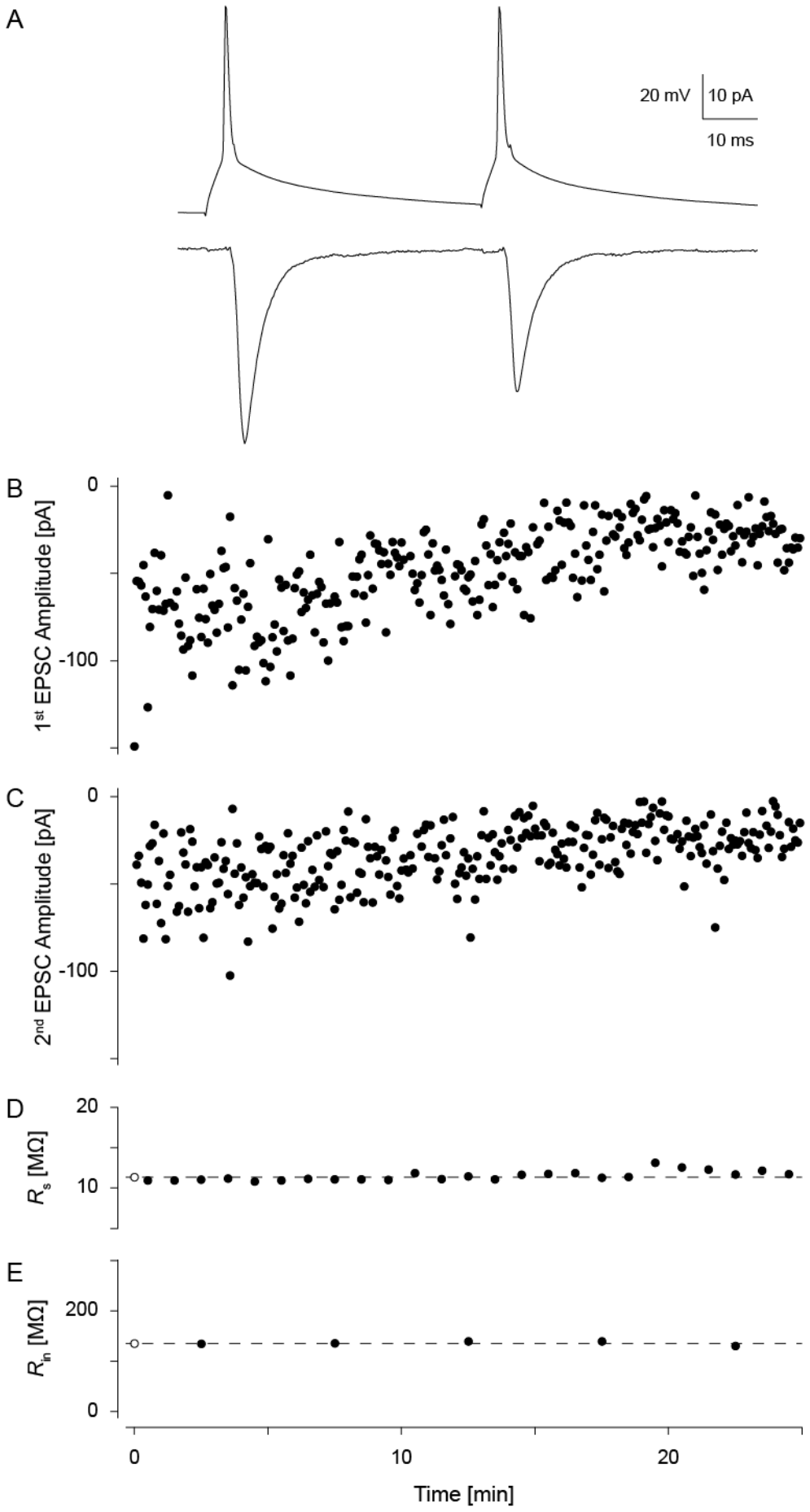
A
20 mV
10 pA
10 ms
B
0
-100
1st EPSC Amplitude [pA]
C
0
-100
2nd EPSC Amplitude [pA]
D
20
10
Rs [MΩ]
E
200
0
Rin [MΩ]
0
10
20
Time [min]

Figure 4.4.1. Typical recording using a paired-pulse protocol.

A. Time courses of the presynaptic membrane potential with two APs (upper trace) and the postsynaptic currents including the average EPSCs (lower trace). B. Individual peak EPSC amplitudes evoked by the 1st AP plotted against time during the experiment. C. Same as in B, but for the 2nd EPSC. D. Minute averages of the postsynaptic R_s for the entire recording period. The average value is indicated by the open circle and the value is plotted for the duration of recording period as the dashed line. E. Same as in D, but for R_{in}, pooled for blocks of 5 min.

The second AP, which was elicited 50 ms after the first one, had the following properties: time to V_{thr} 2.7 ms, V_{thr} -42.7 mV, V_{rel} 26.4 mV, H 68.9 mV, RT 0.6 ms, and W was 0.9 ms.

For each AP elicited in the presynaptic cell, the membrane current for a holding potential of -70 mV in the postsynaptic cell was recorded. The postsynaptic cell in this pair had a R_{in} of 135 MΩ and R_s of 11 MΩ. The recording noise in the baseline (σ_n) was 0.7 pA. Each EPSC amplitude was measured and the respective average time course was formed from 300 trials recorded over a period of 25 min. It is shown as the bottom trace in A with the corresponding AP above. The average EPSC amplitude was -41.6 ± 1.3 pA. The latency from the first AP peak to the EPSC peak (peak latency) was 2.3 ms. The EPSC rise time was 1.7 ms and the half-width 4.1 ms.

The average second EPSC had the following properties: average amplitude of -30.2 ± 0.9 pA, peak latency of 2.2 ms, rise time of 1.6 ms, and half-width of 3.9 ms. The paired-pulse ratio (PPR) for this pair was 0.73 ± 0.03; *i.e*. there was a small depression at this junction.

The individual peak EPSC amplitudes of each of the 300 trials are plotted in B. Note, that the EPSC amplitude was not stationary throughout this recording period. The average peak EPSC amplitude for the first minute was -72.4 ± 9.5 pA. The peak EPSC amplitudes showed a slight facilitation reaching an average amplitude of -84.1 ± 6.0 pA during the fifth minute. This was followed by a slow depression in a single exponential manner (τ = 8.2 min), which finally reached stationarity for the last eight minutes of the recording. During this final stationary period, the average peak amplitudes of the first and the last minutes were not significantly different (-34.3 ± 4.8 *vs.* 34.4 ± 2.2 pA; p_t = 0.99), giving an average peak amplitude of -28.3 ± 1.2 pA for the whole stationary period. In this case and compared to its initial value, there was a significant depression by 61 ± 5% (p_t = $7 \cdot 10^{-4}$).

A similar pattern was observed for the peak amplitudes of the second EPSC, which also reached a stationary period for the last 8 minutes of recording (C). Specifically, the average peak amplitudes were -44.0 ± 5.7 pA in the first minute, -46.1 ± 4.6 pA after the initial facilitation (the fifth minute), and -23.5 ± 1.2 pA during the stationary period (the last eight minutes). These values indicated that a significant slow depression (τ = 11.0 min) by 47 ± 7% ($p_t = 5 \cdot 10^{-3}$) occurred for the second EPSC. Note that when the extents of the slow depression of the first and second EPSCs were tested with a Student's *t*-test, no significant difference was found (p_t = 0.14).

In D, the values of R_s in the postsynaptic cell, after pooling for every minute, are given (solid circles). The open circle, extrapolated with the dashed line, indicates the average value during this recording period; *i.e*. 11 MΩ throughout. This figure suggests that the slow depression observed in this case was not the result of a change in R_s. Likewise, in E, the values of R_{in} in the postsynaptic cell are presented after pooling for five minutes each (solid circles). The open circle, and indicated with the dashed line for the duration of the recording, represents the average value of 135 MΩ obtained from the total sample. Again, no significant changes were seen during the recording period, suggesting that a systematic change in R_{in} could not account for the slow depression either.

I also checked if this slow depression affected the kinetics of the EPSCs (Fig. 4.4.2). For this purpose, I compared the time courses of average first EPSC from 1) all 300 repetitions during the recording (B, black), 2) 60 repetitions during the first 5 min (A and C, dark grey), and 3) 60 repetitions of last 5 min (A and D, light grey). Despite clear differences in amplitude, *i.e*. -41.6 ± 1.3 *vs.* -72.4 ± 3.4 *vs.* -29.3 ± 1.5 pA, respectively (E), there was no difference in the time courses, when all the average EPSCs were overlaid and peak-scaled to the same amplitude (F).

Out of 38 pyramidal pairs studied in this manner, 32 (84%) showed a slow depression in the EPSC amplitudes. On average, the presynaptic cells had R_{in} of 175 ± 15 MΩ and V_{rest} of -76.2 ± 0.8 mV.

The characteristics of the first AP in the presynaptic cell were as follows: time to V_{thr} was 3.8 ± 0.1 ms, V_{thr} -44.1 ± 0.9 mV, V_{rel} 32.1 ± 0.9 mV, *H* 75.0 ± 1.5 mV, *RT* 0.6 ms, and *W* 0.9 ms. For the second AP, the characteristics were: time to V_{thr} was 3.2 ± 0.1 ms, V_{thr} -43.9 ± 0.9 mV, V_{rel} 32.3 ± 0.9 mV, *H* 74.4 ± 1.5 mV, *RT* 0.6 ms, and *W* 0.9 ms.

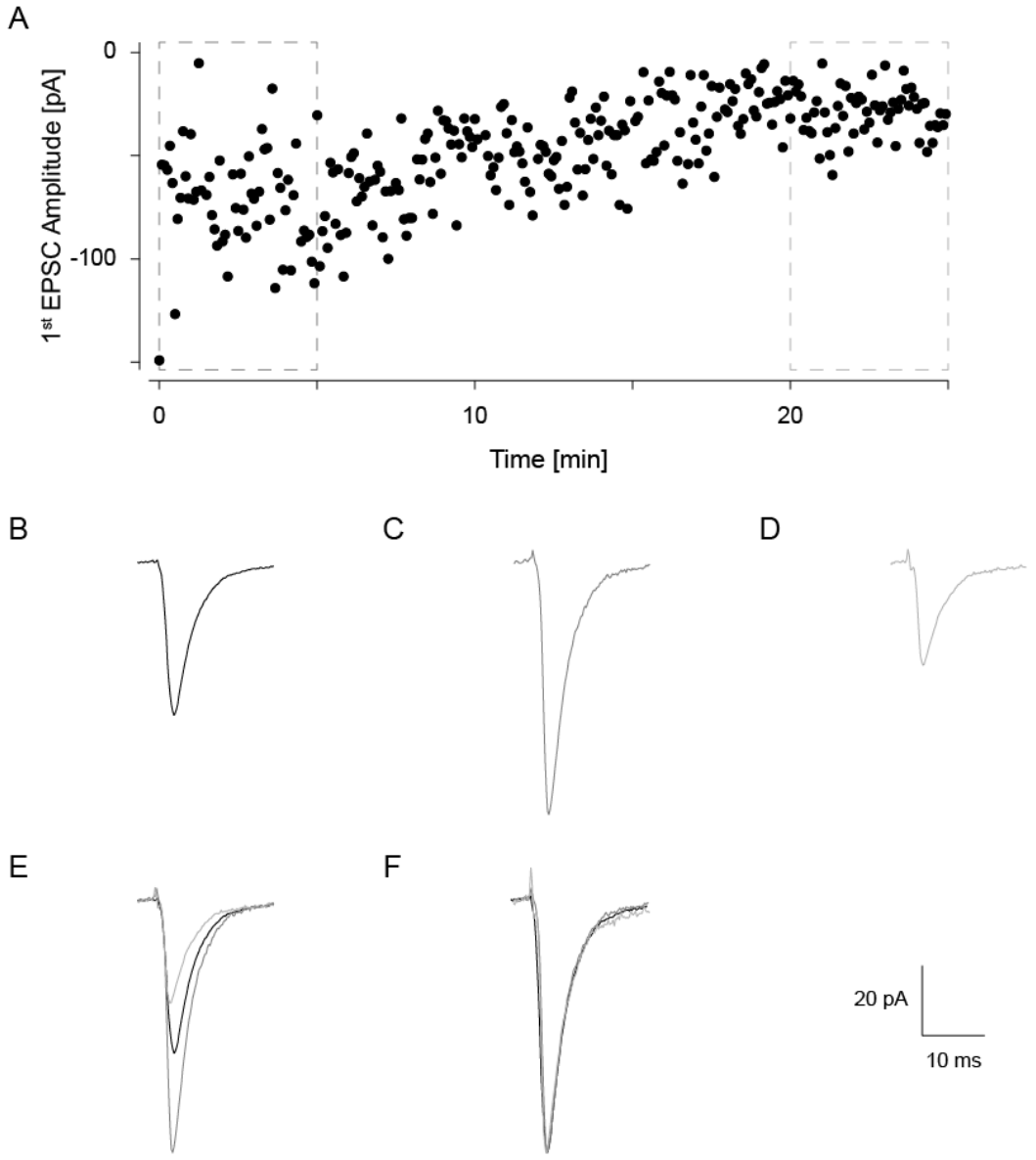

Figure 4.4.2. EPSC time course not affected by slow depression.

A. Individual peak amplitudes of the first EPSCs plotted *vs.* recording time (same data as in Fig. 4.4.1B). The time course of the average EPSC during the whole period is presented in B (black), that bounded by the dashed box to the left is shown in C (dark grey), and D for the box to the right (light grey). E. Superposition of the time courses presented in B – D. F. Same as in E, except that EPSCs are peak-scaled to the same value.

On average, the postsynaptic cells had a R_{in} of 212 ± 20 MΩ and σ_n of 0.9 ± 0.0 pA at a R_s of 15 ± 1 MΩ. The average amplitude of the first EPSC was -28.4 ± 3.7 pA during the first minute of recording. The slow depression occurred at a single exponential rate with an average time constant (τ) of 10.8 ± 2.0 minutes. Consequently, the first EPSC amplitude depressed by 67 ± 2% to -9.4 ± 1.3 pA over the first 15 – 20 minutes of recordings. Thereafter, in most cells, the EPSC did not depress significantly any further;

i.e. it had reached a stationary period for at least 5 minutes, which fulfilled the criterion of stationarity. As the depression had steadied, such periods were accepted for comparisons with subsequent parts of the experiment. The average peak-to-peak latency for the first EPSC was 2.9 ± 0.1 ms, the rise time 1.8 ± 0.1 ms, and half-width 4.5 ± 0.2 ms. There was no relationship between the rate of the depression and R_s as one might have expected (p_{pt} = 0.18).

Similar to the first EPSC, the amplitude of the second also exhibited a slow depression at an exponential rate. At the start, the amplitude was -22.1 ± 3.6 and at the end -6.9 ± 1.3 pA, which corresponded to a depression of 68 ± 3%. This depression was not different from that of the first EPSC (p_{pt} = 0.59). The average value of τ was 9.5 ± 1.4 min, again no different from that of the first EPSC (p_{pt} = 0.56). The other properties of the second EPSC were as follows: peak-to-peak latency 2.7 ± 0.2 ms, rise time 1.7 ± 0.0 ms, and half-width 4.3 ± 0.2 ms.

From this set of data, the following conclusions could be drawn: 1) In the majority of pairs, a significant depression was observed within the first 15 – 20 min of recording. 2) In most cells, the depression had reached a stationary amplitude after about 20 min. 3) The time course of the EPSC was not affected by this depression.

4.4.1.2. Pairs without EPSC Depression

In contrast to the 32 pyramidal pairs with this slow depression, 6 pyramidal pairs maintained a stationary EPSC amplitude throughout the recording period. The data from such a pair are shown in Fig. 4.4.3.

In this case, the presynaptic cell had a R_{in} of 344 MΩ and a V_{rest} of -74.7 mV. Two square current pulses of 1.2 nA amplitude, injected at an interval of 50 ms, elicited two APs in this cell (A, top trace). The time to V_{thr} for the first AP was 3.7 ms. V_{thr} was -44.7 mV, and hence V_{rel} 30.0 mV. The other properties of this first AP were: *H* 74.8 mV, *RT* 0.5 ms, and *W* 0.6 ms. The second AP had the following properties: time to V_{thr} 2.8 ms, V_{thr} -44.1 mV, V_{rel} 30.6 mV, *H* 72.9 mV, *RT* 0.5 ms, and *W* was 0.6 ms.

The bottom trace in A shows the average time courses of EPSCs from the 300 repetitions recorded over 25 minutes. The postsynaptic cell had a R_{in} of 308 MΩ and a σ_n of 1.0 pA at a R_s of 11 MΩ. The respective individual peak amplitudes of the first EPSC were stationary, as shown in B, in which the average value for the first 12 points (corresponding to one minute) is not significantly different to that of the last 12 points (-9.7 ± 3.1 *vs.* -9.3 ± 2.0; p_t = 0.92).

The average value throughout the 25 minutes recording period was -12.4 ± 0.5 pA. Other properties of the average first EPSC were as follows: peak-to-peak latency 2.4 ms, rise time 1.4 ms, and half-width 3.7 ms.

The second EPSC is shown in C and had an average amplitude of -9.4 ± 0.5 pA. Similar to the first, the second EPSC was also stationary as there was no significant difference in the average peak amplitude between the first 12 points and the last 12 points (-8.9 ± 3.2 *vs.* -6.2 ± 1.8; $p_t = 0.46$). The value of PPR was 0.76 ± 0.05, again indicating a small short-term depression. The other properties of this second EPSC were: peak-to-peak latency 2.2 ms, rise time 1.6 ms, and half-width 3.6 ms. In D, the values of R_s in the postsynaptic cell for every minute are shown (solid circles). The open circle represents the average value in this recording. This average value is indicated by the dashed line throughout. The values of the postsynaptic R_{in} for every 5 minutes are shown in E (solid circles), with both the open circle and the dashed line indicating the average value throughout the recording.

In this set of 6 pairs, the presynaptic cells had a R_{in} of 157 ± 43 MΩ and a V_{rest} of -74.8 ± 1.1 mV. The average values of the first AP were: time to V_{thr} 3.8 ± 0.2 ms, V_{thr} -38.5 ± 4.1 mV, V_{rel} 37.6 ± 4.9 mV, *H* 70.7 ± 2.6 mV, *RT* 0.6 ms, and *W* 1.0 ± 0.2 ms. The average values for the second AP were: time to V_{thr} 3.2 ± 0.2 ms, V_{thr} -38.3 ± 4.1 mV, V_{rel} 37.9 ± 4.9 mV, *H* 70.2 ± 2.2 mV, *RT* 0.6 ± 0.1 ms, and *W* 1.1 ± 0.2 ms. The postsynaptic cells had a R_{in} of 163 ± 28 MΩ and σ_n of 0.9 ± 0.0 pA at a R_s of 16 ± 4 MΩ.

The average amplitude for the first EPSC during the first minute of recording (initial EPSC amplitude) was -14.2 ± 3.4 pA, and during the last minute was -16.9 ± 5.2 pA, whilst the average amplitude for whole 25 minute-recording period was -14.3 ± 3.9 pA, clearly showing that a slow depression did not occur in these pairs ($p_{ANOVA} = 0.51$). The average peak-to-peak latency for the first EPSCs was 2.3 ± 0.3 ms, rise time 1.5 ± 0.0 ms, and half-width 4.0 ± 0.4 ms. The average amplitude for the second EPSC was slightly smaller than the first one (-12.1 ± 3.1), giving an average PPR of 0.94 ± 0.11. Other properties of the second EPSC were: peak latency 2.5 ± 0.4 ms, rise time 1.5 ± 0.1 ms, and half-width 3.9 ± 0.3 ms.

Comparing this set of values with those for the pairs with depression revealed that there was no significant difference in the passive membrane and AP properties of the presynaptic cells ($p_t \geq 0.16$). Likewise, the passive membrane properties of the postsynaptic cells did not show any significant differences either ($p_t \geq 0.19$).

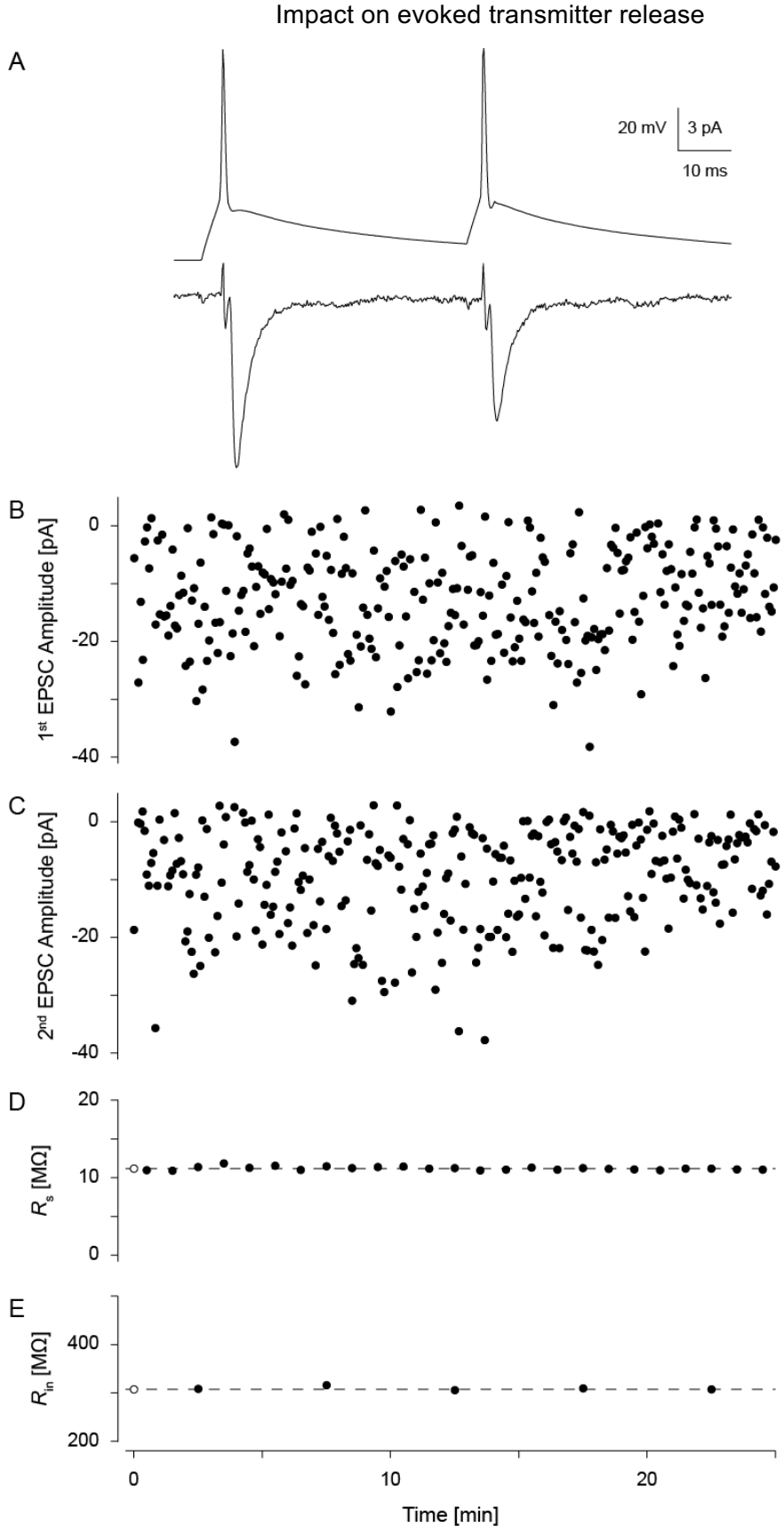

Figure 4.4.3. Paired recording with maintained EPSC amplitudes.

A. Time courses of the membrane potential with two APs (upper trace) and the average EPSCs (lower trace). B. Individual peak EPSC amplitudes evoked by the 1st AP plotted against time during the experiment. C. Same as in B, except for the 2nd AP. D. Minute averages of the postsynaptic R_s for the entire recording period. The average value is

indicated by the open circle and a dashed line drawn for the duration of the experiment. E. Same as in D, except for R_{in} after pooling for 5 min.

However, I observed an obvious difference in the initial EPSC amplitude. Its average value in pairs with a stationary amplitude was only half of that in pairs with a slow depression (-14.2 ± 3.4 *vs.* -28.4 ± 3.7 pA; p_t = 0.01). Interestingly, after the slow depression had become stationary, no significant difference could be observed between the two groups (-14.3 ± 3.9 *vs.* -10.3 ± 1.3 pA; p_t = 0.38). In addition, the first AP peak to the EPSC peak latency in pairs with a stationary amplitude was significantly faster than that that of pairs with a slow depression (2.3 ± 0.3 *vs.* 2.9 ± 0.1 ms; p_t = 0.007). This was also close to significant for the latency from the second AP peak to the second EPSC peak (2.5 ± 0.4 *vs.* 2.7 ± 0.2 ms, respectively; p_t = 0.076). This difference was partially accounted for by a significantly faster rise time of the first (1.5 ± 0.0 *vs.*1.8 ± 0.1; p_t = $3 \cdot 10^{-4}$) and second EPSCs (1.5 ± 0.1 *vs.*1.7 ± 0.0 ms; p_t = 0.017). No significant differences were observed for the half-widths of EPSC (p_t > 0.30) and PPR (p_t > 0.29).

The observed differences in the peak-to-peak latency and EPSC rise time were unlikely caused by different AMPA subunit combinations in these pyramidal cells (Conti *et al.*, 1994). These findings rather indicate a difference in the position of synapses along the axon (latency) and their location on imperfectly space-clamped dendrites (rise time). Specifically, synapses in pairs with a slow depression might be located further away on the axon, and also on more remote dendritic compartments (from the soma).

4.4.1.3. Properties of Presynaptic Cells

As there was no difference between the two groups of pairs in regard to the presynaptic properties (p_t > 0.52), I pooled the respective data. In addition, because the first AP in a 50 Hz train of 20 APs was not different either (p_t > 0.069), data from the other 18 pyramidal pairs were also included to give a total of 56 pairs. The data of these properties are presented in Fig. 4.4.4. in the form of histograms.

V_{rest} ranged from -82.5 to -66.5 mV with an average value of -75.4 ± 0.5 mV. The respective histogram is presented in A, formed using a bin width of 4 mV. The distribution was more or less symmetric around the mean. Likewise, R_{in} ranged from of 38 to 417 MΩ, having an average value of 162 ± 10 MΩ. The distribution for R_{in} is shown in B, with a bin width of 45 MΩ. It had a slightly positive skew (skew = 1.03), with a tail towards larger values of R_{in}.

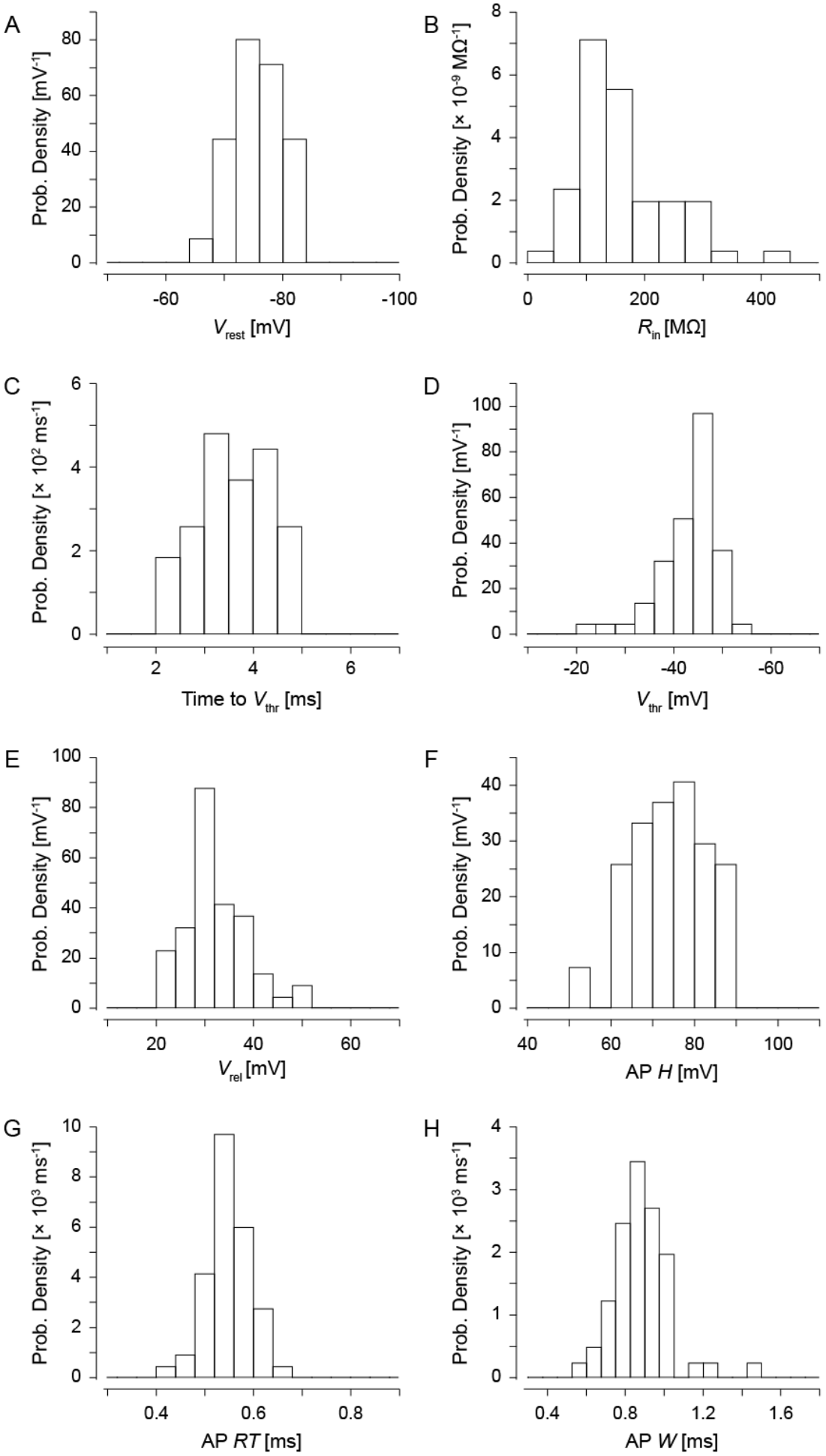
A
Prob. Density [mV-1]
80
60
40
20
0
-60
-80
-100
Vrest [mV]
B
Prob. Density [× 10-9 MΩ-1]
8
6
4
2
0
0
200
400
Rin [MΩ]
C
Prob. Density [× 10² ms-1]
6
4
2
0
2
4
6
Time to Vthr [ms]
D
Prob. Density [mV-1]
100
80
60
40
20
0
-20
-40
-60
Vthr [mV]
E
Prob. Density [mV-1]
100
80
60
40
20
0
20
40
60
Vrel [mV]
F
Prob. Density [mV-1]
40
30
20
10
0
40
60
80
100
AP H [mV]
G
Prob. Density [× 10³ ms-1]
10
8
6
4
2
0
0.4
0.6
0.8
AP RT [ms]
H
Prob. Density [× 10³ ms-1]
4
3
2
1
0
0.4
0.8
1.2
1.6
AP W [ms]

Figure 4.4.4. Properties of the presynaptic cells and APs.
Histograms formed from the passive membrane properties V_{rest} (A), and R_{in} (B). Also shown are the respective probability densities of the time to V_{thr} (C), V_{thr} (D), V_{rel} (E), H (F), RT (G), and W (H).

In regard to the AP, the average time to V_{thr} was 3.6 ± 0.1 ms (range 2.1 to 4.9 ms; C; bin width 0.5 ms). The average V_{thr} was -43.2 ± 0.8 mV (range -52.1 to -23.7 mV; D; bin width 4 mV). V_{rel} had an average value of 32.3 ± 0.9 mV (range 21.1 to 51.3 mV; E; bin width 4 mV). On average, H of the first AP was 73.8 ± 1.2 mV (range 54.7 to 89.7 mV; F; bin width 5 mV), while RT was 0.6 ± 0.0 ms (range 0.4 to 1.6 ms; G; bin width 0.04 ms), and W was 0.9 ± 0.0 ms (range 0.6 to 1.4 ms; H; bin width 0.075 ms). The densities of the time to V_{thr}, and H, RT, and W of the first AP were more or less symmetrical. In comparison, the histograms of V_{thr} and V_{rel} had a distribution with a short tail.

To further characterize the presynaptic cells, I also compared the properties of the two APs elicited at the short interval of 50 ms (Fig. 4.4.5). In this set, the number of pairs corresponded to 38.

In A, the comparison between the time to V_{thr} of the second against that of the first AP for each pair is presented, with the line of identity dashed. The data in almost all cases showed that, for the second AP, the time to V_{thr} was systematically shorter than that for the first. In fact, a significant linear correlation was uncovered by a Pearson's correlation test (r_{38} = 0.91; p_{Pr} = $1 \cdot 10^{-14}$; solid line). Further, I tested if this linear correlation was statistically different from the line of equality by rotating the data points by -45° and then checking if the deviations around zero were random; *i.e*. if the data points in this situation were still correlated with the time to V_{thr}. This was not the case (p_{Pr} = 0.92); *i.e*. the best linear fit to the data points was not significantly different from the line of identity (A, dashed and superpositioned solid line). Note that this outcome most likely resulted because, as compared to D and E for example, the variance around the line of identity was much larger.

Similar comparisons were performed for the other properties. Specifically, V_{thr} (B), V_{rel} (C), H (D), RT (E), and W (F) of the second AP were all linearly correlated to those of the first AP (all $p_{Pr} < 10^{-13}$). Except for the two cases in D and E, the correlations were not different from the line of identity ($p_{Pr} > 0.29$ in all cases).

The linear correlation between H of the second (y) and first (x) AP could be described by y = 0.99 x. The slope of this linear relationship indicates that the second H was slightly (1%) smaller than the first one. Regarding RT, the linear correlation was y = 1.04 x, with

y *RT* of the second and x that of the first AP. The slope indicates that *RT* of the second was slower by 4% compared to that of the first AP. This data suggests that there were minimal changes to the presynaptic APs.

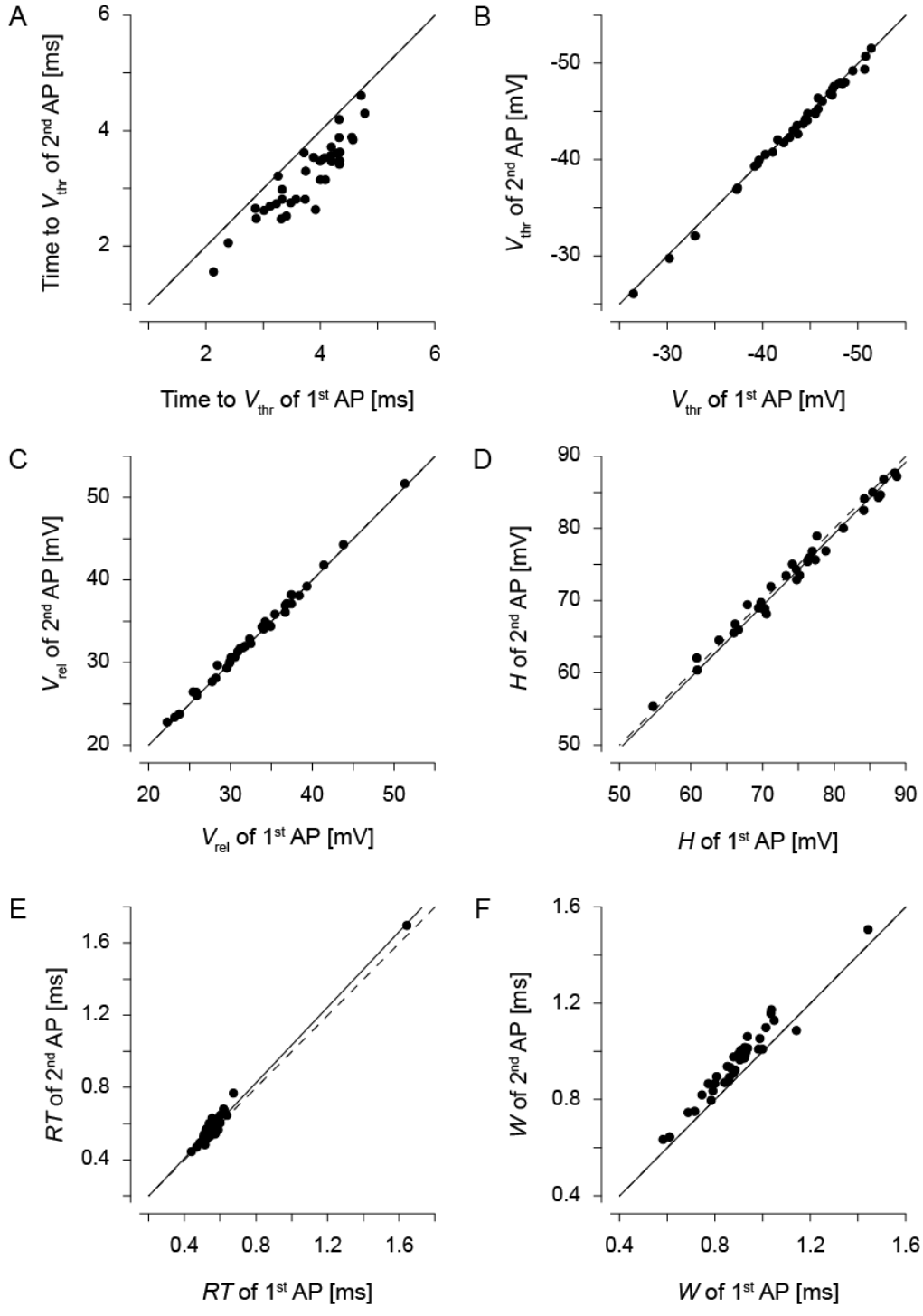

Figure 4.4.5. Comparison of presynaptic properties.

Plots of the second *vs.* first time to V_{thr} (A), V_{thr} (B), V_{rel} (C), *H* (D), *RT* (E), and *W* (F). Solid line represents the best linear fit to the data. Line of identity dashed.

4.4.1.4. Properties of Postsynaptic Cells and EPSCs

Based on 56 pairs, the respective distributions for the passive membrane properties (R_{in}, I_{hold}, and σ_n) and the first EPSC (initial peak amplitude, amplitude during the stationary period, rise time, and half-width) are presented in Fig. 4.4.6.

R_{in} had an average value of 207 ± 16 MΩ and ranged from 64 to 628 MΩ. The distribution of R_{in}, formed with a bin width of 45 MΩ, is shown in A. This density had a positive skew (1.55), *i.e*. it had a long tail towards large values. The holding current, I_{hold}, had an average value of 62.3 ± 7.9 pA (ranging from -100.0 to 195.0 pA). This indicates that the V_{rest} was typically more hyperpolarized than -70 mV. The relevant histogram based on a bin width of 40 pA is presented in in B.

σ_n, for an average R_s of 16 ± 1 MΩ, ranged from 0.66 to 1.22 pA, with an average value of 0.88 ± 0.02 pA. With a bin width of 0.08 pA, the relevant density is presented in C. Note that σ_n in each cell was much smaller than the peak of the unitary EPSC amplitude (E and F), enabling the observation of EPSC amplitudes as small as -1.5 pA. The average peak-to-peak latency was 2.8 ± 0.1 ms (ranging from 1.4 to 4.8 ms; bin width 0.5 ms; D). The initial EPSC amplitude, during the first minute of recording, was -30.2 ± 3.6 pA (ranging from -5.4 to -145.1 pA; bin width 10 pA; E). Its distribution was negatively skewed (-2.16; note that the x axis in E is reversed, with more negative values indicating larger amplitudes). After the slow depression had reached a steady state, the subsequent stationary EPSC amplitudes were binned at 7.5 pA, with the density shown in F. The average peak EPSC amplitude during this stationary period was -14.2 ± 1.6 pA (ranging from -1.4 to -63.7 pA). This indicates that, in this data set (including the stationary pairs), the EPSCs on average depressed by 48 ± 5%. These amplitudes remained negatively skewed despite the depression (skew = -2.03). The density for the rise times is presented in G. The average value was 1.7 ± 0.0 ms (ranging from 1.2 to 2.5 ms; bin width 0.2 ms). The average half-width was 4.5 ± 0.1 ms (ranging from 3.0 to 7.3 ms; bin width 0.5 ms; H). Both distributions are positively skewed (1.15 and 0.86). Histograms of the peak-to-peak latencies, rise times, and half-widths also showed tails towards larger values.

To check how these parameters changed from the first to the second EPSC, their values were plotted against each other (n = 38) in Fig. 4.4.7. The data for the peak-to-peak latency of the second against that of the first EPSCs is shown in A. The data points grouped around the line of identity (dashed). In fact, this data set showed a highly significant correlation ($p_{Pr} < 10^{-15}$), whose best fit was no different to the line of identify (p_{Pr} = 0.99; solid line), suggesting that the latencies after both stimuli were identical.

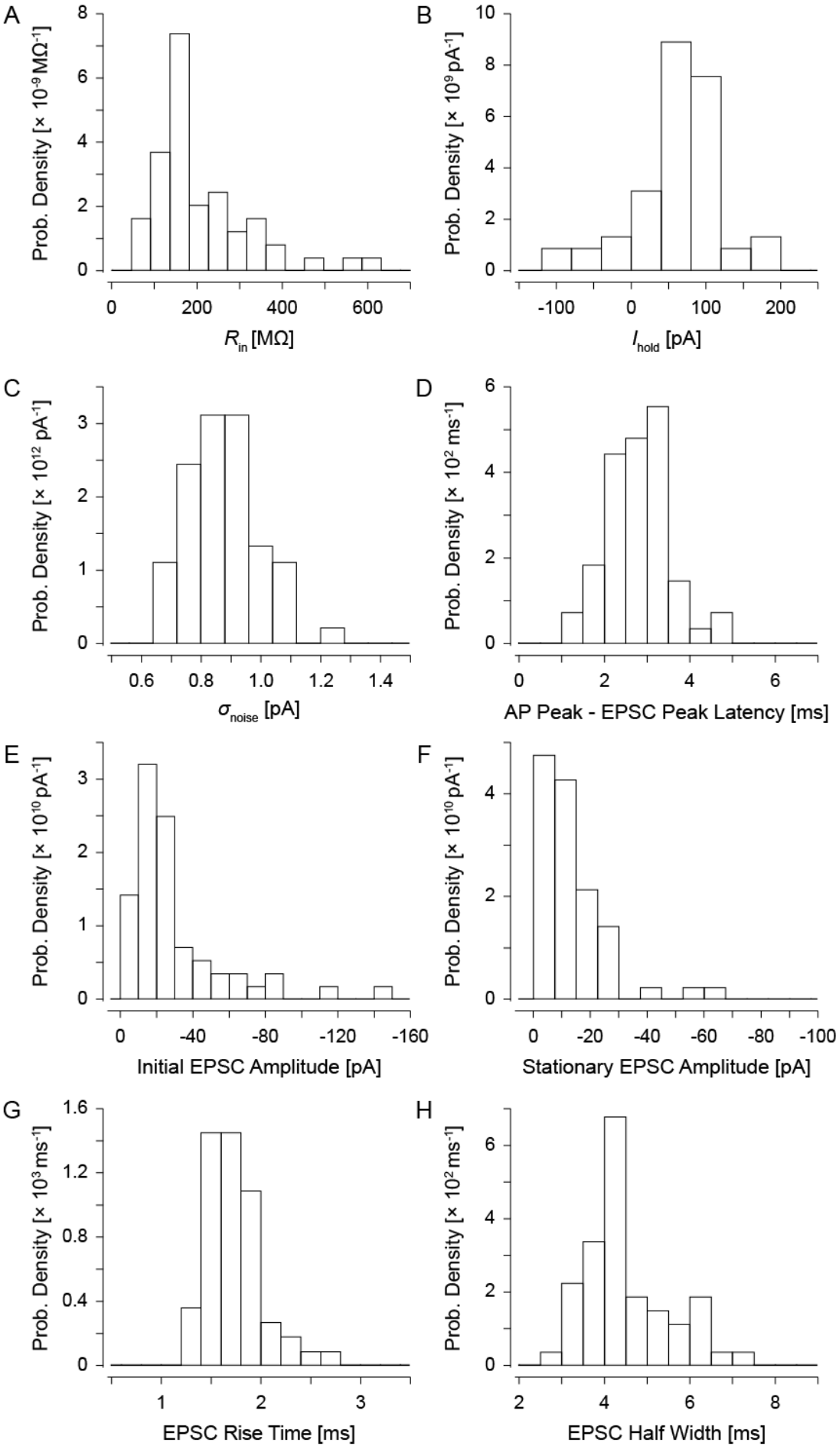
A
Prob. Density [× 10⁻⁹ MΩ⁻¹]
R_{in} [MΩ]
B
Prob. Density [× 10⁹ pA⁻¹]
I_{hold} [pA]
C
Prob. Density [× 10¹² pA⁻¹]
σ_{noise} [pA]
D
Prob. Density [× 10² ms⁻¹]
AP Peak - EPSC Peak Latency [ms]
E
Prob. Density [× 10¹⁰ pA⁻¹]
Initial EPSC Amplitude [pA]
F
Prob. Density [× 10¹⁰ pA⁻¹]
Stationary EPSC Amplitude [pA]
G
Prob. Density [× 10³ ms⁻¹]
EPSC Rise Time [ms]
H
Prob. Density [× 10² ms⁻¹]
EPSC Half Width [ms]

Figure 4.4.6. Histograms of postsynaptic properties and EPSCs.

Histograms of R_{in} (A), I_{hold} (B), σ_n (C), initial peak-to-peak latency (D), initial amplitude (E), stationary amplitude (F), rise time (G), and half-width (F).

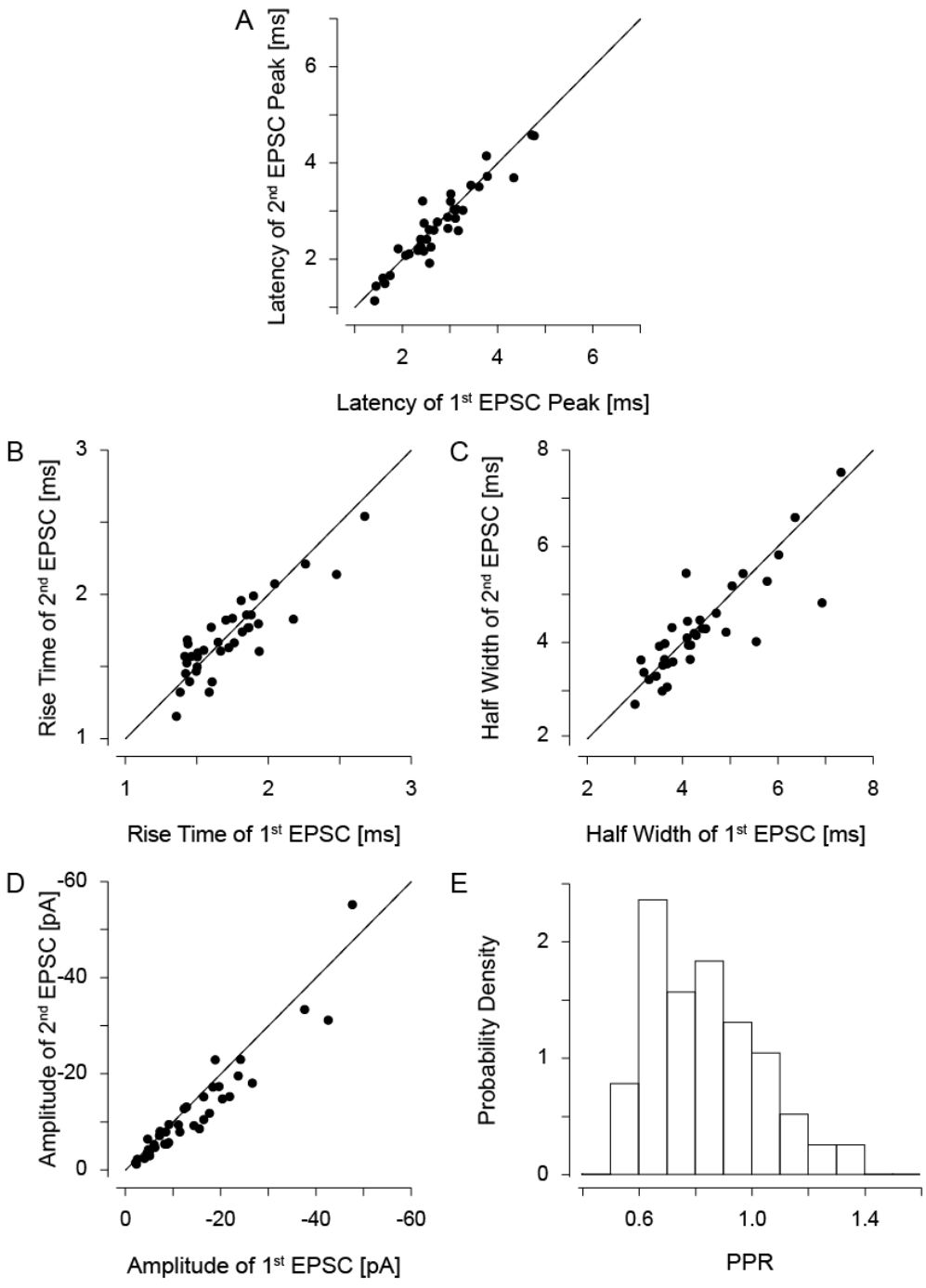

Figure 4.4.7. Comparison of 2nd and 1st EPSCs during paired-pulses.

Plots of the peak-to-peak latencies (A), rise times (B), half-widths (C), and peak amplitudes of the second *vs.* first EPSCs (D). Solid lines represent the best linear fit to the data. Dashed line represents line of equality. E. Histogram of respective PPR values.

Likewise, both of the plots of the EPSC rise times (B) and half-widths (C), were also linearly correlated (both $p_{Pr} < 10^{-10}$) and no different from the line of identity ($p_{Pr} > 0.12$ in both cases).

I then plotted the peak amplitudes of the second *vs.* that of the first EPSCs. The data are presented in D. In most instances, the data points were below the line of identity, indicating that in most cells there was a small amount of short-term depression, consistent with the average value for PPR. It ranged from 0.55 to 1.40, with an average value of 0.83 ± 0.03. Again, this set of data was best fit with a line ($p_{Pr} < 10^{-15}$), however, it was statistically not different from the line of identity suggesting that on average there was no systematic change in PPR. The respective histogram of the values of PPR, with a bin width 0.1, is shown in E. With the peak of the distribution < 1.0, the majority of pyramidal cells (n = 30; 79%) showed a small amount of short-term depression. For the remainder, there was a small amount of facilitation.

4.4.1.5. Evidence for Release-Independence

The concept of release-dependence states that, if synaptic vesicles are released from a finite pool of vesicles in rapid succession, upon a second stimulus, the pool size is reduced. Consequently, due to depletion, the amplitudes of the subsequent EPSCs are smaller. If this is due to vesicle depletion alone, subsequent EPSCs should be anti-correlated; *i.e*. if many vesicles were released, only few can be released subsequently, and *vice versa*. Therefore, in a plot of the second *vs.* the first EPSC amplitudes (Fuhrmann *et al.*, 2004), there would be a significant anticorrelation. I tested if this was the case in the 6 pairs with stationary EPSC amplitudes.

An example for this type of analysis is illustrated in Fig. 4.4.8. In A, the average time course is shown containing the first and second EPSCs from the 300 repetitions. The average peak amplitude of the first EPSC was -12.4 ± 0.5 pA, whilst the average for the second one was -9.4 ± 0.5 pA; *i.e*. there was short-term depression in this case (PPR = 0.76 ± 0.05). B shows the plot of all second *vs.* first peak amplitudes. The horizontal and vertical dashed lines are drawn to indicate zero for both the second and first EPSCs. The horizontal and vertical solid lines indicated the respective average peak amplitudes. When the extent of correlation between the two EPSCs was calculated, p_{Pr} was 0.93; *i.e*. there was no significant correlation in this case. This is consistent with the idea that in this case, the short-term depression was release-independent.

I acknowledge that, strictly speaking, the concept of release-dependence is only defined for depressing synapses (Fuhrmann *et al.*, 2004). However, I tried to extend the same reasoning as above to the two stationary pairs which showed facilitation. Such a case is

illustrated in C and D. In this pair, the average peak amplitude of the first EPSC was -5.8 ± 0.3 pA, whilst the average for the second one was -8.0 ± 0.3 pA, resulting in a PPR of 1.38 ± 0.09. When all second peak amplitudes were plotted against the first ones (D), again no linear correlation was observed (p_{Pr} = 0.93).

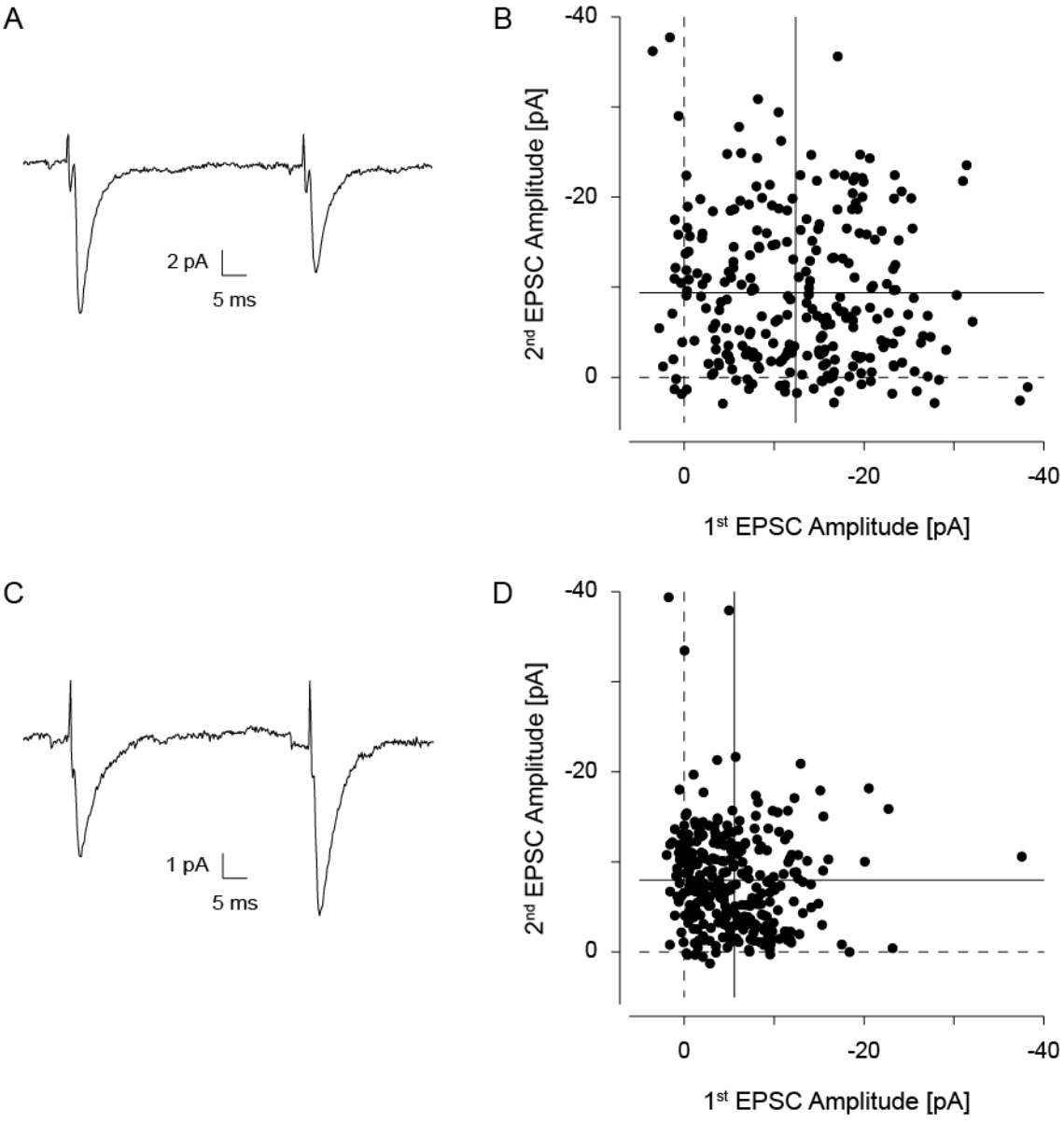

Figure 4.4.8. Evidence of release-independence.

A. Time course of the average EPSCs from 300 repetitions using a paired-pulse with an interval of 50 ms. B. Plot of the respective peak amplitudes of the second *vs.* first EPSCs. Dashed lines indicate the respective failures. The horizontal and vertical solid lines indicate the average peak amplitudes of the second and first EPSCs, respectively. C. Same as in A, but for a pair with short-term facilitation. D. Same as in B, but for the case shown in C.

Within this group of 6 pairs, for the 4 pairs with depressing synapses, the second EPSC amplitudes were not correlated with the first ones ($p_{Pr} > 0.28$). In other words, no anti-correlation was observed in these pairs. Likewise, for the two facilitating pairs, there was no correlation either ($p_{Pr} > 0.93$). Therefore, I conclude from this set of data that the short-term plasticity is not affected by the preceding release, hence, is mostly release-independent.

4.4.2. Serotonergic Depression of Evoked Release

In this section, I will describe the impact of 10 µM 5-HT on evoked glutamate release, and describe the changes of the pre- and postsynaptic properties upon 5-HT exposure. Much of the data will focus on the peak EPSC amplitude, because the largest and most significant change was observed in this parameter. Note that the average peak EPSC amplitude of the control period was from the stationary period after the slow depression had reached a steady-state in the respective pairs.

4.4.2.1. Large EPSC Depression Caused by 5-HT

In the presence of 3 µM gabazine to block $GABA_A$ receptors, 10 µM 5-HT was added to the superfusate, whilst both the presynaptic APs and the postsynaptic EPSCs were recorded. The results of such an experiment in a pair which had a stationary amplitude throughout the control period, are shown in Fig. 4.4.9. During the 25 minutes of the control period (blue), the same paired-pulse stimulation was repeated for 300 times at 0.5 Hz, and the respective EPSCs were recorded postsynaptically. The average first EPSC amplitude was stationary at -12.4 ± 0.5 pA (A, lower trace and C). After the subsequent addition of 10 µM 5-HT (red) and waiting for five minutes until the 5-HT concentration in the bath had stabilised, the first EPSC amplitude depressed by 57 ± 4% to -5.3 ± 0.4 pA ($p_t = 2 \cdot 10^{-26}$; lower trace in B and C). In contrast to the transient increase in mEPSC frequency, this depression was fully established within the five minutes before the resumption and then persisted for the remainder of the recording. The depression was characterized by more failures and smaller EPSCs than during control. Similarly, the second EPSC also depressed by 63 ± 6% from -9.4 ± 0.5 to -3.5 ± 0.5 pA. During control, PPR was 0.69 ± 0.05 and after 5-HT, it remained at 0.62 ± 0.09. Consequently, PPR was not significantly altered during this depression.

Concurrently with the EPSC depression, the presynaptic cell showed a hyperpolarization by 7.3 mV from -74.7 to -82.0 mV (D, left traces). Comparison between the time courses of the first APs in control *vs.* that in 5-HT done by alignment the two traces at V_{thr} (D,

right traces) revealed that except for the hyperpolarization, there were no significant changes.

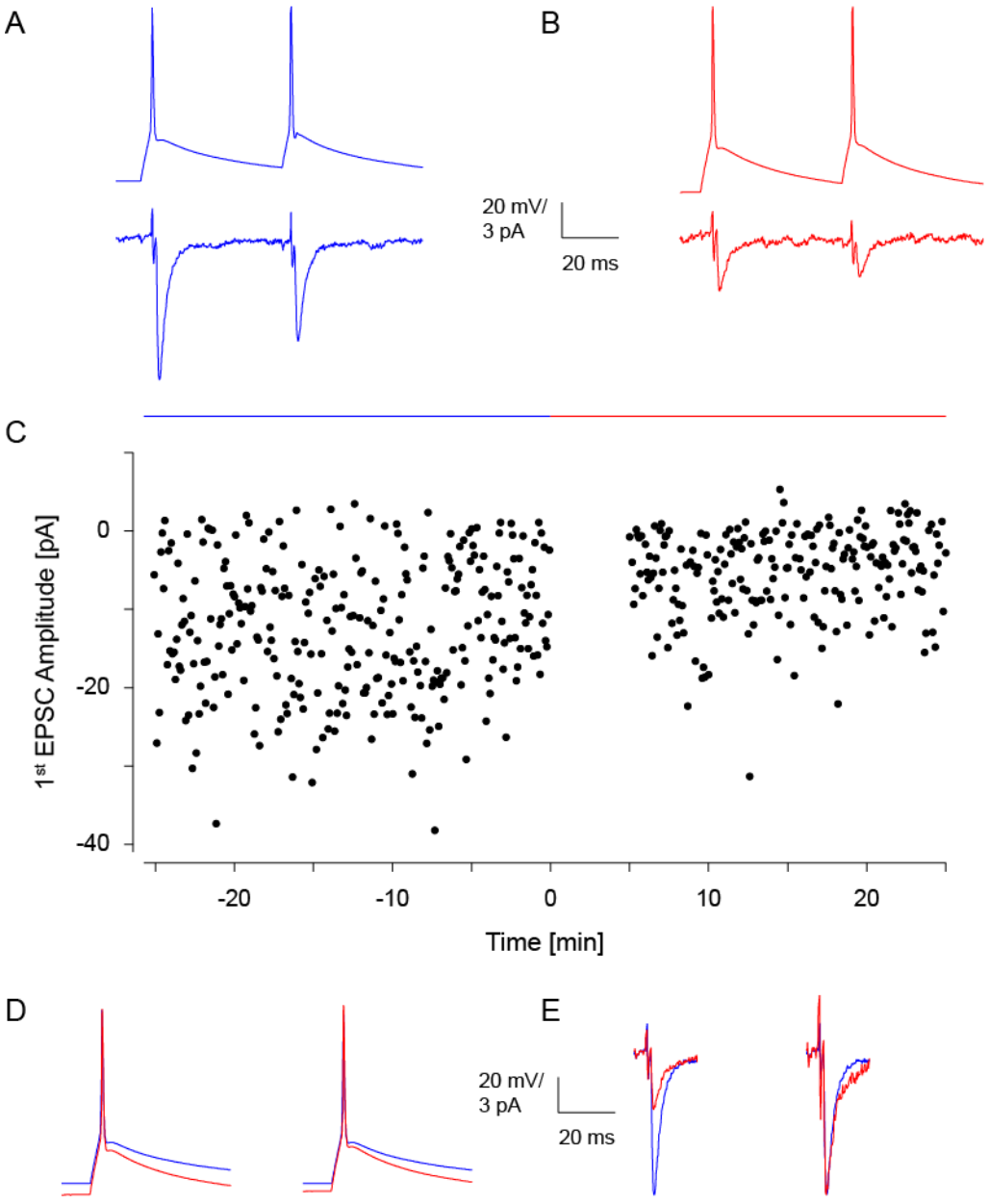

Figure 4.4.9. 5-HT depressed EPSC amplitude.

A. Time courses of the two APs (upper trace) and respective EPSCs (lower trace). B. Same as in A, except after 5-HT application. C. Individual peak amplitudes of the first EPSC plotted against time during the experiment. Time 0 corresponds to when 10 µM 5-HT was added to the superfusate. D. Superposition of the time courses of the first APs during both periods without (left) or with alignment for the same V_{thr} (right). E. Superposition of the time courses of the first EPSCs during both periods (left), and after peak-scaling for the amplitude during control (right).

I also checked if 5-HT affected V_{rest} of the postsynaptic cell. To estimate this value in voltage-clamp, I used Ohm's law and multiplied the peak change in I_{hold} (31 pA) with R_{in} (125 MΩ). This provided a hyperpolarization of 3.9 mV. This value was much smaller than that of the presynaptic cell. The average time courses of the first EPSC were also peak scaled and aligned (E). It revealed a small difference during the late decay phase, but no significant change in either the rise time or half-width.

In Fig. 4.4.10, I show a 5-HT mediated depression in a pair which had a slow depression but which had reached a steady state for 8 min during control. During this period, the average amplitude of the first EPSC was -28.3 ± 1.2 pA (lower trace in A and C). After the addition of 5-HT, the EPSC depressed by 38 ± 4% to -17.8 ± 0.7 pA ($p_t < 8 \cdot 10^{-12}$; lower trace in B and C), and remained stationary throughout the remainder of the recording. PPR during control was 0.73 ± 0.03, and 0.72 ± 0.04 after 5-HT. Hence, the large depression in the first EPSC amplitude was not accompanied by significant change in PPR.

Again, after addition of 5-HT, there was a pronounced hyperpolarization by 8.4 mV from -69.1 to -77.5 mV in the presynaptic cell (D, left). Likewise, the postsynaptic cell showed an increase in I_{hold}, which peaked by 70 pA, corresponding to an estimate of the hyperpolarization by 5.0 mV. The two time courses of the respective first APs after alignment for the same V_{thr} (D, right) did not show any significant change, nor did the EPSC time courses (E). Further details regarding any other change in the pre- and postsynaptic properties of these pyramidal cells will be provided in 4.4.2.2 and 3.

The depression by 10 µM 5-HT was very different to the slow depression seen after obtaining the whole-cell recording condition. The τ of the latter was 10.8 ± 2.0 minutes (see 4.4.1.1), whereas the depression by 5-HT was fully established < 8 min (compare Figs. 4.4.1B with 4.4.10C).

Next, I asked the question if the depression by 5-HT in pairs, which showed a slow depression, was different to that in pairs without. For this purpose, I pooled the 18 pairs from this and subsequent data sets (4.4.2.4 and 4.4.4.1), and compared the 5-HT-induced depression in pairs without (n = 4; two pairs could not be included in this set as these had Gβγ binding peptides in them) with that in pairs with a slow depression (n = 14). The average depression by 5-HT in the former group was 53 ± 9%, compared to 47 ± 3% in the latter group. There was no significant difference (p_t = 0.66). Consequently, the data from the two groups were pooled. This comparison indicates that the depression caused by 5-HT is molecularly very different to of the slow depression.

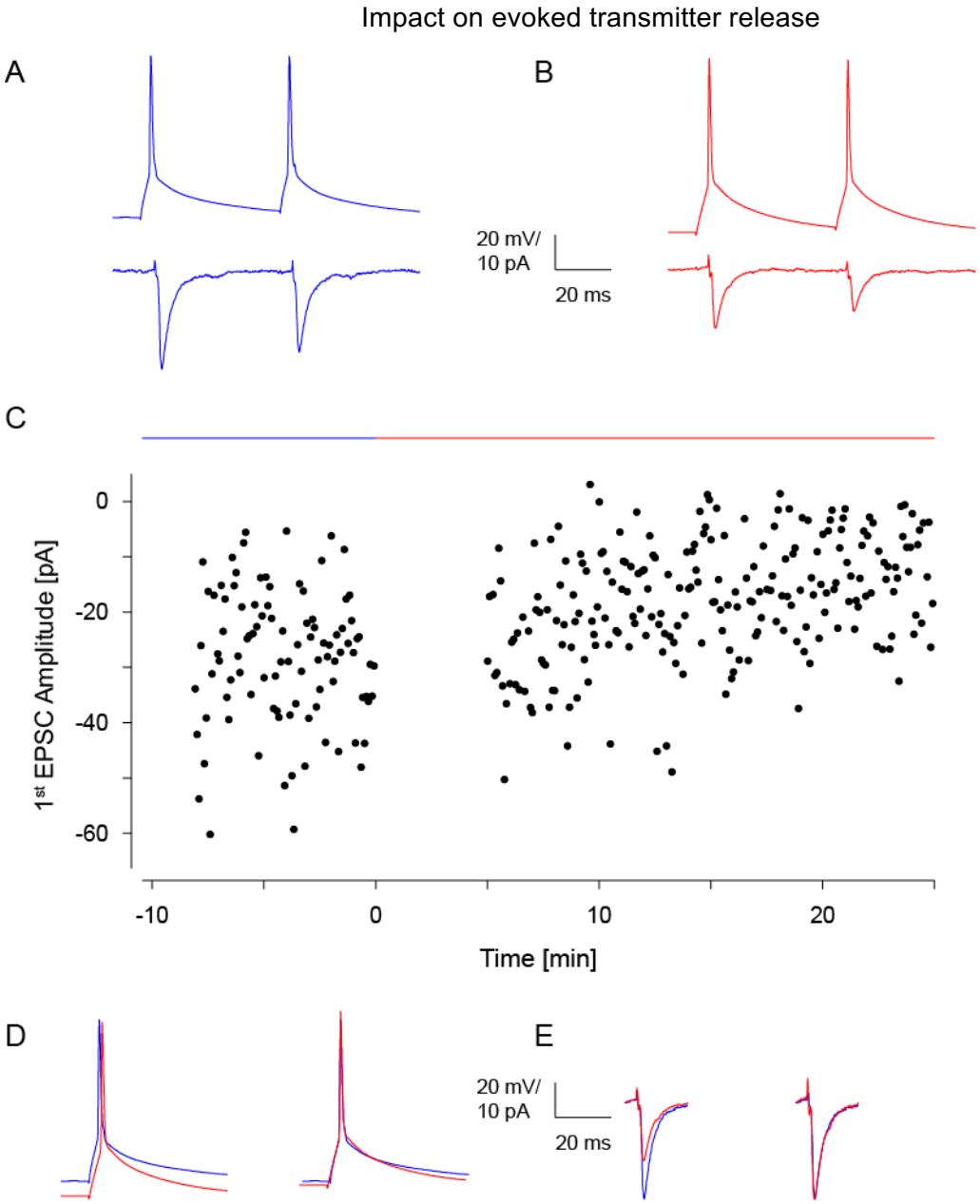

Figure 4.4.10. 5-HT depressed EPSC amplitude despite slow depression.
Same colour code as before. The same figure legend as in Fig. 4.4.9 applies here.

In Fig. 4.4.11, the values for all 8 pairs exposed to 10 µM 5-HT are presented. Each pair showed a significant depression in the EPSC amplitude. On average (n = 8), the peak amplitude of the first EPSC depressed from -10.7 ± 2.8 to -5.8 ± 1.8 pA (p_{pt} = 0.002; A, black) by 46 ± 4% (B). This depression was not accompanied by significant change in PPR (0.70 ± 0.03 *vs.* 0.70 ± 0.04, respectively; p_{pt} = 0.77; C).

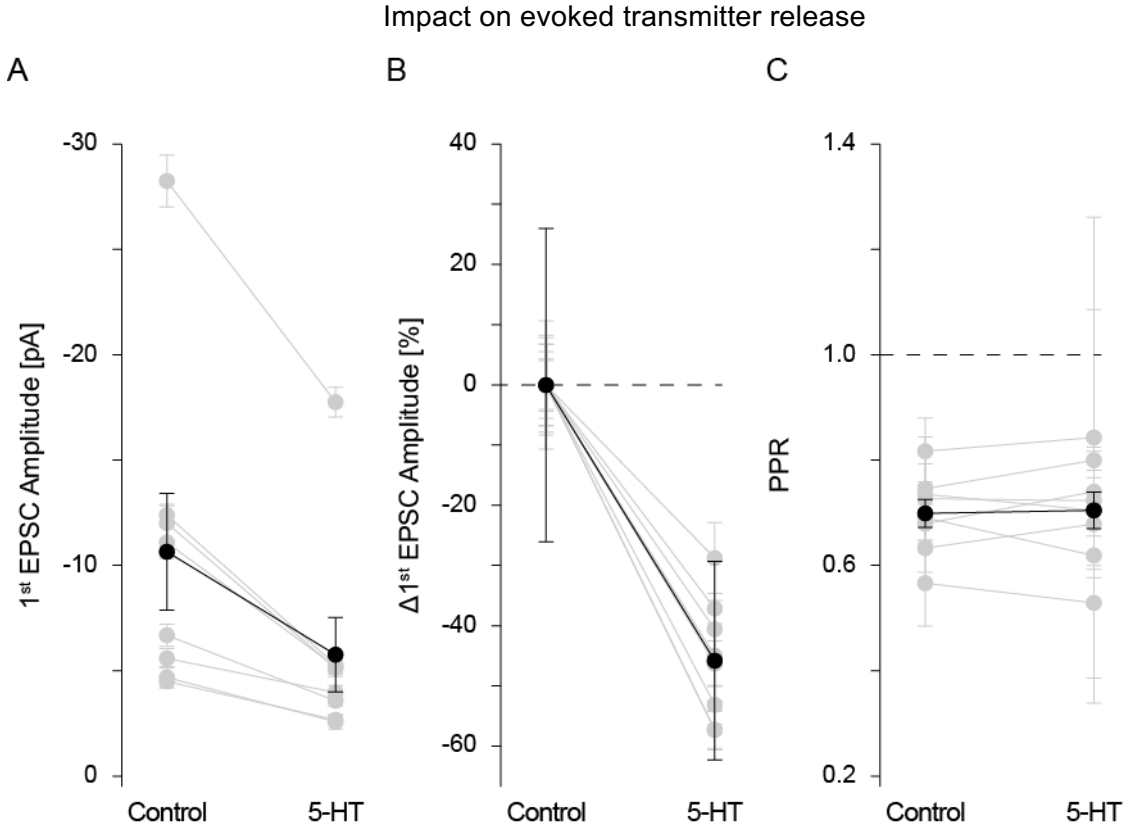

Figure 4.4.11. Depression of EPSC amplitudes.

Individual EPSC amplitudes for each pair during control and after 5-HT shown in grey, with the respective averages. Paired values are joined by a line. B. Same as in A except that in this case, the amplitudes were normalised for a control value of 0. Dashed line indicates no depression. C. Plot of PPR in both conditions for individual experiments and the population averages. Dashed line indicates no change.

4.4.2.2. Presynaptic Changes

5-HT might have caused changes to the presynaptic membrane properties and/or AP, which may have resulted in the observed depression. Hence, I checked the relevant properties, and quantified the respective changes.

In Fig. 4.4.12, I present data showing the typical changes caused by exposure to 5-HT. In this cell, R_{in} decreased by 52 MΩ from 234 to 182 MΩ, consistent with an opening of a considerable conductance. Similar to what was shown in Fig. 4.4.9, V_{rest} hyperpolarized by 3.6 mV from -77.6 to -81.2 mV (A), suggesting that the conductance had a reversal potential more negative than V_{rest}.

In regard to the AP, the values of the first during control and after 5-HT were as follows: time to V_{thr} was 3.3 *vs.* 3.6 ms, V_{thr} -42.2 *vs.* -38.3 mV, V_{rel} 35.4 *vs.* 43.0 mV, *H* 66.6 *vs.* 61.4 mV, *RT* 0.6 *vs.* 0.6 ms, and *W* 1.0 *vs.* 1.1 ms. Changes to the AP were observed for V_{rel} and *H*. The change in V_{rel} was expected because the hyperpolarization by 5-HT

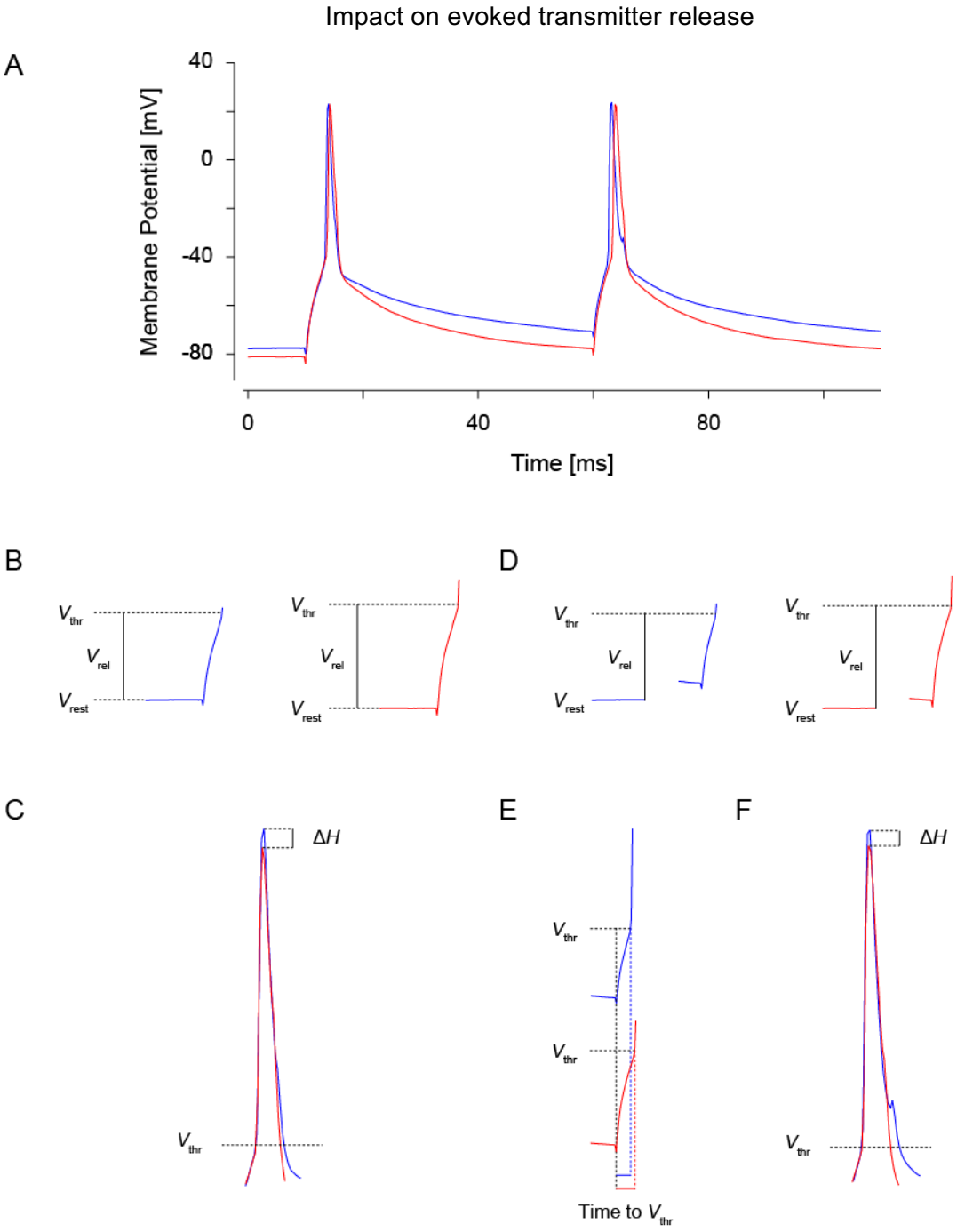

Figure 4.4.12. Changes to V_{rest} and AP.

A. Time courses of membrane voltage with two APs. B. Comparisons of the relative difference in voltage (V_{rel}) for the first AP. C. Superposition of the first APs during control and after 5-HT after adjusting for the same V_{thr}. D. Same as in B, but for the second AP. E. Comparison of time to V_{thr} for the second AP. F. Same as in C, but for the second AP.

made the voltage change to reach V_{thr} larger as shown in B. Although there was no noticeable change in the time course of the fast part of the AP, 5-HT decreased the amplitude (H) by 5.2 mV. This difference is clearly detectable when the two traces were superimposed and aligned at the same value of V_{thr} (C).

The respective values for the second AP were as follows: time to V_{thr} was 2.5 *vs.* 3.2 ms, V_{thr} -41.8 *vs.* -38.6 mV, V_{rel} 35.9 *vs.* 42.7 mV, *H* 66.0 *vs.* 61.8 mV, *RT* 0.7 *vs.* 0.6 ms, and *W* 1.1 *vs.* 1.2 ms. For this second AP, in addition to the changes in V_{rel} and *H*, time to V_{thr} became longer (E). Again, the change in time to V_{thr} was most likely explained by the hyperpolarization. Similar to the first one, there was no noticeable change in the time course of the fast part, but *H* again decreased by 4.2 mV (F). This was likely related to the observed drop in R_{in}.

Table 4.4.1. Presynaptic changes.

	Control	5-HT	Δ	p_{pt}
Basic Properties (*n* = 39)				
R_{in} [MΩ]	171 ± 11	138 ± 11	-33 ± 13	0.013 *
V_{rest} [mV]	-75.0 ± 0.8	-77.1 ± 0.9	-2.1 ± 0.9	0.023 *
Properties of 1st AP (*n* = 34)				
Time to V_{thr} [ms]	3.6 ± 0.1	3.6 ± 0.1	0.0 ± 0.1	0.58
V_{thr} [ms]	-41.7 ± 1.1	-40.9 ± 1.7	0.8 ± 1.0	0.43
V_{rel} [ms]	33.6 ± 1.3	35.7 ± 1.5	2.1 ± 0.8	0.014 *
H [mV]	71.7 ± 1.4	68.0 ± 1.5	-3.7 ± 0.8	$5 \cdot 10^{-5}$ **
RT [ms]	0.6	0.6	0.0 ± 0.0	0.41
W [ms]	0.9	0.9	-0.0 ± 0.0	0.16
Properties of 2nd AP (*n* = 23)				
Time to V_{thr} [ms]	3.1 ± 0.1	3.5 ± 0.2	0.4 ± 0.1	0.002 **
V_{thr} [ms]	-41.3 ± 1.2	-41.6 ± 2.0	-0.3 ± 1.2	0.82
V_{rel} [ms]	34.0 ± 1.6	36.3 ± 1.7	2.4 ± 0.8	0.010 **
H [mV]	71.6 ± 1.5	68.5 ± 1.5	-3.1 ± 0.6	$5 \cdot 10^{-5}$ **
RT [ms]	0.6	0.6	-0.0 ± 0.0	0.56
W [ms]	1.0	0.9	-0.1 ± 0.0	0.013 *

Respective parameters during control and after 5-HT (or full agonist) addition, together with the calculated differences. Values for RT and W are given without errors as those were smaller than the A/D sampling time. Significances were based on paired t-tests. Significant differences are highlighted on a grey background. * for $p_{pt} < 0.05$ and ** for < 0.01.

Pooling the data from all pairs (n = 39), I found that the addition of 5-HT or relevant full agonist caused significant changes which are given in Table 4.4.1. For the first AP, these were 1) R_{in}, 2) V_{rest}, 3) V_{rel} and 4) H. For the second, 5) time to V_{thr}, 6) V_{rel}, 7) H, and 8) W. Specifically, R_{in} of the presynaptic cell decreased by 33 ± 13 from 171 ± 11 to 138 ± 11 MΩ (n = 39; p_{pt} = 0.013). V_{rest} hyperpolarized by 2.1 ± 0.9 from -75.0 ± 0.8 to -77.1 ± 0.9 mV (p_{pt} = 0.023). This value was very likely a slight underestimate because in the pairs exposed to the 5-HT_2R agonist α-methyl-5-HT (n = 6), the agonist caused a depression without a hyperpolarization of the presynaptic cell (see 4.4.2.4 below).

After 5-HT addition, V_{rel} of the first AP increased on average by 2.1 ± 0.8 mV from 33.6 ± 1.3 to 35.7 ± 1.5 mV (n = 34; p_{pt} = 0.014). Likewise, V_{rel} of the second AP increased by 2.4 ± 0.8 from 34.0 ± 1.6 to 36.3 ± 1.7 mV (p_{pt} = 0.010). H of both the first and second AP decreased by 3.7 ± 0.8 mV from 71.7 ± 1.4 to 68.0 ± 1.5 mV ($p_{pt} = 5 \cdot 10^{-5}$), and 3.1 ± 0.6 from 71.6 ± 1.5 to 68.5 ± 1.5 mV ($p_{pt} = 5 \cdot 10^{-5}$), respectively. Lastly, W of the second AP decreased by 0.1 from 1.0 to 0.9 ms (p_{pt} = 0.013). This shortening was likely related to the smaller H as a consequence of the drop in R_{in}.

Although there were several significant changes to the AP, these were quite small and, therefore, unlikely the explanation for the depression by 49 ± 3% (see 4.4.2.3). This conclusion is further supported by a set of experiments to be presented later, in which the depression could be fully blocked, while both decreases in H and W remained (see 4.4.4.2 and 3).

To summarise, 5-HT caused some small and significant changes to the presynaptic cell and the APs, but these likely had minimal impacts on the depression.

4.4.2.3. Postsynaptic Changes

A postsynaptic depression could have been caused if for example the membrane resistivity was lowered at synapses which escaped the imposed space-clamp (Spruston *et al.*, 1993; Williams & Mitchell, 2008). To rule out this possibility, I checked the membrane and EPSC properties of the respective postsynaptic cells.

In Fig. 4.4.13, I present relevant data from a single cell. The time courses of the respective membrane voltages and currents are presented in A for the first and in B the second AP and EPSC during control (top) and after 5-HT (bottom). After the exposure to 5-HT, R_{in} decreased by 63 MΩ from 135 to 72 MΩ, again indicating the opening of a slightly larger conductance. At the same time, I_{hold} increased by 70 from 160 to 230 pA; *i.e.* the cell hyperpolarized. In keeping with the finding for the presynaptic cell, this

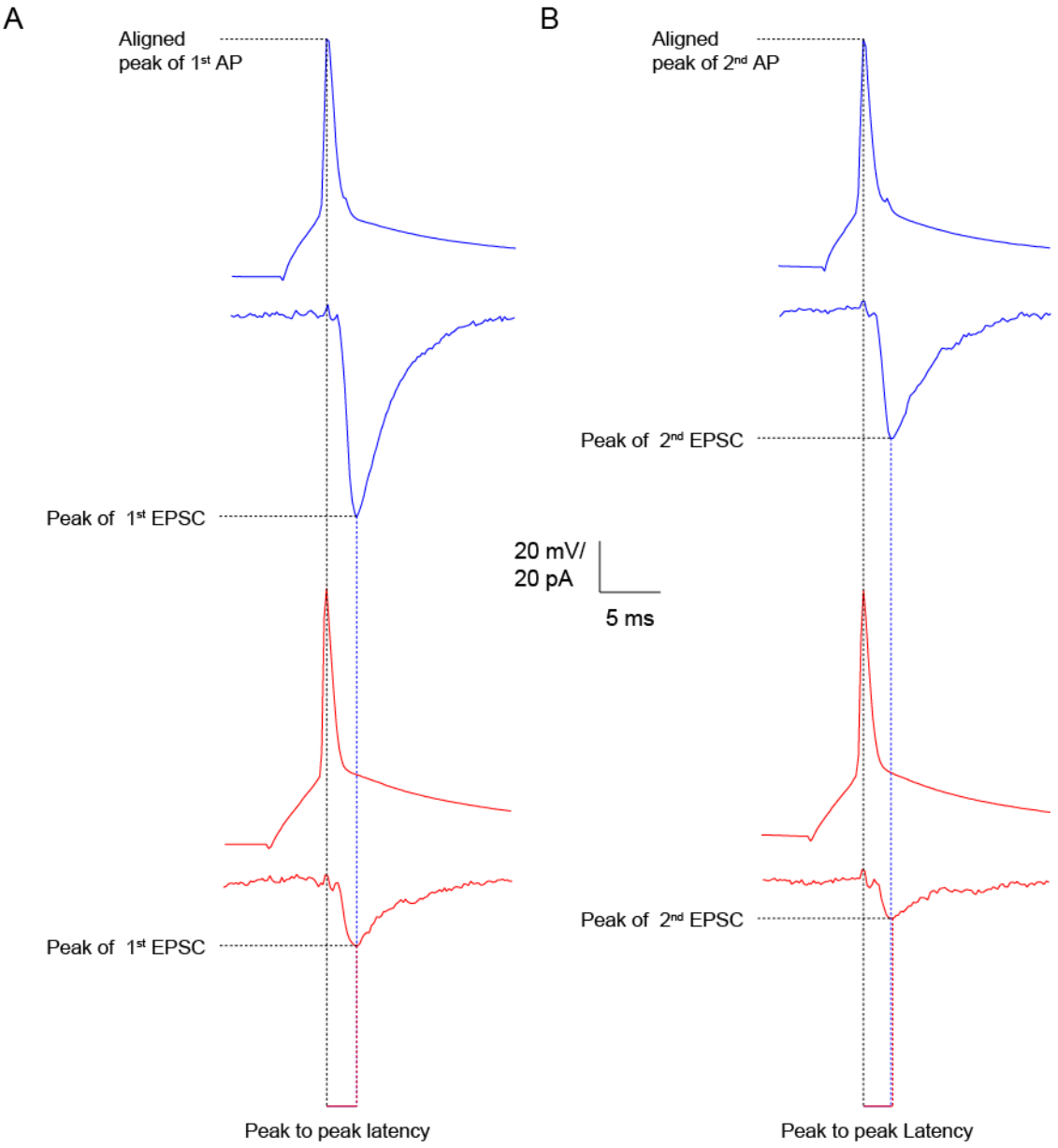
A
Aligned
peak of 1st AP
Peak of 1st EPSC
Peak of 1st EPSC
Peak to peak latency
B
Aligned
peak of 2nd AP
Peak of 2nd EPSC
Peak of 2nd EPSC
Peak to peak Latency
20 mV/
20 pA
5 ms

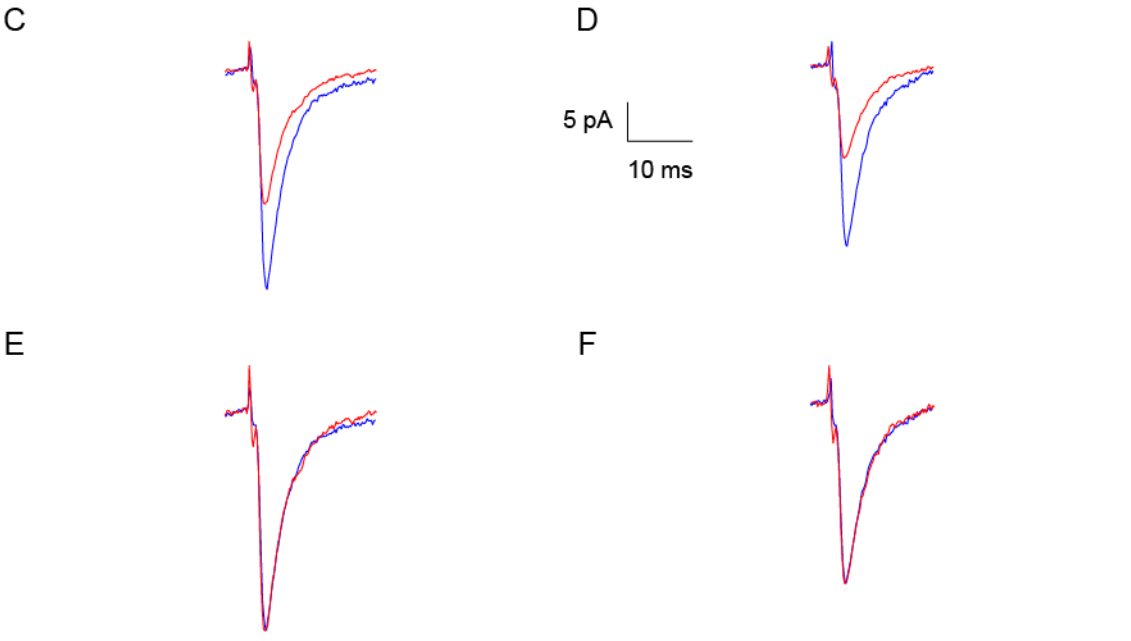
C
D
5 pA
10 ms
E
F

Figure 4.4.13. Changes to EPSC properties.

A. Comparison of the peak-to-peak latencies of first APs and EPSCs during control (top) and in 5-HT (bottom). Dashed lines are given to facilitate comparisons. B. Same as in A, except for the second APs and EPSCs. Superposition of the average time courses of the first (C) and second (D) EPSCs before and after addition of 5-HT. E. Same as C, except for peak scaling to the amplitude during control. Both D and F are similar to C and E, except for the second EPSCs.

indicated that the reversal potential of this conductance was more negative than V_{rest}. Furthermore, during control, σ_n for a R_s of 11 MΩ was 0.7 pA. After 5-HT, and despite the drop in R_{in}, σ_n for a R_s of 10 MΩ remained 0.7 pA.

During control, the average peak amplitude of the first EPSC was -28.3 ± 1.2 pA (A, top). After 5-HT (A, bottom), the EPSC amplitude depressed by 38 ± 4% to -17.8 ± 0.7 pA ($p_t < 8 \cdot 10^{-12}$; C). The remaining characteristics of the first EPSC before and after 5-HT addition were as follows: the peak-to-peak latencies were 2.3 *vs.* 2.4 ms, the rise times 1.7 *vs.* 1.6 ms, and the half-widths 4.1 *vs.* 4.0 ms. When the time courses of the average EPSCs were superimposed without (D) and after peak scaling (E), only minimal differences were found for the latter, suggesting that the time courses of EPSCs remained largely unchanged. Therefore, the only significant change to the EPSC was its depression.

A similar set of findings was made for the second EPSCs (B, D, and F). Specifically, the peak-to-peak latencies were 2.2 *vs.* 2.3 ms, rise times 1.6 *vs.* 1.5 ms, the half-widths 3.9 *vs.* 4.0 ms, and PPR 0.73 *vs.* 0.72. No significant changes to the time courses were found either. These data further support the findings that there were minimal changes to the second EPSC (F), but a large depression (D) with no significant change to PPR (p_{pt} = 0.3).

Pooling the data from all pairs (n = 40), I found that 5-HT or the full agonist caused a large decrease in R_{in} in all postsynaptic cells, together with a pronounced depression in the EPSC amplitude (Table 4.4.2). Specifically, R_{in} decreased on average by 55 ± 17 from 198 ± 17 to 143 ± 14 MΩ (28 ± 9%; p_{pt} = 0.002). The decrease in R_{in} was not accompanied by any significant change in I_{hold} (66.7 ± 8.2 *vs.* 69.0 ± 16.6 pA; p_{pt} = 0.83), suggesting that the conductance(s) in this case had a (combined) reversal potential(s) close to the holding potential, which is different to what was found for the presynaptic cells.

The first EPSC amplitude depressed by 8.3 ± 1.5 from -16.4 ± 2.6 to -8.1 ± 1.3 pA (49 ± 3%, n = 30; $p_{pt} = 4 \cdot 10^{-6}$). I averaged the PPR from all possible 18 pairs, and found that

the PPR remained the same, *i.e*. 0.78 ± 0.05 *vs.* 0.79 ± 0.05 for control *vs.* after 5-HT (p_{pt} = 0.69). These data showed that the second EPSC amplitude also depressed by 51% from its control value. The peak latencies and time courses of both EPSCs were not altered by 5-HT (p_{pt} > 0.18), indicating that the depression was unlikely caused by any change to the kinetics of the postsynaptic AMPA receptors.

Table 4.4.2. Postsynaptic changes.

	Control	5-HT	Δ	p_{pt}
Basic Properties (*n* = 40)				
R_s [MΩ]	15 ± 1	16 ± 1	1 ± 1	0.13
R_{in} [MΩ]	198 ± 17	143 ± 14	-55 ± 17	0.002**
I_{hold} [pA]	66.7 ± 8.2	69.0 ± 16.6	2.3 ± 10.6	0.83
Properties of 1st EPSC (*n* = 30)				
σ_n [pA]	0.9 ± 0.0	0.9 ± 0.0	0.0 ± 0.0	0.07
Amplitude [pA]	-16.4 ± 2.6	-8.1 ± 1.3	8.3 ± 1.5	$4 \cdot 10^{-6}$**
Peak latency [ms]	2.7 ± 0.1	2.9 ± 0.2	0.2 ± 0.1	0.18
Rise time [ms]	1.7 ± 0.0	1.8 ± 0.1	0.1 ± 0.1	0.55
Half-width [ms]	4.2 ± 0.2	4.3 ± 0.2	0.1 ± 0.2	0.70
Properties of 2nd EPSC (*n* = 18)				
PPR	0.78 ± 0.05	0.79 ± 0.05	0.01 ± 0.02	0.69
Peak latency [ms]	2.5 ± 0.2	2.4 ± 0.2	-0.1 ± 0.2	0.63
Rise time [ms]	1.6 ± 0.1	1.7 ± 0.1	0.1 ± 0.1	0.38
Half-width [ms]	3.8 ± 0.2	4.0 ± 0.3	0.3 ± 0.2	0.23

Relevant parameters during control and after 5-HT (or full agonist addition), along with the estimated differences. Significances were determined based on paired *t*-tests. Significant differences are highlighted on a grey background. * for p_{pt} < 0.05 and ** for < 0.01.

In the two sections above and here, I have provided data to indicate that 5-HT (or the relevant full agonist) altered properties of both the pre- and postsynaptic cells. One finding worth stressing was that R_{in} decreased in both the pre- and the postsynaptic cells.

This result reminded me of the differences found for responders and non-responders in Part 3 (see 3.4.3.3). This will be addressed later in 4.4.5.

4.4.2.4. Depression Mediated via Activation of 5-HT_2R

In this section, I determined the identity of the 5-HT receptor(s) mediating this depression. Given that the reversal potential in the postsynaptic cell associated with the change in R_{in} was unlikely solely caused by GIRK channels, and anticipating a possible similarity with the findings in Part 3, where 5-HT_2R were involved, I started off by applying the pan-5-HT_2R agonist α-methyl-5-HT.

A typical such recording is shown in Fig. 4.4.14. The time courses of the APs and respective EPSCs are shown during the control period in A and after 5-HT in B. The average peak amplitude of the first EPSC was -11.8 ± 0.6 pA (A, bottom). With the resumption of the recording 5 min after exposure to 20 µM α-methyl-5-HT (B, bottom), the first EPSC amplitude had depressed by 52 ± 4% to -5.7 ± 0.4 pA ($p_t = 5 \cdot 10^{-14}$). In C, the individual peak amplitudes of the first EPSCs are presented, showing that these were stationary during the control period. After agonist application and resumption of the recording (t > 5 min), the EPSC remained stationary, but had depressed within 5 min, which persisted for the remainder of the recording. Consistent with Figs. A and B, PPR during control was 0.65 ± 0.05, and after α-methyl-5-HT 0.68 ± 0.12, which was not significantly different ($p_t = 0.17$).

After the exposure to this agonist, the presynaptic cell only showed a small hyperpolarization by 0.6 mV from -73.0 to -73.6 mV (D, left). The comparison between the time courses of the first AP, after alignment at the same threshold, revealed no significant changes to the early part of the AP (D, right).

The postsynaptic cell showed a small increase in I_{hold} by 15 pA, which corresponded to a slight hyperpolarization after the exposure to 5-HT. Again, when the average time courses of the first EPSC were peak-scaled (E, right), no significant changes were found.

In all 6 pairs studied, α-methyl-5-HT depressed the peak amplitude of all first EPSCs, on average by 49 ± 5 % from -10.3 ± 2.5 to -5.3 ± 1.6 pA ($p_{pt} = 0.003$; F and G, black). Overall, this depression was not accompanied by any significant change in PPR (0.89 ± 0.13 *vs.* 0.86 ± 0.11; $p_{pt} = 0.65$; H, black).

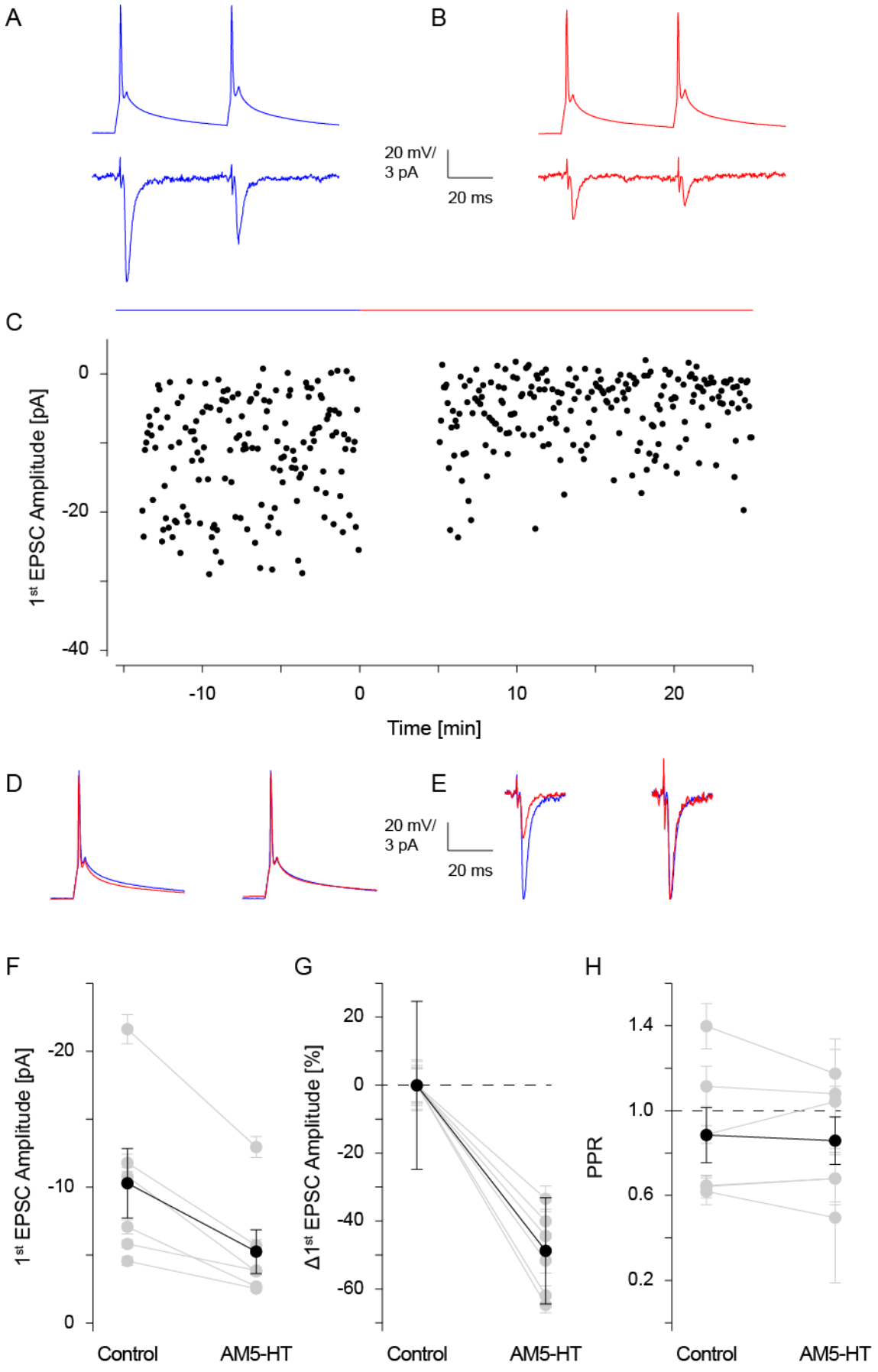
A
B
20 mV/
3 pA
20 ms
C
1st EPSC Amplitude [pA]
0
-20
-40
-10
0
10
20
Time [min]
D
E
20 mV/
3 pA
20 ms
F
1st EPSC Amplitude [pA]
-20
-10
0
Control
AM5-HT
G
Δ1st EPSC Amplitude [%]
20
0
-20
-40
-60
Control
AM5-HT
H
PPR
1.4
1.0
0.6
0.2
Control
AM5-HT

Figure 4.4.14. α-Methyl-5-HT mimicked 5-HT in causing EPSC depression.

A. Time courses of the membrane potential with two APs (upper trace) and the currents containing the respective EPSCs (lower trace) during control. B. Same as in A, except after addition of α-methyl-5-HT. C. Individual peak amplitudes of the first EPSC plotted against time during the recording. 20 μM α-methyl-5-HT was added to the superfusion at t = 0. D. Superposition of the first APs during both periods without (left) and with (right) aligning for the same V_{thr}. E. Superposition of the first EPSCs in both periods (left), and after peak-scaling (right). F. Plot of individual average EPSC amplitudes during control and after α-methyl-5-HT (AM5-HT) with the paired values joined by a line. Grey circles for individual, and the black for the average of these data. G. Plot of the depression in each pair, including the respective sample average. Dashed line indicates no depression. H. Plot of PPR values for each experiment in both conditions.

Comparing the depression by 5-HT to that by α-methyl-5-HT, both of which persisted for the remainder of the recording, there was no significant difference (46 ± 4 *vs.* 49 ± 5%; p_t = 0.57). This observation suggests that α-methyl-5-HT is a full agonist at these receptors. In addition, as with 5-HT, PPR also remained unchanged after agonist addition. However, whilst 5-HT caused a significant hyperpolarization by 7.2 ± 2.6 mV from -75.2 ± 1.4 to -82.5 ± 2.3 in the presynaptic cell (p_{pt} = 0.027), α-methyl-5-HT did not cause a significant hyperpolarization (-76.1 ± 1.6 *vs.* -71.4 ± 4.2 mV; p_{pt} = 0.38). This difference is likely explained as follows. 20 μM α-methyl-5-HT activated only 5-HT_2R. In contrast, 5-HT also activated 5-HT_1R, which then caused the opening of GIRK channels, resulting in the hyperpolarization observed (Andrade *et al.*, 1986).

Altogether, the data from this set of experiments showed that α-methyl-5-HT is a full agonist at these receptors and mimicked the action of 5-HT on the depression of the EPSC amplitude but not in regard to the hyperpolarization in the presynaptic cells. This is consistent with the idea that the depression is caused by 5-HT_2R but the presynaptic hyperpolarization is caused by 5-HT_1R.

4.4.3. Comparison with Modulation by NA

The depression observed with 5-HT and a 5-HT_2R agonist reminded me of that observed with 10 μM NA observed earlier in this laboratory. Before going any further, I will present some data on how NA modulated excitatory transmitter release in these cells. In 4.4.3.1, I present data for the noradrenergic modulation of spontaneous release, and point out the mechanism(s) involved. In 4.4.3.2, I present data on how NA modulated evoked release. The mechanism involved in the EPSC depression will be provided in 4.4.3.3. Note that most of the data in sections 4.4.3.1 and 4.4.3.2 was acquired by Drs. Julian Choy and Li Li (Choy, 2011), when working in the laboratory. However, I contributed

crucial data as to the molecular mechanism in 4.4.3.3. Some of these data will appear in joint publications (Choy *et al.*, 2017a; Choy *et al.*, 2017b).

4.4.3.1. Involvement of Store Release in NA-Mediated mEPSC Frequency Increase

Any receptor that is capable of activating the classical G_q cascade, may release Ca^{2+} from stores to modulate transmitter release. Some potential candidates, such as the group I metabotropic glutamate receptors (Simkus & Stricker, 2002a) and α_1-AR were investigated in this laboratory. The impact of α_1-AR activation on spontaneous release is shown in Fig. 4.4.15. In A, the individual mEPSC frequencies during the control period (blue bar) and after addition of 10 µM NA (red bar) are presented. The average mEPSC frequency during control was 39 ± 1 Hz, and the amplitude -13.0 ± 0.1 pA. After addition of NA at t = 0, and the resumption of the recording after another 5 min, the average mEPSC frequency increased by 34 ± 3% to 53 ± 1 Hz (A, D). Minute averages of the mEPSC frequency were normalised to the average value during control, and are shown in B. Note that, in contrast to the case with 5-HT, the mEPSC frequency increase persisted for the whole period after addition of NA. The mEPSC amplitude remained unchanged (-13.0 ± 0.1 pA; C), not significantly different from control (E). When the average time courses of mEPSCs were superimposed (F) there was no significant change by NA.

When all such experiments were analysed (n = 49), it was found that 24 (49%) pyramidal cells showed a sustained increase in the mEPSC frequency as described above. Like in Part 3, these cells were referred to as responders. On average, NA increased the mEPSC frequency by 56 ± 7% from 39 ± 2 to 59 ± 3 Hz ($p_{pt} < 10^{-8}$; Fig. G) in these responders. This increase persisted throughout the recording. The rest did not show any significant increase in the mEPSC frequency (non-responders). A significantly smaller mEPSC frequency during the control period was observed in responders than non-responders (39 ± 2 *vs.* 53 ± 4 Hz; $p_t < 10^{-3}$). In addition, the NA and agonists caused a significant decrease of R_{in} only in responders (9 ± 7% from 122 ± 8 to 103 ± 7 MΩ; p_{pt} = 0.01).

The mechanisms causing the increase in mEPSC frequency were identified as follows (Choy *et al.*, 2017a). 1) NA acted via α_1-ARs, which in turn 2) activated PLCβ, resulting in 3) PIP_2 hydrolysis to produce IP_3 and DAG. 4) The former bound to IP_3R on presynaptic stores to cause 5) Ca^{2+} release from stores, which then 6) drove vesicle fusion, observed as an increase in mEPSC frequency.

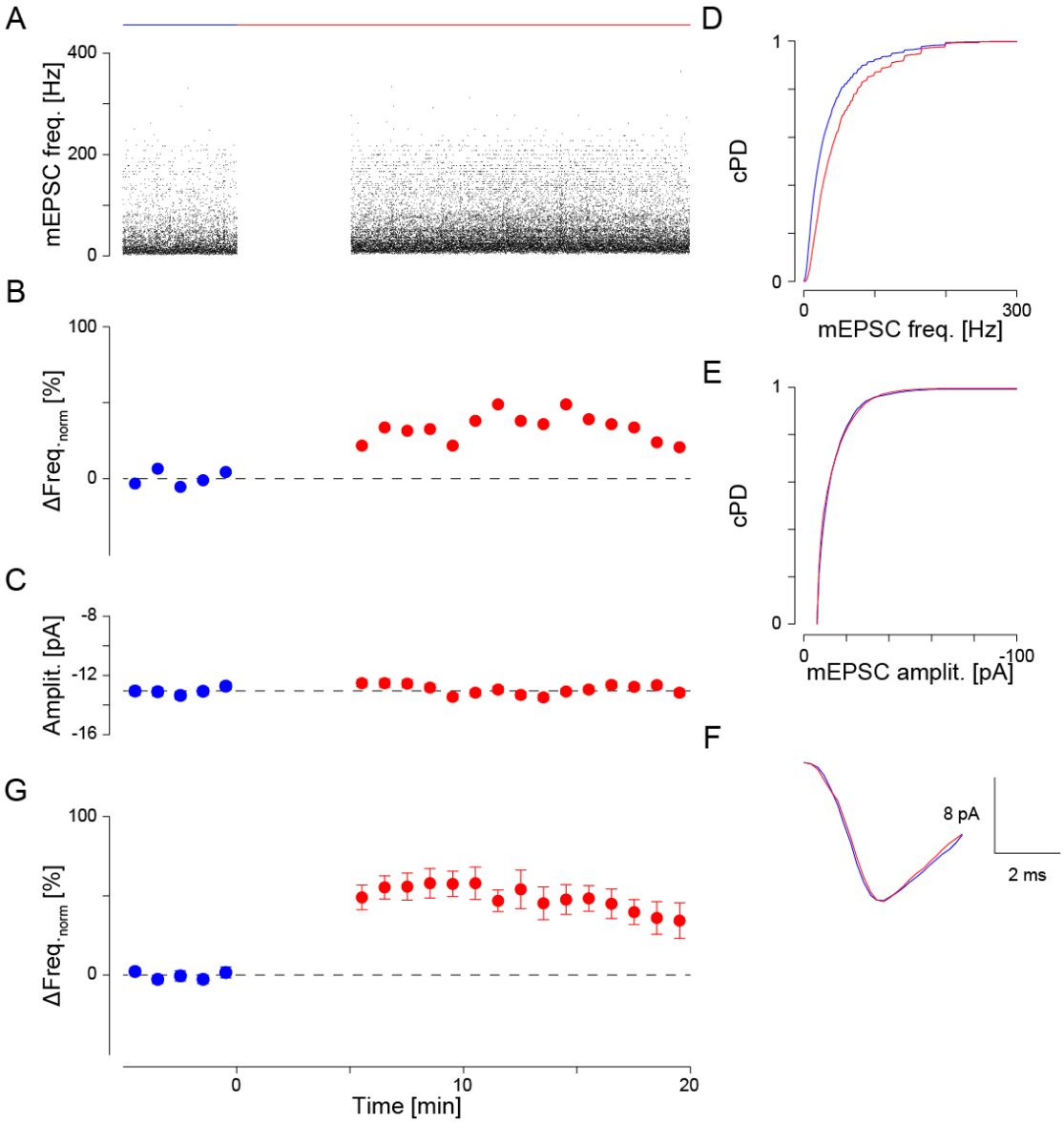

Figure 4.4.15. NA increased the mEPSC persistently.

A. Individual instantaneous mEPSC frequencies in a single pyramidal cell shown during control (t < 0 min), and after addition of NA (t ≥ 0 min). B. Minute averages of the data in A after normalising the average control value to 0%, including the respective error bars which were smaller than the diameter of the dots. Dashed line indicates no change. C. Same as in B, but for the mEPSC amplitude. D. cPDFs of the instantaneous frequencies during control and after NA. E. Same as in F, but for the mEPSC amplitude. F. Superposition of the average mEPSC time courses during control and in NA. G. Minute averages of the pooled mEPSC frequency change in responders, after normalising as in B.

Consequently, in regard to spontaneous transmitter release, both NA and 5-HT 1) increased the mEPSC frequency without affecting its amplitude. 2) The increase in mEPSC frequency was restricted to a subset of pyramidal cells (responders). 3) Both agonists signalled via a classical G_q cascade to increase the mEPSC frequency via

presynaptic Ca^{2+} release from stores. However, in contrast to NA, the increase in mEPSC frequency by 5-HT was transient, but become maintained after PKC was blocked. The impact of NA on evoked transmitter release, and how it compared with 5-HT, will be presented next.

4.4.3.2. EPSCs Depression by NA

Different from what was expected from its impact on spontaneous release, NA also depressed evoked glutamate release in this layer.

The results obtained in a paired-recording after exposure to 10 µM NA is illustrated in Fig. 4.4.16. In A, the time course of the presynaptic AP (top) with the evoked average EPSC (bottom) during control is presented. The average peak EPSC amplitude was -47.2 ± 1.2 pA. Addition of NA depressed the EPSC amplitude by 71 ± 5% to -13.7 ± 0.9 pA (B). Individual peak amplitudes during control and after NA are plotted in C. It shows that NA caused a persisting depression within 5 min of exposure. The time courses of the respective EPSCs are given in D, with the traces superimposed (left) and peak-scaled for comparison (right).

Seven such experiments are presented in E, where the paired values of the amplitudes in control and NA for the respective pairs are joined by a grey line. The average EPSC amplitude during control was -24.0 ± 5.6 pA, but depressed by 62 ± 7% to -8.3 ± 2.0 pA (p_{pt} = 0.01) after addition of NA. Even though this depression was strictly not larger than the one caused by 5-HT, it was close to significant (62 ± 7 *vs*. 49 ± 3%; p_t = 0.06).

The depression by NA was caused by α_1-AR activation (Choy *et al.*, 2017b). Specifically, application of the α_1-AR agonist cirazoline (5 µM) caused a constant EPSC depression by 54 ± 18% from -8.2 ± 1.5 to -3.1 ± 0.3 pA (n = 4; $p_{pt} < 0.05$). Compared to NA, the extent of the depression caused by the α_1-AR agonist was indistinguishable (p_t = 0.40). This depression persisted in the presence of α_2- and β-AR blockers yohimbine and propranolol, respectively (1 µM in both cases; n = 5), further strengthening the idea that α_1-AR caused this depression. It is also important to add that in all cases tested PPR was not significantly altered (p_{pt} = 0.37).

Comparing the impacts of NA on transmitter release with those of 5-HT, the following observations can be made: 1) Both, NA and 5-HT considerably depressed the EPSC amplitude, but increased spontaneous transmitter release. 2) Both, the depression and the increase in m EPSC frequency were downstream of a G_q-linked signalling cascade. 3) In both cases, despite a large EPSC depression, on average PPR was not altered.

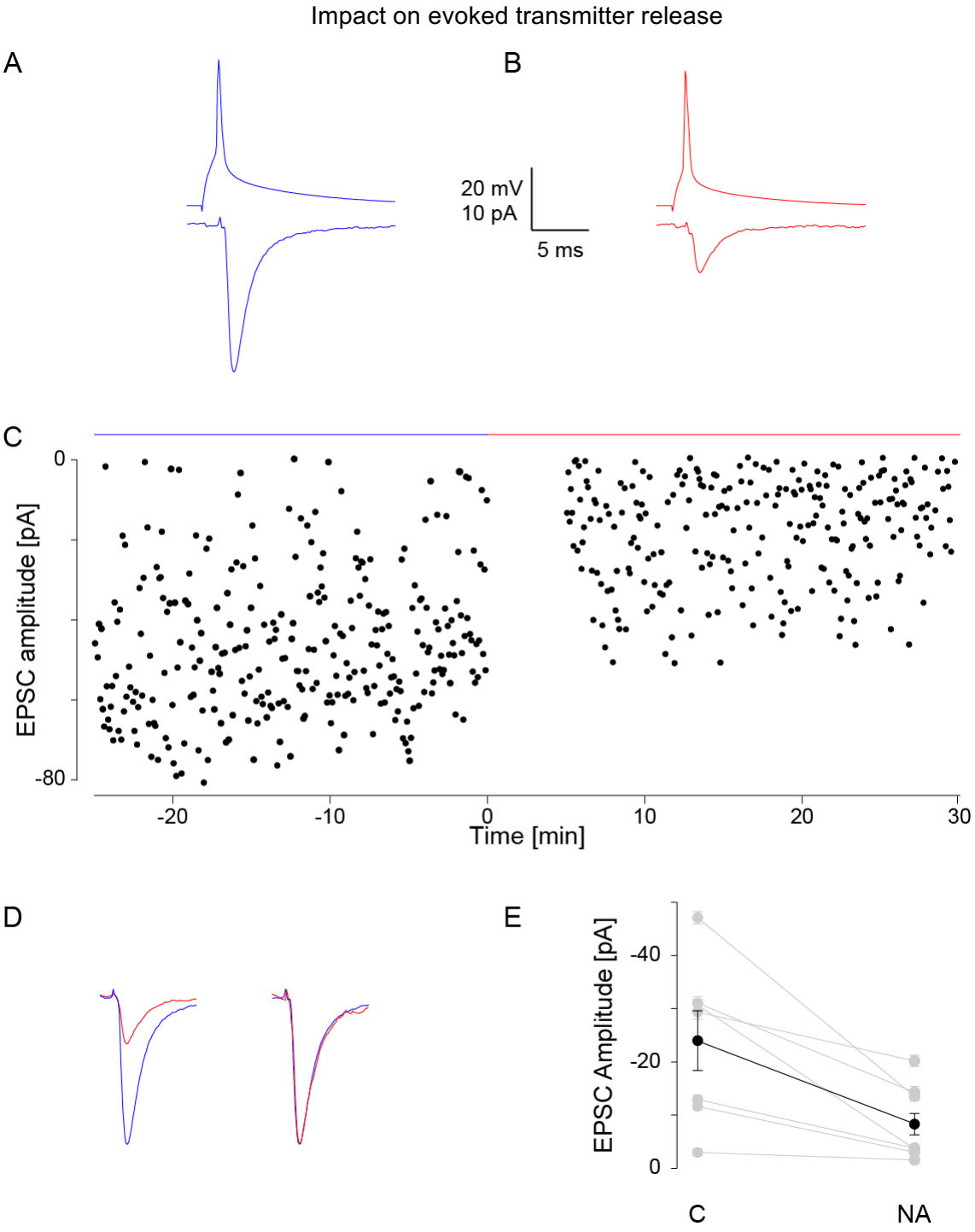

Figure 4.4.16. NA depressed the evoked EPSC amplitude.

Control in blue and exposure to NA in red. A. Time courses of the first presynaptic AP and the average EPSC during control. B. Same as in A, but in the presence of NA. C. Individual first peak EPSC amplitudes before and after addition of NA at time 0 min. D. Overlaid average EPSC time courses before and after NA (left) and after peak scaling for the control amplitude (right). E. Pair-wise plot of different experiments for the first EPSC amplitudes during control and after addition of NA. Data from the same experiment are joined by a line.

These comparisons suggested that the activation of both receptors very likely employed the same or very similar molecular mechanisms to modulate transmitter release.

4.4.3.3. Presynaptic Gβγ Signalling Causing NA-Induced Depression

Because of the dissociation of the increase in spontaneous, but the depression in evoked release, I checked at which step downstream of α_1-AR activation the signalling diverged. This line of investigation was started at the first step in this cascade, which is the activation of PLCβ.

After blocking PLCβ with 30 µM edelfosine, NA still depressed the EPSC by 61 ± 11% (p_{pt} = 0.004; Choy *et al.*, 2017b), suggesting that the relevant signalling occurred before this step, most likely at the level of the G protein. Since receptor activation produces Gα and Gβγ from the trimeric G protein, both of which have been found to initiate downstream signalling (Betke *et al.*, 2012), and cognisant of the fact that Gβγ has been found to directly bind to the SNARE complex and inhibit transmitter release (Gerachshenko *et al.*, 2005), we hypothesised that the latter was responsible for the depression.

To test this possibility, I performed experiments in which I utilized the commercially available synthetic peptide mSIRK, which scavenges Gβγ (Goubaeva *et al.*, 2003) and therefore blocks its action. Different from previous conditions, in which pharmacological agents were added to the superfusate, in this case, mSIRK was added to the presynaptic patch solution and allowed to diffuse into the cell after break-in. Since the relevant nerve terminals were on average 91 ± 47 µm away from the soma, and due to its dilution by the cell volume, we chose a concentration of 100 µM. A loading time of at least 20 minutes was allowed until the data were considered for analysis. This time was sufficiently long given the relationship between molecular weight and diffusion rate (Pusch & Neher, 1988).

After loading the presynaptic cell with mSIRK for at least 20 minutes, EPSCs were evoked in the postsynaptic cell again in response to the normal paired-pulse stimulus protocol. Data was taken before (control) and after addition of 10 µM NA to the superfusate. Such a recording is presented in Fig. 4.4.17. In this experiment, the first EPSC had an average peak amplitude of -3.8 ± 0.5 pA during the control period (A, bottom trace). Subsequent application of NA prevented the depression as the EPSC amplitude remained at -3.8 ± 0.3 pA (p_t = 0.98; B, bottom trace). The individual peak amplitudes of the first EPSC are plotted in C for the control period and after exposure to NA showing that the release process remained stationary. As expected, PPR was not altered either (0.89 ± 0.06 in control *vs.* 0.95 ± 0.08 in NA; p_t = 0.14). The time courses

of the first AP (D, right traces) and the first EPSC (E, right traces) in control *vs.* after NA showed no significant change.

In 7 pairs studied, the peak amplitude of the first EPSC during control period was -4.5 ± 1.1 pA. The subsequent application of NA failed to cause any significant depression, as the amplitude remained at -4.3 ± 1.2 pA (p_{pt} = 0.55; F and G). Neither was there on average a significant change in PPR (0.78 ± 0.08 *vs.* 0.78 ± 0.10 for control *vs.* NA; p_{pt} = 0.98; H).

These results strongly suggest that NA caused the large presynaptic EPSC depression via Gβγ signalling downstream of α_1-AR activation. Because of the similarities between NA and 5-HT, I hypothesized that downstream of 5-HT_2R activation, the depression is also caused via Gβγ signalling. In the following section, I will provide data in support of this idea.

4.4.4. Mechanism of EPSC Depression by 5-HT

As indicated above, the most likely mechanism how 5-HT caused the EPSC depression is via the production of Gβγ upon receptor activation. The following section addresses this hypothesis but also rules out the alternative possibility that it may have been caused by activation of PKC. In 4.4.4.1, I will present data from experiments in which PKC was blocked. This data set served as a control, to rule out the possibility that the depression was caused by the production of DAG downstream of PLCβ and the subsequent activation of PKC (see also Part 3). In 4.4.4.2, the addition of the Gβγ scavenger mSIRK to the presynaptic recording solution in the patch pipette successfully blocked the depression by 5-HT. In 4.4.4.3, I will provide additional data with another Gβγ-binding peptide, which also blocked the depression observed. In 4.4.4.4, I will provide data to indicate the downstream target(s) of Gβγ by comparing the recovery from short-term depression with that in NA. With this neuromodulator, Gβγ most likely bound to the c-terminus of SNAP-25. In 4.4.4.5, I will present results from quantal analyses of individual EPSCs (Stricker & Redman, 1994; Stricker *et al.*, 1994; Stricker *et al.*, 1996b, a) and compare these with similar ones with NA, where a significant reduction in quantal size was observed, consistent with Gβγ binding to SNAP-25.

4.4.4.1. PKC Block

Because the transient mEPSC frequency increases became sustained when PKC was blocked (see 3.4.4.6), I checked if PKC activation was involved in the depression of evoked release.

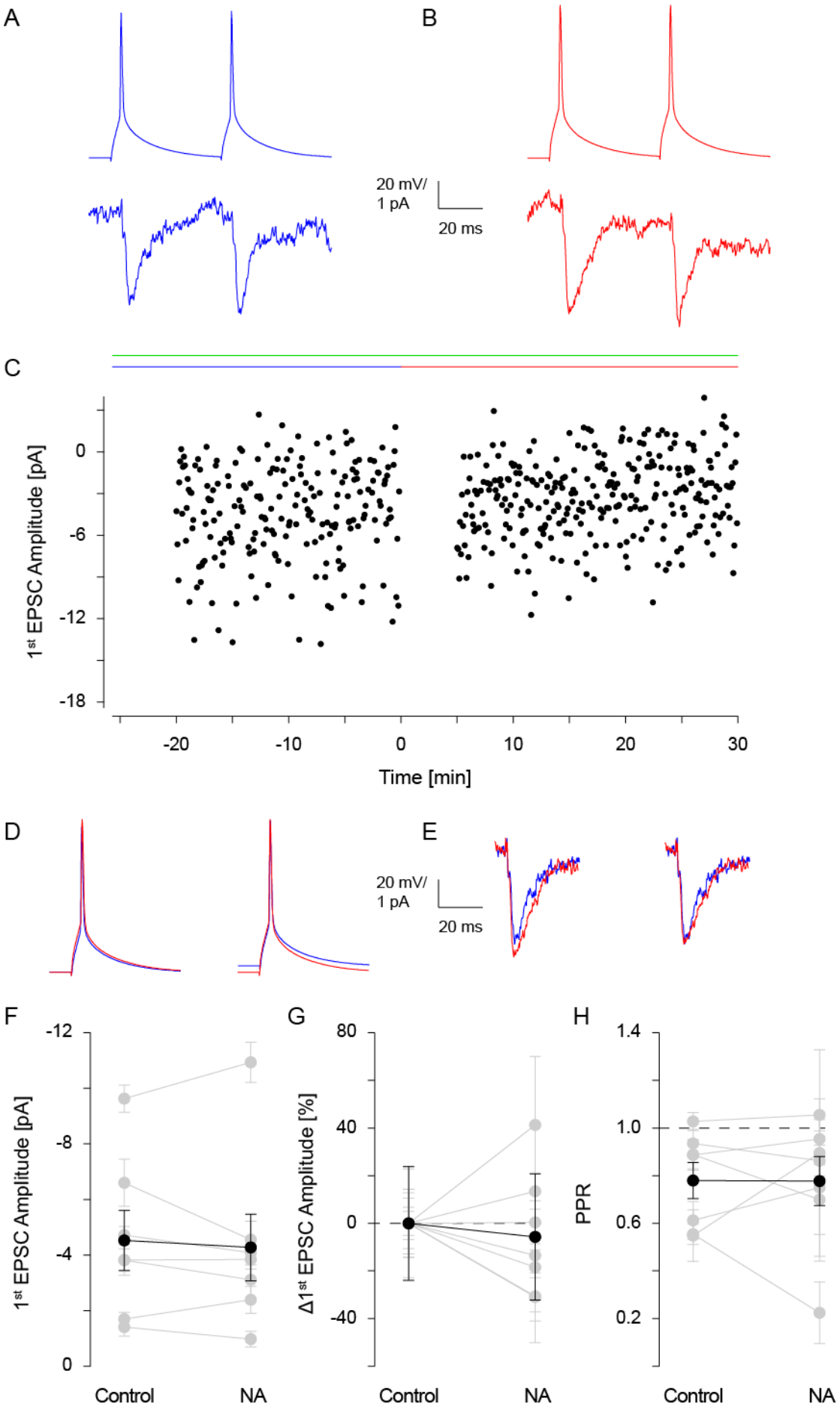
A
B
20 mV/
1 pA
20 ms
C
1st EPSC Amplitude [pA]
0
-6
-12
-18
-20
-10
0
10
20
30
Time [min]
D
E
20 mV/
1 pA
20 ms
F
1st EPSC Amplitude [pA]
-12
-8
-4
0
Control
NA
G
Δ1st EPSC Amplitude [%]
80
40
0
-40
Control
NA
H
PPR
1.4
1.0
0.6
0.2
Control
NA

Figure 4.4.17. Depression by NA was blocked by mSIRK.

The same figure legend as for Fig. 4.4.14 also applies here, with the additions that red codes for NA, and green indicates the presence of mSIRK in the recording pipette.

Data from an experiment with PKC blocked with 100 nM Gö 6983, and $GABA_A$ receptors with 3 µM gabazine, are illustrated in Fig. 4.4.18. In A, the time courses of the respective APs and EPSCs recorded during control are shown. Control experiments for the action of the PKC blocker revealed that Gö 6983 itself did not significantly change the pre- and postsynaptic properties (n = 4; $p_{pt} \geq 0.23$). In this experiment, during control, the average first EPSC amplitude was -5.7 ± 0.5 pA. In the presence of Gö 6983 and after the addition of 5-HT for five minutes (B), the first EPSC amplitude still depressed by 53 ± 7% to -2.7 ± 0.3 pA ($p_t < 2 \cdot 10^{-7}$). This depression was largely established within the first five minutes in 5-HT and persisted for the remainder of the recording (C). PPR in this pair did not change (0.77 ± 0.10 in control vs. 0.84 ± 0.32 in 5-HT; p_t = 0.17).

After the addition of 5-HT, the membrane potential in the presynaptic cell showed a depolarization by 4.6 from -76.5 to -71.9 mV (D, left traces). The comparison between the two AP time courses after aligning for V_{thr} showed no significant change in either *RT* or *W*. However, *H* of the AP was reduced by 3.6 from 66.0 to 62.4 mV.

The postsynaptic cell showed a decrease in I_{hold} by 65 pA from 55 to -10 pA. At a R_{in} of 142 MΩ, this change would have corresponded to a depolarization by 9.2 mV. When the time courses of the first EPSC were aligned and peak-scaled (E, right traces), no change was observed.

This set of experiments consisted of four pairs. Because in two out of four presynaptic cells, V_m required a bias current to keep then at <-70 mV, I am unable to comment on the change in the presynaptic membrane potential following 5-HT. However, I am able to comment on that in the postsynaptic cell, there was on average no significant change to I_{hold} (32.8 ± 33.2 *vs.* 31.5 ± 61.1 pA; p_{pt} = 0.98). The EPSC time courses including rise time and half-width remained unaltered ($p_{pt} \geq 0.36$).

In the 4 pairs studied, 5-HT still consistently depressed the EPSC amplitude by 51 ± 9% from -13.9 ± 5.5 to -6.7 ± 3.1 pA (p_{pt} = 0.04; F and G, black) despite PKC block. This depression was also accompanied by no change in PPR (0.80 ± 0.08 *vs.* 0.89 ± 0.04; p_{pt} = 0.24; H black). The extent of depression with or without PKC inhibition was indistinguishable (51 ± 9 *vs.* 46 ± 4%; p_t = 0.57), as was PPR. Therefore, I conclude that

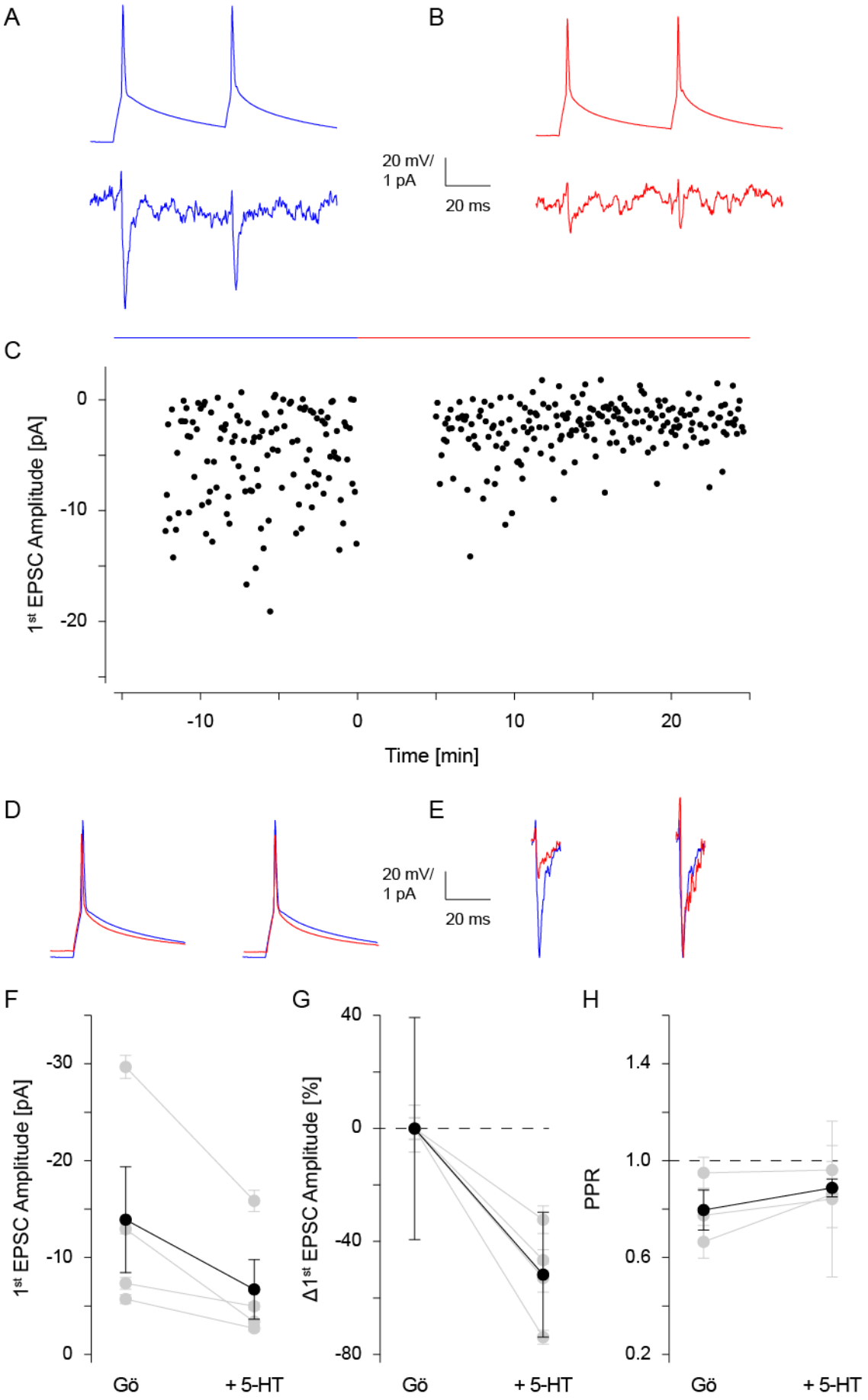
A
B
20 mV/
1 pA
20 ms
C
1st EPSC Amplitude [pA]
0
-10
-20
-10
0
10
20
Time [min]
D
E
20 mV/
1 pA
20 ms
F
1st EPSC Amplitude [pA]
-30
-20
-10
0
Gö
+ 5-HT
G
Δ1st EPSC Amplitude [%]
40
0
-40
-80
Gö
+ 5-HT
H
PPR
1.4
1.0
0.6
0.2
Gö
+ 5-HT

Figure 4.4.18. EPSC depression persists despite PKC block.

This figure is made similarly to that shown in Fig. 4.4.14 and therefore the legend there applies here, with the exception that this experiment was performed with PKC blocked throughout.

PKC is not significantly involved in causing the EPSC depression. Since the depression is brought about by receptor signalling proximal to PKC, the most likely candidate, therefore, is Gβγ.

4.4.4.2. Depression Blocked by mSIRK

Because scavenging Gβγ by mSIRK blocked the depression caused by NA (see 4.4.3.3 above), I tested the impact of this peptide on the depression. 100 μM mSIRK was added to only the patch solution of the presynaptic cell. As above, after re-patching the presynaptic cell with an intracellular solution containing mSIRK, it was allowed to diffuse for > 20 minutes before 5-HT was added to the superfusion.

When I compared the presynaptic properties immediately after re-patching with those after loading mSIRK for > 20 minutes (n = 13), I found that for the first AP, significant changes were observed in regard to V_{thr}, V_{rel}, H, RT, and W. Specifically, V_{thr} depolarized by 6.5 ± 1.6 from -45.4 ± 1.3 to -38.9 ± 1.5 mV ($p_{pt} = 2 \cdot 10^{-3}$), V_{rel} increased by 6.0 ± 1.9 from 31.8 ± 1.9 to 37.8 ± 2.2 mV (p_{pt} = 0.011), H decreased by 7.2 ± 1.7 from 79.6 ± 2.0 to 72.5 ± 2.4 mV ($p_{pt} = 2 \cdot 10^{-3}$), RT was prolonged by 0.1 from 0.5 to 0.6 ms ($p_{pt} = 7 \cdot 10^{-5}$) and W broadened by 0.1 ms from 0.9 to 1.0 ms ($p_{pt} = 9 \cdot 10^{-4}$). Similar changes were also observed for the second AP. V_{thr} depolarized by 6.5 ± 1.5 from -45.1 ± 1.3 to -38.6 ± 1.5 mV ($p_{pt} = 2 \cdot 10^{-3}$), V_{rel} increased by 6.0 ± 1.9 from 32.1 ± 1.8 to 38.1 ± 2.2 mV (p_{pt} = 0.01), H decreased by 7.1 ± 1.5 from 79.0 ± 1.8 to 71.9 ± 2.2 mV ($p_{pt} = 7 \cdot 10^{-4}$), and W broadened by 0.1 ms from 1.0 to 1.1 ms ($p_{pt} = 2 \cdot 10^{-4}$).

Despite the changes indicated above, V_{rest} remained the same (-77.3 ± 1.5 *vs.* -77.0 ± 1.2 mV; p_{pt} = 0.77). Because R_{in} was not measured 20 minutes after loading, I am unable to present direct evidence if R_{in} was affected by mSIRK. However, since the change in R_{in} estimated before mSIRK loading and after addition of 5-HT in its presence was not significantly different from that in “plain” experiments (p_t = 0.68), R_{in} was unlikely affected by mSIRK.

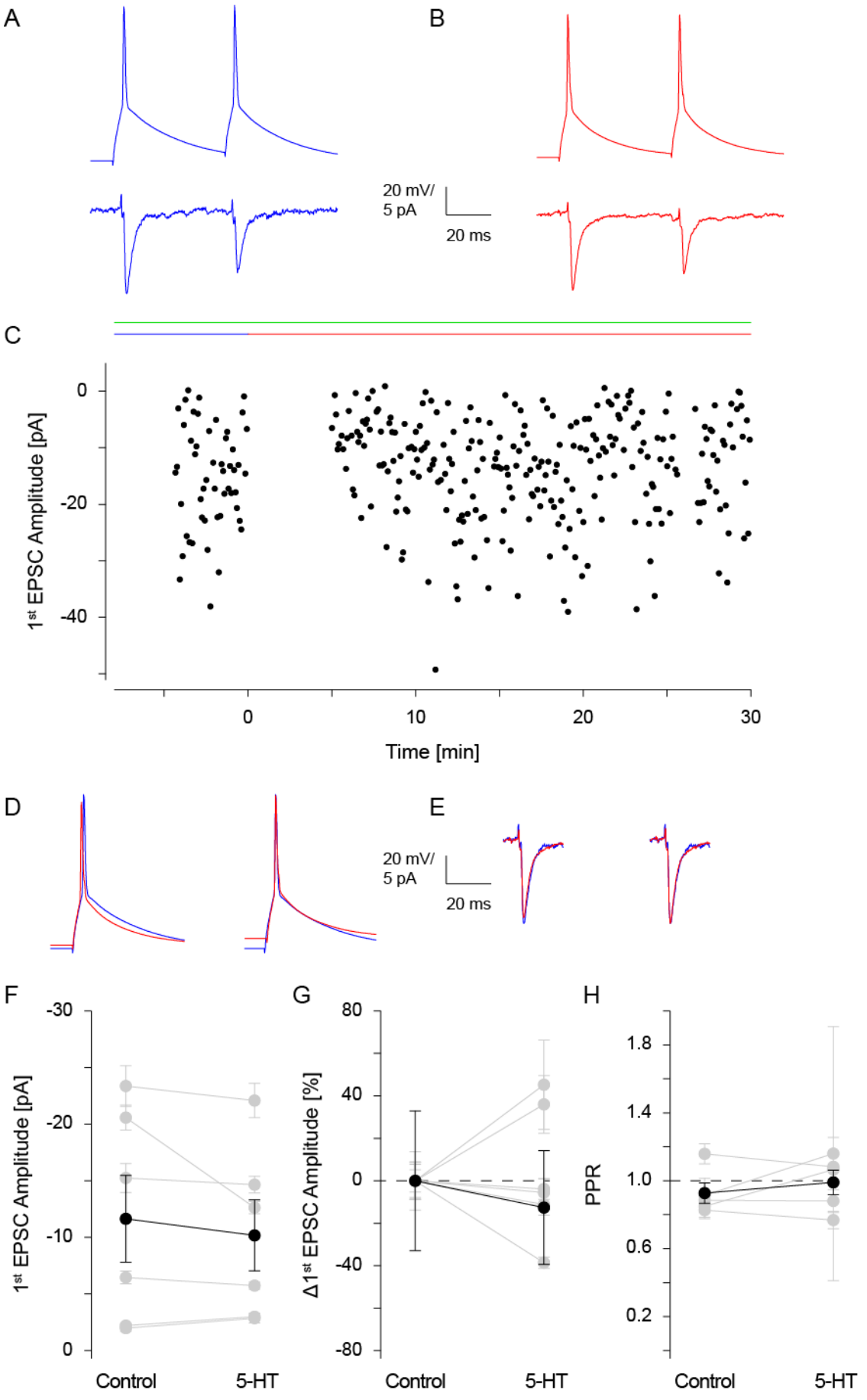
A
B
20 mV/
5 pA
20 ms
C
1st EPSC Amplitude [pA]
0
-20
-40
0
10
20
30
Time [min]
D
E
20 mV/
5 pA
20 ms
F
1st EPSC Amplitude [pA]
-30
-20
-10
0
Control
5-HT
G
Δ1st EPSC Amplitude [%]
80
40
0
-40
-80
Control
5-HT
H
PPR
1.8
1.4
1.0
0.6
0.2
Control
5-HT

Figure 4.4.19. Depression was blocked with mSIRK in the presynaptic solution.
The same legend as in Fig. 4.4.17 applies here, except that the slices were exposed to 10 μM 5-HT.

How 5-HT affected the presynaptic APs and the postsynaptic EPSCs after mSIRK being loaded to the presynaptic cell is shown in Fig. 4.4.19. Specifically, after 20 minutes of mSIRK loading of the presynaptic cell, the time courses of the APs and average EPSCs during the control period are presented in A. The first EPSC had an average amplitude of -15.2 ± 1.3 pA (A, bottom). Subsequent exposure to 5-HT failed to cause any significant depression, as the average amplitude remained at -14.7 ± 0.8 pA (p_t = 0.70; B, bottom). The individual peak amplitudes of the EPSCs before and after 5-HT addition are presented in C indicating that the EPSC remained stationary during both recording periods. As expected, PPR did not change significantly either (0.83 ± 0.04 in control *vs.* 0.77 ± 0.05 in 5-HT; p_t = 0.09).

Upon exposure to 5-HT, the presynaptic cell depolarized by 2.7 from -78.7 to -76.0 mV (D, left). The comparison between the two time courses of the first AP, after aligning for the V_{thr} (D, right), revealed no change in *RT* and *W*, but a small decrease in *H* by 1.6 from 71.0 to 69.4 mV. The postsynaptic cell showed an increase in I_{hold} by 53 pA, which corresponded to a hyperpolarization by 5.3 mV for a R_{in} of 100 MΩ. When the time courses of the first EPSC were aligned and peak-scaled (E, right), no significant change was observed.

After exposure to 5-HT, the presynaptic cells did not show any significant change in V_{rest} (-75.9 ± 1.5 *vs.* -75.7 ± 1.3 mV; p_{pt} = 0.84). With the exception of *H*, other properties of the AP were not significantly altered either ($p_{pt} \geq 0.08$). On average, *H* of the first AP still decreased by 2.6 ± 0.5 from 73.0 ± 3.1 to 70.4 ± 2.9 mV (p_{pt} = 0.003), and the second by 2.5 ± 0.5 from 72.1 ± 2.9 to 69.6 ± 2.7 mV (p_{pt} = 0.004). Neither I_{hold} (64 ± 35 *vs.* 26 ± 93 pA; p_{pt} = 0.57), nor any other property of the postsynaptic cells were significantly altered by 5-HT ($p_{pt} \geq 0.051$).

The presence of mSIRK in the presynaptic patch pipette prevented a significant depression in 5 out 6 pairs. In one pair, a significant depression by 39 ± 4% from -20.6 ± 1.1 to -12.6 ± 0.5 pA remained ($p_t = 5 \cdot 10^{-9}$). One likely explanation for this observation was that the larger R_s associated with this presynaptic cell (~18 MΩ) slowed the diffusion of mSIRK to the nerve terminals. However, in comparison with experiments without mSIRK, the number of pairs with no depression increased significantly (0 out of 7 *vs.* 5 out of 6; p_{χ^2} = 0.001).

On average, after mSIRK was loaded into all presynaptic cells, the peak amplitude of the first EPSC during control period was -11.6 ± 3.8 pA. The subsequent addition of 5-HT did not cause any significant depression, as the peak amplitude remained at -10.2 ± 3.1 pA (p_t = 0.32; F black). In addition, no significant change was observed for PPR either (0.93 ± 0.06 *vs.* 0.99 ± 0.07; p_t = 0.41; H black).

These results indicated that when mSIRK bound Gβγ, the EPSC depression by 5-HT was largely abolished. However, because in this case 5-HT still reduced *H* of the AP, without any depression of the EPSC, under physiological conditions the depression observed is not due to a smaller AP. Furthermore, because mSIRK also blocked the presynaptic hyperpolarization, which was also not observed when the 5-HT_2R agonist was used (see 4.4.2.4), the hyperpolarization likely occurred via the activation of 5-HT_1R, which signalled via Gβγ subunits to activate GIRK channels (Lüscher *et al.*, 1997).

4.4.4.3. Depression Also Blocked by ct-SNAP-25

Because mSIRK is myristoylated to allow for membrane penetration, a potential conjecture could be that its action was not restricted to the presynaptic nerve terminals as it could have diffused out of the cell, and in doing so, could have affected nerve terminals and dendrites nearby. This then could have somehow blocked the depression observed.

To rule such a scenario out, I performed another set of experiments, this time using a peptide of 14 amino-acids corresponding to the C-terminal of SNAP-25 (ct-SNAP-25), to which physiologically Gβγ binds (Gerachshenko *et al.*, 2005). Specifically, the peptide sequence is DEANQRATKMLGSG. Again, this peptide was added to the presynaptic solution at a concentration of 5.4 mM. Otherwise, these experiments were conducted in the same way as with mSIRK. However, because of a small sample size (*n* = 3), the presentation will be restricted to the ability of ct-SNAP-25 to block the depression.

One of these experiments is illustrated in Fig. 4.4.20. The time courses of the AP and the average EPSC during the control period are presented in A. The first EPSC had an average peak amplitude of -14.1 ± 1.0 pA (A, bottom). Subsequent addition of 5-HT did not result in a significant depression (-12.6 ± 0.8 pA; p_t = 0.25; B, bottom). Individual peak amplitudes of the first EPSCs for the periods before and after 5-HT are shown in C, further corroborating that there was no significant depression. At the same time, PPR remained unchanged throughout recording (0.93 ± 0.04 in control *vs.* 0.95 ± 0.06 in 5-HT; p_t = 0.13).

The presynaptic cell, loaded with ct-SNAP-25, showed a depolarization by 2.4 from -76.9 to -74.5 mV after 5-HT was added (D, left). After aligning the two time courses for V_{thr}, the comparison of the first APs before and after 5-HT (D, right) revealed no change in *RT* and *W*. However, *H* showed a small decrease by 1.4 from 77.2 to 75.9 mV.

I_{hold} of the postsynaptic cell showed a very small increase by 8 pA at a R_{in} of 109 MΩ, which corresponded to a hyperpolarization by 0.9 mV. When the time courses of the first EPSC during control and in 5-HT were aligned and peak-scaled (E, right), no significant change was observed.

On average, the peak amplitude of the first EPSC was -15.2 ± 3.0 pA during control. Subsequent addition of 5-HT did not cause a significant depression (G black) as the EPSC amplitude remained at -13.8 ± 2.5 pA (p_{pt} = 0.11; F black). In support, PPR in this data set did not show any significant change either (0.88 ± 0.11 *vs.* 0.91 ± 0.08; p_{pt} = 0.44; H black).

Admittedly based on a small sample size, these experiments still strengthen the idea that when Gβγ was bound to ct-SNAP-25 instead of its physiological target, the depression by 5-HT was largely blocked. Because the outcome of this set of experiments was no different from that with mSIRK, it was unlikely that mSIRK significantly affected signalling outside of the respective nerve terminals to prevent the depression.

4.4.4.4. No Speed-Up of the Recovery Rate from Depression

After confirming that 5-HT caused the EPSC depression via Gβγ signalling, insights into the respective targets were sought. Based on previous studies, there are two known mechanisms by which Gβγ might cause the observed depression. In the first mechanism, Gβγ binds to high voltage-activated Ca^{2+} channels to limit Ca^{2+} influx (Ikeda, 1996). In the second, it directly binds to SNAP-25 of the SNARE complex, to inhibit subsequent membrane fusion (Blackmer *et al.*, 2005).

In the latter case, Gβγ competes with Ca^{2+}/synaptotagmin 1 for binding to the SNARE complex in a Ca^{2+}-dependent way. At high Ca^{2+} concentrations, Gβγ unbinds from SNAP-25 and Ca^{2+}/synaptotagmin 1 rebinds to cause a temporary relief from depression (Yoon *et al.*, 2007), seen as a speed-up in the rate of recovery from depression. When Gβγ binds to the distal part of SNAP-25, it reduces the quantal amplitude by altering the fusion pore (Photowala *et al.*, 2006; Schwartz *et al.*, 2007; Fang *et al.*, 2008). It has previously been shown in this laboratory that this mechanism is most likely responsible

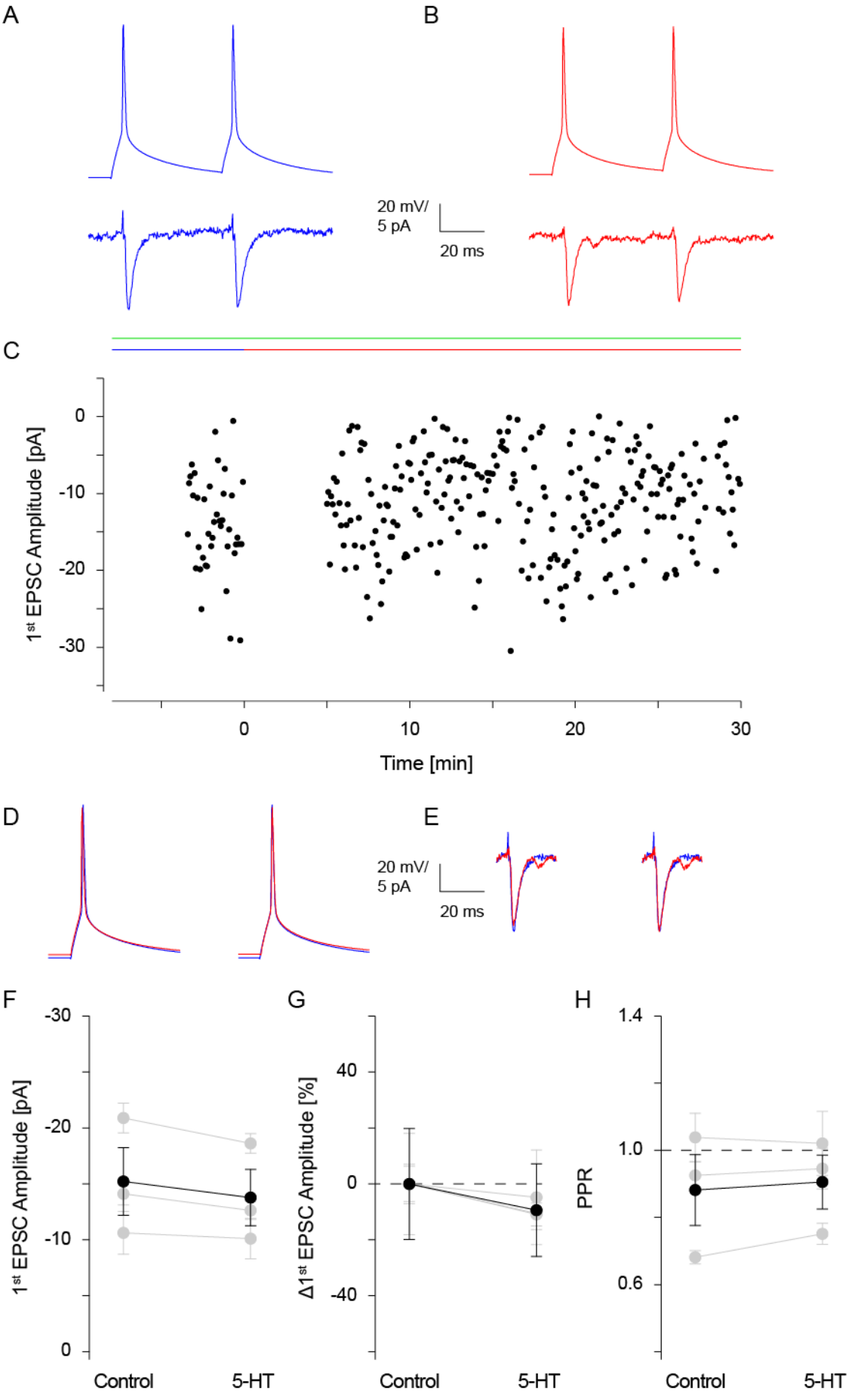
A
B
20 mV/
5 pA
20 ms
C
1st EPSC Amplitude [pA]
0
-10
-20
-30
0
10
20
30
Time [min]
D
E
20 mV/
5 pA
20 ms
F
1st EPSC Amplitude [pA]
-30
-20
-10
0
Control
5-HT
G
Δ1st EPSC Amplitude [%]
40
0
-40
Control
5-HT
H
PPR
1.4
1.0
0.6
Control
5-HT

Figure 4.4.20. Depression was also blocked by ct-SNAP-25.
The figure legend for Fig. 4.4.19 also applies here, with the exception that green indicates the presence of ct-SNAP-25 in presynaptic cell.

for the depression by NA, as evidenced by a speed-up in the recovery rate from depression and a reduced quantal size, both implicating the critical role of Gβγ binding to SNAP-25 in this process (Choy *et al.*, 2017b).

A protocol was designed (see 4.3.2) to test if the rate of recovery from depression was accelerated by 5-HT. For this purpose, short-term depression was induced by a burst of 20 APs at a rate of 50 Hz. 500 ms later, another AP was evoked to gauge the rate of recovery. Such a set of stimuli was repeated 20 times every 25 s as higher rates incurred a powerful depression. From these repetitions, an average time course was formed. Based on this time course, the recovery from (short-term) depression was quantified as R_{50}, as described in Methods, section 4.3.5. A value of R_{50} = -1 indicates no recovery, 0 full recovery within 500 ms, and values > 0 denote that the recovery EPSC is larger than the first EPSC in the train.

Before proceeding further, I summarise data from experiments with NA. Exposure to 10 μM NA caused a significant increase in R_{50} from -0.20 ± 0.06 during control to 0.51 ± 0.29 (n = 5; p_{pt} = 0.03; Choy *et al.*, 2017b). This result was consistent with the idea that, in the case of NA, after α_1 receptor activation Gβγ most likely bound to SNAP-25. If 5-HT also caused the depression via the same mechanism, a significant increase in R_{50} would be uncovered.

Such an experiment is illustrated in Fig. 4.4.21. During the control period (A), the average peak amplitude of the first EPSC was -40.4 ± 2.1 pA. At this set of synapses, after 20 APs, there was a steady-state depression by 57 ± 3% to -17.3 ± 0.5 pA. The peak amplitude of the recovery EPSC was -38.3 ± 1.9 pA, resulting in a value for R_{50} of -0.09 ± 0.12. This indicated that within 500 ms, the EPSC recovered just about back to the amplitude of the first EPSC in the train. After exposure to 5-HT (B), the first EPSC in the burst depressed by 42 ± 5% to -23.4 ± 1.6 pA, consistent with my previous findings (see 4.4.2.1). After 20 APs, the steady state amplitude depressed to -8.8 ± 0.8 pA. The recovery EPSC amplitude remained slightly smaller than the first EPSC in the stimulus sequence, *i.e*. -22.0 ± 2.0 pA *vs.* -23.4 ± 1.6 pA, respectively. Consequently, in this case R_{50} was -0.10 ± 0.18, not different from the starting value (p_t = 0.50).

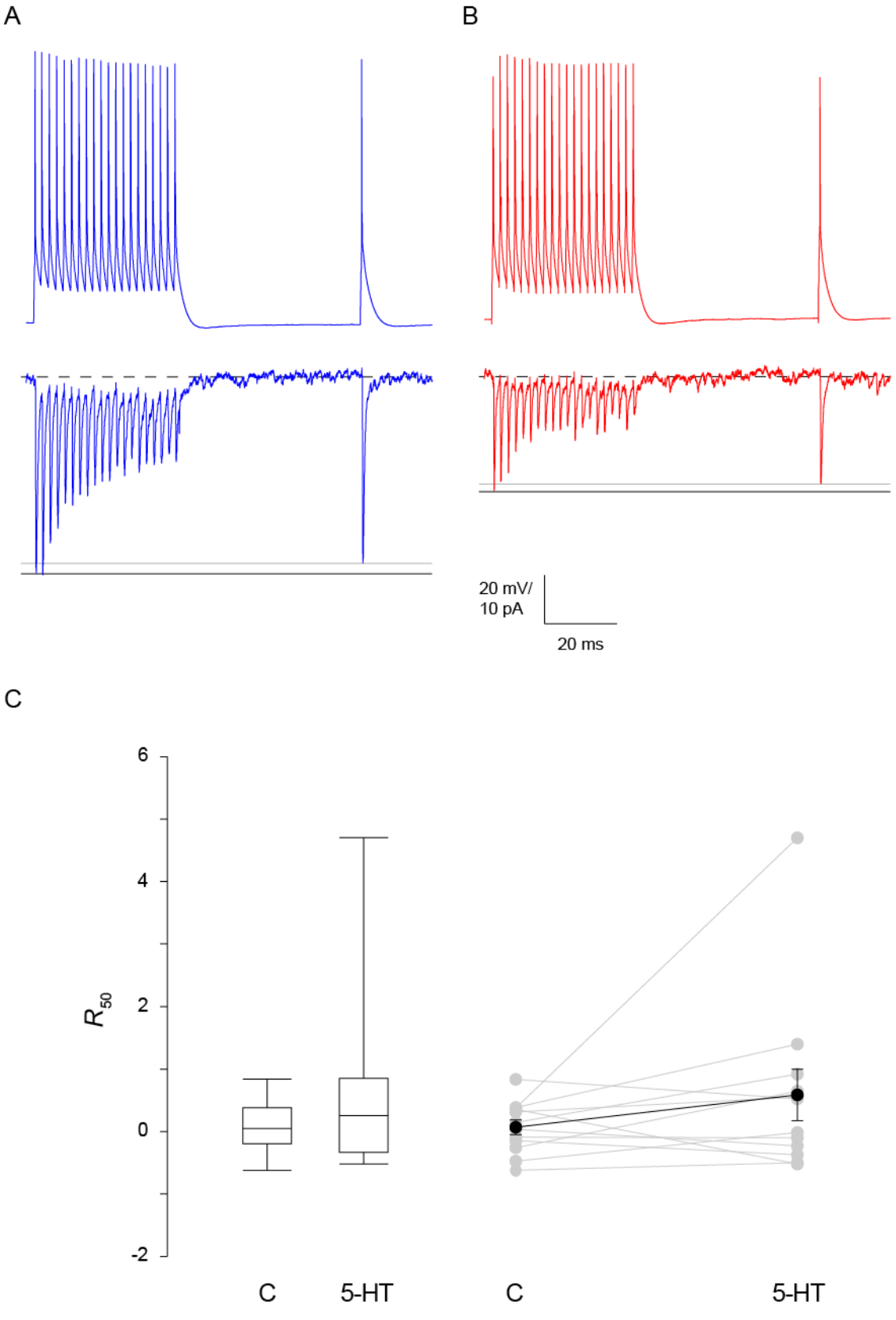

Figure 4.4.21. 5-HT did not speed-up recovery from depression.

A. Average time courses of the presynaptic APs and postsynaptic EPSCs elicited by 20 APs at 50 Hz, followed by eliciting a single AP with a 500 ms delay and measuring the respective EPSC. The black line indicates the amplitude of the 1st EPSC, the grey one the amplitude of the recovery EPSC. The dashed line indicates the baseline against which the

amplitudes were measured B. Same as in A, but after addition of 5-HT. C. Whisker plot of the values for R_{50} during control period (n = 18) and in 5-HT (n = 12). D. Pair-wise values of R_{50} plotted before and after 5-HT addition with the values in the respective experiment joined by a line. The black values represent the population averages with the respective errors.

During control, in 18 pyramidal pairs, R_{50} ranged from -0.62 ± 0.09 to 0.84 ± 0.80, with a median value of 0.05 ± 0.02 (C) and a mean of 0.07 ± 0.09. I was able to extract the values of R_{50} before and after 5-HT in 12 out of those 18 pairs (D). On average, R_{50} did not significantly change with 5-HT (0.07 ± 0.12 *vs.* 0.59 ± 0.41; p_{pt} = 0.10).

Because 5-HT did not alter R_{50} significantly, I conclude that Gβγ downstream of 5-HT_2R activation unlikely binds to the C-terminus of SNAP-25. These results then point towards the idea that in the case of 5-HT, the targets of Gβγ may likely be VDCC. If that were the case, then the quantal size should remain unaltered, in contrast to what was found in the case of NA.

4.4.4.5. Quantal Analysis on 5-HT-Induced EPSC Depression

To further explore the molecular targets through which the depression was incurred, quantal analysis was performed on a subset of such recordings. This was done in keeping with how NA affected the quantal parameters (Choy *et al.*, 2017b). Specifically, in that data set, a significant drop in quantal size by 39 ± 5% was uncovered. Because this decrease was restricted to the presynaptic terminal, this observation is consistent with Gβγ binding to SNAP-25, in competition with Ca^{2+}, to most likely cause fusion pore limitation.

For this purpose, I performed a density-based quantal analysis. To be included in this analysis, a data set should have had at least about 100 – 300 stationary EPSCs evoked during the control period, and about an equal number after the addition of 5-HT. An example of such data set is given in Fig. 4.4.22. Individual peak amplitudes of the first EPSC during the control period (solid black) and after 5-HT exposure (open) are shown in A. The average value for the 279 measured EPSCs during control period was -12.0 ± 0.5 pA, with a coefficient of variation (CV) of 0.67. The respective noise standard deviation (σ_n) was 0.91 pA. The density of these amplitudes, formed using a Gaussian kernel of 0.27 pA, is illustrated in B (solid line). After the addition of 5-HT, the average peak EPSC amplitude was -5.1 ± 0.3 pA, with a CV of 0.95 and σ_n of 1.04 pA. Using a kernel size of 0.31 pA, the density of these amplitudes was formed and is shown in C (solid line).

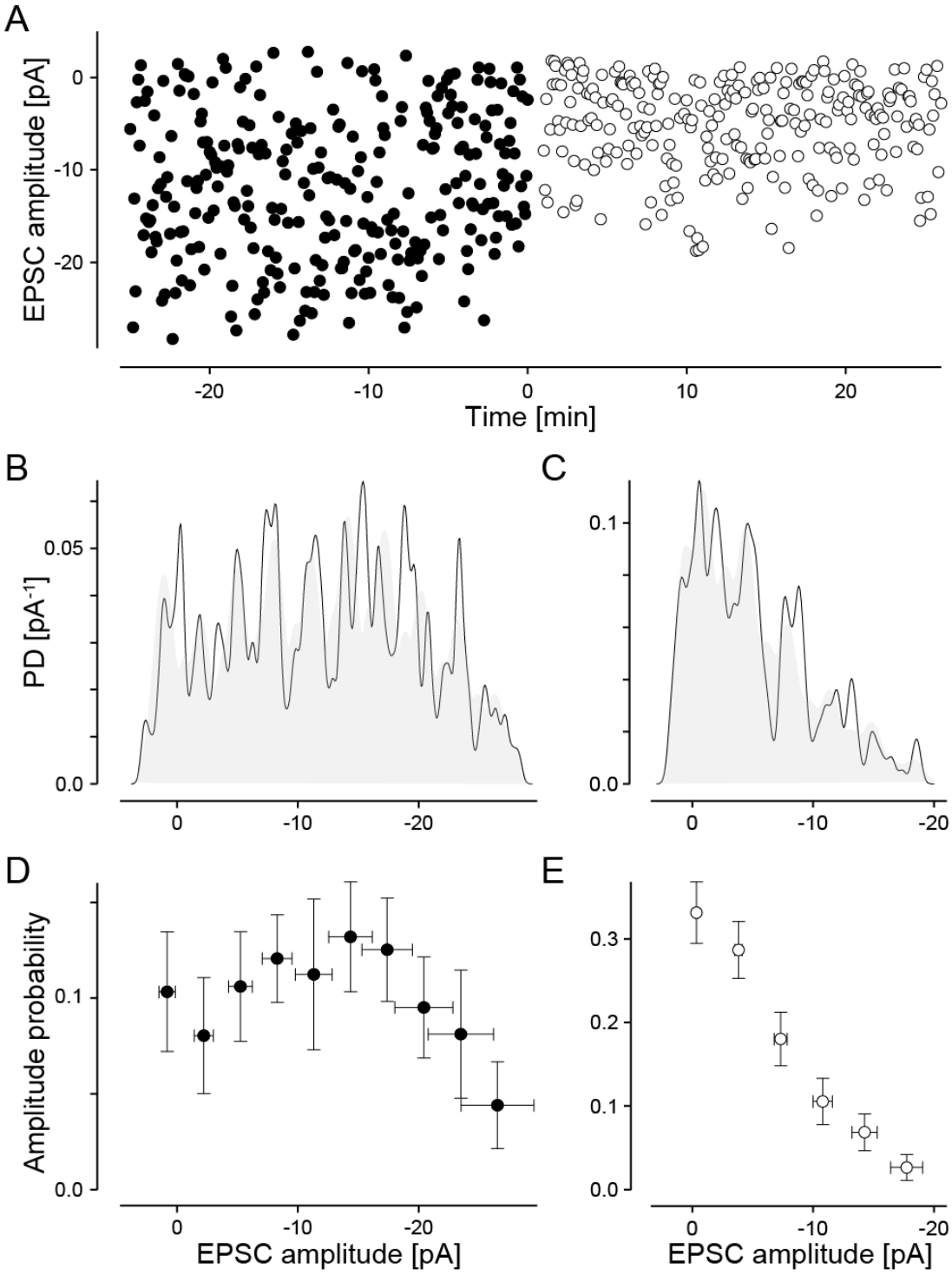

Figure 4.4.22. Quantal analysis of 5-HT mediated EPSC depression.

A. Individual peak EPSC amplitudes during the control period (solid) and after addition of 5-HT (open). B. Probability density of the EPSC amplitudes during control (solid line) and with the best fit (grey). C. Same as for B, but after exposure to 5-HT. D. Estimates of the amplitude probabilities and quantal amplitudes, including the respective error bars for the best model during control. E. Same as in D, but for the best model in the presence of 5-HT.

The best model during the control period was an unconstrained quantal process with 10 modes and a quantal size (Q) of -3.0 ± 0.3 pA (B, grey density). Consequently, the quantal content (m) was estimated to be 3.9 ± 0.5, with a failure rate (P_0) of 0.10 ± 0.03. After addition of 5-HT, the best model remained an unconstrained quantal process, but this time only with 6 modes and a Q of -3.5 ± 0.3 pA (C, grey density). Based on this value, m equalled 1.5 ± 0.1 and P_0 was 0.33 ± 0.04. The respective amplitudes and associated probabilities, together with the respective error bars, are presented in Fig. D for the control and E for the period with 5-HT. Note how the error bars for the amplitudes become larger with the number of modes due to the accumulation of the respective error in quantal size. A comparison between Q during control and after 5-HT reveals that these values were indistinguishable (p_t = 0.07).

Because there was no difference in the outcomes when 5-HT (n = 8) or the agonist α-methyl-5-HT (n = 6) was used, the data sets were pooled. From these 14 data sets, 6 passed the unimodality tests (43%). The average peak EPSC amplitude during control was -11.2 ± 2.3 pA, based on an average sample size of 197 ± 36. σ_n was 0.94 ± 0.07 pA (kernel size 0.30 ± 0.02 pA). After the addition of 5-HT, the average peak EPSC amplitude was -4.6 ± 0.9 pA based on an average sample size of 212 ± 16. σ_n was of 0.89 ± 0.05 pA (kernel size 0.30 ± 0.02 pA). These numbers correspond to an average depression in peak EPSC amplitude by 55 ± 7%, which was not different from that in the overall sample (p_t = 0.42).

Similar to the example presented above, all data sets were well fit with an unconstrained quantal model without variance. The average value of Q during control was -2.9 ± 0.1 pA. After 5-HT, Q remained the same (-2.9 ± 0.2 pA; p_t = 0.65). The values for each experiment are presented in Fig. 4.4.23. In A, the dashed line indicates the line of identity. Note that all data points group around it. This finding is in contrast to that with NA, where a reduction in Q by 39 ± 5% was uncovered (Choy *et al.*, 2017b). Based on the individual values of Q, the average value of m was estimated to be 3.8 ± 0.7 and 1.6 ± 0.3 during control and after 5-HT, respectively. This is shown in B, where the respective values are plotted with the line of identity dashed. In fact, there is a significant correlation between $m_{5\text{-HT}}$ and m_C when the offset was constrained to 0 (B, solid line; slope 0.40 ± 0.05, r = 0.77, p_{Pr} = 0.045). When the depression in m was plotted against the EPSC depression (C), all data points grouped around the line of identity, indicating that the EPSC depression was mostly due to a reduction in m. Again, this is different to what was seen with NA, suggesting that in this case, Gβγ did not primarily bind to the C-terminal of SNAP-25.

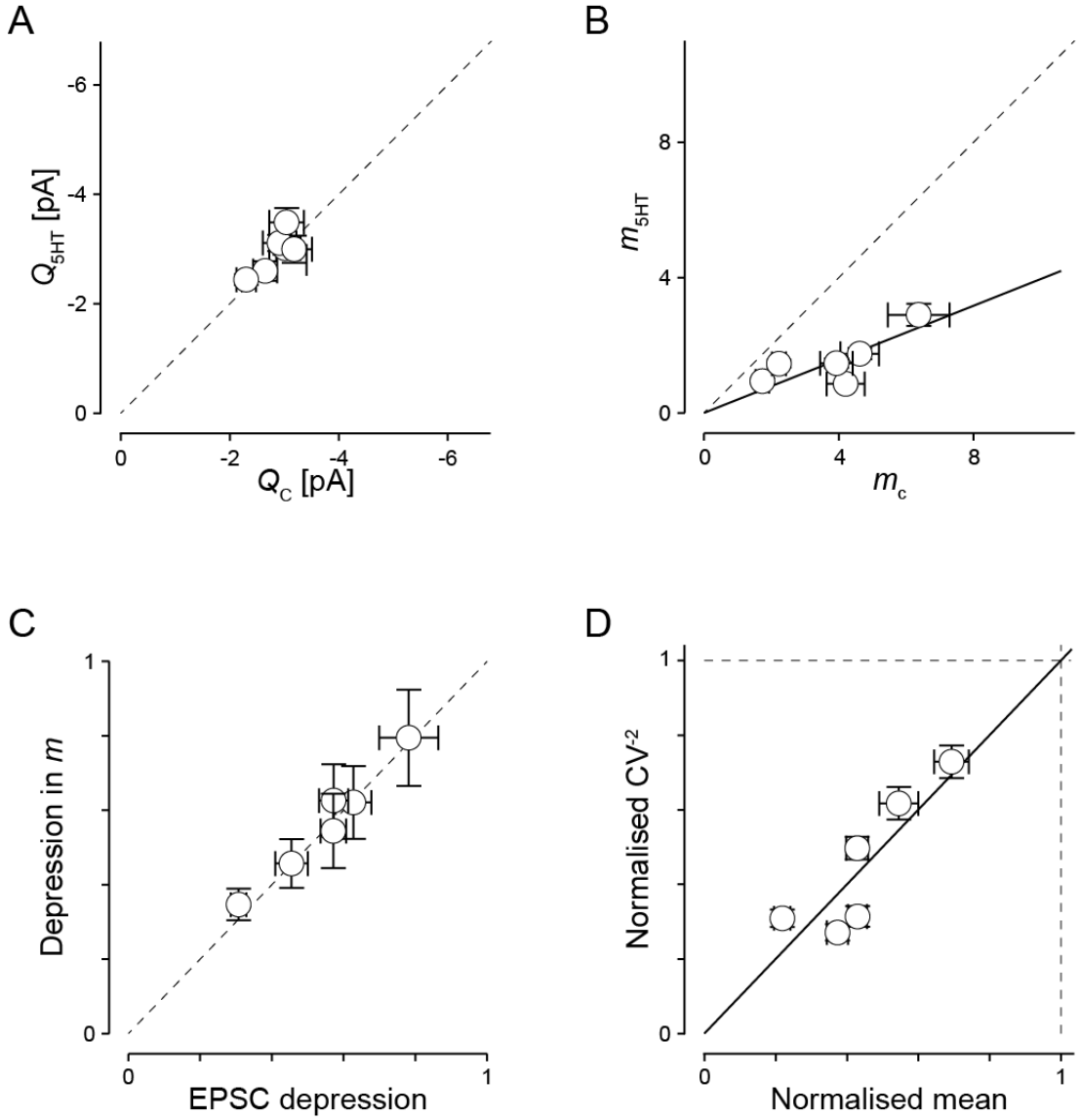

Figure 4.4.23. Reduction in quantal content, but not size.

A. Quantal size (*Q*) after addition of 5-HT plotted against that during the control period with their respective error bars. Line of identity dashed. B. Same as in A, but for quantal content (*m*). C. Depression in *m* plotted against that of the EPSC amplitude. D. CV^{-2} analysis of the same data set. Both values normalised to the control condition. Dashed lines indicate values of 1 for both CV^{-2} and mean, and delineate the area of depression between values of 0 and 1. The solid line is the best fit to the data set, but also the line of identify. Values on and below the line are interpreted as due to a change in release probability.

To cross-check the outcomes of the density based estimation, the data set was subject to a CV^{-2} analysis (Del Castillo & Katz, 1954b; Bekkers & Stevens, 1990; Malinow & Tsien, 1990). This is illustrated in D. In its classic interpretation, any change associated with the quantal size should not change CV^{-2}, but affect the mean (points would fall into the triangle above the line of identity), whereas changes in release probability strongly affect both the relative CV^{-2}, but to a lesser extent the relative mean (points would fall

into the line of identity or below). In the case of the depression incurred by 5-HT, all 6 data points fell near or onto the line of identity. In fact, the best fit to this data was the line of identity (r = 0.88; p_{Pr} = 0.02). This finding supports the conclusion drawn above that most, if not all the depression is due to a change in release probability.

This set of analyses further supported the idea that 5-HT caused the EPSC depression through a mechanism different to that of NA, *i.e*. consequently, most likely by limiting Ca^{2+} influx via N- and/or P/Q Ca^{2+} channels or a yet to be discovered mechanism.

4.4.5. Network Specificity of Modulation by 5-HT

In this section, I will show that the serotonergic modulation of glutamate release was specific within the network of layer II pyramidal cells. Specifically, in 4.4.5.1, I will provide analyses and comparisons that link together the conceptions of responders and non-responders as defined in Part 3, extending it to include the pre- and postsynaptic cells. In 4.4.5.2, I will present further evidence that in the postsynaptic cells which corresponded to responders, together with the depression observed, there was a concurrent increase in spontaneous glutamate release after exposure to 5-HT. This finding further strengthens the conclusion drawn in 4.4.5.1, by showing that the serotonergic modulation is restricted to specific synapses in the network. In 4.4.5.3, I will present further data in support of this idea by experimentally testing in paired recordings the conclusion drawn in 4.4.5.1 and 2.

4.4.5.1. Non-Responders Are Mostly Presynaptic, Responders Postsynaptic

In Part 3, responders were functionally defined as showing an increase in mEPSC frequency. About half of the cells were captured in this definition. However, in this part, depression was not restricted to a subset, but was observed in all postsynaptic cells. This result raised the question if the modulation of glutamate release by 5-HT was restricted to a specific set of synapses that preferentially connected onto pyramidal cells. Or in other words, only very specific cells that form connections in this layer were modulated by 5-HT, hence, form a specific network.

If 5-HT specifically modulated glutamate release at synapses that linked pyramidal cells, the responders and the postsynaptic cells should show identical changes in both R_{in} and I_{hold} after 5-HT exposure. Furthermore, there should be no statistical difference between the percentages of cells, which showed a net inward ($-\Delta I_{hold}$) or a net outward current ($+\Delta I_{hold}$). Data to make such comparisons are presented in Table 4.4.3.

As shown in Part 3, after exposure to 5-HT, the decrease in R_{in} for responders was -56 ± 13 from 197 ± 15 to 141 ± 8 MΩ (n = 36; $p_{pt} = 10^{-4}$; Table 4.4.3). Similarly, the reduction in R_{in} for the postsynaptic cells in the pairs presented in this part was also -55 ± 17 from 198 ± 17 to 143 ± 14 MΩ (n = 40; p_{pt} = 0.002). Under the null hypothesis (H_0) that there was no difference between the two samples, when the two decreases in R_{in} were compared, H_0 had to be accepted at p_t = 0.97. This result indicates that, on a statistical basis, the postsynaptic pyramidal cells in the pairs correspond to responders.

Table 4.4.3. Comparison of spontaneous and evoked data sets.

Changes by 5-HT	**Spontaneous** *vs.* **Evoked**				
Parameter	**Non-Responder (*n*)**		**Presynaptic (*n*)**		**Statistics**
ΔR_{in} [MΩ]	-30 ± 11	(67)	-33 ± 13	(39)	p_t = 0.83
ΔI_{hold} [pA]	34.4 ± 4.2	(51)	-		-
ΔV_m [mV]	-		-3.4 ± 1.3	(21)	-
$-\Delta I_{hold} / +\Delta V_m$ [%]	6	(3)	19	(4)	p_{χ^2} = 0.09
$+\Delta I_{hold} / -\Delta V_m$ [%]	94	(48)	81	(17)	
	Responder (*n*)		**Postsynaptic (*n*)**		
ΔR_{in} [MΩ]	-56 ± 13	(36)	-55 ± 17	(40)	p_t = 0.97*
ΔI_{hold} [pA]	6.3 ± 7.8	(25)	2.3 ± 10.6	(43)	p_t = 0.76
$-\Delta I_{hold}$ [%]	40	(10)	42	(18)	p_{χ^2} = 0.88
$+\Delta I_{hold}$ [%]	60	(15)	58	(25)	

The significant change is marked with a grey background and by * for a value > 0.95.

This specificity was further supported by the following analysis. After exposure to 5-HT or the full agonist α-methyl-5-HT, responders in Part 3 on average showed no significant change in I_{hold} (78.9 ± 8.4 *vs*. 85.2 ± 12.6 pA, n = 25; p_{pt} = 0.43; Table 4.4.3). In this part (4.4.2.3), the postsynaptic cells also had an insignificant change in I_{hold} (66.7 ± 8.2 *vs*. 69.0 ± 16.6 pA, n = 43; p_{pt} = 0.83). Again, when these two values were compared, there was no significance (p_t = 0.76), further strengthening the idea that the postsynaptic cells in the pairs correspond to responders.

Because the average changes in holding current for both data sets were made up of cells showing either a net inward or outward current, a further refined analysis was done by counting the respective numbers of cells and asking if based on a χ^2-test, there was a difference in the make-up. As presented previously in Part 3, 10 out of 25 responders showed a net inward and, consequently, 15 had a net outward current (Table 4.4.3). An identical set of numbers was found in Part 4 for the postsynaptic cells. 18 out of 43 cells showed a net inward, and the remaining 25 a net outward current. Based on a χ^2-test, there was no significant difference either (p_{χ^2} = 0.88), further strengthening the conclusion that responders are the postsynaptic elements in the layer II microcircuit. This conclusion implies that in the same postsynaptic pyramidal cell, besides the EPSC depression, there are concurrent changes in mEPSC frequency. Experimental data supporting this conclusion will be provided in the next section.

If responders are postsynaptic, non-responders are most likely presynaptic. In analogy to the analysis above, I checked the possibility if non-responders were indeed the presynaptic cells within the network.

On average, the reduction in R_{in} in non-responders in Part 3 was -30 ± 11 MΩ (191 ± 10 *vs*. 161 ± 7 MΩ, n = 67; p_{pt} = 0.003; Table 4.4.3). For comparison, the reduction in R_{in} for the presynaptic cells in this part was also -33 ± 13 MΩ (171 ± 11 *vs*. 138 ± 11 MΩ, n = 39; p_{pt} = 0.013). When comparing these reductions, no significant difference was found (p_t = 0.83), suggesting that the idea that non-responders are the presynaptic cells, cannot be rejected.

Furthermore, non-responders In Part 3 showed a significant increase in the outward current (+ΔI_{hold}) of 34.4 ± 4.2 pA (75.4 ± 5.3 *vs*. 109.8 ± 7.4 pA, n = 51; p_{pt} = 0.001; Table 4.4.3). Because the presynaptic cells were held in current-clamp to evoke action potentials, a direct comparison was not possible. But because an outward current in voltage-clamp corresponds to a hyperpolarization in current-clamp, after 5-HT a hyperpolarization (-ΔV_m) was expected in the presynaptic cells. In fact, the average change in membrane potential of the presynaptic cells was indeed -3.4 ± 1.3 mV (-74.3 ± 1.2 *vs*. -77.7 ± 1.4 mV, n = 21; p_{pt} = 0.015). This further strengthens the idea that the presynaptic cells correspond to non-responders.

In addition, I compared the number of cells showing either an inward current or a depolarization (-ΔI_{hold} / +ΔV_m) *vs.* outward current or a hyperpolarization (+ΔI_{hold} / -ΔV_m) in both data sets. As shown in Part 3, only 3 out of 51 non-responders showed an inward (-ΔI_{hold}), but 48 an outward current (+ΔI_{hold}; Table 4.4.3). In the data set in this part, 4 out of 21 presynaptic cells showed a depolarization (+ΔV_m) whereas the remaining 17 a

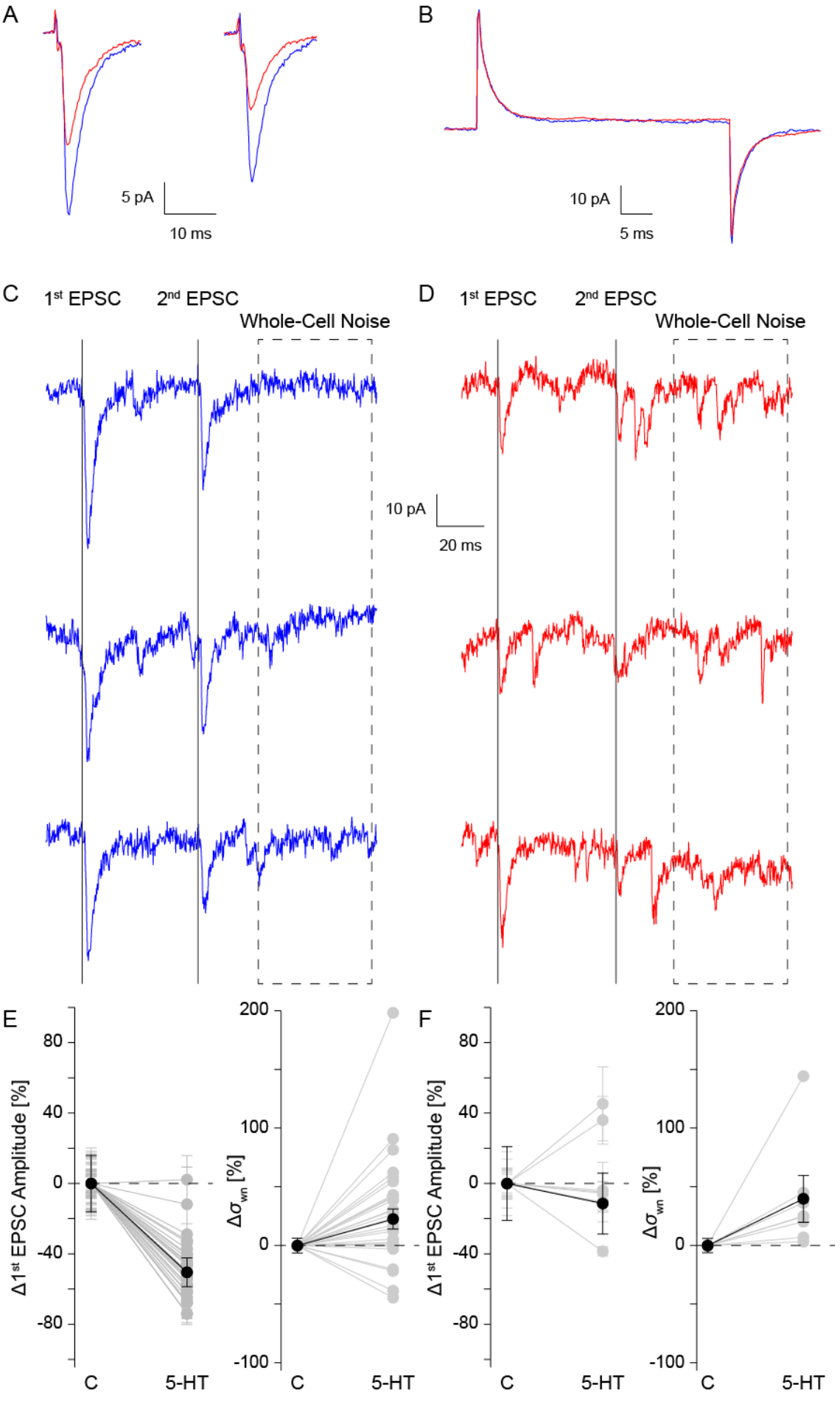
A
5 pA
10 ms
B
10 pA
5 ms
C
1st EPSC
2nd EPSC
Whole-Cell Noise
D
1st EPSC
2nd EPSC
Whole-Cell Noise
10 pA
20 ms
E
Δ1st EPSC Amplitude [%]
80
40
0
-40
-80
Δσwn [%]
200
100
0
-100
C
5-HT
C
5-HT
F
Δ1st EPSC Amplitude [%]
80
40
0
-40
-80
Δσwn [%]
200
100
0
-100
C
5-HT
C
5-HT

Figure 4.4.24. EPSC depression and concomitant increase in σ_{wn}.
A. Average time courses of the first (left) and second (right) EPSCs during control and after 5-HT. B. Superposition of the respective current transients to a voltage step of 0.5 mV reflecting R_s and R_{in}. C. Raw traces of three evoked trials containing the two EPSCs before (left) and after 5-HT (right). EPSC onset times are indicated by solid lines. The dashed rectangles indicate the time windows during which σ_{wn} was determined. E. Relative EPSC amplitude during control and after 5-HT (left). The average values are presented in black. Change in σ_{wn} before and after exposure to 5-HT. F. Same as in E, except for the dataset, in which either mSIRK or ct-SNAP-25 were present.

hyperpolarization ($-\Delta V_m$). It can be seen that in both sets, most cells underwent a hyperpolarization after 5-HT. When the two sets were compared using a χ^2-test, a significant difference was hardly uncovered ($p_{\chi^2} = 0.09$), further supporting the idea that non-responders are the presynaptic cells in the network.

4.4.5.2. Postsynaptic Whole-Cell Noise after 5-HT

To find further evidence in support of the conclusion just drawn, the standard deviation of the whole-cell noise (σ_{wn}) in the postsynaptic cells before and after exposure to 5-HT was determined. This indirect measure was chosen, because TTX would have abolished AP generation and, hence, the resulting EPSC. A long time window was chosen, over which σ_{wn} was measured, to deliberately include spontaneous EPSCs (sEPSCs). Notably, σ_{wn} is different from σ_{noise} in 3.4.1.2 and part 4, because the latter excludes visible spontaneous glutamate currents.

Such an analysis is illustrated in Fig. 4.4.24. In A, the average peak amplitudes of the first EPSC (left traces) before and after 5-HT addition are shown. During control, the size of the first EPSC was -28.3 ± 1.2 pA. The addition of 10 µM 5-HT depressed the amplitude by 38 ± 4% to -17.8 ± 0.7 pA ($p_t < 8 \cdot 10^{-12}$). As mentioned above (4.4.2.1), it is critical for this kind of comparison that R_s did not change by more than 10% between the two conditions. Specifically, in this example, R_s of the postsynaptic cell during control was estimated after rounding to be 9 and after 5-HT 10 MΩ (B), not significantly altering the current decay after a voltage step of 0.5 mV.

Next, I determined σ_{wn} in the postsynaptic cell. In C and D, three individual traces are presented which were acquired during control and 5-HT, respectively, with the onsets of the first and second EPSCs indicated by solid lines. The periods, during which σ_{wn} was measured, are indicated by dashed rectangles. Specifically, 30 ms after the second EPSC was elicited, σ_{wn} was determined over the duration of 48 ms. σ_{wn} during the control

period was 4.1 pA. After exposure to 5-HT, it increased to 5.7 pA consistent with the idea that spontaneous release increased. Note that after exposure to 5-HT, at the same time, a large depression in the first and second EPSCs was also evident.

In a set of 36 experiments where this type of analysis could be done, 5-HT depressed the average peak amplitude of the first EPSC by 49 ± 3% from -16.4 ± 2.6 to -8.1 ± 1.3 pA ($p_{pt} = 4 \cdot 10^{-6}$; E, left set). Consistent with the idea above, this depression was typically accompanied by a significant increase in σ_{wn} by 28 ± 9% from 3.5 ± 0.2 to 4.2 ± 0.3 pA ($p_{pt} = 0.004$; E, right set). Together these results support the idea that the evoked EPSC depression and increase in spontaneous transmitter release occur concurrently in the same postsynaptic cell.

I extended the same analysis also to the pairs loaded either with mSIRK or ct-SNAP-25. In these cells, 5-HT failed to cause any significant depression of the EPSCs (-12.8 ± 2.7 *vs.* -11.4 ± 2.2 pA; $p_{pt} = 0.14$; F, left set). However, σ_{wn} still increased by 38 ± 16% from 2.5 ± 0.1 to 3.4 ± 0.5 pA ($p_{pt} = 0.026$; F right set). These findings make one important point, namely that the signalling for spontaneous and evoked release could be dissociated at the level of the G protein.

4.4.5.3. Testing for Network Specificity

To directly test the prediction that the postsynaptic cells correspond to responders and the presynaptic to non-responders, I performed a set of experiments in which I first obtained a connected pair. Having determined which of the cells was pre- and postsynaptic and their respective membrane properties, among them R_{in}, 1 µM TTX was added to the superfusate, and mEPSCs were recorded before and after the addition of 5-HT.

A recording from such a pair with unidirectional connectivity is presented in Fig. 4.4.25. Specifically, in A, a schematic of the respective connection is drawn together with the respective time courses of the APs (presynaptic) and the EPSCs (postsynaptic). In B – F the data from the presynaptic, and in G – L that of the postsynaptic cell are illustrated.

First, data for the presynaptic cell will be presented with the prediction that these should be consistent with the properties of non-responders. In this cell, the mEPSC frequency during the control period was 80 ± 4 Hz (B0). After 5-HT had been added, there was no significant increase (81 ± 3 Hz; B1 – 3, C, D, and E). The respective amplitudes were -5.6 ± 0.1 and -5.6 ± 0.1 pA (B0 – 3 and F), with an average rise time of 0.7 and 0.7 ms, and half-width of 2.0 and 1.9 ms, respectively. There was no significant change in any of these properties. In contrast, after the addition of 5-HT, R_{in} decreased by 19 from 141

to 122 MΩ, but I_{hold} increased by 35.0 from 50.0 to 85.0 pA, reflecting a small hyperpolarization by 0.7 mV. These data were then clearly consistent with the prediction that the presynaptic cell displayed all the hallmarks of a non-responder.

I now present data from the postsynaptic cell with the expectation that the properties should be consistent with those of responders. Specifically, during the control period, the instantaneous mEPSC frequency was 64 ± 2 Hz (G0). After addition of 5-HT to the superfusate, the frequency increased initially to 84 ± 4 Hz; *i.e*. by 31 ± 7% (G1, H, I, and J). The frequency then gradually decreased to 65 ± 3 Hz, which was not different from the control value (G2). Subsequently, it resurged back by 29 ± 9% to reach another peak at 83 ± 5 Hz (G3 and K). Throughout, the mEPSC amplitude did not show any significant change, as it remained at the control value of -10.0 ± 0.1 pA (L). There was not change in the average time courses of the mEPSCs during control and after 5-HT (data not shown), with the average rise time and half-width also remaining at 0.6 and 1.8 ms, respectively. After 5-HT, I observed a decrease in R_{in} by 34 from 124 to 90 MΩ, which was accompanied by a small increase in I_{hold} by 18 pA (106 *vs.* 124 pA). In comparison to the presynaptic cell above, the decrease in R_{in} was larger, but the increase in I_{hold} was smaller. These data were then clearly consistent with the prediction that the postsynaptic cell displayed all the hallmarks of a responder.

Overall, I was able to perform such mEPSC recordings in 4 pairs, each of which showed connectivity only in one direction. For the presynaptic cells, there was no significant mEPSC increase in any of the cells. In addition, they had all the hallmarks of non-responders, namely a drop in R_{in} on average by 21 ± 45 from 173 ± 34 to 152 ± 28 MΩ (p_{pt} = 0.34), associated with an outward current of 38.0 ± 1.3 pA (p_{pt} = $4 \cdot 10^{-5}$). When these changes in R_{in} and I_{hold} were compared to those of non-responders (see table 4.4.3), no significant differences were found (p_t = 0.86 and 0.43, respectively). Altogether, these findings are consistent with the prediction.

In 2 out of the 4 postsynaptic cells, there were transient mEPSC frequency increases after 5-HT addition; *i.e*. consistent with the notion of responders. If the 8 cells were considered as a “random” sample, as in Part 3, the percentage of responders in these recordings was not significantly different from that has been reported earlier (25 *vs.* 47%; p_{χ^2} = 0.31). After exposure to 5-HT, R_{in} changed on average by 60 ± 39 from 175 ± 40 to 115 ± 2 MΩ (p_{pt} = 0.11). Even though the respective number was larger, it was not different, likely due to the limited sample size. Concomitantly, an outward current was observed.

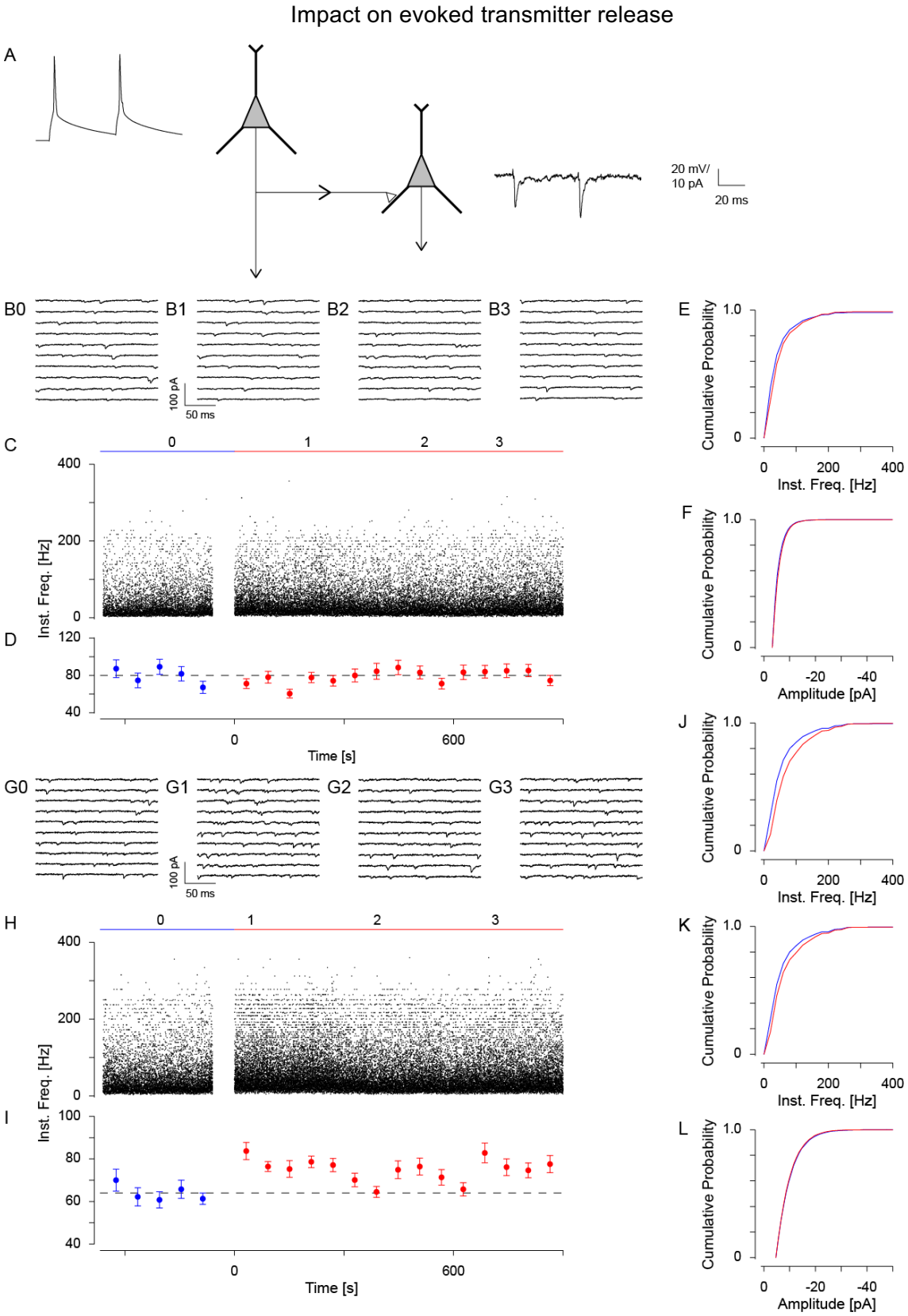

Figure 4.4.25. Modulation of mEPSCs in a pre- *vs.* postsynaptic cell.

A. Schematic of the unidirectional recording configuration with the average time courses of the presynaptic voltage and postsynaptic current shown. B. Representative traces of mEPSCs in the presynaptic cell during control (B0) and after 5-HT exposure (B1 – 3) at different points in time as indicated in C (top). C. Plot of the instantaneous mEPSC frequencies during the recording. D. Minute averages of the mEPSC frequencies. The

dashed line indicates the average value during control. E. cPDFs of the mEPSC frequencies during control and at time point 1 indicated in C. F. cPDFs of mEPSC amplitudes during control and during the last five minutes with 5-HT. G – I. The same legends as for B – D apply, except that the data were recorded postsynaptically. J and K. Comparisons between cPDFs of the frequencies during control and after 5-HT at the time points indicated in H by number 1 and 3, respectively. L. cPDFs of amplitudes in control and during the last five minutes with 5-HT.

So far, the data presented were consistent with pre- corresponding to non-responders, and postsynaptic cells to responders. This conception would preclude reciprocal connectivity. If there were reciprocal connectivity, such topologies would constitute the exceptions from the rule established. Therefore, I checked if there were reciprocal pairs in my data set and estimated, if the observed connectivity was different from random connectivity.

Indeed, in my data set, I found 7 reciprocal connections out of the 56 pairs recorded from, which corresponded to a probability of one in eight (0.13). To check if this probability was consistent with random connectivity, I did the following estimation. My experience tells that the connectivity between pyramidal cells within a target radius of 20 µM is about 0.25. Given that random connectivity could exist, the respective probability would be $0.25^2 = 0.06$. Based on a χ^2-test, there was no significant difference between the expected and the observed probability ($p_{\chi^2} = 0.16$). Hence, this observation is consistent with random reciprocal connectivity. Given that only a few reciprocal connections existed in the data set, these would unlikely have swayed the rules established.

4.5. Discussion

In this part of my thesis, I have investigated how 5-HT modulated evoked glutamate release in a set of 56 connected cell pairs. These pairs were *post hoc* verified histologically, and confirmed to be pyramidal cells in layer II.

The most surprising finding was that, despite the fact that 10 µM 5-HT increased the rate of spontaneous transmitter release as shown in Part 3, the same concentration consistently depressed the evoked EPSC amplitude by about half in all pairs studied, except one. Consistent with Part 3, though, this depression was also mediated by 5-HT_2R activation.

Subsequent analyses revealed that 5-HT had some "specificity" to its action. Specifically, the postsynaptic cells of connected pairs corresponded to what was described earlier as responders, whereas the presynaptic cells belonged to the group of non-responders. This network specificity was further supported by experimental data showing that, consistent with Part 3, the membrane current noise in the postsynaptic cell, as a proxy for spontaneous release, increased after addition of 5-HT. In addition, I provided direct evidence for this specificity by showing that, after having obtained a cell pair, no increase in the mEPSC frequency was detectable in the presynaptic, but only in the postsynaptic cells.

I then showed that this depression was mostly due to a presynaptic mechanism. When either the Gβγ-binding peptide mSIRK or ct-SNAP-25 was added to the presynaptic patch solution, the depression was abolished, suggesting that the crucial signalling molecule downstream of receptor activation was Gβγ. I propose that the depression seen in this case was most likely caused by Gβγ binding to N- and/or P/Q-type VDCC, thereby limiting the Ca^{2+} influx resulting in a considerable depression of the EPSCs (Ikeda 1996; Trombley 1994). This mechanism is most likely different to the one seen with NA, whereby direct binding of Gβγ to the SNARE complex caused the depression (Yoon et al. 2007). Two lines of evidence for this idea are provided. 1) In contrast to the mechanism seen with noradrenaline (NA), where the recovery rate from short-term depression following a train of 20 APs at 50 Hz was much accelerated, 5-HT failed to speed up this rate. 2) Whilst NA consistently reduced the quantal size in accordance with SNARE inhibition, the quantal size in 5-HT remained unaltered.

4.5.1. Properties of Pyramidal Cell Pairs in Layer II

I recorded from 56 pairs in 15 – 20 day-old rats at physiological temperature. Subsequent histological verification confirmed that the location of pairs was in the layer II, with few were located on the border with layer III. In regard to R_{in}, these cells were not different to those presented in Part 3 (184 ± 10 here *vs.* 187 ± 6 MΩ in Part 3; $p_t = 0.78$).

As the postsynaptic cells were kept in voltage-clamp, the AP parameters were determined for presynaptic cells only, in most cases in the presence of gabazine. When comparisons were made between these average values *vs.* the data from Part 3, I found that there was no difference in either V_{rest} (-75.4 ± 0.5 *vs.* -76.6 ± 0.3 mV; $p_t = 0.06$) or H (73.8 ± 1.2 *vs.* 74.0 ± 0.4 mV; $p_t = 0.90$). There were small but significant differences found for V_{thr} (-43.2 ± 0.8 *vs.* -38.0 ± 0.3 mV; $p_t = 9 \cdot 10^{-8}$) and W (0.9 ± 0.0 *vs.* 1.0 ± 0.0 ms; $p_t = 2 \cdot 10^{-6}$), which may have likely resulted from the presence of gabazine in the ACSF in these pairs. This is because of the fact that there is typically a tonic $GABA_A$ conductance present in these cells (Otis *et al.*, 1991). Because V_m was typically more negative than the chloride equilibrium potential (E_{Cl}) in these cells, there would have been a depolarising current present at rest. The block would have turned this inward current off, which resulted in a hyperpolarisation, causing the small effects seen. Note that in these recordings, I did not correct for the liquid junction potential.

Consequently, and compared to the data presented in Part 3, I am confident that I was unlikely dealing with a biased sample. Therefore, comparisons with other reports from this laboratory are justified (Choy, 2011; Choy *et al.*, 2017a; Choy *et al.*, 2017b).

4.5.2. 5-HT Affects AP and Postsynaptic Properties

The depression observed could have been caused by 5-HT affecting either the AP or the postsynaptic (*i.e*. dendritic) membrane properties. I was able to rule out most such considerations.

4.5.2.1. Modulation of AP

Consistent with the idea put forward in Part 3, most of the effect of 5-HT on the AP very likely reflected the activation of 5-HT_{1A}R and the subsequent activation of GIRK channels by Gβγ (Andrade & Nicoll, 1987; Lüscher *et al.*, 1997). Specifically, this most likely caused the hyperpolarization of V_{rest} by about 2 mV. 5-HT also reduced the amplitude of the APs. Different from the hyperpolarization mentioned above, the mechanism for this decrease was independent of presynaptic Gβγ signalling because it persisted when Gβγ was bound by mSIRK and ct-SNAP-25. A concern might be that this decrease in H might

have been responsible for the EPSC depression. However, as *H* was also reduced in the presence of mSIRK and ct-SNAP-25, when the depression was abolished, this possibility is very unlikely.

4.5.2.2. Modulation of Dendritic Properties

I observed that exposure of 5-HT caused a small reduction in R_{in} in non-responders, but a large one in responders. Consequently, owing to the expression of distinct 5-HTR in the two groups of cells, there is most likely a differential impact on synaptic integration (Kia *et al.*, 1996; Cornea-Hébert *et al.*, 1999). This would mean that the time window of integration in responders is significantly shorter than that in non-responders. This could further be accentuated as it is known that 5-HT_2R activation also inhibits sodium currents and dendritic excitability via a PKC-dependent cascade (Franceschetti *et al.*, 2000; Carr *et al.*, 2002; Carlier *et al.*, 2006). However, nothing is known if this mechanism may be differentially expressed in the two subtypes of pyramidal cells.

Whilst I recorded synaptic currents generated at synapses most likely onto basal dendrites (Feldmeyer *et al.*, 2006), I admit that the recorded currents were subject to space-clamp issues. Therefore, the underlying currents at these synapses were likely much faster and larger (Spruston *et al.*, 1993; Williams & Mitchell, 2008). Or expressed differently, the EPSC decay times most likely were affected by the membrane time constant as is the case of EPSPs. Given that R_{in} decreased considerably upon 5-HT exposure, the EPSC amplitudes, affected by the escape from space-clamp, should have become smaller, and the time constant shorter. Consequently, it could be that some of the depression observed might have been due to the decrease in R_{in}. Whilst I cannot rule out a small contribution of this factor to the overall depression, I think that such a mechanism was unlikely at work here. My main argument is that in this case, a depressed EPSC should have been associated with a faster decay time, something not observed in this data set. Likewise, when the depression was blocked presynaptically by Gβγ-binding peptides, the time courses did not change either, strengthening the idea that the postsynaptic effects on the dendritic membranes were likely minimal. However, given the considerable reduction in R_{in} in responders, it remains surprising that no or minimal changes to the EPSC time courses were detectable. This may well be linked to the co-expression of “opposing” receptors, like 5-HT_1R and 5-HT_2R (Amargós-Bosch *et al.*, 2004) and/or the differential signalling downstream of the respective receptors, which may result in “counter-balancing” the effects on EPSCs.

4.5.3. Network Specificity

The most intriguing finding in this part is that non-responders were congruent with the pre- and responders with the postsynaptic cells. This was surprising, as such a clear distinction was not found with NA (Choy *et al.*, 2017a; Choy *et al.*, 2017b) in the same layer. This might suggest that the effect of 5-HT on the network made up of these cells is likely distinct to that of NA.

This observation was further strengthened by the following additional evidence. First, I provided data confirming that, after addition of 5-HT to the superfusate, the whole-cell recording noise increased in postsynaptic cells. Whilst this was an indirect proxy for the increase in the sEPSC frequency, it was consistent with the idea put forward. More direct support was gained after obtaining a paired recording and then measuring mEPSCs in pre- and postsynaptic cells, respectively. The data provided was consistent with the prediction made; all presynaptic cells were consistent with non-responders, whereas the postsynaptic neurons were mostly responders. One reason that most but not necessarily all postsynaptic neurons fitted this classification was likely linked to the strictness of significance level set for the KS statistic, which, after all, was rather *ad hoc*.

It is important to restate that the specificity of connectivity is not absolute. As alluded above, I found reciprocal connectivity in 7 out of 56. This number is small and may contain a bias. To avoid this, the data from all pairs in layer II obtained in this laboratory over more than 8 years were pooled. In a total set of 306 pairs, 13 reciprocal connections were found; *i.e*. the rate of reciprocal connectivity was 4.3%, smaller than the value in the sample here. This value is very close to that estimated for a random connectivity assuming a connectivity rate of 0.25. This suggests that, besides the specificity observed, random connectivity coexisted. This random connectivity could also underlie the observation, that no depression was found for one EPSC. It is also important to point out that these few reciprocal connections would not have much affected the conclusions reached for responders and non-responders.

A further discussion and a consideration of potential functional implications of this network specificity will be discussed below (see 5.4).

4.5.4. Properties of EPSCs

The amplitudes of the EPSCs evoked during the first minute of recording were in the range from -5.4 to -145.1 pA, with an average of -30.2 ± 3.6 pA, similar to that presented in Choy *et al.* (2017b). Because these data were recorded in voltage-clamp, a direct comparison with a similar data set by Feldmeyer *et al.* (2006), mostly made in current

clamp, is problematic. However, their average EPSC amplitude in the small sample they recorded in voltage-clamp was slightly larger but not significantly different (n = 7; -58 ± 35 *vs.*-30.2 ± 3.6 pA; p_t = 0.27).

I chose voltage-clamp because of the lower noise conditions obtained in this recording mode, compared to that with current clamp amplifiers. Note, however, that I do not claim that the EPSCs were voltage-clamped, as most of them would have been subject to space-clamp escape (Spruston *et al.*, 1993; Williams & Mitchell, 2008) and, therefore, the time courses would have been subject to dendritic filtering. Because of that, in regard to both latency and amplitude, the values were comparable to Feldmeyer *et al.* (2006). But the values for the rise times were much slower in this data set. This is most likely due to the fact that, in order to keep the recording noise to a minimum (important for quantal analysis, see later), no series resistance compensation was made. I do not think that the slightly older age bracket (17 – 23) of animals in Feldmeyer *et al.* (2006) was a significant contributing factor to the differences reported.

I note that in this data set, EPSCs were evoked using a paired-pulse stimulus with an interval of 50 ms repeated every 5 s. PPR in this data set ranged from 0.55 to 1.40, with an average value of 0.83 ± 0.3, comparable to that found by Feldmeyer *et al.* (2006). Overall, the average PPR in this data set was slightly smaller than 1; *i.e*. it was biased towards depression, but variable over a considerable range, with both facilitation as well as depression seen at these synapses.

Classically, the interpretation of PPR relies on the release-dependence of subsequent EPSCs. Specifically, an anti-correlation is expected between the second and the first EPSCs if the depression is due to vesicle depletion. Such correlations were found for EPSCs from pairs in layers IV (Cowan & Stricker, 2004) and V (Fuhrmann *et al.*, 2004). However, in this data set, there was no such correlation; *i.e*. transmitter release was mostly release-independent consistent with the findings in Choy (2011). The mechanisms causing release-independence remained unclear.

4.5.5. 5-HT Quickly Depresses the EPSC Amplitude

In contrast to Part 3, where 5-HT caused a transient increase in the mEPSC frequency, the same neuromodulator caused a fast-onset and large depression of EPSCs by 49 ± 3% in the recorded pairs. Consistent with the ideas by Katz, a potentiation/facilitation would have been expected.

Ever since the first reports of the functional impact of 5-HT on neurons in the central nervous system, it was recognised that it depressed the excitability of some nerve cells

as assayed in single unit recordings (Krnjevic & Phillis, 1963; Wang & Aghajanian, 1977). This is consistent with the data presented here. It is also consistent with studies on its impact on synapses reporting depressions in the spinal cord of lamprey (Buchanan & Grillner, 1991; Takahashi *et al.*, 2001) and rat (Singer *et al.*, 1996), in the brainstem (Umemiya & Berger, 1995), the raphe nucleus itself (Lemos *et al.*, 2006), at the reticulo-geniculate synapse (Chen & Regehr, 2003), in the suprachiasmatic nucleus (Bramley *et al.*, 2005), amygdala (Wang & Aghajanian, 1977), hippocampus (Segal, 1980), cingulate (Tanaka & North, 1993), entorhinal (Schmitz *et al.*, 1998), ventrolateral orbital (Huo *et al.*, 2010), and human prefrontal cortex (Komlosi *et al.*, 2012). However, it is at odds with several reports suggesting a facilitatory contribution to the EPSC (Delaney *et al.*, 1991; Hori *et al.*, 1996; Aghajanian & Marek, 1997; Hasuo *et al.*, 2002; Beique *et al.*, 2007; Austgen *et al.*, 2012; Barre *et al.*, 2016). It needs to be pointed out that in most of the studies mentioned, the receptor types involved were not well characterised. However, the opposing effects seen with 5-HT likely suggest that its action is specific to the cells recorded from and their respective location, the receptors involved (see below), and the downstream signalling targets implicated. From the observations made here, it is therefore most likely inappropriate to generalise to other areas of the brain.

Because this synaptic depression was evident in paired recordings, and since the presynaptic stimulation was restricted to a single axon, it is highly unlikely that activity within a network was generated via second order cells, to the extent that other presynaptic mechanisms would have to be taken into account. I base this statement on the fact that, after stimulating the presynaptic cell, in none of the pairs recorded from, an AP was ever elicited.

Without 5-HT, in most pairs recorded from, a slowly evolving depression of the EPSC was observed during the control period, which after about 10 – 20 minutes had stabilised and reached a constant value. The reason(s) for this depression remain unclear. Feldmeyer *et al.* (2006) mentioned that this depression was avoided by stimulating at a rate of 0.03 – 0.05 Hz. I was unable to confirm this, as a depression remained even at much lower stimulus rates, but admittedly, the rate of depression was much slowed (Li *et al.*, 2010). An interesting clue may be that no depression was seen when the PKC inhibitor Gö 6883 was used in a subset of experiments. This preliminary observation awaits further experimental verification, but may suggest that a critical phosphorylation is most likely involved, which then leads to the slow depression. I don't think that the targets of this phosphorylation are AMPA receptors (Lüscher *et al.*, 1999), as there was no evidence that the quantal size (see below), nor the mEPSC amplitude (Part 3) changed with 5-HT. In addition, it is unlikely that 5-HT_2R were the target either, as the

size of the depression in cells with and without the slow depression was the same and the increase in sEPSC frequency also remained (see below).

It is important to stress that the slow depression was independent of that produced by 5-HT. In my hands, the former typically set in over a time of 10 – 20 minutes, and then persisted for the entire time of the recording, whereas the one by 5-HT was established within 3 – 5 minutes, a time consistent with a complete solution exchange within the chamber used. To make this clear, I showed that even in pairs which had undergone the slow depression, 5-HT still produced a depression together with an increase in the sEPSC frequency. The extent of this depression was no different to that in the set of cells that did not show the slow depression; *i.e*. the two were independent of each other. Both points suggest that the molecular mechanism of the 5-HT-mediated depression is distinct from that of the slow depression.

It is also unlikely, that the EPSC depression was caused by an evolving receptor desensitisation (Roth *et al.*, 1995; Berg *et al.*, 2001). Whilst there are admittedly slight differences between the different types of 5-HT_2R, at 10 µM 5-HT, desensitisation occurs on a time scale of several minutes. In expression systems, after about 5 minutes, desensitisation is ~90%. Consequently, a significant, but not a full desensitisation may likely have occurred during the time of wash-in. However, an increasing depression in the early minutes should have been seen in our recordings, something that was not observed. In addition, the extent of desensitisation at 10 µM 5-HT is about 70% (Berg *et al.*, 2001), much larger than the actual depression observed. Furthermore, the block of PKC (see also below) should have affected the extent of desensitisation (Berg *et al.*, 2001), something that we did not observe either. Whilst I cannot exclude a contribution of desensitisation to the depression observed, I am convinced that at best it was small.

4.5.6. Involvement of 5-HT_2R

My data clearly shows that the depression of EPSCs was mimicked by the pan-5-HT_2R agonist α-methyl-5-HT. This conclusion relies on the fact that the depression evoked by α-methyl-5-HT was not different to the one by 5-HT (p_t = 0.57). This finding is consistent with previous reports (Singer *et al.*, 1996; Komlosi *et al.*, 2012; Nozaki *et al.*, 2016). Given that the depression by α-methyl-5-HT accounted for the full depression, and at the concentration used, does not activate 5-HT_1R, it is unlikely that there was any significant contribution by the latter, something reported in other preparations (Schmitz *et al.*, 1998; Nozaki *et al.*, 2016). Due to time constraints, I was unable to further dissect the pharmacological characteristics of the receptors involved, but it is likely that the same receptors involved in driving spontaneous are also causing the depression of evoked

release. Therefore, the most likely candidate is 5-HT_{2C}R, but admittedly, 5-HT_{2A}R could also participate, as both receptors have been found to be associated with nerve terminals. In addition, the affinity of α-methyl-5-HT is about the same at both receptors (Di Giovanni & De Deurwaerdere, 2016). This idea is consistent with other reports (Abramowski *et al.*, 1995; Willins *et al.*, 1997; Cornea-Hébert *et al.*, 1999; Jansson *et al.*, 2001).

In both parts I have mostly added 10 µM 5-HT to the superfusate. The question arises if this concentration was sufficient to activate 5-HT_2R and cause the depression observed. The affinity of 5-HT at 5-HT_{2A}R and 5-HT_{2C}R as assayed in binding studies using expression systems is 6 and 16 nM, respectively (Knight *et al.*, 2004). It is, however, important to note that the EC_{50} measured *in situ* and in expression systems was much higher, namely about 324 and 51 nM, respectively (Xu & Chuang, 1987; Berg *et al.*, 2001). Consequently, 10 µM is a more than sufficient concentration for receptor activation, consistent with earlier reports also using a similar concentration (Hasuo *et al.*, 2002; Beique *et al.*, 2007). However, it is smaller than others have used (Aghajanian & Marek, 1999; Marek & Aghajanian, 1999).

4.5.7. Downstream Signalling

Downstream of G-protein-coupled receptor activation, Gα and Gβγ are produced. The classical signalling cascade is turned on by either of these, then results in the activation of PLCβ (Day *et al.*, 2002), which then causes the formation of IP_3 and DAG from PIP_2, with IP_3 causing presynaptic store release. Indeed, these steps were verified in Part 3 for miniature transmitter release.

However, similar to NA (Choy *et al.*, 2017b), the depression seen with 5-HT was dependent on Gβγ. When either mSIRK (Goubaeva *et al.*, 2003) or ct-SNAP-25 (Gutierrez *et al.*, 1997) was contained in the presynaptic pipette solution, the EPSC depression was blocked, suggesting that the signalling downstream of 5-HT_2R was independent of the “classical” cascade. In addition to the report mentioned above, Gβγ-dependent EPSC depressions have also been described for 5-HT_1R (Gerachshenko *et al.*, 2005), α_2-ARs (Delaney *et al.*, 2007) and group II metabotropic glutamate receptors (Zhang *et al.*, 2011), which, with the exception of α_1-ARs (Choy *et al.*, 2017b), are all coupled to $G_{i/o}$ proteins.

We chose two different Gβγ-binding peptides as mSIRK is myristoylated and, therefore, membrane permeant. Consequently, a small chance existed that the action of mSIRK was not restricted to the patched presynaptic cell, but could potentially have spread to

nearby terminals. To exclude this possibility, ct-SNAP-25 was chosen, which is a peptide that contains the binding region of Gβγ to SNAP-25 and, therefore, should also bind it. I found that with both peptides, the 5-HT mediated depression was blocked. After re-patching with the solution containing the respective peptide, I waited for at least 20 minutes until data were gathered; in most situations, during the time when the peptide diffused from the tip of the electrode into the cell, the respective control measurements were obtained. Consequently, within this time, the peptides should have well reached the nerve terminals (Pusch & Neher, 1988). I would like to point out that I am not claiming that in the presence of both peptides, the depression was fully blocked, as I admit that some small depression might have persisted but remained undetectable within the statistical comparison. However, even if a small amount remained, it does not detract from the fact that both peptides were able to block most of the depression.

The concentrations used in the patch solution in both cases were ≥ 100 µM. This concentration is higher than the 10 µM typically chosen for mSIRK (Goubaeva *et al.*, 2003). I chose the former concentration to speed-up the diffusion into the nerve terminals, and to be sure that a sufficiently high concentration was reached in the cytosol to efficiently bind most Gβγ. A similar concentration was used by Zhang *et al.* (2011) when mSIRK was extracellularly puffed onto nerve terminals.

The experiments using these two peptides also shed some light on the idea if there is tonic Gβγ production in these nerve terminals. In fact, in some of the recordings, it did look as if after peptide infusion, the EPSCs slowly grew in amplitude. However, this was far from a large effect. Consequently, it may be that Gβγ was produced in the absence of respective receptor activation. Indeed, G-protein signalling without receptor activation has been linked to activators of G-protein signalling (AGS; Blumer *et al.*, 2007) of which there are three different groups (I – III) and about 10 isoforms, some of which are also known as G-protein signalling modulators (GPSM1 – 3). In fact, AGS1 is markedly expressed in prefrontal cortex, and after a single dose of amphetamine upregulated within 3 hours (Schwendt & McGinty, 2010). In addition, AGS3 is also expressed in the prefrontal cortex. It is involved in cocaine craving (Bowers *et al.*, 2004), and upregulated after trauma to the brain (Wang *et al.*, 2013). It is commonly believed that these proteins are likely involved in the fine tuning of synapses (Andreeva *et al.*, 2007; Crawford *et al.*, 2011).

I would also like to point out that the depression was not linked to PKC activation either, as it made no difference to the EPSC depression if PKC was blocked. I tested this because there is some evidence in the literature that PKC activation is linked to 5-HT_{2A}R internalisation (Bhattacharyya *et al.*, 2002; Raote *et al.*, 2013). As a consequence, the

receptor “sensitivity” would decrease and result in either a smaller or even no depression. However, based on the study cited, the time scale of this mechanism is quite slow. Endocytosis was stopped in a ligand-specific manner within 2.5 hours, much slower than the depression observed here.

As Gβγ binding prevented the depression, the important point is what the physiological target(s) downstream of 5-HT_2R activation was/were. So far, two mechanisms have been identified in which Gβγ binds to specific molecular targets that can inhibit transmitter release. The first target is the high voltage-activated Ca^{2+} channels (Trombley, 1994; Ikeda, 1996). According to this mechanism, Gβγ-binding to the Ca_V2 family of channels (Tedford & Zamponi, 2006) in the nerve terminals limits Ca^{2+} influx, and as less becomes available for the activation of the release complex, a depression results. Specifically, the Gβγ-binding site has been identified to be located on the I – II linker region on the N-terminus of the α_1-subunit of VGCC (for review see Tedford & Zamponi, 2006). The other target is SNAP-25. In this case Gβγ directly binds to an element of the SNARE complex, and in doing so, prevents the SNARE zipping to limit vesicle fusion, which also results in depression (Blackmer *et al.*, 2005; Gerachshenko *et al.*, 2005; Yoon *et al.*, 2007). I am not aware of a third target of Gβγ, which resulted in a depression of evoked transmitter release.

Unfortunately, it is not possible to comment on the role of Gβγ and $G\alpha_q$ in the activation of PLCβ1 (Kim *et al.*, 1997). Even though the whole-cell current noise, indicative of an increased rate of sEPSCs, increased in my experiments, the restricted diffusion of the Gβγ-binding peptides into a single axon unlikely filled a sufficiently large number of nerve terminals that a reduction in the sEPSC rate became detectable. I note that such an experiment would be possible with mSIRK as it could be applied to all presynaptic structures via the superfusate. However, it would require quite a considerable amount (and cost) as the target concentration is about 10 µM at a molecular weight of about 2’000 Da.

4.5.8. Comparison with NA

Some experiments where I have used NA in contrast to 5-HT shed some light on the molecular mechanism(s) involved. First, it is important to point out that like 5-HT, NA also increased the mEPSC frequency, but the frequency increase persisted for the remainder of the recording. This is an important point as it renders the possibility very unlikely that the transient nature of the mEPSC frequency increase was a recording artefact (see also Part 3 for a further discussion). In addition, 10 µM NA also caused a large depression of the EPSC. I noted that the depression seen with NA was 62 ± 7, whereas that for 5-HT

was 49 ± 3%. The comparison was very close to be significant (p_t = 0.06), suggesting that the mechanism of the NA-mediated depression may not be identical to that of 5-HT. Second, like with NA, the depression was established largely within the time of a full solution exchange in the recording chamber (3 – 5 minutes). Third, whilst NA could be displaced by competitive antagonists, and α_1-AR agonists could be washed-out, I was not able to satisfactorily wash 5-HT out; *i.e*. even after 1 hour, a considerable depression remained. This observation is most likely linked to the much higher affinity of 5-HT_2R compared to α_1-AR (Xu & Chuang, 1987). Consequently, a much longer unbinding time would be expected. This was also observed by others (Hori *et al.*, 1996). Fourth, when mSIRK was used in the presynaptic patch pipette, the depression was also blocked, suggesting that in both cases Gβγ is the crucial signalling molecule downstream of receptor activation.

In addition, it is important to point out that in contrast to NA, the changes in R_{in} were much more striking. In particular, in non-responders, there was no significant drop in R_{in} with NA, but one with 5-HT (-19 ± 8%), whereas in responders, the drop in NA was much less (-9 ± 7 *vs.* -28 ± 9%). This indicates that in these cells, 5-HT has a much larger effect on postsynaptic membrane conductances than NA. This observation is further supported by the fact that I_{hold} in NA did not change significantly, something that was certainly the case with 5-HT for non-responders but much less so in responders.

4.5.9. Unaltered Recovery from Depression

Normally, the recovery time constant from short-term depression is in the range of about 1 s for neocortical nerve terminals (Markram & Tsodyks, 1996). There are several reports in the literature, in which the recovery from depression was accelerated when Ca^{2+} rose in the respective nerve terminals (Dittman & Regehr, 1998; Wang & Kaczmarek, 1998; Fuhrmann *et al.*, 2004). The point of the experiment in 4.4.4.4 was to gain additional insight into the molecular mechanism downstream of receptor activation, besides that gained by quantal analysis (see below). In the case of Gβγ binding to SNAP-25, the binding to SNARE complex is in competition with Ca^{2+}/synaptotagmin 1, in a Ca^{2+}-dependent way. This means that at a high Ca^{2+} concentration, as after a burst of action potentials at 50 Hz, Gβγ unbinds from SNAP-25 causing a temporary relief from depression. This is then seen as a speed-up of the recovery from depression (Yoon *et al.*, 2007). At the same time, the same Gβγ binding to SNAP-25 also causes a reduction in the quantal size (see below).

Consistent with this idea, in the case of NA, after a burst of 20 APs at 50 Hz, an additional AP elicited after 500 ms caused an EPSC, which was much larger than the first in the

burst. This speed-up in recovery was quantified as R_{50}, where -1 indicates no recovery within the 500 ms, 0 full recovery, and 1 a recovery, which is larger than the amplitude of the first EPSC. In NA, R_{50} was on average 0.51 ± 0.29, clearly indicating an increased recovery. With 5-HT, however, R_{50} was on average 0.07 ± 0.09, not different from zero. Whilst the change in R_{50} from control to NA was significant (p_{pt} = 0.03), in the case of 5-HT it was not (p_{pt} = 0.10). These data then suggest that in the case of 5-HT, the mechanism of depression unlikely involves the binding of Gβγ to the SNARE complex. This is somewhat surprising, as this mechanism was identified in the lamprey spinal cord where 5-HT was acting via 5-HT_1R (Blackmer *et al.*, 2001; Blackmer *et al.*, 2005; Yoon *et al.*, 2007; Gerachshenko *et al.*, 2009; Zurawski *et al.*, 2016).

It is worth pointing out that this idea is representative of most data points in this data set, except one, which may be considered an outlier. However, looking at it with the mechanism for NA in mind, there was clearly a speed-up in recovery, consistent with the idea of Gβγ binding to SNAP-25. This observation, whilst admittedly taken with caution, may suggest that, in the case of 5-HT, the mechanism of depression could potentially vary downstream of receptor activation and, for example, be specific to particular axons, or reflect the proximity of the Gβγ producing receptors to the respective target (see 5.2 for more on this point).

4.5.10. Quantal Properties of EPSC Depression

The point of quantal analysis was to further provide evidence for the molecular mechanism involved in the depression observed. With NA in the superfusate, a consistent and significant reduction in the quantal size by 39 ± 5% was observed, consistent with the idea that Gβγ interacted at the C-terminus of SNAP-25 (Choy *et al.*, 2017b). In support of this idea are studies which also showed that when Gβγ bound to SNAP-25, the quantal size decreased (Photowala *et al.*, 2006). In addition, when this C-terminus region was mutated, the fusion mode was altered (Gil *et al.*, 2002; Fang *et al.*, 2008).

For this study, I successfully performed quantal analyses on data from 14 pairs, of which 6 passed the stringent unimodality tests. This rate is comparable to what was observed in other cortical areas (Stricker *et al.*, 1996a, b; Stricker *et al.*, 1999; Cowan & Stricker, 2004; Choy *et al.*, 2017b). In addition, σ_n (1.2 ± 0.1 *vs.* 0.9 ± 0.1 pA; p_t = 0.15), The average EPSC amplitude (-19.9 ± 0.7 *vs.* -11.2 ± 2.3 pA; p_t = 0.14), the quantal size (-3.9 ± 0.3 *vs.* -2.8 ± 0.1 pA; p_t = 0.10), the quantal content (4.8 ± 0.5 *vs.* 3.8 ± 0.7 pA; p_t = 0.22) and the failure rate (0.12 ± 0.03 *vs.* 0.15 ± 0.05; p_t = 0.32) were comparable to

what was found before (Choy *et al.*, 2017b). Insofar, this limited data set was not different to what was estimated before.

The overall finding was that in contrast to NA, 5-HT did not cause any reduction in quantal size, with the other quantal parameters indistinguishable from those obtained in a previous study (Choy *et al.*, 2017b). This was backed-up by a CV^{-2} analysis, which also indicated that there was mostly a reduction in release probability. Conversely, in the context with 5-HT, the whole depression was solely due to a decrease in quantal content. In addition, based on a χ^2-test, the outcomes in this case were indeed very different to what was observed with NA (6:0 *vs.* 0:9; $p_{\chi^2} = 10^{-4}$).

This outcome is consistent with a presynaptic mechanism of depression as the Gβγ-binding peptides were applied to the presynaptic axon only. In addition, despite the fact that the analysed sample was quite small, the findings using quantal analysis were uniformly similar in all cases. Together with the finding above, that there was also no speed-up in recovery from depression, these data suggest that despite Gβγ being the signalling molecule downstream of $5\text{-}HT_2R$ activation, the molecular target is unlikely SNAP-25 but VDCC.

4.5.11. Molecular Mechanism of Depression

In contrast to the data obtained with NA, and despite the fact that in both cases Gβγ was the relevant signalling molecule downstream of $5\text{-}HT_2R$ activation, I conclude that 5-HT caused the depression without binding to SNAP-25 (Blackmer *et al.*, 2001; Blackmer *et al.*, 2005; Yoon *et al.*, 2007; Wells *et al.*, 2012; Zurawski *et al.*, 2016). In this case, I suggest that Gβγ most likely binds to VDCC of the Ca_V2 family (Tedford & Zamponi, 2006), which contain the P/Q- (2.1, α_{1A}), N- (2.2, α_{1B}), and R-types (2.3, α_{1E}). As a consequence, Ca^{2+} influx into the nerve terminals is inhibited. However, it needs to be pointed out that also a modulation of an alternative channel(s) by Gβγ may be possible.

Ca^{2+} current inhibition has originally been described in dorsal root ganglion cells in the chicken (Dunlap & Fischbach, 1978). Subsequently, it was identified for a number of G-protein-coupled receptors, which typically signal via $G_{i/o}$, like μ-opioid (Bourinet *et al.*, 1996), α_2-adrenergic (Herlitze *et al.*, 1996; Ikeda, 1996), 5-HT1 (Penington *et al.*, 1991; Foehring, 1996), purinergic (Currie & Fox, 1997), dopaminergic (Marchetti *et al.*, 1986; Mirotznik *et al.*, 2000), neuropeptide Y (Plummer *et al.*, 1991), and muscarinic receptors (M1 and M3; Bernheim *et al.*, 1991; but also M2 and M4; Currie & Fox, 1997). For some of the latter, though, the identity of the associated G-protein was not clear at the time of

their writing. It is important to note that the effect of current inhibition seems to be larger for N- than for P/Q-type channels (Tedford & Zamponi, 2006).

Two conceptional mechanisms have been described resulting in Ca^{2+} current inhibition (for review see Shapiro & Gamper, 2009). In fact, the two can co-exist to potently modulate Ca^{2+} channels (Beech *et al.*, 1992). One of them is acting fast (~ 400 ms), the other slower (~ 30 s). Because both times are shorter than the exchange time of 5-HT in my bath, I am unable to distinguish between the two. The first was originally described by Bean (1989) without knowing that it was mediated by Gβγ. He noticed that the current inhibition was voltage-dependent. He correctly identified that the activation curve of the Ca^{2+} channels was shifted to much more positive voltages without actually affecting the maximal flux. He suggested that the channels were in a "willing" mode at rest, but upon exposure to a neuromodulator, changed into a "reluctant" mode, without any effect on the voltage-dependence of inactivation suggesting that the switch between the two modes could occur fast. This model implicated that the G protein binding to the channel was voltage-dependent. Subsequent work confirmed these observations and found that when Gβγ bound to N-type VDCC, the channels switched to the reluctant mode (Boland & Bean, 1993). In addition, the inhibition could be relieved by a large depolarization to +100 mV also known as "pre-pulse facilitation" (Bean, 1989). (Brody & Yue, 2000) used AP waveforms as the voltage-protocols and showed that the voltage-dependent unblock described by Bean with large steps also occurs with these more physiological stimuli. The implication is that the modulation is effective at low rates of stimuli but trains of APs can reverse it. This Ca^{2+} current disinhibition (Brody & Yue, 2000) may be reminiscent of the Ca^{2+}-dependent unbinding of Gβγ from SNAP-25. This "facilitation" was dominant at P/Q-, but close to absent at N-type channels (Rozov *et al.*, 2001). This is consistent with the published data that most of the Ca^{2+} current at synapses in layer II is made up of a large P/Q-current component (Rozov *et al.*, 2001). Given that when 20 APs were evoked at 50 Hz, no facilitaory response was observed suggests that this mechanism may not be operating in these nerve terminals.

The second mechanism consists of a set of processes all linked to signalling cascades around PLC. In contrast to the first, the action on VDCC in this set is voltage-independent. One such mechanism was first characterised for M_1 receptors (Bernheim *et al.*, 1991) and involved a Ca^{2+}-sensitive step in the signalling cascade. It was later found that it was linked to PLCδ and the availability of PIP_2 in the membrane (Gamper *et al.*, 2004) with a reduction resulting in a current inhibition. Another mechanism employs signalling downstream of of PLCβ. In this case, DAG lipase forms arachidonic acid (Irvine, 1982) from DAG, which then inhibits Ca^{2+} channels (Piomelli *et al.*, 1987). Because of the involvement of several enzymes in the cascade, it is not surprising that

this set of mechanisms can take tens of seconds to minutes to take place. Yet another alternative is linked to the fact that some PLCβ isoforms can be activated by Gβγ (see also below), but the required concentrations might be quite high. Downstream signalling, via for example the DAG lipase path, would then result in the Ca^{2+} current depression (Diversé-Pierluissi *et al.*, 1995).

In future experiments, it would be possible to evaluate the extent of the involvement of the two mechanisms. One could block PLC isoforms with edelfosine to prevent downstream signalling associated with the second set of mechanisms. Alternatively, one could attempt to perform large conditioning voltage-steps to +100 mV for several hundred ms followed by evoking an action current at the soma to evoked transmitter release. The idea here is that it may be possible if the nerve terminals are not too remote to mimic “pre-pulse” facilitation (see above).

Based on my dataset, and assuming a Ca^{2+} cooperativity of four (Dodge & Rahamimoff, 1967; Borst & Sakmann, 1996) between EPSC and the Ca^{2+} current, the extent of the AP-associated Ca^{2+} current depression can be estimated to be ~16 ± 1%. This extent should be detectable when doing Ca^{2+} imaging directly from single nerve terminals. Similar measurements have been made (Chen & Regehr, 2003). An extension of this work should attempt to reveal and quantify the Ca^{2+} current depression associated with a single action potential.

It should also be noted that whilst the Ca^{2+} current depression is the most likely explanation for the depression observed, I cannot rule out the possibility that another mechanism may exist which depresses transmitter release downstream of Gβγ. One such mechanism may act via K^+ channels. As indicated above, the family of GIRK channels (K_{IR}) can be activated by Gβγ (Logothetis *et al.*, 1987). Synaptic depression would then be the result of a hyperpolarised nerve terminal, in which the Ca^{2+} influx becomes limited. However, at least in hippocampus, there is little evidence that GIRK channels are involved and cause a synaptic depression (Lüscher *et al.*, 1997). Alternative K^+ channels include $K_v7.4$ (Stott *et al.*, 2015) and TASK-2 channels (Añazco *et al.*, 2013). The latter are of the family of two-pore potassium channels, which contribute to the leak conductance and pH homeostasis. These channels seem to be inhibited by Gβγ (Lüscher *et al.*, 1997), which would result in an increase in input resistance and a depolarisation and may facilitate transmitter release if expressed in nerve terminals. However, the expression of TASK-2 channels is low in the brain (Gabriel *et al.*, 2002), which makes this possibility rather unlikely.

Channels of the family of K_v7 (KCNQ) channels are widely expressed in the brain (for example see Schroeder *et al.*, 2000) and are often associated with the M-current (Brown

& Adams, 1980) setting the excitability in nerve cells. These channels are certainly expressed in myelinated axons in layer V cells (Battefeld *et al.*, 2014) and are activated by Gβγ (Logothetis *et al.*, 1987; Stott *et al.*, 2015) reducing the overall excitability and hyperpolarising the neuron. Indeed, some are expressed on nerve terminals (Huang & Trussell, 2011). When blocked, they increase the postsynaptic current by about 10 – 20% without affecting overall the time course of short-term depression. Conversely, when activated, they should slightly reduce the amplitude of the postsynaptic EPSC, however, unlikely by about 50% as in reported here. Whilst they may contribute to the depression, they are unlikely majorly involved here.

4.5.12. Alternative Targets of Gβγ

I cannot rule out alternative targets that Gβγ may bind to and modulate transmitter release, but perhaps to a lesser extent. As mentioned above, relevant proteins in the presynapse also include phospholipase A (PLA) and PLCβ isoforms. In the case of PLCβ, Gβγ binding activates it, but only at high concentrations (see also discussion in 3.5.8.1).

Another potential target is the plasma membrane Ca^{2+}-ATPase (PMCA) (Lotersztajn *et al.*, 1992). However, it is unlikely that this mechanism is significantly at work here because the PMCA provides typically a continuous, but low transport capacity (Fierro *et al.*, 1998). As a consequence, the increase in transport activity is unlikely to significantly affect the Ca^{2+} concentration in nerve terminals, which renders this possibility unlikely.

It has been reported that IP_3R are also the target of Gβγ modulation. Specifically, Gβγ is capable of activating IP_3R on stores and generate Ca^{2+} oscillations (Zeng *et al.*, 2003). Whilst I cannot rule a small contribution out, it is highly unlikely that this mechanism is majorly at work as increased release from intracellular stores would augment Ca^{2+} in the nerve terminal and facilitate release, which is not consistent with the depression observed.

Gβγ also inhibits phospho-inositide 3-kinase (PI3K; Stephens *et al.*, 1994), the enzyme synthesising phosphatidylinositol (3,4,5)-trisphosphate (PIP_3) from PIP_2, which is the substrate of PLCβ. From a signalling perspective, inhibition of PI3K may lead to accumulation of PIP_2 and in doing so either re-direct more substrate towards PLCβ, and increase the production of IP_3 and therefore, Ca^{2+} release from stores. In addition, the increase in membrane PIP_2 may cause a Ca^{2+} current facilitation. This was not observed. Therefore, this is also an unlikely mechanism.

Likewise, adenylyl cyclase can also be a target of Gβγ, however, the actions are different depending on the isotype. As most types are expressed in the brain (Sadana & Dessauer, 2009), the picture is complex. Whilst isotypes 2, 4 – 7 and 9 are activated, isotypes 1, 3, 8 are inhibited (Tang & Gilman, 1991). The result would be either an in- or decrease in cAMP and associated signalling. As cAMP levels modulate synaptic plasticity (Byrne & Kandel, 1996), the outcomes are not necessarily predictable. I cannot exclude the possibility that such a mechanism may partake in the slow mechanism of Ca^{2+} current inhibition.

5. Overall Discussion and Conclusions

This study focussed on the mechanisms of how 5-HT modulated both spontaneous and evoked transmitter release. The outcomes were contrasted to similar findings made in this laboratory for NA (Choy, 2011; Choy *et al.*, 2017a; Choy *et al.*, 2017b).

5.1. mEPSC Frequency Increase *vs*. EPSC Depression

In Part 3, I reported that the activation of 5-HT_{2C}R by 5-HT resulted in the activation of a classical G_q-mediated signalling cascade, causing the release of Ca^{2+} from presynaptic Ca^{2+} stores, which was seen as an increase in mEPSC frequency. No significant change in its amplitude was observed. However, the increase in mEPSC frequency was transient within the first 5 minutes, and later waned and waxed again. However, when PKC was inhibited using Gö 6983, the mEPSC frequency increase became sustained for the duration of the experiment, suggesting a critical phosphorylation downstream of 5-HT_2R activation.

In contrast, in Part 4, I observed that the activation of 5-HT_2R depressed the evoked EPSCs by 49 ± 3%, however, without any indication of waxing and waning. These two mutually exclusive observations lend further support to the idea that the mechanisms resulting in the transient frequency increase are most likely downstream of the separation of the adaptor G-protein from its receptor and the subsequent dissociation of the Gα subunit from the Gβγ dimer.

The molecular mechanisms involved in both instances, as presented in Parts 3 and 4, are schematically illustrated in Fig. 5.1.1. The case for evoked release is shown on the left, whilst that for spontaneous release on the right. The explanation can be found in the figure legend.

5.2. Comparison with NA

Similar to NA, the frequency of mEPSC increased due to store release. However, with NA, this increase persisted throughout the recording and did not wax and wane. Because both NA and 5-HT activated signalling via the G_q protein, the two outcomes downstream of the same G protein were clearly different. It remains unclear how the specificity downstream of G_q activation was preserved for both cascades. It may well be

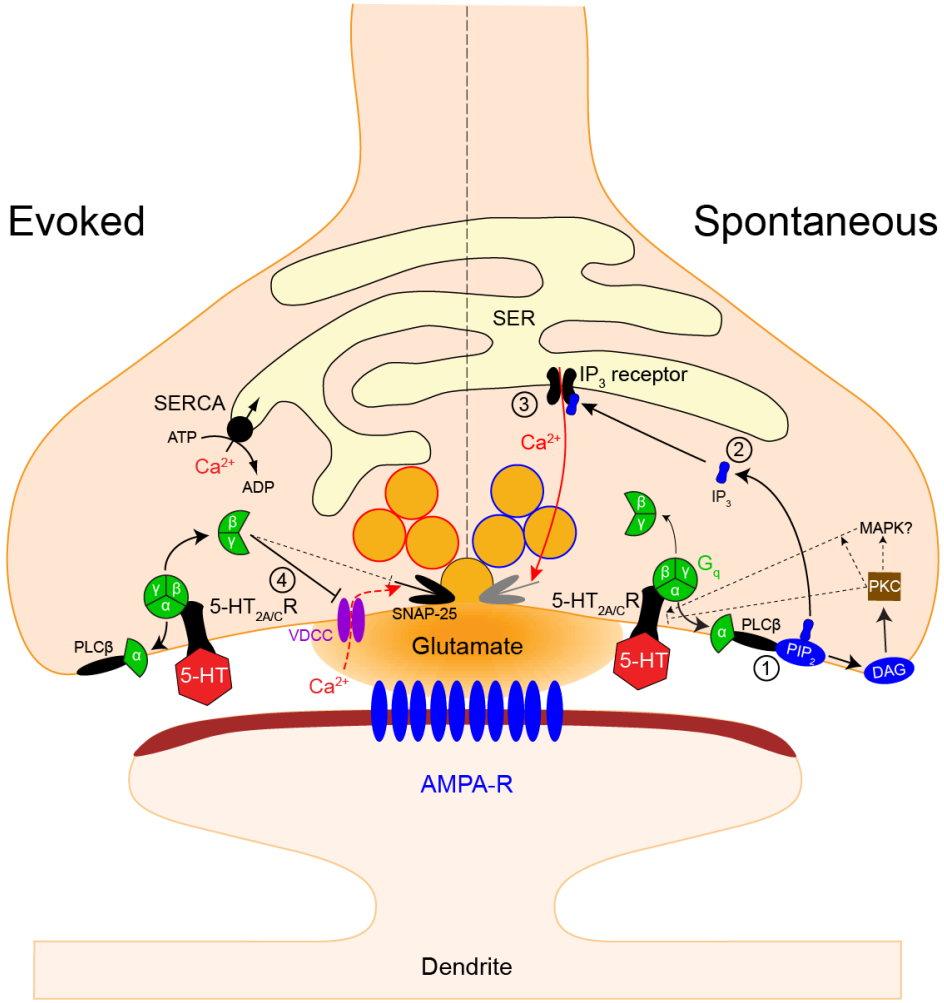

Figure 5.1.1. Modulation of spontaneous and evoked glutamate release.
Mechanisms involved in spontaneous glutamate release (mEPSCs) are shown on the right, whereas those for evoked are on the left. Arrows indicate activation whereas end bars inhibition. **Right**: Upon ligand binding, presynaptic 5-$HT_{2A/C}$R are activated beyond their constitutive activity and initiate the classical G_q-mediated signalling cascade by firstly activating PLCβ (1), which then hydrolyses PIP_2 to produce IP_3 (2) and DAG. The IP_3 binds to IP_3R on presynaptic Ca^{2+} stores, causing store release (3). This Ca^{2+} binds to a Ca^{2+} sensor likely around the SNARE complex (grey), causing increased release of vesicles, observed as an increased mEPSC frequency. The other product, DAG most likely activates PKC to phosphorylate 5-HT_2R and thereby inhibiting their activity (dashed line). Alternatively, and/or additionally, DAG is also capable of activating MAPK and its various elements, the result of which is a further positive feedback onto 5-HT_2R (dashed line with arrow). MAPK activity itself is sensitive to PKC block (dashed). **Left**: In the case of evoked transmitter release, 5-HT also activates presynaptic 5-$HT_{2A/C}$R. Upon activation, the G_q dissociates into Gα and Gβγ subunits, the former most likely activating PLCβ and the latter directly or indirectly inhibiting VDCC (4). This inhibition of Ca^{2+} influx curtails evoked glutamate release, resulting in a large depression in the EPSC amplitude. It may be that in some cases, Gβγ can bind to SNAP-25 to inhibit transmitter release at the level of the SNARE complex (black, dashed).

that this specificity was maintained by other proteins in proximity to the activated receptors; in other words, it may well be that the local biochemical microdomains around the two receptors are different and, consequently, the signalling outcomes become distinct (see also below).

Likewise, evoked transmitter release in both cases was depressed; notably slightly more for NA than 5-HT. Furthermore, in both cases, the depression was sensitive to Gβγ binding peptides. However, it is most likely that the targets of Gβγ in both cases are very different. With NA, the most likely target of Gβγ was at the distal end of SNAP-25. The evidence for this stemmed from two lines of evidence. First, the increased value of R_{50} and second, the reduction in quantal size. Both of these observations are consistent with a target on the distal end of SNAP-25. However, in the case of 5-HT, the target was most likely different, as neither R_{50} nor the quantal size changed. Because the depression was incurred within the presynaptic nerve terminal, where the peptides were applied to, the most parsimonious explanation is that the target is VDCCs. As noted in the discussion in Part 4, I did observe that in at least one case, R_{50} increased, but unfortunately, this case could not be subjected to quantal analysis. Likewise, even in the case with NA, a single case without a speed-up in recovery was seen, potentially suggesting that the molecular target may not be uniformly identical but depend on local factors (proximity).

The fact that with NA, evoked transmitter release depressed but spontaneous increased, and given that SNAP-25 was the target, suggested that there were at least two populations of vesicles in these nerve terminals, as depression was only seen for evoked but not spontaneous release (Choy *et al.*, 2017a; Choy *et al.*, 2017b). However, in the case with 5-HT where the likely target was VDCCs, there is no need to postulate the existence of two vesicle pools, unless there is some weight given to the observation, that in one case R_{50} increased. This is simply because spontaneous release in this case was independent of Ca^{2+} influx via VDCCs (Katz & Miledi, 1963). However, this conclusion does not rule the idea of two pools out either (see two differently outlined vesicle populations in Fig. 5.1.1).

Given that it is very likely that both receptors are expressed on the same nerve terminals (even though I have not studied this aspect directly), an interesting question arises, namely why in the case of 5-HT the target is the VDCCs, whereas with NA, it is SNAP-25? A likely explanation is that there is a difference in the proximity to the target. “Shielding” by (an) adaptor protein(s) may restrict the availability of a potential target. Another possible explanation is that different Gβγ dimers are at play. A similar micro-organisation was found for the case with 5-HT_1R and $GABA_B$R (Hamid *et al.*, 2014), in which the signalling downstream of receptor activation is also driven by Gβγ. Specifically,

in regard to the molecular micro-organisation, this could mean that in the case of 5-HT, VDCCs and 5-HT_2R are very much closer, whereas α_1-AR are in much closer proximity to the SNARE complex. This is something that may be resolved by the FRET interaction (Herrick-Davis *et al.*, 2006) between the receptor and the target, or using single-molecule detection microscopy (for an idea see Saka & Rizzoli, 2012). Alternatively, there is evidence that different types of Gβ and Gγ are expressed in cortex, which may give rise to the formation of different dimer combinations (Betke *et al.*, 2014). Using different purified dimer combinations contained in the presynaptic patch pipette may be able to clarify this idea.

5.3. Constitutive 5-HT_2R Activity

Another feature distinct to that of NA was that there is evidence of constitutive 5-HT_2R activity despite having severed the relevant axons during slicing. With NA, and consistent with an earlier report from this laboratory (Simkus & Stricker, 2002b, a), there was evidence that only PLCβ was tonically active in both instances, a fact reported by others before (Hardie *et al.*, 2004).

The evidence for constitutive 5-HT_2R activity was obtained in a set of experiments, during which 5-$HT_{2A/C}$R antagonists were utilised while recording mEPSCs. When these antagonists were applied to the superfusate, an increase in mEPSC frequency by 23 ± 11% was observed consistent with other reports (De Deurwaerdere *et al.*, 2004; Austgen *et al.*, 2012). It suggests that the 5-HT_2R/signalling cascade was in a desensitised state, which was relieved when exposed to the antagonist. This then resulted in a higher mEPSC frequency. This is most likely the mechanism responsible for the antidepressant activity of some 5-HT_2R antagonists (Di Giovanni & De Deurwaerdere, 2016).

I noted that, within the data set obtained while doing paired recordings, no evidence for constitutive activity was uncovered. The reason for this lack of evidence was because so far, no antagonists were used in this context. In the near future, it would be important to investigate if constitutive activity can also be seen when doing paired recordings. The prediction would be that upon exposure to the antagonists, the EPSCs would become larger by some 20 – 30%. This experiment is important, as it remains unknown if the increase in mEPSCs is downstream of the same subtype of 5-HT_2R as that of the EPSC depression.

5.4. Specificity within Neocortical Networks

One of the most surprising findings in this study was that a simple *ad hoc* classification based on the impact on the mEPSC frequency, as presented in Part 3, had a mirror image in Part 4, where I found that non-responders were typically pre- and responders postsynaptic (Fig. 5.4.1). This idea was further underpinned by the fact that, statistically speaking, the null hypothesis in the case of the presynaptic cells (*i.e*. non-responders) had to be accepted ($p_t > 0.97$); *i.e*. it is with very high confidence that presynaptic cells belonged to the class of non-responders. The case of having to accept the null hypothesis in the context of a *t*-test is rather unusual in biology. This further lends strength to this classification. In hindsight, it is also interesting to point out that, within the confines of this thesis, the significance level chosen for the KS statistic was very likely appropriate.

These novel results are consistent with two earlier studies, which found that the effect of 5-HT was largely restricted to cortical projection neurons (Dembrow *et al.*, 2010; Avesar & Gulledge, 2012). It is important to point out that both of these studies assessed properties that mostly reflected those of the postsynaptic dendrite (Dembrow *et al.*, 2010) and its excitability (Avesar & Gulledge, 2012). This study, though, is different in that the specificity was related to the expression of 5-HTR on notably presynaptic terminals onto these responders (autoreceptors). A similar finding was obtained in prefrontal cortex (Beique *et al.*, 2007). Whilst I cannot exclude the possibility that most of these nerve terminals were associated with pyramidal cells that would predominantly project outside of the cortex, as suggested by the two studies cited, it is unlikely to be the case here for the following three reasons. First, I did find reciprocal connections (7 out of 56 pairs), which, by itself, challenges the conception of specific wiring beyond that of randomness (for a more detailed discussion see below). Second, given that the sEPSC rate in these cells (52 ± 6 Hz), and its increase by 5-HT (28 ± 8 %) was sizeable, a considerable number of nerve terminals expressing 5-HT_2R must exist in this layer, which is unlikely made up from axon collaterals of projection neurons only. And, third, using immuno-histochemistry (data obtained for a different project by Le-Thuy-Van Tran in the laboratory), after randomly filling pyramidal cells in this layer for this part, we did not observe that some axons were devoid of 5-HT_2R expression as implicated by the specific wiring idea; *i.e*. in all cells imaged, 5-HT_2R were expressed along the axon.

All three considerations suggest that the presynaptic nerve terminals when making contact to a responder were appropriately “matched” to operate as a single entity (Fig.

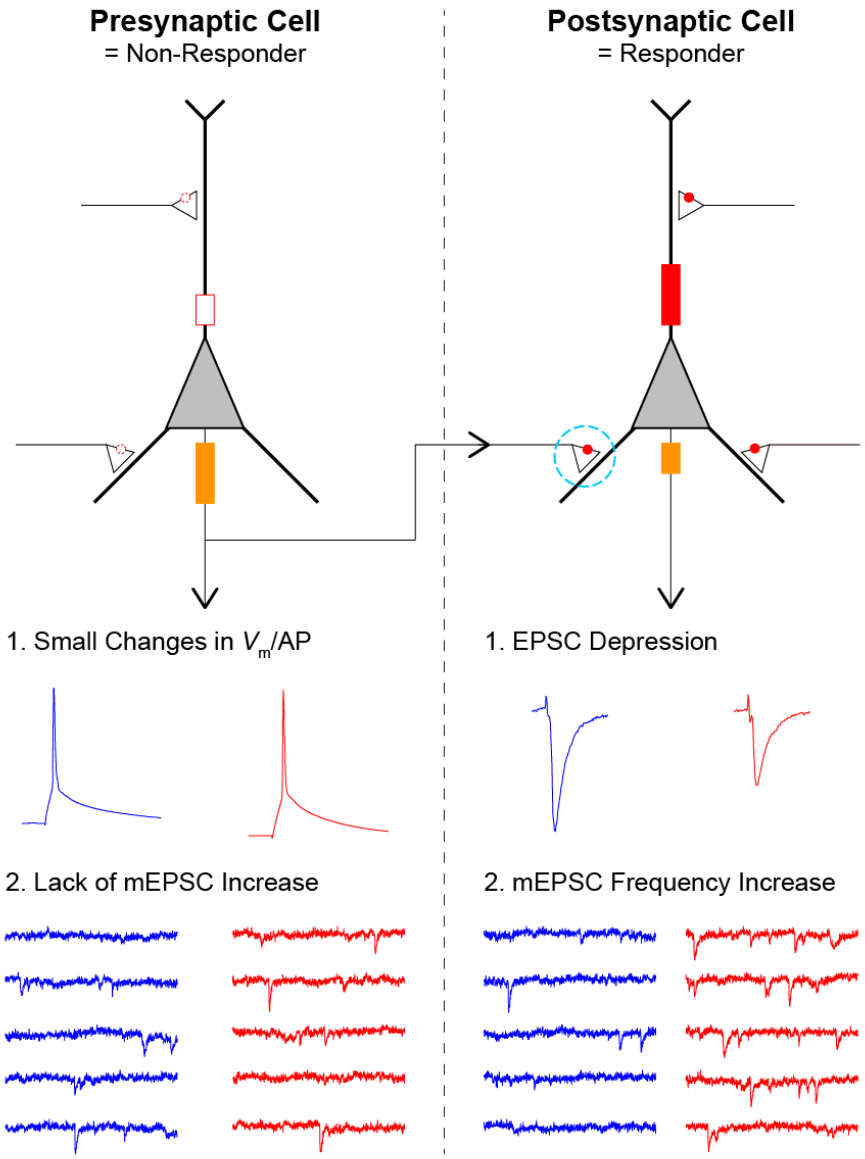

Figure 5.4.1. Network specificity and impact on glutamate release.

In a cell pair (typical one-way connectivity), non-responders are very likely presynaptic (blue for control). These express a large (axonal) conductance activated by 5-HT_1R (orange), and send axonal projections expressing 5-HT_2R (red dot) to form synapses with postsynaptic cells. These are the responders, which also express a larger number of dendritic 5-HT_2R (filled red rectangle) than non-responders. At such a connection, in presynaptic cells, 5-HT (red) caused an insignificant increase in mEPSC frequency with small changes to the AP, together with a large hyperpolarization. Conversely, in postsynaptic cells, there were concomitant transient increases in mEPSC frequency together with a large EPSC depression, associated with a large reduction in R_{in}, but a small hyperpolarization. Consequently, signal transmission is weakened because of EPSC depression on an increased background noise caused by s/mEPSCs.

5.4.1); *i.e*. both the pre- and the postsynaptic cells responded simultaneously to 5-HT via 5-HT_2R. The idea of matching pre- with postsynaptic properties has gained little attention in the literature (Mohan *et al.*, 2013) outside the conception of homeostatic plasticity (Turrigiano *et al.*, 1998). It may suggest that the postsynaptic element determines the presynaptic characteristics via some form of retrograde message (target specificity; see also Scanziani *et al.*, 1996; Reyes *et al.*, 1998; Mohrmann *et al.*, 1999; Schinder *et al.*, 2000; Toth & McBain, 2000; Harney & Jones, 2002; Cowan & Stricker, 2004; Dugue *et al.*, 2005; Koester & Johnston, 2005; Buchanan *et al.*, 2012; Rubio *et al.*, 2014). Except in the case of synaptic plasticity, the nature of this retrograde message remains elusive, but likely mediators are Eph receptors together with their ephrin ligands, and cell surface proteins like *N*-cadherin, sidekicks, flamingo, SYG-1 and 2 (Shen, 2004).

The fact that, based on immunohistochemistry (see above), all axons labelled with biocytin also expressed 5-HT_2R, suggests that the receptors were present on most nerve terminals in layer II. However, their functional state differed; *i.e*. onto non-responders, the receptors are likely silenced (open circles on nerve terminals in Fig. 5.4.1) or non-responsive. It is unclear if in the first case, the respective receptors like AMPAR remained in endosomal vesicles, ready to be inserted (Hayashi *et al.*, 2000), or, in the second case the receptors were in the membrane, but required for their activation, for example, phosphorylation (Sheffler *et al.*, 2006; Strachan *et al.*, 2009; Strachan *et al.*, 2010), or another post-translational modification, which rendered them unresponsive.

5.5. Systems Impact of Serotonergic Modulation

These data suggest that in specific neocortical networks, increased activity in the raphe nuclei could cause a large depression of sensory input and/or local recurrent excitation, resulting in depressed EPSCs, and consequently reduced firing. Accordingly, firing may become restricted to connections with initially large EPSCs and thereby, “sharpening” of the respective receptive fields may occur as other connections “drop out” (Williams *et al.*, 2002; Lottem *et al.*, 2016). However, at the same time, the same 5-HT also transiently increased spontaneous transmitter release via store activation, which was seen as noise (Fig. 5.4.1). Under conditions where the EPSC is depressed on an increased background “noise”, spike de-correlations may occur, which have been reported in this context (Favero *et al.*, 2012; Castro-Alamancos & Gulati, 2014; Kapoor *et al.*, 2016).

However, I am unsure about the impact and value of a waxing and waning background noise, as it may not be relevant for sensory processing (too slow). I note that this observation was obtained under pharmacological conditions, *i.e*. after exposure to 10 µM 5-HT. This concentration is likely very much higher than that under physiological

conditions, where, using microdialysis, it was estimated that 5-HT rose by a factor of about two to ~15 nM (Fujino *et al.*, 2002). The concentration used in my experiments may have forced 5-HT_2R into a desensitised and altered state, which may have caused the waxing and waning.

5.6. Relevance to Disease

The 5-HT-mediated EPSC depression could result in a dampening of cortical "excitability" when predominantly driven by synapses. This has indeed been reported (Buchanan *et al.*, 2014). Or alternatively, neocortical excitability increased when 5-HT_2R were knocked-out (Tecott *et al.*, 1995) or dysfunctional (Bagdy *et al.*, 2007). In addition, 5-HT has been found to reduce the incidence of absence seizures (Ohno *et al.*, 2010; for review see Guiard & Di Giovanni, 2015). In fact, it has been known for 60 years, that the antiepileptic drug phenytoin augments the 5-HT concentration in brain tissue (Bonnycastle *et al.*, 1957). Admittedly, in this generalisation, the molecular actions are likely highly diverse, with both direct actions on glutamatergic and GABAergic transmission reported as well as direct effects on membrane conductances (Carr *et al.*, 2002).

With epidemiological data suggesting a correlation between epilepsy and depression, and, conversely, depression also linked to some forms of epilepsy (Kanner, 2003; Di Giovanni *et al.*, 2016; Palacios *et al.*, 2017), it is well established that depression is typically linked to a hypofunction of the serotonergic system (Pytliak *et al.*, 2011; Lutz, 2013; Olivier, 2015; Chagraoui *et al.*, 2016). Therapeutically, selective serotonin re-uptake inhibitors (SSRI) are among the drugs used to treat patients suffering from this disease. These compounds augment the 5-HT concentration in brain tissue by blocking the respective re-uptake into glia and neurons. It may well be that one of the major actions in this regard rests upon the ability of 5-HT_2R to transactivate, *i.e*. mimic the action of some neurotrophins (Tsuchioka *et al.*, 2008; Kruk *et al.*, 2015).

Furthermore, it has been reported that decreased serotonergic activity is a key player in β-amyloid oligomer-induced depressive-like behaviour in mice, a model of Alzheimer disease (Ledo *et al.*, 2016). In addition, the same disease is linked to increased Ca^{2+} store content (Berridge, 2010), which may well alter the extent of the transient mEPSC frequency increase, but more importantly, the activation of the β-secretase (Green *et al.*, 2008; for review see Green & LaFerla, 2008) and in doing so, accelerate the accumulation and toxicity of β-amyloid oligomers in the extracellular space. A detailed understanding of store involvement may provide crucial insights into the pathophysiology and potential drug targets in Alzheimer disease.

Beyond the classical understanding of dimerization of 5-HT_2R, these receptors are involved in signalling via forming heterodimers beyond the same class of receptors. For example, heterodimeric receptors are involved in weight control (Tecott *et al.*, 1995; Yadav *et al.*, 2009; Schellekens *et al.*, 2013; Schellekens *et al.*, 2015), motor function (Albizu *et al.*, 2011; Lukasiewicz *et al.*, 2011), mood disorder (Kamal *et al.*, 2015), and psychotic disease (Gonzalez-Maeso *et al.*, 2008; Moreno *et al.*, 2012). Consequently, a vast complexity exists in association with 5-HT_2R, which is just beginning to be recognized and their clinical implications appreciated. A lot more knowledge needs to be generated until a full picture emerges of how 5-HT alters various properties and functions of neocortical microcircuits (Douglas & Martin, 1991; Földy *et al.*, 2005; Grillner *et al.*, 2005).

6. References

Abdi H. (2007). Bonferonni and Sidăk corrections for multiple comparisons. *In Neil Salkind (Ed) Encyclopedia of Measurement and Statistics* 103-107.

Abramowski D, Rigo M, Duc D, Hoyer D & Staufenbiel M. (1995). Localization of the 5-hydroxytryptamine$_{2C}$ receptor protein in human and rat brain using specific antisera. *Neuropharmacology* **34,** 1635-1645.

Acuna-Castillo C, Villalobos C, Moya PR, Saez P, Cassels BK & Huidobro-Toro JP. (2002). Differences in potency and efficacy of a series of phenylisopropylamine/phenylethylamine pairs at 5-HT$_{2A}$ and 5-HT$_{2C}$ receptors. *Br J Pharmacol* **136,** 510-519.

Adams JP & Sweatt JD. (2002). Molecular psychology: roles for the ERK MAP kinase cascade in memory. *Annu Rev Pharmacol Toxicol* **42,** 135-163.

Aghajanian GK & Marek GJ. (1997). Serotonin induces excitatory postsynaptic potentials in apical dendrites of neocortical pyramidal cells. *Neuropharmacology* **36,** 589-599.

Aghajanian GK & Marek GJ. (1999). Serotonin, via 5-HT$_{2A}$ receptors, increases EPSCs in layer V pyramidal cells of prefrontal cortex by an asynchronous mode of glutamate release. *Brain Res* **825,** 161-171.

Alberini CM, Ghirardi M, Metz R & Kandel ER. (1994). C/EBP is an immediate-early gene required for the consolidation of long-term facilitation in *Aplysia*. *Cell* **76,** 1099-1114.

Albizu L, Holloway T, Gonzalez-Maeso J & Sealfon SC. (2011). Functional crosstalk and heteromerization of serotonin 5-HT$_{2A}$ and dopamine D$_2$ receptors. *Neuropharmacology* **61,** 770-777.

Amargós-Bosch M, Bortolozzi A, Puig MV, Serrats J, Adell A, Celada P, Toth M, Mengod G & Artigas F. (2004). Co-expression and *in vivo* interaction of serotonin$_{1A}$ and serotonin$_{2A}$ receptors in pyramidal neurons of prefrontal cortex. *Cereb Cortex* **14,** 281-299.

Añazco C, Peña-Münzenmayer G, Araya C, Cid LP, Sepúlveda FV & Niemeyer MI. (2013). G protein modulation of K2P potassium channel TASK-2 : a role of basic residues in the C terminus domain. *Pflugers Arch* **465,** 1715-1726.

Andrade R, Malenka RC & Nicoll RA. (1986). A G protein couples serotonin and GABA$_B$ receptors to the same channels in hippocampus. *Science* **234,** 1261-1265.

Andrade R & Nicoll RA. (1987). Pharmacologically distinct actions of serotonin on single pyramidal neurones of the rat hippocampus recorded in vitro. *J Physiol* **394,** 99-124.

Andreae LC, Fredj NB & Burrone J. (2012). Independent vesicle pools underlie different modes of release during neuronal development. *J Neurosci* **32,** 1867-1874.

Andreeva AV, Kutuzov MA & Voyno-Yasenetskaya TA. (2007). Scaffolding proteins in G-protein signaling. *J Mol Signal* **2,** 13.

Apostolides PF & Trussell LO. (2013). Regulation of interneuron excitability by gap junction coupling with principal cells. *Nat Neurosci* **16,** 1764-1772.

Arac D, Chen X, Khant HA, Ubach J, Ludtke SJ, Kikkawa M, Johnson AE, Chiu W, Sudhof TC & Rizo J. (2006). Close membrane-membrane proximity induced by Ca^{2+}-dependent multivalent binding of synaptotagmin-1 to phospholipids. *Nat Struct Mol Biol* **13,** 209-217.

Araneda R & Andrade R. (1991). 5-Hydroxytryptamine$_2$ and 5-hydroxytryptamine$_{1A}$ receptors mediate opposing responses on membrane excitability in rat association cortex. *Neuroscience* **40,** 399-412.

Araque A, Sanzgiri RP, Parpura V & Haydon PG. (1998). Calcium elevation in astrocytes causes an NMDA receptor-dependent increase in the frequency of miniature synaptic currents in cultured hippocampal neurons. *J Neurosci* **18,** 6822-6829.

Artigas F. (2013). Serotonin receptors involved in antidepressant effects. *Pharmacol Ther* **137,** 119-131.

Arvanov VL, Liang X, Magro P, Roberts R & Wang RY. (1999). A pre- and postsynaptic modulatory action of 5-HT and the 5-HT$_{2A, 2C}$ receptor agonist DOB on NMDA-evoked responses in the rat medial prefrontal cortex. *Eur J Neurosci* **11,** 2917-2934.

Austgen JR, Dantzler HA, Barger BK & Kline DD. (2012). 5-hydroxytryptamine 2C receptors tonically augment synaptic currents in the nucleus tractus solitarii. *J Neurophysiol* **108,** 2292-2305.

Avesar D & Gulledge AT. (2012). Selective serotonergic excitation of callosal projection neurons. *Front Neural Circuits* **6,** 12.

Azmitia EC, Gannon PJ, Kheck NM & Whitaker-Azmitia PM. (1996). Cellular localization of the 5-HT$_{1A}$ receptor in primate brain neurons and glial cells. *Neuropsychopharmacology* **14,** 35-46.

Bagdy G, Kecskemeti V, Riba P & Jakus R. (2007). Serotonin and epilepsy. *J Neurochem* **100,** 857-873.

Bai D, del Corsso C, Srinivas M & Spray DC. (2006). Block of specific gap junction channel subtypes by 2-aminoethoxydiphenyl borate (2-APB). *J Pharmacol Exp Ther* **319,** 1452-1458.

Bai F, Yin T, Johnstone EM, Su C, Varga G, Little SP & Nelson DL. (2004). Molecular cloning and pharmacological characterization of the guinea pig 5-HT$_{1E}$ receptor. *Eur J Pharmacol* **484,** 127-139.

Bal M, Leitz J, Reese AL, Ramirez DM, Durakoglugil M, Herz J, Monteggia LM & Kavalali ET. (2013). Reelin mobilizes a VAMP7-dependent synaptic vesicle pool and selectively augments spontaneous neurotransmission. *Neuron* **80,** 934-946.

Barker EL, Westphal RS, Schmidt D & Sanders-Bush E. (1994). Constitutively active 5-hydroxytryptamine$_{2C}$ receptors reveal novel inverse agonist activity of receptor ligands. *J Biol Chem* **269,** 11687-11690.

Barnes NM, Hales TG, Lummis SC & Peters JA. (2009). The 5-HT$_3$ receptor--the relationship between structure and function. *Neuropharmacology* **56,** 273-284.

Barnes NM & Sharp T. (1999). A review of central 5-HT receptors and their function. *Neuropharmacology* **38,** 1083-1152.

Barre A, Berthoux C, De Bundel D, Valjent E, Bockaert J, Marin P & Becamel C. (2016). Presynaptic serotonin 2A receptors modulate thalamocortical plasticity and associative learning. *Proc Natl Acad Sci U S A* **113,** E1382-1391.

Barry PH. (1994). JPCalc, a software package for calculating liquid junction potential corrections in patch-clamp, intracellular, epithelial and bilayer measurements and for correcting junction potential measurements. *J Neurosci Methods* **51,** 107-116.

Battefeld A, Tran BT, Gavrilis J, Cooper EC & Kole MH. (2014). Heteromeric K_V7.2/7.3 channels differentially regulate action potential initiation and conduction in neocortical myelinated axons. *J Neurosci* **34,** 3719-3732.

Baxter G, Kennett G, Blaney F & Blackburn T. (1995). 5-HT$_2$ receptor subtypes: a family re-united? *Trends Pharmacol Sci* **16,** 105-110.

Bean BP. (1989). Neurotransmitter inhibition of neuronal calcium currents by changes in channel voltage dependence. *Nature* **340,** 153-156.

Beck SG, Pan YZ, Akanwa AC & Kirby LG. (2004). Median and dorsal raphe neurons are not electrophysiologically identical. *J Neurophysiol* **91,** 994-1005.

Beech DJ, Bernheim L & Hille B. (1992). Pertussis toxin and voltage dependence distinguish multiple pathways modulating calcium channels of rat sympathetic neurons. *Neuron* **8,** 97-106.

Beique JC, Campbell B, Perring P, Hamblin MW, Walker P, Mladenovic L & Andrade R. (2004a). Serotonergic regulation of membrane potential in developing rat prefrontal cortex: coordinated expression of 5-hydroxytryptamine (5-HT)$_{1A}$, 5-HT$_{2A}$, and 5-HT$_7$ receptors. *J Neurosci* **24,** 4807-4817.

Beique JC, Chapin-Penick EM, Mladenovic L & Andrade R. (2004b). Serotonergic facilitation of synaptic activity in the developing rat prefrontal cortex. *J Physiol* **556,** 739-754.

Beique JC, Imad M, Mladenovic L, Gingrich JA & Andrade R. (2007). Mechanism of the 5-hydroxytryptamine 2A receptor-mediated facilitation of synaptic activity in prefrontal cortex. *Proc Natl Acad Sci U S A* **104,** 9870-9875.

Bekkers JM & Stevens CF. (1990). Presynaptic mechanism for long-term potentiation in the hippocampus. *Nature* **346,** 724-729.

Bennett MV & Zukin RS. (2004). Electrical coupling and neuronal synchronization in the Mammalian brain. *Neuron* **41,** 495-511.

Berendse HW & Groenewegen HJ. (1991). Restricted cortical termination fields of the midline and intralaminar thalamic nuclei in the rat. *Neuroscience* **42,** 73-102.

Berg KA, Harvey JA, Spampinato U & Clarke WP. (2005). Physiological relevance of constitutive activity of 5-HT_{2A} and 5-HT_{2C} receptors. *Trends Pharmacol Sci* **26,** 625-630.

Berg KA, Maayani S, Goldfarb J, Scaramellini C, Leff P & Clarke WP. (1998). Effector pathway-dependent relative efficacy at serotonin type 2A and 2C receptors: evidence for agonist-directed trafficking of receptor stimulus. *Mol Pharmacol* **54,** 94-104.

Berg KA, Stout BD, Maayani S & Clarke WP. (2001). Differences in rapid desensitization of 5-hydroxytryptamine$_{2A}$ and 5-hydroxytryptamine$_{2C}$ receptor-mediated phospholipase C activation. *J Pharmacol Exp Ther* **299,** 593-602.

Berger M, Gray JA & Roth BL. (2009). The expanded biology of serotonin. *Annu Rev Med* **60,** 355-366.

Berman RM, Fava M, Thase ME, Trivedi MH, Swanink R, McQuade RD, Carson WH, Adson D, Taylor L, Hazel J & Marcus RN. (2009). Aripiprazole augmentation in major depressive disorder: a double-blind, placebo-controlled study in patients with inadequate response to antidepressants. *CNS Spectr* **14,** 197-206.

Bernheim L, Beech DJ & Hille B. (1991). A diffusible second messenger mediates one of the pathways coupling receptors to calcium channels in rat sympathetic neurons. *Neuron* **6,** 859-867.

Berridge MJ. (1987). Inositol trisphosphate and diacylglycerol: two interacting second messengers. *Annu Rev Biochem* **56,** 159-193.

Berridge MJ. (2010). Calcium hypothesis of Alzheimer's disease. *Pflugers Arch* **459,** 441-449.

Berridge MJ & Irvine RF. (1984). Inositol trisphosphate, a novel second messenger in cellular signal transduction. *Nature* **312,** 315-321.

Betke KM, Rose KL, Friedman DB, Baucum AJ, 2nd, Hyde K, Schey KL & Hamm HE. (2014). Differential localization of G protein *βγ* subunits. *Biochemistry* **53,** 2329-2343.

Betke KM, Wells CA & Hamm HE. (2012). GPCR mediated regulation of synaptic transmission. *Prog Neurobiol* **96,** 304-321.

Bettler B, Boulter J, Hermans-Borgmeyer I, O'Shea-Greenfield A, Deneris ES, Moll C, Borgmeyer U, Hollmann M & Heinemann S. (1990). Cloning of a novel glutamate receptor subunit, GluR5: expression in the nervous system during development. *Neuron* **5,** 583-595.

Bhattacharyya S, Puri S, Miledi R & Panicker MM. (2002). Internalization and recycling of 5-HT_{2A} receptors activated by serotonin and protein kinase C-mediated mechanisms. *Proc Natl Acad Sci U S A* **99,** 14470-14475.

Bienenstock EL, Cooper LN & Munro PW. (1982). Theory for the development of neuron selectivity: orientation specificity and binocular interaction in visual cortex. *J Neurosci* **2,** 32-48.

Bilmen JG, Wootton LL, Godfrey RE, Smart OS & Michelangeli F. (2002). Inhibition of SERCA Ca^{2+} pumps by 2-aminoethoxydiphenyl borate (2-APB). 2-APB reduces both Ca^{2+} binding and phosphoryl transfer from ATP, by interfering with the pathway leading to the Ca^{2+}-binding sites. *Eur J Biochem* **269,** 3678-3687.

Birdwell JA, Solomon JH, Thajchayapong M, Taylor MA, Cheely M, Towal RB, Conradt J & Hartmann MJ. (2007). Biomechanical models for radial distance determination by the rat vibrissal system. *J Neurophysiol* **98,** 2439-2455.

Blackmer T, Larsen EC, Bartleson C, Kowalchyk JA, Yoon EJ, Preininger AM, Alford S, Hamm HE & Martin TF. (2005). G protein βγ directly regulates SNARE protein fusion machinery for secretory granule exocytosis. *Nat Neurosci* **8,** 421-425.

Blackmer T, Larsen EC, Takahashi M, Martin TF, Alford S & Hamm HE. (2001). G protein βγ subunit-mediated presynaptic inhibition: regulation of exocytotic fusion downstream of Ca^{2+} entry. *Science* **292,** 293-297.

Blakely RD, De Felice LJ & Hartzell HC. (1994). Molecular physiology of norepinephrine and serotonin transporters. *J Exp Biol* **196,** 263-281.

Blumer JB, Smrcka AV & Lanier SM. (2007). Mechanistic pathways and biological roles for receptor-independent activators of G-protein signaling. *Pharmacol Ther* **113,** 488-506.

Boddeke HW, Hoffman BJ, Palacios JM & Hoyer D. (1993). Calcineurin inhibits desensitization of cloned rat 5-HT_{1C} receptors. *Naunyn Schmiedebergs Arch Pharmacol* **348,** 221-224.

Boehm S. (1999). Presynaptic α_2-adrenoceptors control excitatory, but not inhibitory, transmission at rat hippocampal synapses. *J Physiol* **519 Pt 2,** 439-449.

Boland LM & Bean BP. (1993). Modulation of N-type calcium channels in bullfrog sympathetic neurons by luteinizing hormone-releasing hormone: kinetics and voltage dependence. *J Neurosci* **13,** 516-533.

Bonaventure P, Hall H, Gommeren W, Cras P, Langlois X, Jurzak M & Leysen JE. (2000). Mapping of serotonin 5-HT_4 receptor mRNA and ligand binding sites in the post-mortem human brain. *Synapse* **36,** 35-46.

Bonhaus DW, Weinhardt KK, Taylor M, DeSouza A, McNeeley PM, Szczepanski K, Fontana DJ, Trinh J, Rocha CL, Dawson MW, Flippin LA & Eglen RM. (1997). RS-102221: a novel high affinity and selective, 5-HT_{2C} receptor antagonist. *Neuropharmacology* **36,** 621-629.

Bonisch H & Bruss M. (2006). The norepinephrine transporter in physiology and disease. *Handb Exp Pharmacol***,** 485-524.

Bonnycastle DD, Giarman NJ & Paasonen MK. (1957). Anticonvulsant compounds and 5-hydroxytryptamine in rat brain. *Br J Pharmacol Chemother* **12,** 228-231.

Borst JG & Sakmann B. (1996). Calcium influx and transmitter release in a fast CNS synapse. *Nature* **383,** 431-434.

Bourinet E, Soong TW, Stea A & Snutch TP. (1996). Determinants of the G protein-dependent opioid modulation of neuronal calcium channels. *Proc Natl Acad Sci U S A* **93,** 1486-1491.

Bowers MS, McFarland K, Lake RW, Peterson YK, Lapish CC, Gregory ML, Lanier SM & Kalivas PW. (2004). Activator of G protein signaling 3: a gatekeeper of cocaine sensitization and drug seeking. *Neuron* **42,** 269-281.

Bowie D & Lange GD. (2002). Functional stoichiometry of glutamate receptor desensitization. *J Neurosci* **22,** 3392-3403.

Bowker RM. (1986). Serotonergic and peptidergic inputs to the primate ventral spinal cord as visualized with multiple chromagens on the same tissue section. *Brain Res* **375,** 345-350.

Bowker RM, Westlund KN, Sullivan MC & Coulter JD. (1982). Organization of descending serotonergic projections to the spinal cord. *Prog Brain Res* **57,** 239-265.

Bramley JR, Sollars PJ, Pickard GE & Dudek FE. (2005). 5-HT_{1B} receptor-mediated presynaptic inhibition of GABA release in the suprachiasmatic nucleus. *J Neurophysiol* **93,** 3157-3164.

Brock LG, Coombs JS & Eccles JC. (1952). The recording of potentials from motoneurones with an intracellular electrode. *J Physiol* **117,** 431-460.

Brody DL & Yue DT. (2000). Relief of G-protein inhibition of calcium channels and short-term synaptic facilitation in cultured hippocampal neurons. *J Neurosci* **20,** 889-898.

Bronk P, Deak F, Wilson MC, Liu X, Sudhof TC & Kavalali ET. (2007). Differential effects of SNAP-25 deletion on Ca^{2+} -dependent and Ca^{2+} -independent neurotransmission. *J Neurophysiol* **98,** 794-806.

Brown DA & Adams PR. (1980). Muscarinic suppression of a novel voltage-sensitive K^+ current in a vertebrate neurone. *Nature* **283,** 673-676.

Brown TH, Wong RK & Prince DA. (1979). Spontaneous miniature synaptic potentials in hippocampal neurons. *Brain Res* **177,** 194-199.

Bruinvels AT, Palacios JM & Hoyer D. (1993). Autoradiographic characterisation and localisation of 5-HT_{1D} compared to 5-HT_{1B} binding sites in rat brain. *Naunyn Schmiedebergs Arch Pharmacol* **347,** 569-582.

Brunger AT. (2005). Structure and function of SNARE and SNARE-interacting proteins. *Q Rev Biophys* **38,** 1-47.

Buchanan GF, Murray NM, Hajek MA & Richerson GB. (2014). Serotonin neurones have anti-convulsant effects and reduce seizure-induced mortality. *J Physiol* **592,** 4395-4410.

Buchanan JT & Grillner S. (1991). 5-Hydroxytryptamine depresses reticulospinal excitatory postsynaptic potentials in motoneurons of the lamprey. *Neurosci Lett* **122,** 71-44.

Buchanan KA, Blackman AV, Moreau AW, Elgar D, Costa RP, Lalanne T, Tudor Jones AA, Oyrer J & Sjostrom PJ. (2012). Target-specific expression of presynaptic NMDA receptors in neocortical microcircuits. *Neuron* **75,** 451-466.

Buhl DL, Harris KD, Hormuzdi SG, Monyer H & Buzsaki G. (2003). Selective impairment of hippocampal gamma oscillations in connexin-36 knock-out mouse *in vivo*. *J Neurosci* **23,** 1013-1018.

Bylund DB, Eikenberg DC, Hieble JP, Langer SZ, Lefkowitz RJ, Minneman KP, Molinoff PB, Ruffolo RR, Jr. & Trendelenburg U. (1994). International Union of Pharmacology nomenclature of adrenoceptors. *Pharmacol Rev* **46,** 121-136.

Byrne JH & Kandel ER. (1996). Presynaptic facilitation revisited: state and time dependence. *J Neurosci* **16,** 425-435.

Carlier E, Sourdet V, Boudkkazi S, Deglise P, Ankri N, Fronzaroli-Molinieres L & Debanne D. (2006). Metabotropic glutamate receptor subtype 1 regulates sodium currents in rat neocortical pyramidal neurons. *J Physiol* **577,** 141-154.

Carr DB, Cooper DC, Ulrich SL, Spruston N & Surmeier DJ. (2002). Serotonin receptor activation inhibits sodium current and dendritic excitability in prefrontal cortex via a protein kinase C-dependent mechanism. *J Neurosci* **22,** 6846-6855.

Carta M, Fievre S, Gorlewicz A & Mulle C. (2014). Kainate receptors in the hippocampus. *Eur J Neurosci* **39,** 1835-1844.

Carter AG & Regehr WG. (2002). Quantal events shape cerebellar interneuron firing. *Nat Neurosci* **5,** 1309-1318.

Castro-Alamancos MA & Gulati T. (2014). Neuromodulators produce distinct activated states in neocortex. *J Neurosci* **34,** 12353-12367.

Celada P, Puig MV & Artigas F. (2013). Serotonin modulation of cortical neurons and networks. *Front Integr Neurosci* **7,** 25.

Chagraoui A, Thibaut F, Skiba M, Thuillez C & Bourin M. (2016). 5-HT_{2C} receptors in psychiatric disorders: A review. *Prog Neuropsychopharmacol Biol Psychiatry* **66,** 120-135.

Chalmers DT & Watson SJ. (1991). Comparative anatomical distribution of 5-HT_{1A} receptor mRNA and 5-HT_{1A} binding in rat brain--a combined in situ hybridisation/in vitro receptor autoradiographic study. *Brain Res* **561,** 51-60.

Charney DS, Krystal JH, Delgado PL & Heninger GR. (1990). Serotonin-specific drugs for anxiety and depressive disorders. *Annu Rev Med* **41,** 437-446.

Cheetham SC, Yamaguchi Y & Horton RW. (1989). [^{3}H]5-hydroxytryptamine binding sites in postmortem human brain. *Neuropharmacology* **28,** 1055-1060.

Chen C & Jonas P. (2017). Synaptotagmins: That's Why So Many. *Neuron* **94,** 694-696.

Chen C & Regehr WG. (2003). Presynaptic modulation of the retinogeniculate synapse. *J Neurosci* **23,** 3130-3135.

Chen CY, Ling Eh EH, Horowitz JM & Bonham AC. (2002). Synaptic transmission in nucleus tractus solitarius is depressed by Group II and III but not Group I presynaptic metabotropic glutamate receptors in rats. *J Physiol* **538,** 773-786.

Chen TY & Hwang TC. (2008). CLC-0 and CFTR: chloride channels evolved from transporters. *Physiol Rev* **88,** 351-387.

Chinopoulos C, Gerencser AA, Doczi J, Fiskum G & Adam-Vizi V. (2004). Inhibition of glutamate-induced delayed calcium deregulation by 2-APB and La^{3+} in cultured cortical neurones. *J Neurochem* **91,** 471-483.

Choi DS & Maroteaux L. (1996). Immunohistochemical localisation of the serotonin 5-HT2B receptor in mouse gut, cardiovascular system, and brain. *FEBS Lett* **391,** 45-51.

Choi IS, Cho JH, Kim JT, Park EJ, Lee MG, Shin HI, Choi BJ & Jang IS. (2007). Serotoninergic modulation of GABAergic synaptic transmission in developing rat CA3 pyramidal neurons. *J Neurochem* **103,** 2342-2353.

Choi UB, Strop P, Vrljic M, Chu S, Brunger AT & Weninger KR. (2010). Single-molecule FRET-derived model of the synaptotagmin 1-SNARE fusion complex. *Nat Struct Mol Biol* **17,** 318-324.

Choy J. (2011). Adrenergic neuromodulation of transmitter release in rat neocortex. In *Neuroscience*. Australian National University, Canberra

Choy JM, Agahari FA, Li L & Stricker C. (2017a). Noradrenaline increases mEPSC frequency in Pyramidal Cells in Layer II of rat barrel cortex via calcium release from presynaptic stores. *under revision for J Neurophysiol*.

Choy JM, Li L, Agahari FA & Stricker C. (2017b). Noradrenaline depresses evoked EPSCs in layer II pyramidal cells of the rat barrel ccrtex. *under revision for J Neurophysiol*.

Chu Z, Galarreta M & Hestrin S. (2003). Synaptic interactions of late-spiking neocortical neurons in layer 1. *J Neurosci* **23,** 96-102.

Chubakov AR, Gromova EA, Konovalov GV, Sarkisova EF & Chumasov EI. (1986). The effects of serotonin on the morpho-functional development of rat cerebral neocortex in tissue culture. *Brain Res* **369,** 285-297.

Clarke WB & Bowsher D. (1962). Terminal distribution of primary afferent trigeminal fibers in the rat. *Exp Neurol* **6,** 372-383.

Clem RL & Huganir RL. (2013). Norepinephrine enhances a discrete form of long-term depression during fear memory storage. *J Neurosci* **33,** 11825-11832.

Clements JD & Bekkers JM. (1997). Detection of spontaneous synaptic events with an optimally scaled template. *Biophys J* **73,** 220-229.

Colomo F & Erulkar SD. (1968). Miniature synaptic potentials at frog spinal neurones in the presence of tertodotoxin. *J Physiol* **199,** 205-221.

Connors BW. (2017). Synchrony and so much more: Diverse roles for electrical synapses in neural circuits. *Dev Neurobiol* **77,** 610-624.

Connors BW, Benardo LS & Prince DA. (1983). Coupling between neurons of the developing rat neocortex. *J Neurosci* **3,** 773-782.

Connors BW, Gutnick MJ & Prince DA. (1982). Electrophysiological properties of neocortical neurons in vitro. *J Neurophysiol* **48,** 1302-1320.

Connors BW & Long MA. (2004). Electrical synapses in the mammalian brain. *Annu Rev Neurosci* **27,** 393-418.

Conti F, Minelli A & Brecha NC. (1994). Cellular localization and laminar distribution of AMPA glutamate receptor subunits mRNAs and proteins in the rat cerebral cortex. *J Comp Neurol* **350,** 241-259.

Cornea-Hébert V, Riad M, Wu C, Singh SK & Descarries L. (1999). Cellular and subcellular distribution of the serotonin 5-HT2A receptor in the central nervous system of adult rat. *J Comp Neurol* **409,** 187-209.

Cortes R, Mengod G, Celada P & Artigas F. (1993). *p*-chlorophenylalanine increases tryptophan-5-hydroxylase mRNA levels in the rat dorsal raphe: a time course study using in situ hybridization. *J Neurochem* **60,** 761-764.

Cowan AI & Stricker C. (2004). Functional connectivity in layer IV local excitatory circuits of rat somatosensory cortex. *J Neurophysiol* **92,** 2137-2150.

Crawford DC, Chang CY, Hyrc KL & Mennerick S. (2011). Calcium-independent inhibitory G-protein signaling induces persistent presynaptic muting of hippocampal synapses. *J Neurosci* **31,** 979-991.

Currie KP & Fox AP. (1997). Comparison of N- and P/Q-type voltage-gated calcium channel current inhibition. *J Neurosci* **17,** 4570-4579.

Czyrak A, Czepiel K, Mackowiak M, Chocyk A & Wedzony K. (2003). Serotonin 5-HT1A receptors might control the output of cortical glutamatergic neurons in rat cingulate cortex. *Brain Res* **989,** 42-51.

Davidson C, Ho M, Price GW, Jones BJ & Stamford JA. (1997). (+)-WAY 100135, a partial agonist, at native and recombinant 5-$HT_{1B/1D}$ receptors. *Br J Pharmacol* **121,** 737-742.

Davletov BA & Sudhof TC. (1993). A single C_2 domain from synaptotagmin I is sufficient for high affinity Ca^{2+}/phospholipid binding. *J Biol Chem* **268,** 26386-26390.

Day M, Olson PA, Platzer J, Striessnig J & Surmeier DJ. (2002). Stimulation of 5-HT_2 receptors in prefrontal pyramidal neurons inhibits $Ca_v1.2$ L type Ca^{2+} currents via a PLCβ/IP3/calcineurin signaling cascade. *J Neurophysiol* **87,** 2490-2504.

De Deurwaerdere P, Navailles S, Berg KA, Clarke WP & Spampinato U. (2004). Constitutive activity of the serotonin2C receptor inhibits *in vivo* dopamine release in the rat striatum and nucleus accumbens. *J Neurosci* **24,** 3235-3241.

de Juan-Sanz J, Holt GT, Schreiter ER, de Juan F, Kim DS & Ryan TA. (2017). Axonal endoplasmic reticulum Ca^{2+} content controls release probability in CNS nerve terminals. *Neuron* **93,** 867-881 e866.

DeFelipe J & Farinas I. (1992). The pyramidal neuron of the cerebral cortex: morphological and chemical characteristics of the synaptic inputs. *Prog Neurobiol* **39,** 563-607.

DeFelipe J, Lopez-Cruz PL, Benavides-Piccione R, Bielza C, Larranaga P, Anderson S, Burkhalter A, Cauli B, Fairen A, Feldmeyer D, Fishell G, Fitzpatrick D, Freund TF, Gonzalez-Burgos G, Hestrin S, Hill S, Hof PR, Huang J, Jones EG, Kawaguchi Y, Kisvarday Z, Kubota Y, Lewis DA, Marin O, Markram H, McBain CJ, Meyer HS, Monyer H, Nelson SB, Rockland K, Rossier J, Rubenstein JL, Rudy B, Scanziani M, Shepherd GM, Sherwood CC, Staiger JF, Tamas G, Thomson A, Wang Y, Yuste R & Ascoli GA. (2013). New insights into the classification and nomenclature of cortical GABAergic interneurons. *Nat Rev Neurosci* **14,** 202-216.

Del Castillo J & Katz B. (1954a). The effect of magnesium on the activity of motor nerve endings. *J Physiol* **124,** 553-559.

Del Castillo J & Katz B. (1954b). Quantal components of the end-plate potential. *J Physiol* **124,** 560-573.

Delaney AJ, Crane JW & Sah P. (2007). Noradrenaline modulates transmission at a central synapse by a presynaptic mechanism. *Neuron* **56,** 880-892.

Delaney K, Tank DW & Zucker RS. (1991). Presynaptic calcium and serotonin-mediated enhancement of transmitter release at crayfish neuromuscular junction. *J Neurosci* **11,** 2631-2643.

Dembrow NC, Chitwood RA & Johnston D. (2010). Projection-specific neuromodulation of medial prefrontal cortex neurons. *J Neurosci* **30,** 16922-16937.

Deschenes M, Timofeeva E, Lavallee P & Dufresne C. (2005). The vibrissal system as a model of thalamic operations. *Prog Brain Res* **149,** 31-40.

Devay P, McGehee DS, Yu CR & Role LW. (1999). Target-specific control of nicotinic receptor expression at developing interneuronal synapses in chick. *Nat Neurosci* **2,** 528-534.

Di Giovanni G & De Deurwaerdere P. (2016). New therapeutic opportunities for 5-HT_{2C} receptor ligands in neuropsychiatric disorders. *Pharmacol Ther* **157,** 125-162.

Di Giovanni G, Svob Strac D, Sole M, Unzeta M, Tipton KF, Muck-Seler D, Bolea I, Della Corte L, Nikolac Perkovic M, Pivac N, Smolders IJ, Stasiak A, Fogel WA & De Deurwaerdere P. (2016). Monoaminergic and histaminergic strategies and treatments in brain diseases. *Front Neurosci* **10,** 541.

Ding S, Li L & Zhou FM. (2013). Presynaptic serotonergic gating of the subthalamonigral glutamatergic projection. *J Neurosci* **33,** 4875-4885.

Dittman JS & Regehr WG. (1998). Calcium dependence and recovery kinetics of presynaptic depression at the climbing fiber to Purkinje cell synapse. *J Neurosci* **18,** 6147-6162.

Diversé-Pierluissi M, Goldsmith PK & Dunlap K. (1995). Transmitter-mediated inhibition of N-type calcium channels in sensory neurons involves multiple GTP-binding proteins and subunits. *Neuron* **14,** 191-200.

Dobrydneva Y & Blackmore P. (2001). 2-Aminoethoxydiphenyl borate directly inhibits store-operated calcium entry channels in human platelets. *Mol Pharmacol* **60,** 541-552.

Dodge FA, Jr. & Rahamimoff R. (1967). Co-operative action a calcium ions in transmitter release at the neuromuscular junction. *J Physiol* **193,** 419-432.

Doi A, Ishibashi H, Jinno S, Kosaka T & Akaike N. (2002). Presynaptic inhibition of GABAergic miniature currents by metabotropic glutamate receptor in the rat CNS. *Neuroscience* **109,** 299-311.

Douglas RJ & Martin KA. (1991). A functional microcircuit for cat visual cortex. *J Physiol* **440,** 735-769.

Douglas RJ & Martin KA. (2004). Neuronal circuits of the neocortex. *Annu Rev Neurosci* **27,** 419-451.

Dugue GP, Dumoulin A, Triller A & Dieudonne S. (2005). Target-dependent use of co-released inhibitory transmitters at central synapses. *J Neurosci* **25,** 6490-6498.

Dunlap K & Fischbach GD. (1978). Neurotransmitters decrease the calcium component of sensory neurone action potentials. *Nature* **276,** 837-839.

Duxon MS, Flanigan TP, Reavley AC, Baxter GS, Blackburn TP & Fone KC. (1997). Evidence for expression of the 5-hydroxytryptamine-2B receptor protein in the rat central nervous system. *Neuroscience* **76,** 323-329.

Eccles JC & McGeer PL. (1979). Ionotropic and Metabotropic Neurotransmission. *TINS* **2,** 39-40.

Edgar DM, Miller JD, Prosser RA, Dean RR & Dement WC. (1993). Serotonin and the mammalian circadian system: II. Phase-shifting rat behavioral rhythms with serotonergic agonists. *J Biol Rhythms* **8,** 17-31.

Edwards FA, Konnerth A, Sakmann B & Takahashi T. (1989). A thin slice preparation for patch clamp recordings from neurones of the mammalian central nervous system. *Pflugers Arch* **414,** 600-612.

Egan C, Herrick-Davis K & Teitler M. (1998). Creation of a constitutively activated state of the 5-HT_{2A} receptor by site-directed mutagenesis: revelation of inverse agonist activity of antagonists. *Ann N Y Acad Sci* **861,** 136-139.

Eisensamer B, Rammes G, Gimpl G, Shapa M, Ferrari U, Hapfelmeier G, Bondy B, Parsons C, Gilling K, Zieglgansberger W, Holsboer F & Rupprecht R. (2003). Antidepressants are functional antagonists at the serotonin type 3 (5-HT_3) receptor. *Mol Psychiatry* **8,** 994-1007.

Elhanany E & White EL. (1990). Intrinsic circuitry: synapses involving the local axon collaterals of corticocortical projection neurons in the mouse primary somatosensory cortex. *J Comp Neurol* **291,** 43-54.

Eliot LS, Kandel ER, Siegelbaum SA & Blumenfeld H. (1993). Imaging terminals of *Aplysia* sensory neurons demonstrates role of enhanced Ca^{2+} influx in presynaptic facilitation. *Nature* **361,** 634-637.

Elston GN, Pow DV & Calford MB. (1997). Neuronal composition and morphology in layer IV of two vibrissal barrel subfields of rat cortex. *Cereb Cortex* **7,** 422-431.

Emptage NJ, Reid CA & Fine A. (2001). Calcium stores in hippocampal synaptic boutons mediate short-term plasticity, store-operated Ca^{2+} entry, and spontaneous transmitter release. *Neuron* **29,** 197-208.

Enyedi P & Czirjak G. (2010). Molecular background of leak K^+ currents: two-pore domain potassium channels. *Physiol Rev* **90,** 559-605.

Erickson JD, Schafer MK, Bonner TI, Eiden LE & Weihe E. (1996). Distinct pharmacological properties and distribution in neurons and endocrine cells of two isoforms of the human vesicular monoamine transporter. *Proc Natl Acad Sci U S A* **93,** 5166-5171.

Erzurumlu RS & Kind PC. (2001). Neural activity: sculptor of 'barrels' in the neocortex. *Trends Neurosci* **24,** 589-595.

Evans BA, Papaioannou M, Hamilton S & Summers RJ. (1999). Alternative splicing generates two isoforms of the β_3-adrenoceptor which are differentially expressed in mouse tissues. *Br J Pharmacol* **127,** 1525-1531.

Exton JH. (1994). Phosphoinositide phospholipases and G proteins in hormone action. *Annu Rev Physiol* **56,** 349-369.

Fang Q, Berberian K, Gong LW, Hafez I, Sorensen JB & Lindau M. (2008). The role of the C terminus of the SNARE protein SNAP-25 in fusion pore opening and a model for fusion pore mechanics. *Proc Natl Acad Sci U S A* **105,** 15388-15392.

Fatt P & Katz B. (1950). Some observations on biological noise. *Nature* **166,** 597-598.

Fatt P & Katz B. (1952). Spontaneous subthreshold activity at motor nerve endings. *J Physiol* **117,** 109-128.

Favero M, Varghese G & Castro-Alamancos MA. (2012). The state of somatosensory cortex during neuromodulation. *J Neurophysiol* **108,** 1010-1024.

Feldmeyer D, Lübke J & Sakmann B. (2006). Efficacy and connectivity of intracolumnar pairs of layer 2/3 pyramidal cells in the barrel cortex of juvenile rats. *J Physiol* **575,** 583-602.

Fernandez-Chacon R, Shin OH, Konigstorfer A, Matos MF, Meyer AC, Garcia J, Gerber SH, Rizo J, Sudhof TC & Rosenmund C. (2002). Structure/function analysis of Ca^{2+} binding to the C_2A domain of synaptotagmin 1. *J Neurosci* **22,** 8438-8446.

Fierro L, DiPolo R & Llano I. (1998). Intracellular calcium clearance in Purkinje cell somata from rat cerebellar slices. *J Physiol* **510 (Pt 2),** 499-512.

Fink KB & Göthert M. (2007). 5-HT receptor regulation of neurotransmitter release. *Pharmacol Rev* **59,** 360-417.

Fitzpatrick PF. (1991). Studies of the rate-limiting step in the tyrosine hydroxylase reaction: alternate substrates, solvent isotope effects, and transition-state analogues. *Biochemistry* **30,** 6386-6391.

Foehring RC. (1996). Serotonin modulates N- and P-type calcium currents in neocortical pyramidal neurons via a membrane-delimited pathway. *J Neurophysiol* **75,** 648-659.

Foehring RC, Schwindt PC & Crill WE. (1989). Norepinephrine selectively reduces slow Ca^{2+}- and Na^{+}-mediated K^{+} currents in cat neocortical neurons. *J Neurophysiol* **61,** 245-256.

Foehring RC, van Brederode JF, Kinney GA & Spain WJ. (2002). Serotonergic modulation of supragranular neurons in rat sensorimotor cortex. *J Neurosci* **22,** 8238-8250.

Földy C, Dyhrfjeld-Johnsen J & Soltesz I. (2005). Structure of cortical microcircuit theory. *J Physiol* **562,** 47-54.

Franceschetti S, Taverna S, Sancini G, Panzica F, Lombardi R & Avanzini G. (2000). Protein kinase C-dependent modulation of Na^{+} currents increases the excitability of rat neocortical pyramidal neurones. *J Physiol* **528 Pt 2,** 291-304.

Franklin JM & Carrasco GA. (2015). Cocaine potentiates multiple 5-HT_{2A} receptor signaling pathways and is associated with decreased phosphorylation of 5-HT_{2A} receptors in vivo. *J Mol Neurosci* **55,** 770-777.

Fredj NB & Burrone J. (2009). A resting pool of vesicles is responsible for spontaneous vesicle fusion at the synapse. *Nat Neurosci* **12,** 751-758.

Fuhrmann G, Cowan A, Segev I, Tsodyks M & Stricker C. (2004). Multiple mechanisms govern the dynamics of depression at neocortical synapses of young rats. *J Physiol* **557,** 415-438.

Fujino K, Yoshitake T, Inoue O, Ibii N, Kehr J, Ishida J, Nohta H & Yamaguchi M. (2002). Increased serotonin release in mice frontal cortex and hippocampus induced by acute physiological stressors. *Neurosci Lett* **320,** 91-95.

Funahashi M, Mitoh Y & Matsuo R. (2004). Activation of presynaptic 5-HT_3 receptors facilitates glutamatergic synaptic inputs to area postrema neurons in rat brain slices. *Methods Find Exp Clin Pharmacol* **26,** 615-622.

Furshpan EJ & Potter DD. (1959). Transmission at the giant motor synapses of the crayfish. *J Physiol* **145,** 289-325.

Gabriel A, Abdallah M, Yost CS, Winegar BD & Kindler CH. (2002). Localization of the tandem pore domain K^+ channel KCNK5 (TASK-2) in the rat central nervous system. *Brain Res Mol Brain Res* **98,** 153-163.

Galarreta M, Erdelyi F, Szabo G & Hestrin S. (2004). Electrical coupling among irregular-spiking GABAergic interneurons expressing cannabinoid receptors. *J Neurosci* **24,** 9770-9778.

Galarreta M & Hestrin S. (1999). A network of fast-spiking cells in the neocortex connected by electrical synapses. *Nature* **402,** 72-75.

Galarreta M & Hestrin S. (2001). Electrical synapses between GABA-releasing interneurons. *Nat Rev Neurosci* **2,** 425-433.

Galarreta M & Hestrin S. (2002). Electrical and chemical synapses among parvalbumin fast-spiking GABAergic interneurons in adult mouse neocortex. *Proc Natl Acad Sci U S A* **99,** 12438-12443.

Gamper N, Reznikov V, Yamada Y, Yang J & Shapiro MS. (2004). Phosphatidylinositol 4,5-bisphosphate signals underlie receptor-specific $G_{q/11}$-mediated modulation of N-type Ca^{2+} channels. *J Neurosci* **24,** 10980-10992.

Gasparini S & DiFrancesco D. (1999). Action of serotonin on the hyperpolarization-activated cation current (I_h) in rat CA1 hippocampal neurons. *Eur J Neurosci* **11,** 3093-3100.

Gehlert DR, Gackenheimer SL, Wong DT & Robertson DW. (1991). Localization of 5-HT_3 receptors in the rat brain using [^{3}H]LY278584. *Brain Res* **553,** 149-154.

Gerachshenko T, Blackmer T, Yoon EJ, Bartleson C, Hamm HE & Alford S. (2005). Gβγ acts at the C terminus of SNAP-25 to mediate presynaptic inhibition. *Nat Neurosci* **8,** 597-605.

Gerachshenko T, Schwartz E, Bleckert A, Photowala H, Seymour A & Alford S. (2009). Presynaptic G-protein-coupled receptors dynamically modify vesicle fusion, synaptic cleft glutamate concentrations, and motor behavior. *J Neurosci* **29,** 10221-10233.

Gérard C, Martres MP, Lefevre K, Miquel MC, Verge D, Lanfumey L, Doucet E, Hamon M & el Mestikawy S. (1997). Immuno-localization of serotonin 5-HT_6 receptor-like material in the rat central nervous system. *Brain Res* **746,** 207-219.

Geurts FJ, De Schutter E & Timmermans JP. (2002). Localization of 5-HT2A, 5-HT3, 5-HT5A and 5-HT7 receptor-like immunoreactivity in the rat cerebellum. *J Chem Neuroanat* **24,** 65-74.

Gibson JR, Beierlein M & Connors BW. (2005). Functional properties of electrical synapses between inhibitory interneurons of neocortical layer 4. *J Neurophysiol* **93,** 467-480.

Gil A, Gutierrez LM, Carrasco-Serrano C, Alonso MT, Viniegra S & Criado M. (2002). Modifications in the C terminus of the synaptosome-associated protein of 25 kDa (SNAP-25) and in the complementary region of synaptobrevin affect the final steps of exocytosis. *J Biol Chem* **277,** 9904-9910.

Glickfeld LL, Andermann ML, Bonin V & Reid RC. (2013). Cortico-cortical projections in mouse visual cortex are functionally target specific. *Nat Neurosci* **16,** 219-226.

Gonzales RA & Crews FT. (1985). Guanine nucleotides stimulate production of inositol trisphosphate in rat cortical membranes. *Biochem J* **232,** 799-804.

Gonzalez-Maeso J, Ang RL, Yuen T, Chan P, Weisstaub NV, Lopez-Gimenez JF, Zhou M, Okawa Y, Callado LF, Milligan G, Gingrich JA, Filizola M, Meana JJ & Sealfon SC. (2008). Identification of a serotonin/glutamate receptor complex implicated in psychosis. *Nature* **452,** 93-97.

Gonzalez-Maeso J, Weisstaub NV, Zhou M, Chan P, Ivic L, Ang R, Lira A, Bradley-Moore M, Ge Y, Zhou Q, Sealfon SC & Gingrich JA. (2007). Hallucinogens recruit specific cortical 5-HT_{2A} receptor-mediated signaling pathways to affect behavior. *Neuron* **53,** 439-452.

Goodfellow NM, Benekareddy M, Vaidya VA & Lambe EK. (2009). Layer II/III of the prefrontal cortex: Inhibition by the serotonin 5-HT_{1A} receptor in development and stress. *J Neurosci* **29,** 10094-10103.

Goubaeva F, Ghosh M, Malik S, Yang J, Hinkle PM, Griendling KK, Neubig RR & Smrcka AV. (2003). Stimulation of cellular signaling and G protein subunit dissociation by G protein *βγ* subunit-binding peptides. *J Biol Chem* **278,** 19634-19641.

Gray JA, Bhatnagar A, Gurevich VV & Roth BL. (2003). The interaction of a constitutively active arrestin with the arrestin-insensitive 5-HT_{2A} receptor induces agonist-independent internalization. *Mol Pharmacol* **63,** 961-972.

Green KN, Demuro A, Akbari Y, Hitt BD, Smith IF, Parker I & LaFerla FM. (2008). SERCA pump activity is physiologically regulated by presenilin and regulates amyloid β production. *J Cell Biol* **181,** 1107-1116.

Green KN & LaFerla FM. (2008). Linking calcium to Aβ and Alzheimer's disease. *Neuron* **59,** 190-194.

Greger IH, Watson JF & Cull-Candy SG. (2017). Structural and functional architecture of AMPA-type glutamate receptors and their auxiliary proteins. *Neuron* **94,** 713-730.

Grewal JS, Luttrell LM & Raymond JR. (2001). G protein-coupled receptors desensitize and down-regulate epidermal growth factor receptors in renal mesangial cells. *J Biol Chem* **276,** 27335-27344.

Grillner S, Markram H, De Schutter E, Silberberg G & LeBeau FE. (2005). Microcircuits in action--from CPGs to neocortex. *Trends Neurosci* **28,** 525-533.

Grossman CJ, Kilpatrick GJ & Bunce KT. (1993). Development of a radioligand binding assay for 5-HT_4 receptors in guinea-pig and rat brain. *Br J Pharmacol* **109,** 618-624.

Gruner JE, Hirsch JC & Sotelo C. (1974). Ultrastructural features of the isolated suprasylvian gyrus in the cat. *J Comp Neurol* **154,** 1-27.

Gschwendt M, Dieterich S, Rennecke J, Kittstein W, Mueller HJ & Johannes FJ. (1996). Inhibition of protein kinase C μ by various inhibitors. Differentiation from protein kinase c isoenzymes. *FEBS Lett* **392,** 77-80.

Guiard BP & Di Giovanni G. (2015). Central serotonin-2A (5-HT2A) receptor dysfunction in depression and epilepsy: the missing link? *Front Pharmacol* **6,** 46.

Gupta A, Wang Y & Markram H. (2000). Organizing principles for a diversity of GABAergic interneurons and synapses in the neocortex. *Science* **287,** 273-278.

Gutierrez LM, Viniegra S, Rueda J, Ferrer-Montiel AV, Canaves JM & Montal M. (1997). A peptide that mimics the C-terminal sequence of SNAP-25 inhibits secretory vesicle docking in chromaffin cells. *J Biol Chem* **272,** 2634-2639.

Haas HL & Konnerth A. (1983). Histamine and noradrenaline decrease calcium-activated potassium conductance in hippocampal pyramidal cells. *Nature* **302,** 432-434.

Hall H, Farde L, Halldin C, Lundkvist C & Sedvall G. (2000). Autoradiographic localization of 5-HT_{2A} receptors in the human brain using [^{3}H]M100907 and [^{11}C]M100907. *Synapse* **38,** 421-431.

Hamada S, Senzaki K, Hamaguchi-Hamada K, Tabuchi K, Yamamoto H, Yamamoto T, Yoshikawa S, Okano H & Okado N. (1998). Localization of 5-HT2A receptor in rat cerebral cortex and olfactory system revealed by immunohistochemistry using two antibodies raised in rabbit and chicken. *Brain Res Mol Brain Res* **54,** 199-211.

Hamid E, Church E, Wells CA, Zurawski Z, Hamm HE & Alford S. (2014). Modulation of neurotransmission by GPCRs is dependent upon the microarchitecture of the primed vesicle complex. *J Neurosci* **34,** 260-274.

Hancock MB & Fougerousse CL. (1976). Spinal projections from the nucleus locus coeruleus and nucleus subcoeruleus in the cat and monkey as demonstrated by the retrograde transport of horseradish peroxidase. *Brain Res Bull* **1,** 229-234.

Hardie RC, Gu Y, Martin F, Sweeney ST & Raghu P. (2004). *In vivo* light-induced and basal phospholipase C activity in *Drosophila* photoreceptors measured with genetically targeted phosphatidylinositol 4,5-bisphosphate-sensitive ion channels (Kir2.1). *J Biol Chem* **279,** 47773-47782.

Hardingham NR & Larkman AU. (1998). Rapid report: the reliability of excitatory synaptic transmission in slices of rat visual cortex *in vitro* is temperature dependent. *J Physiol* **507 (Pt 1),** 249-256.

Harney SC & Jones MV. (2002). Pre- and postsynaptic properties of somatic and dendritic inhibition in dentate gyrus. *Neuropharmacology* **43,** 584-594.

Hartig PR, Hoyer D, Humphrey PP & Martin GR. (1996). Alignment of receptor nomenclature with the human genome: classification of 5-HT_{1B} and 5-HT_{1D} receptor subtypes. *Trends Pharmacol Sci* **17,** 103-105.

Harvey JA. (2003). Role of the serotonin 5-HT_{2A} receptor in learning. *Learn Mem* **10,** 355-362.

Hasuo H, Matsuoka T & Akasu T. (2002). Activation of presynaptic 5-hydroxytryptamine 2A receptors facilitates excitatory synaptic transmission via protein kinase C in the dorsolateral septal nucleus. *J Neurosci* **22,** 7509-7517.

Hattox A, Li Y & Keller A. (2003). Serotonin regulates rhythmic whisking. *Neuron* **39,** 343-352.

Haviland MG. (1990). Yates's correction for continuity and the analysis of 2 x 2 contingency tables. *Stat Med* **9,** 363-367; discussion 369-383.

Hayashi T, McMahon H, Yamasaki S, Binz T, Hata Y, Sudhof TC & Niemann H. (1994). Synaptic vesicle membrane fusion complex: action of clostridial neurotoxins on assembly. *Embo J* **13,** 5051-5061.

Hayashi T, Yamasaki S, Nauenburg S, Binz T & Niemann H. (1995). Disassembly of the reconstituted synaptic vesicle membrane fusion complex *in vitro*. *Embo J* **14,** 2317-2325.

Hayashi Y, Shi SH, Esteban JA, Piccini A, Poncer JC & Malinow R. (2000). Driving AMPA receptors into synapses by LTP and CaMKII: requirement for GluR1 and PDZ domain interaction. *Science* **287,** 2262-2267.

Heal DJ, Smith SL, Fisas A, Codony X & Buschmann H. (2008). Selective 5-HT_6 receptor ligands: progress in the development of a novel pharmacological approach to the treatment of obesity and related metabolic disorders. *Pharmacol Ther* **117,** 207-231.

Hedlund PB. (2009). The 5-HT_7 receptor and disorders of the nervous system: an overview. *Psychopharmacology (Berl)* **206,** 345-354.

Hensler JG. (2006). Serotonergic modulation of the limbic system. *Neurosci Biobehav Rev* **30,** 203-214.

Herlitze S, Garcia DE, Mackie K, Hille B, Scheuer T & Catterall WA. (1996). Modulation of Ca^{2+} channels by G-protein βγ subunits. *Nature* **380,** 258-262.

Herndon JL, Ismaiel A, Ingher SP, Teitler M & Glennon RA. (1992). Ketanserin analogues: structure-affinity relationships for 5-HT_2 and 5-HT_{1C} serotonin receptor binding. *J Med Chem* **35,** 4903-4910.

Herrick-Davis K, Grinde E, Harrigan TJ & Mazurkiewicz JE. (2005). Inhibition of serotonin 5-hydroxytryptamine2c receptor function through heterodimerization: receptor dimers bind two molecules of ligand and one G-protein. *J Biol Chem* **280,** 40144-40151.

Herrick-Davis K, Weaver BA, Grinde E & Mazurkiewicz JE. (2006). Serotonin 5-HT_{2C} receptor homodimer biogenesis in the endoplasmic reticulum: real-time visualization with confocal fluorescence resonance energy transfer. *J Biol Chem* **281,** 27109-27116.

Hieble JP, Bondinell WE & Ruffolo RR, Jr. (1995). *α*- and *β*-adrenoceptors: from the gene to the clinic. 1. Molecular biology and adrenoceptor subclassification. *J Med Chem* **38,** 3415-3444.

Hirst GD, Hashitani H & Suzuki H. (2008). Cellular mechanism of the voltage-dependent change in slow potentials generated in circular smooth muscle of the guinea-pig gastric corpus. *J Physiol* **586,** 5521-5536.

Hirst WD, Cheung NY, Rattray M, Price GW & Wilkin GP. (1998). Cultured astrocytes express messenger RNA for multiple serotonin receptor subtypes, without functional coupling of 5-HT_1 receptor subtypes to adenylyl cyclase. *Brain Res Mol Brain Res* **61,** 90-99.

Holmberg M, Scheinin M, Kurose H & Miettinen R. (1999). Adrenergic α_{2C}-receptors reside in rat striatal GABAergic projection neurons: comparison of radioligand binding and immunohistochemistry. *Neuroscience* **93,** 1323-1333.

Hori Y, Endo K & Takahashi T. (1996). Long-lasting synaptic facilitation induced by serotonin in superficial dorsal horn neurones of the rat spinal cord. *J Physiol* **492 (Pt 3),** 867-876.

Horowitz LF, Hirdes W, Suh BC, Hilgemann DW, Mackie K & Hille B. (2005). Phospholipase C in living cells: activation, inhibition, Ca^{2+} requirement, and regulation of M current. *J Gen Physiol* **126,** 243-262.

Hosford PS, Mifflin SW & Ramage AG. (2014). 5-hydroxytryptamine-mediated neurotransmission modulates spontaneous and vagal-evoked glutamate release in the nucleus of the solitary tract effect of uptake blockade. *J Pharmacol Exp Ther* **349,** 288-296.

Hosokawa Y, Sciancalepore M, Stratta F, Martina M & Cherubini E. (1994). Developmental changes in spontaneous $GABA_A$-mediated synaptic events in rat hippocampal CA3 neurons. *Eur J Neurosci* **6,** 805-813.

Hoyer D, Clarke DE, Fozard JR, Hartig PR, Martin GR, Mylecharane EJ, Saxena PR & Humphrey PP. (1994). International Union of Pharmacology classification of receptors for 5-hydroxytryptamine (Serotonin). *Pharmacol Rev* **46,** 157-203.

Hoyer D, Engel G & Kalkman HO. (1985). Molecular pharmacology of 5-HT_1 and 5-HT_2 recognition sites in rat and pig brain membranes: radioligand binding studies with [^{3}H]5-HT, [^{3}H]8-OH-DPAT, (-)[^{125}I]iodocyanopindolol, [^{3}H]mesulergine and [^{3}H]ketanserin. *Eur J Pharmacol* **118,** 13-23.

Hoyer D, Pazos A, Probst A & Palacios JM. (1986a). Serotonin receptors in the human brain. I. Characterization and autoradiographic localization of 5-

HT_{1A} recognition sites. Apparent absence of 5-HT_{1B} recognition sites. *Brain Res* **376,** 85-96.

Hoyer D, Pazos A, Probst A & Palacios JM. (1986b). Serotonin receptors in the human brain. II. Characterization and autoradiographic localization of 5-HT_{1C} and 5-HT_2 recognition sites. *Brain Res* **376,** 97-107.

Hu H & Agmon A. (2015). Properties of precise firing synchrony between synaptically coupled cortical interneurons depend on their mode of coupling. *J Neurophysiol* **114,** 624-637.

Hua Y, Sinha R, Martineau M, Kahms M & Klingauf J. (2010). A common origin of synaptic vesicles undergoing evoked and spontaneous fusion. *Nat Neurosci* **13,** 1451-1453.

Huang H & Trussell LO. (2011). KCNQ5 channels control resting properties and release probability of a synapse. *Nat Neurosci* **14,** 840-847.

Huo FQ, Huang FS, Lv BC, Chen T, Feng J, Qu CL, Tang JS & Li YQ. (2010). Activation of serotonin 1A receptors in ventrolateral orbital cortex depresses persistent nociception: a presynaptic inhibition mechanism. *Neurochem Int* **57,** 749-755.

Hylden JL, Hayashi H, Ruda MA & Dubner R. (1986). Serotonin innervation of physiologically identified lamina I projection neurons. *Brain Res* **370,** 401-404.

Ikeda SR. (1996). Voltage-dependent modulation of N-type calcium channels by G-protein βγ subunits. *Nature* **380,** 255-258.

Irvine RF. (1982). How is the level of free arachidonic acid controlled in mammalian cells? *Biochem J* **204,** 3-16.

Jakab RL & Goldman-Rakic PS. (1998). 5-Hydroxytryptamine$_{2A}$ serotonin receptors in the primate cerebral cortex: possible site of action of hallucinogenic and antipsychotic drugs in pyramidal cell apical dendrites. *Proc Natl Acad Sci U S A* **95,** 735-740.

Jansson A, Tinner B, Bancila M, Verge D, Steinbusch HW, Agnati LF & Fuxe K. (2001). Relationships of 5-hydroxytryptamine immunoreactive terminal-like varicosities to 5-hydroxytryptamine-2A receptor-immunoreactive neuronal processes in the rat forebrain. *J Chem Neuroanat* **22,** 185-203.

Jhaveri DJ, Mackay EW, Hamlin AS, Marathe SV, Nandam LS, Vaidya VA & Bartlett PF. (2010). Norepinephrine directly activates adult hippocampal precursors via β_3-adrenergic receptors. *J Neurosci* **30,** 2795-2806.

Jin I, Puthanveettil S, Udo H, Karl K, Kandel ER & Hawkins RD. (2012a). Spontaneous transmitter release is critical for the induction of long-term and intermediate-term facilitation in *Aplysia*. *Proc Natl Acad Sci U S A* **109,** 9131-9136.

Jin I, Udo H, Rayman JB, Puthanveettil S, Kandel ER & Hawkins RD. (2012b). Spontaneous transmitter release recruits postsynaptic mechanisms of long-term and intermediate-term facilitation in *Aplysia*. *Proc Natl Acad Sci U S A* **109,** 9137-9142.

Johnson JW & Ascher P. (1987). Glycine potentiates the NMDA response in cultured mouse brain neurons. *Nature* **325,** 529-531.

Jones LS, Gauger LL & Davis JN. (1986). Localization of α_1-adrenergic receptors in normal and weaver mouse brain with in vitro ^{125}I-HEAT autoradiography. *Neurosci Lett* **65,** 259-264.

Kamal M, Gbahou F, Guillaume JL, Daulat AM, Benleulmi-Chaachoua A, Luka M, Chen P, Kalbasi Anaraki D, Baroncini M, Mannoury la Cour C, Millan MJ, Prevot V, Delagrange P & Jockers R. (2015). Convergence of melatonin and serotonin (5-HT) signaling at MT_2/5-HT_{2C} receptor heteromers. *J Biol Chem* **290,** 11537-11546.

Kanner AM. (2003). Depression in epilepsy: prevalence, clinical semiology, pathogenic mechanisms, and treatment. *Biol Psychiatry* **54,** 388-398.

Kapoor V, Provost AC, Agarwal P & Murthy VN. (2016). Activation of raphe nuclei triggers rapid and distinct effects on parallel olfactory bulb output channels. *Nat Neurosci* **19,** 271-282.

Katz B. (1962). The transmission of impulses from nerve to muscle, and the subcellular unit of synaptic action. *Proc R Soc Lond B Biol Sci* **155,** 455-477.

Katz B & Miledi R. (1963). A study of spontaneous miniature potentials in spinal motoneurones. *J Physiol* **168,** 389-422.

Kaufman MJ, Hartig PR & Hoffman BJ. (1995). Serotonin 5-HT_{2C} receptor stimulates cyclic GMP formation in choroid plexus. *J Neurochem* **64,** 199-205.

Kawaguchi Y & Kubota Y. (1996). Physiological and morphological identification of somatostatin- or vasoactive intestinal polypeptide-containing cells among GABAergic cell subtypes in rat frontal cortex. *J Neurosci* **16,** 2701-2715.

Kawaguchi Y & Kubota Y. (1997). GABAergic cell subtypes and their synaptic connections in rat frontal cortex. *Cereb Cortex* **7,** 476-486.

Kawaguchi Y & Kubota Y. (1998). Neurochemical features and synaptic connections of large physiologically-identified GABAergic cells in the rat frontal cortex. *Neuroscience* **85,** 677-701.

Keinanen K, Wisden W, Sommer B, Werner P, Herb A, Verdoorn TA, Sakmann B & Seeburg PH. (1990). A family of AMPA-selective glutamate receptors. *Science* **249,** 556-560.

Keller A & White EL. (1987). Synaptic organization of GABAergic neurons in the mouse SmI cortex. *J Comp Neurol* **262,** 1-12.

Kelley SP, Bratt AM & Hodge CW. (2003). Targeted gene deletion of the 5-HT_{3A} receptor subunit produces an anxiolytic phenotype in mice. *Eur J Pharmacol* **461,** 19-25.

Kennett GA, Wood MD, Bright F, Cilia J, Piper DC, Gager T, Thomas D, Baxter GS, Forbes IT, Ham P & Blackburn TP. (1996). *In vitro* and *in vivo* profile of SB 206553, a potent 5-HT_{2C}/5-HT_{2B} receptor antagonist with anxiolytic-like properties. *Br J Pharmacol* **117,** 427-434.

Kennett GA, Wood MD, Glen A, Grewal S, Forbes I, Gadre A & Blackburn TP. (1994). *In vivo* properties of SB 200646A, a 5-$HT_{2C/2B}$ receptor antagonist. *Br J Pharmacol* **111,** 797-802.

Kepecs A & Fishell G. (2014). Interneuron cell types are fit to function. *Nature* **505,** 318-326.

Kia HK, Miquel MC, Brisorgueil MJ, Daval G, Riad M, El Mestikawy S, Hamon M & Verge D. (1996). Immunocytochemical localization of serotonin$_{1A}$ receptors in the rat central nervous system. *J Comp Neurol* **365,** 289-305.

Kia HK, Miquel MC, McKernan RM, Laporte AM, Lombard MC, Bourgoin S, Hamon M & Verge D. (1995). Localization of 5-HT_3 receptors in the rat spinal cord: immunohistochemistry and in situ hybridization. *Neuroreport* **6,** 257-261.

Kidd FL & Isaac JT. (1999). Developmental and activity-dependent regulation of kainate receptors at thalamocortical synapses. *Nature* **400,** 569-573.

Kim D, Jun KS, Lee SB, Kang NG, Min DS, Kim YH, Ryu SH, Suh PG & Shin HS. (1997). Phospholipase C isozymes selectively couple to specific neurotransmitter receptors. *Nature* **389,** 290-293.

King PR, Gundlach AL & Louis WJ. (1995). Quantitative autoradiographic localization in rat brain of α_2-adrenergic and non-adrenergic I-receptor binding sites labelled by [^{3}H]rilmenidine. *Brain Res* **675,** 264-278.

Kisvarday ZF, Martin KA, Freund TF, Magloczky Z, Whitteridge D & Somogyi P. (1986). Synaptic targets of HRP-filled layer III pyramidal cells in the cat striate cortex. *Exp Brain Res* **64,** 541-552.

Kjaerby C, Athilingam J, Robinson SE, Iafrati J & Sohal VS. (2016). Serotonin 1B receptors regulate prefrontal function by gating callosal and hippocampal inputs. *Cell Rep* **17,** 2882-2890.

Knauer CS, Campbell JE, Chio CL & Fitzgerald LW. (2009). Pharmacological characterization of mitogen-activated protein kinase activation by recombinant human 5-HT_{2C}, 5-HT_{2A}, and 5-HT_{2B} receptors. *Naunyn Schmiedebergs Arch Pharmacol* **379,** 461-471.

Knight AR, Misra A, Quirk K, Benwell K, Revell D, Kennett G & Bickerdike M. (2004). Pharmacological characterisation of the agonist radioligand binding site of 5-HT_{2A}, 5-HT_{2B} and 5-HT_{2C} receptors. *Naunyn Schmiedebergs Arch Pharmacol* **370,** 114-123.

Koek W, Jackson A & Colpaert FC. (1992). Behavioral pharmacology of antagonists at 5-HT_2/5-HT_{1C} receptors. *Neurosci Biobehav Rev* **16,** 95-105.

Koester HJ & Johnston D. (2005). Target cell-dependent normalization of transmitter release at neocortical synapses. *Science* **308,** 863-866.

Kojic L, Dyck RH, Gu Q, Douglas RM, Matsubara J & Cynader MS. (2000). Columnar distribution of serotonin-dependent plasticity within kitten striate cortex. *Proc Natl Acad Sci U S A* **97,** 1841-1844.

Kole MH & Stuart GJ. (2008). Is action potential threshold lowest in the axon? *Nat Neurosci* **11,** 1253-1255.

Komlosi G, Molnar G, Rozsa M, Olah S, Barzo P & Tamas G. (2012). Fluoxetine (prozac) and serotonin act on excitatory synaptic transmission to suppress single layer 2/3 pyramidal neuron-triggered cell assemblies in the human prefrontal cortex. *J Neurosci* **32,** 16369-16378.

Korn H, Burnod Y & Faber DS. (1987). Spontaneous quantal currents in a central neuron match predictions from binomial analysis of evoked responses. *Proc Natl Acad Sci U S A* **84,** 5981-5985.

Kosofsky BE & Molliver ME. (1987). The serotoninergic innervation of cerebral cortex: different classes of axon terminals arise from dorsal and median raphe nuclei. *Synapse* **1,** 153-168.

Koyama Y, Kondo M & Shimada S. (2017). Building a 5-HT3A Receptor Expression Map in the Mouse Brain. *Sci Rep* **7,** 42884.

Krause KM, Pearce J & Govind CK. (1998). Regeneration of phasic motor axons on a crayfish tonic muscle: neuron specifies synapses. *J Neurophysiol* **80,** 994-997.

Krnjevic K & Phillis JW. (1963). Actions of certain amines on cerebral cortical neurones. *Br J Pharmacol Chemother* **20,** 471-490.

Kroeze WK, Hufeisen SJ, Popadak BA, Renock SM, Steinberg S, Ernsberger P, Jayathilake K, Meltzer HY & Roth BL. (2003). H_1-histamine receptor affinity predicts short-term weight gain for typical and atypical antipsychotic drugs. *Neuropsychopharmacology* **28,** 519-526.

Kruk JS, Vasefi MS, Gondora N, Ahmed N, Heikkila JJ & Beazely MA. (2015). Fluoxetine-induced transactivation of the platelet-derived growth factor type β receptor reveals a novel heterologous desensitization process. *Mol Cell Neurosci* **65,** 45-51.

Kubota Y, Karube F, Nomura M, Gulledge AT, Mochizuki A, Schertel A & Kawaguchi Y. (2011). Conserved properties of dendritic trees in four cortical interneuron subtypes. *Sci Rep* **1,** 89.

Kuno M. (1964). Quantal components of excitatory synaptic potentials in spinal motoneurones. *J Physiol* **175,** 81-99.

Kurrasch-Orbaugh DM, Parrish JC, Watts VJ & Nichols DE. (2003). A complex signaling cascade links the serotonin$_{2A}$ receptor to phospholipase A_2 activation: the involvement of MAP kinases. *J Neurochem* **86,** 980-991.

Kursar JD, Nelson DL, Wainscott DB & Baez M. (1994). Molecular cloning, functional expression, and mRNA tissue distribution of the human 5-hydroxytryptamine$_{2B}$ receptor. *Mol Pharmacol* **46,** 227-234.

Lambe EK, Goldman-Rakic PS & Aghajanian GK. (2000). Serotonin induces EPSCs preferentially in layer V pyramidal neurons of the frontal cortex in the rat. *Cereb Cortex* **10,** 974-980.

Landisman CE, Long MA, Beierlein M, Deans MR, Paul DL & Connors BW. (2002). Electrical synapses in the thalamic reticular nucleus. *J Neurosci* **22,** 1002-1009.

Larkman AU. (1991). Dendritic morphology of pyramidal neurones of the visual cortex of the rat: III. Spine distributions. *J Comp Neurol* **306,** 332-343.

Larkman PM & Kelly JS. (1992). Ionic mechanisms mediating 5-hydroxytryptamine- and noradrenaline-evoked depolarization of adult rat facial motoneurones. *J Physiol* **456,** 473-490.

Ledo JH, Azevedo EP, Beckman D, Ribeiro FC, Santos LE, Razolli DS, Kincheski GC, Melo HM, Bellio M, Teixeira AL, Velloso LA, Foguel D, De Felice FG & Ferreira ST. (2016). Cross talk between brain innate immunity and serotonin signaling underlies depressive-like behavior induced by Alzheimer's amyloid-*β* oligomers in mice. *J Neurosci* **36,** 12106-12116.

Lee JJ, Hahm ET, Lee CH & Cho YW. (2008). Serotonergic modulation of GABAergic and glutamatergic synaptic transmission in mechanically isolated rat medial preoptic area neurons. *Neuropsychopharmacology* **33,** 340-352.

Lee S, Hjerling-Leffler J, Zagha E, Fishell G & Rudy B. (2010). The largest group of superficial neocortical GABAergic interneurons expresses ionotropic serotonin receptors. *J Neurosci* **30,** 16796-16808.

Lei S. (2012). Serotonergic modulation of Neural activities in the entorhinal cortex. *Int J Physiol Pathophysiol Pharmacol* **4,** 201-210.

Lemos JC, Pan YZ, Ma X, Lamy C, Akanwa AC & Beck SG. (2006). Selective 5-HT receptor inhibition of glutamatergic and GABAergic synaptic activity in the rat dorsal and median raphe. *Eur J Neurosci* **24,** 3415-3430.

Leonhardt S, Gorospe E, Hoffman BJ & Teitler M. (1992). Molecular pharmacological differences in the interaction of serotonin with 5-hydroxytryptamine$_{1C}$ and 5-hydroxytryptamine$_2$ receptors. *Mol Pharmacol* **42,** 328-335.

Leonhardt S, Herrick-Davis K & Titeler M. (1989). Detection of a novel serotonin receptor subtype (5-HT$_{1E}$) in human brain: interaction with a GTP-binding protein. *J Neurochem* **53,** 465-471.

Lesch KP & Waider J. (2012). Serotonin in the modulation of neural plasticity and networks: implications for neurodevelopmental disorders. *Neuron* **76,** 175-191.

Letty S, Child R, Dumuis A, Pantaloni A, Bockaert J & Rondouin G. (1997). 5-HT$_4$ receptors improve social olfactory memory in the rat. *Neuropharmacology* **36,** 681-687.

Leysen JE, Janssen PM, Schotte A, Luyten WH & Megens AA. (1993). Interaction of antipsychotic drugs with neurotransmitter receptor sites in vitro and in vivo in relation to pharmacological and clinical effects: role of 5HT$_2$ receptors. *Psychopharmacology (Berl)* **112,** S40-54.

Li L, Choy JM & Stricker C. (2010). Long-term depression caused by low frequency stimulation revealed in paired recordings of pyramidal cells of layer II/III of rat barrel cortex. *SfN Abstract* **141.17**.

Li QH, Nakadate K, Tanaka-Nakadate S, Nakatsuka D, Cui Y & Watanabe Y. (2004). Unique expression patterns of 5-HT$_{2A}$ and 5-HT$_{2C}$ receptors in the

rat brain during postnatal development: Western blot and immunohistochemical analyses. *J Comp Neurol* **469,** 128-140.

Liang Y, Yuan LL, Johnston D & Gray R. (2002). Calcium signaling at single mossy fiber presynaptic terminals in the rat hippocampus. *J Neurophysiol* **87,** 1132-1137.

Lidow MS, Goldman-Rakic PS, Gallager DW, Geschwind DH & Rakic P. (1989). Distribution of major neurotransmitter receptors in the motor and somatosensory cortex of the rhesus monkey. *Neuroscience* **32,** 609-627.

Litosch I. (1987). Guanine nucleotide and NaF stimulation of phospholipase C activity in rat cerebral-cortical membranes. Studies on substrate specificity. *Biochem J* **244,** 35-40.

Lodato S & Arlotta P. (2015). Generating neuronal diversity in the mammalian cerebral cortex. *Annu Rev Cell Dev Biol* **31,** 699-720.

Lodato S, Shetty AS & Arlotta P. (2015). Cerebral cortex assembly: generating and reprogramming projection neuron diversity. *Trends Neurosci* **38,** 117-125.

Loewy AD & McKellar S. (1981). Serotonergic projections from the ventral medulla to the intermediolateral cell column in the rat. *Brain Res* **211,** 146-152.

Logothetis DE, Kurachi Y, Galper J, Neer EJ & Clapham DE. (1987). The βγ subunits of GTP-binding proteins activate the muscarinic K^+ channel in heart. *Nature* **325,** 321-326.

Lopez-Gil X, Artigas F & Adell A. (2010). Unraveling monoamine receptors involved in the action of typical and atypical antipsychotics on glutamatergic and serotonergic transmission in prefrontal cortex. *Curr Pharm Des* **16,** 502-515.

Lorenzon NM & Foehring RC. (1993). The ontogeny of repetitive firing and its modulation by norepinephrine in rat neocortical neurons. *Brain Res Dev Brain Res* **73,** 213-223.

Lorenzon NM & Foehring RC. (1995). Alterations in intracellular calcium chelation reproduce developmental differences in repetitive firing and afterhyperpolarizations in rat neocortical neurons. *Brain Res Dev Brain Res* **84,** 192-203.

Lotersztajn S, Pavoine C, Deterre P, Capeau J, Mallat A, LeNguyen D, Dufour M, Rouot B, Bataille D & Pecker F. (1992). Role of G protein βγ subunits in the regulation of the plasma membrane Ca^{2+} pump. *J Biol Chem* **267,** 2375-2379.

Lottem E, Lorincz ML & Mainen ZF. (2016). Optogenetic activation of dorsal raphe serotonin neurons rapidly inhibits spontaneous but not odor-evoked activity in olfactory cortex. *J Neurosci* **36,** 7-18.

Loughlin SE, Foote SL & Grzanna R. (1986). Efferent projections of nucleus locus coeruleus: morphologic subpopulations have different efferent targets. *Neuroscience* **18,** 307-319.

Lowther S, De Paermentier F, Crompton MR & Horton RW. (1992). The distribution of 5-HT_{1D} and 5-HT_{1E} binding sites in human brain. *Eur J Pharmacol* **222,** 137-142.

Lübke J, Roth A, Feldmeyer D & Sakmann B. (2003). Morphometric analysis of the columnar innervation domain of neurons connecting layer 4 and layer 2/3 of juvenile rat barrel cortex. *Cereb Cortex* **13,** 1051-1063.

Lucaites VL, Krushinski JH, Schaus JM, Audia JE & Nelson DL. (2005). [^{3}H]LY334370, a novel radioligand for the 5-HT_{1F} receptor. II. Autoradiographic localization in rat, guinea pig, monkey and human brain. *Naunyn Schmiedebergs Arch Pharmacol* **371,** 178-184.

Lucas G, Rymar VV, Du J, Mnie-Filali O, Bisgaard C, Manta S, Lambas-Senas L, Wiborg O, Haddjeri N, Pineyro G, Sadikot AF & Debonnel G. (2007). Serotonin$_4$ (5-HT_4) receptor agonists are putative antidepressants with a rapid onset of action. *Neuron* **55,** 712-725.

Lucchelli A, Santagostino-Barbone MG, Barbieri A, Candura SM & Tonini M. (1995). The interaction of antidepressant drugs with central and peripheral (enteric) 5-HT_3 and 5-HT_4 receptors. *Br J Pharmacol* **114,** 1017-1025.

Lukasiewicz S, Faron-Gorecka A, Kedracka-Krok S & Dziedzicka-Wasylewska M. (2011). Effect of clozapine on the dimerization of serotonin 5-HT_{2A} receptor and its genetic variant 5-HT_{2A}H425Y with dopamine D_2 receptor. *Eur J Pharmacol* **659,** 114-123.

Lüscher C, Jan LY, Stoffel M, Malenka RC & Nicoll RA. (1997). G protein-coupled inwardly rectifying K^+ channels (GIRKs) mediate postsynaptic but not presynaptic transmitter actions in hippocampal neurons. *Neuron* **19,** 687-695.

Lüscher C, Xia H, Beattie EC, Carroll RC, von Zastrow M, Malenka RC & Nicoll RA. (1999). Role of AMPA receptor cycling in synaptic transmission and plasticity. *Neuron* **24,** 649-658.

Lutz PE. (2013). Multiple serotonergic paths to antidepressant efficacy. *J Neurophysiol* **109,** 2245-2249.

Ma J, Ye N & Cohen BM. (2006). Expression of noradrenergic α1, serotoninergic 5HT2a and dopaminergic D2 receptors on neurons activated by typical and atypical antipsychotic drugs. *Prog Neuropsychopharmacol Biol Psychiatry* **30,** 647-657.

Madison DV & Nicoll RA. (1982). Noradrenaline blocks accommodation of pyramidal cell discharge in the hippocampus. *Nature* **299,** 636-638.

Maeshima T, Ito R, Hamada S, Senzaki K, Hamaguchi-Hamada K, Shutoh F & Okado N. (1998). The cellular localization of 5-HT_{2A} receptors in the spinal cord and spinal ganglia of the adult rat. *Brain Res* **797,** 118-124.

Malinow R & Tsien RW. (1990). Presynaptic enhancement shown by whole-cell recordings of long-term potentiation in hippocampal slices. *Nature* **346,** 177-180.

Maravall M, Stern EA & Svoboda K. (2004). Development of intrinsic properties and excitability of layer 2/3 pyramidal neurons during a critical period for sensory maps in rat barrel cortex. *J Neurophysiol* **92,** 144-156.

Marchetti C, Carbone E & Lux HD. (1986). Effects of dopamine and noradrenaline on Ca channels of cultured sensory and sympathetic neurons of chick. *Pflugers Arch* **406,** 104-111.

Marchetti-Gauthier E, Roman FS, Dumuis A, Bockaert J & Soumireu-Mourat B. (1997). BIMU1 increases associative memory in rats by activating 5-HT_4 receptors. *Neuropharmacology* **36,** 697-706.

Marek GJ & Aghajanian GK. (1998). 5-Hydroxytryptamine-induced excitatory postsynaptic currents in neocortical layer V pyramidal cells: suppression by μ-opiate receptor activation. *Neuroscience* **86,** 485-497.

Marek GJ & Aghajanian GK. (1999). 5-HT_{2A} receptor or α_1-adrenoceptor activation induces excitatory postsynaptic currents in layer V pyramidal cells of the medial prefrontal cortex. *Eur J Pharmacol* **367,** 197-206.

Markram H & Tsodyks M. (1996). Redistribution of synaptic efficacy between neocortical pyramidal neurons. *Nature* **382,** 807-810.

Martin KC, Michael D, Rose JC, Barad M, Casadio A, Zhu H & Kandel ER. (1997). MAP kinase translocates into the nucleus of the presynaptic cell and is required for long-term facilitation in *Aplysia*. *Neuron* **18,** 899-912.

Maruyama T, Kanaji T, Nakade S, Kanno T & Mikoshiba K. (1997). 2APB, 2-aminoethoxydiphenyl borate, a membrane-penetrable modulator of Ins(1,4,5)P_3-induced Ca^{2+} release. *J Biochem* **122,** 498-505.

Mateo Z & Porter JT. (2007). Group II metabotropic glutamate receptors inhibit glutamate release at thalamocortical synapses in the developing somatosensory cortex. *Neuroscience* **146,** 1062-1072.

Mathie A. (2007). Neuronal two-pore-domain potassium channels and their regulation by G protein-coupled receptors. *J Physiol* **578,** 377-385.

Mathur BN, Capik NA, Alvarez VA & Lovinger DM. (2011). Serotonin induces long-term depression at corticostriatal synapses. *J Neurosci* **31,** 7402-7411.

Mayer ML. (2006). Glutamate receptors at atomic resolution. *Nature* **440,** 456-462.

McBain C & Dingledine R. (1992). Dual-component miniature excitatory synaptic currents in rat hippocampal CA3 pyramidal neurons. *J Neurophysiol* **68,** 16-27.

McCormick DA & Pape HC. (1990). Noradrenergic and serotonergic modulation of a hyperpolarization-activated cation current in thalamic relay neurones. *J Physiol* **431,** 319-342.

McCormick DA, Pape HC & Williamson A. (1991). Actions of norepinephrine in the cerebral cortex and thalamus: implications for function of the central noradrenergic system. *Prog Brain Res* **88,** 293-305.

McKinney RA, Capogna M, Durr R, Gahwiler BH & Thompson SM. (1999). Miniature synaptic events maintain dendritic spines via AMPA receptor activation. *Nat Neurosci* **2,** 44-49.

Medvedev GS. (2009). Electrical coupling promotes fidelity of responses in the networks of model neurons. *Neural Comput* **21,** 3057-3078.

Mengod G, Nguyen H, Le H, Waeber C, Lubbert H & Palacios JM. (1990). The distribution and cellular localization of the serotonin 1C receptor mRNA in the rodent brain examined by *in situ* hybridization histochemistry. Comparison with receptor binding distribution. *Neuroscience* **35,** 577-591.

Mengod G, Vilaro MT, Raurich A, Lopez-Gimenez JF, Cortes R & Palacios JM. (1996). 5-HT receptors in mammalian brain: receptor autoradiography and in situ hybridization studies of new ligands and newly identified receptors. *Histochem J* **28,** 747-758.

Merriam EB, Netoff TI & Banks MI. (2005). Bistable network behavior of layer I interneurons in auditory cortex. *J Neurosci* **25,** 6175-6186.

Middlemiss DN & Hutson PH. (1990). The 5-HT_{1B} receptors. *Ann N Y Acad Sci* **600,** 132-147; discussion 347-148.

Mirotznik RR, Zheng X & Stanley EF. (2000). G-Protein types involved in calcium channel inhibition at a presynaptic nerve terminal. *J Neurosci* **20,** 7614-7621.

Mitchell HA & Weinshenker D. (2010). Good night and good luck: norepinephrine in sleep pharmacology. *Biochem Pharmacol* **79,** 801-809.

Mitrano DA, Schroeder JP, Smith Y, Cortright JJ, Bubula N, Vezina P & Weinshenker D. (2012). alpha-1 Adrenergic receptors are localized on presynaptic elements in the nucleus accumbens and regulate mesolimbic dopamine transmission. *Neuropsychopharmacology* **37,** 2161-2172.

Mogami H, Lloyd Mills C & Gallacher DV. (1997). Phospholipase C inhibitor, U73122, releases intracellular Ca^{2+}, potentiates Ins(1,4,5)P_3-mediated Ca^{2+} release and directly activates ion channels in mouse pancreatic acinar cells. *Biochem J* **324 (Pt 2),** 645-651.

Mohan A, McDonnell MD & Stricker C. (2013). Interaction of short-term depression and firing dynamics in shaping single neuron encoding. *Front Comput Neurosci* **7,** 41.

Mohrmann R, Werner M, Hatt H & Gottmann K. (1999). Target-specific factors regulate the formation of glutamatergic transmitter release sites in cultured neocortical neurons. *J Neurosci* **19,** 10004-10013.

Molyneaux BJ, Arlotta P, Menezes JR & Macklis JD. (2007). Neuronal subtype specification in the cerebral cortex. *Nat Rev Neurosci* **8,** 427-437.

Monyer H, Sprengel R, Schoepfer R, Herb A, Higuchi M, Lomeli H, Burnashev N, Sakmann B & Seeburg PH. (1992). Heteromeric NMDA receptors: molecular and functional distinction of subtypes. *Science* **256,** 1217-1221.

Moreno JL, Muguruza C, Umali A, Mortillo S, Holloway T, Pilar-Cuellar F, Mocci G, Seto J, Callado LF, Neve RL, Milligan G, Sealfon SC, Lopez-Gimenez JF,

Meana JJ, Benson DL & Gonzalez-Maeso J. (2012). Identification of three residues essential for 5-hydroxytryptamine 2A-metabotropic glutamate 2 (5-HT_{2A}.mGlu2) receptor heteromerization and its psychoactive behavioral function. *J Biol Chem* **287,** 44301-44319.

Morilak DA & Ciaranello RD. (1993). Ontogeny of 5-hydroxytryptamine$_2$ receptor immunoreactivity in the developing rat brain. *Neuroscience* **55,** 869-880.

Moutkine I, Quentin E, Guiard BP, Maroteaux L & Doly S. (2017). Heterodimers of serotonin receptor subtypes 2 are driven by 5-HT_{2C} protomers. *J Biol Chem*.

Myme CI, Sugino K, Turrigiano GG & Nelson SB. (2003). The NMDA-to-AMPA ratio at synapses onto layer 2/3 pyramidal neurons is conserved across prefrontal and visual cortices. *J Neurophysiol* **90,** 771-779.

Nicholas AP, Pieribone VA, Elde R & Hokfelt T. (1991). Initial observations on the localization of mRNA for *α* and *β* adrenergic receptors in brain and peripheral tissues of rat using *in situ* hybridization. *Mol Cell Neurosci* **2,** 344-350.

Nishijo T & Momiyama T. (2016). Serotonin 5-HT_{1B} receptor-mediated calcium influx-independent presynaptic inhibition of GABA release onto rat basal forebrain cholinergic neurons. *Eur J Neurosci* **44,** 1747-1760.

Niswender CM, Copeland SC, Herrick-Davis K, Emeson RB & Sanders-Bush E. (1999). RNA editing of the human serotonin 5-hydroxytryptamine 2C receptor silences constitutive activity. *J Biol Chem* **274,** 9472-9478.

Nocjar C, Alex KD, Sonneborn A, Abbas AI, Roth BL & Pehek EA. (2015). Serotonin-2C and -2a receptor co-expression on cells in the rat medial prefrontal cortex. *Neuroscience* **297,** 22-37.

North RA & Uchimura N. (1989). 5-Hydroxytryptamine acts at 5-HT2 receptors to decrease potassium conductance in rat nucleus accumbens neurones. *J Physiol* **417,** 1-12.

Nozaki K, Kubo R & Furukawa Y. (2016). Serotonin modulates the excitatory synaptic transmission in the dentate granule cells. *J Neurophysiol* **115,** 2997-3007.

Nygren LG & Olson L. (1977). A new major projection from locus coeruleus: the main source of noradrenergic nerve terminals in the ventral and dorsal columns of the spinal cord. *Brain Res* **132,** 85-93.

O'Dell TJ, Connor SA, Guglietta R & Nguyen PV. (2015). β-Adrenergic receptor signaling and modulation of long-term potentiation in the mammalian hippocampus. *Learn Mem* **22,** 461-471.

Ohno Y, Sofue N, Imaoku T, Morishita E, Kumafuji K, Sasa M & Serikawa T. (2010). Serotonergic modulation of absence-like seizures in groggy rats: a novel rat model of absence epilepsy. *J Pharmacol Sci* **114,** 99-105.

Olivier B. (2015). Serotonin: a never-ending story. *Eur J Pharmacol* **753,** 2-18.

Olson L & Fuxe K. (1971). On the projections from the locus coeruleus noradrealine neurons: the cerebellar innervation. *Brain Res* **28,** 165-171.

Opal MD, Klenotich SC, Morais M, Bessa J, Winkle J, Doukas D, Kay LJ, Sousa N & Dulawa SM. (2014). Serotonin 2C receptor antagonists induce fast-onset antidepressant effects. *Mol Psychiatry* **19,** 1106-1114.

Otis TS, Staley KJ & Mody I. (1991). Perpetual inhibitory activity in mammalian brain slices generated by spontaneous GABA release. *Brain Res* **545,** 142-150.

Ouanounou A, Zhang L, Tymianski M, Charlton MP, Wallace MC & Carlen PL. (1996). Accumulation and extrusion of permeant Ca^{2+} chelators in attenuation of synaptic transmission at hippocampal CA1 neurons. *Neuroscience* **75,** 99-109.

Ozaki N, Manji H, Lubierman V, Lu SJ, Lappalainen J, Rosenthal NE & Goldman D. (1997). A naturally occurring amino acid substitution of the human serotonin 5-HT_{2A} receptor influences amplitude and timing of intracellular calcium mobilization. *J Neurochem* **68,** 2186-2193.

Palacios JM, Pazos A & Hoyer D. (2017). A short history of the 5-HT_{2C} receptor: from the choroid plexus to depression, obesity and addiction treatment. *Psychopharmacology (Berl)* **234,** 1395-1418.

Palacios JM, Probst A & Cortes R. (1983). The distribution of serotonin receptors in the human brain: high density of [^{3}H]LSD binding sites in the raphe nuclei of the brainstem. *Brain Res* **274,** 150-155.

Palay SL. (1956). Synapses in the central nervous system. *J Biophys Biochem Cytol* **2,** 193-202.

Palmer LM & Stuart GJ. (2006). Site of action potential initiation in layer 5 pyramidal neurons. *J Neurosci* **26,** 1854-1863.

Pan ZZ, Wessendorf MW & Williams JT. (1993). Modulation by serotonin of the neurons in rat nucleus raphe magnus *in vitro*. *Neuroscience* **54,** 421-429.

Papay R, Gaivin R, Jha A, McCune DF, McGrath JC, Rodrigo MC, Simpson PC, Doze VA & Perez DM. (2006). Localization of the mouse α_{1A}-adrenergic receptor (AR) in the brain: α_{1A}AR is expressed in neurons, GABAergic interneurons, and NG2 oligodendrocyte progenitors. *J Comp Neurol* **497,** 209-222.

Pape HC & McCormick DA. (1989). Noradrenaline and serotonin selectively modulate thalamic burst firing by enhancing a hyperpolarization-activated cation current. *Nature* **340,** 715-718.

Pare D, Shink E, Gaudreau H, Destexhe A & Lang EJ. (1998). Impact of spontaneous synaptic activity on the resting properties of cat neocortical pyramidal neurons In vivo. *J Neurophysiol* **79,** 1450-1460.

Park YK, Galik J, Ryu PD & Randic M. (2004). Activation of presynaptic group I metabotropic glutamate receptors enhances glutamate release in the rat spinal cord substantia gelatinosa. *Neurosci Lett* **361,** 220-224.

Parkinson D, Coscia E & Daw NW. (1988). Identification and localization of adrenergic receptors in cat visual cortex. *Brain Res* **457,** 70-78.

Parpura V, Basarsky TA, Liu F, Jeftinija K, Jeftinija S & Haydon PG. (1994). Glutamate-mediated astrocyte-neuron signalling. *Nature* **369,** 744-747.

Pasti L, Volterra A, Pozzan T & Carmignoto G. (1997). Intracellular calcium oscillations in astrocytes: a highly plastic, bidirectional form of communication between neurons and astrocytes *in situ*. *J Neurosci* **17,** 7817-7830.

Pazos A, Probst A & Palacios JM. (1987). Serotonin receptors in the human brain--III. Autoradiographic mapping of serotonin-1 receptors. *Neuroscience* **21,** 97-122.

Peinado A, Yuste R & Katz LC. (1993). Extensive dye coupling between rat neocortical neurons during the period of circuit formation. *Neuron* **10,** 103-114.

Penington NJ, Kelly JS & Fox AP. (1991). A study of the mechanism of Ca^{2+} current inhibition produced by serotonin in rat dorsal raphe neurons. *J Neurosci* **11,** 3594-3609.

Pereda AE, Curti S, Hoge G, Cachope R, Flores CE & Rash JE. (2013). Gap junction-mediated electrical transmission: regulatory mechanisms and plasticity. *Biochim Biophys Acta* **1828,** 134-146.

Peroutka SJ & Snyder SH. (1979). Multiple serotonin receptors: differential binding of [^{3}H]5-hydroxytryptamine, [^{3}H]lysergic acid diethylamide and [^{3}H]spiroperidol. *Mol Pharmacol* **16,** 687-699.

Perrais D, Veran J & Mulle C. (2010). Gating and permeation of kainate receptors: differences unveiled. *Trends Pharmacol Sci* **31,** 516-522.

Peter D, Liu Y, Sternini C, de Giorgio R, Brecha N & Edwards RH. (1995). Differential expression of two vesicular monoamine transporters. *J Neurosci* **15,** 6179-6188.

Petersen CC & Sakmann B. (2001). Functionally independent columns of rat somatosensory barrel cortex revealed with voltage-sensitive dye imaging. *J Neurosci* **21,** 8435-8446.

Pfister C & Goworek K. (1978). [Effects of 5-hydroxytryptamine creatinine sulfate on development of the in vitro cultivated explants of the cerebrocortex of neonatal rats (author's transl)]. *Acta Histochem* **63,** 137-148.

Photowala H, Blackmer T, Schwartz E, Hamm HE & Alford S. (2006). G protein βγ-subunits activated by serotonin mediate presynaptic inhibition by regulating vesicle fusion properties. *Proc Natl Acad Sci U S A* **103,** 4281-4286.

Piomelli D, Volterra A, Dale N, Siegelbaum SA, Kandel ER, Schwartz JH & Belardetti F. (1987). Lipoxygenase metabolites of arachidonic acid as second messengers for presynaptic inhibition of *Aplysia* sensory cells. *Nature* **328,** 38-43.

Plested AJ, Vijayan R, Biggin PC & Mayer ML. (2008). Molecular basis of kainate receptor modulation by sodium. *Neuron* **58,** 720-735.

Plummer MR, Rittenhouse A, Kanevsky M & Hess P. (1991). Neurotransmitter modulation of calcium channels in rat sympathetic neurons. *J Neurosci* **11,** 2339-2348.

Pompeiano M, Palacios JM & Mengod G. (1994). Distribution of the serotonin 5-HT_2 receptor family mRNAs: comparison between 5-HT_{2A} and 5-HT_{2C} receptors. *Brain Res Mol Brain Res* **23,** 163-178.

Powis G, Seewald MJ, Gratas C, Melder D, Riebow J & Modest EJ. (1992). Selective inhibition of phosphatidylinositol phospholipase C by cytotoxic ether lipid analogues. *Cancer Res* **52,** 2835-2840.

Price RD & Sanders-Bush E. (2000). RNA editing of the human serotonin 5-HT_{2C} receptor delays agonist-stimulated calcium release. *Mol Pharmacol* **58,** 859-862.

Pusch M & Neher E. (1988). Rates of diffusional exchange between small cells and a measuring patch pipette. *Pflugers Arch* **411,** 204-211.

Pytliak M, Vargova V, Mechirova V & Felsoci M. (2011). Serotonin receptors - from molecular biology to clinical applications. *Physiol Res* **60,** 15-25.

Qi YX, Xia RY, Wu YS, Stanley D, Huang J & Ye GY. (2014). Larvae of the small white butterfly, Pieris rapae, express a novel serotonin receptor. *J Neurochem* **131,** 767-777.

Qian J & Noebels JL. (2001). Presynaptic Ca^{2+} channels and neurotransmitter release at the terminal of a mouse cortical neuron. *J Neurosci* **21,** 3721-3728.

Quinn JC, Johnson-Farley NN, Yoon J & Cowen DS. (2002). Activation of extracellular-regulated kinase by 5-hydroxytryptamine$_{2A}$ receptors in PC12 cells is protein kinase C-independent and requires calmodulin and tyrosine kinases. *J Pharmacol Exp Ther* **303,** 746-752.

Qvigstad E, Sjaastad I, Brattelid T, Nunn C, Swift F, Birkeland JA, Krobert KA, Andersen GO, Sejersted OM, Osnes JB, Levy FO & Skomedal T. (2005). Dual serotonergic regulation of ventricular contractile force through 5-HT_{2A} and 5-HT_4 receptors induced in the acute failing heart. *Circ Res* **97,** 268-276.

Rainbow TC, Parsons B & Wolfe BB. (1984). Quantitative autoradiography of β_1- and β_2-adrenergic receptors in rat brain. *Proc Natl Acad Sci U S A* **81,** 1585-1589.

Rainnie DG. (1999). Serotonergic modulation of neurotransmission in the rat basolateral amygdala. *J Neurophysiol* **82,** 69-85.

Ramirez DM, Khvotchev M, Trauterman B & Kavalali ET. (2012). Vti1a identifies a vesicle pool that preferentially recycles at rest and maintains spontaneous neurotransmission. *Neuron* **73,** 121-134.

Ramón y Cajal S. (1904). *La textura del sistema nerviosa del hombre y los vertebrados*. Moya, Madrid.

Raote I, Bhattacharyya S & Panicker MM. (2013). Functional selectivity in serotonin receptor 2A (5-HT_{2A}) endocytosis, recycling, and phosphorylation. *Mol Pharmacol* **83,** 42-50.

Rash BG & Grove EA. (2006). Area and layer patterning in the developing cerebral cortex. *Curr Opin Neurobiol* **16,** 25-34.

Ray TS. (2010). Psychedelics and the human receptorome. *PLoS One* **5,** e9019.

Regan MC, Romero-Hernandez A & Furukawa H. (2015). A structural biology perspective on NMDA receptor pharmacology and function. *Curr Opin Struct Biol* **33,** 68-75.

Reyes A, Lujan R, Rozov A, Burnashev N, Somogyi P & Sakmann B. (1998). Target-cell-specific facilitation and depression in neocortical circuits. *Nat Neurosci* **1,** 279-285.

Reyes A & Sakmann B. (1999). Developmental switch in the short-term modification of unitary EPSPs evoked in layer 2/3 and layer 5 pyramidal neurons of rat neocortex. *J Neurosci* **19,** 3827-3835.

Rhee SG. (2001). Regulation of phosphoinositide-specific phospholipase C. *Annu Rev Biochem* **70,** 281-312.

Rhee SG & Bae YS. (1997). Regulation of phosphoinositide-specific phospholipase C isozymes. *J Biol Chem* **272,** 15045-15048.

Riahi G, Morissette M, Samadi P, Parent M & Di Paolo T. (2013). Basal ganglia serotonin 1B receptors in parkinsonian monkeys with L-DOPA-induced dyskinesia. *Biochem Pharmacol* **86,** 970-978.

Rosse G & Schaffhauser H. (2010). 5-HT_6 receptor antagonists as potential therapeutics for cognitive impairment. *Curr Top Med Chem* **10,** 207-221.

Roth BL, Palvimaki EP, Berry S, Khan N, Sachs N, Uluer A & Choudhary MS. (1995). 5-Hydroxytryptamine$_{2A}$ (5-HT_{2A}) receptor desensitization can occur without down-regulation. *J Pharmacol Exp Ther* **275,** 1638-1646.

Roychowdhury S, Zwierzchowski AN, Garcia-Oscos F, Olguin RC, Delgado RS & Atzori M. (2014). Layer- and area-specificity of the adrenergic modulation of synaptic transmission in the rat neocortex. *Neurochem Res* **39,** 2377-2384.

Rozov A, Burnashev N, Sakmann B & Neher E. (2001). Transmitter release modulation by intracellular Ca^{2+} buffers in facilitating and depressing nerve terminals of pyramidal cells in layer 2/3 of the rat neocortex indicates a target cell-specific difference in presynaptic calcium dynamics. *J Physiol* **531,** 807-826.

Ruat M, Molliver ME, Snowman AM & Snyder SH. (1995). Calcium sensing receptor: molecular cloning in rat and localization to nerve terminals. *Proc Natl Acad Sci U S A* **92,** 3161-3165.

Ruat M, Traiffort E, Arrang JM, Tardivel-Lacombe J, Diaz J, Leurs R & Schwartz JC. (1993a). A novel rat serotonin (5-HT_6) receptor: molecular cloning, localization and stimulation of cAMP accumulation. *Biochem Biophys Res Commun* **193,** 268-276.

Ruat M, Traiffort E, Leurs R, Tardivel-Lacombe J, Diaz J, Arrang JM & Schwartz JC. (1993b). Molecular cloning, characterization, and localization of a high-affinity serotonin receptor (5-HT_7) activating cAMP formation. *Proc Natl Acad Sci U S A* **90,** 8547-8551.

Rubio ME, Fukazawa Y, Kamasawa N, Clarkson C, Molnar E & Shigemoto R. (2014). Target- and input-dependent organization of AMPA and NMDA receptors in synaptic connections of the cochlear nucleus. *J Comp Neurol* **522,** 4023-4042.

Rudnick G. (2006). Serotonin transporters--structure and function. *J Membr Biol* **213,** 101-110.

Ryu SH, Kim UH, Wahl MI, Brown AB, Carpenter G, Huang KP & Rhee SG. (1990). Feedback regulation of phospholipase C-*β* by protein kinase C. *J Biol Chem* **265,** 17941-17945.

Sadalge A, Coughlin L, Fu H, Wang B, Valladares O, Valentino R & Blendy JA. (2003). α1d Adrenoceptor signaling is required for stimulus induced locomotor activity. *Mol Psychiatry* **8,** 664-672.

Sadana R & Dessauer CW. (2009). Physiological roles for G protein-regulated adenylyl cyclase isoforms: insights from knockout and overexpression studies. *Neurosignals* **17,** 5-22.

Saka S & Rizzoli SO. (2012). Super-resolution imaging prompts re-thinking of cell biology mechanisms: selected cases using stimulated emission depletion microscopy. *Bioessays* **34,** 386-395.

Salgado H, Trevino M & Atzori M. (2016). Layer- and area-specific actions of norepinephrine on cortical synaptic transmission. *Brain Res* **1641,** 163-176.

Sallese M, Mariggio S, D'Urbano E, Iacovelli L & De Blasi A. (2000). Selective regulation of Gq signaling by G protein-coupled receptor kinase 2: direct interaction of kinase N terminus with activated Gαq. *Mol Pharmacol* **57,** 826-831.

Sandén N, Thorlin T, Blomstrand F, Persson PA & Hansson E. (2000). 5-Hydroxytryptamine$_{2B}$ receptors stimulate Ca^{2+} increases in cultured astrocytes from three different brain regions. *Neurochem Int* **36,** 427-434.

Sangare A, Dubourget R, Geoffroy H, Gallopin T & Rancillac A. (2016). Serotonin differentially modulates excitatory and inhibitory synaptic inputs to putative sleep-promoting neurons of the ventrolateral preoptic nucleus. *Neuropharmacology* **109,** 29-40.

Santana N, Mengod G & Artigas F. (2013). Expression of α_1-adrenergic receptors in rat prefrontal cortex: cellular co-localization with 5-HT_{2A} receptors. *Int J Neuropsychopharmacol* **16,** 1139-1151.

Satake T, Mitani H, Nakagome K & Kaneko K. (2008). Individual and additive effects of neuromodulators on the slow components of afterhyperpolarization currents in layer V pyramidal cells of the rat medial prefrontal cortex. *Brain Res* **1229,** 47-60.

Scanziani M, Gahwiler BH & Charpak S. (1998). Target cell-specific modulation of transmitter release at terminals from a single axon. *Proc Natl Acad Sci U S A* **95,** 12004-12009.

Scanziani M, Gahwiler BH & Thompson SM. (1993). Presynaptic inhibition of excitatory synaptic transmission mediated by *α* adrenergic receptors in area CA3 of the rat hippocampus in vitro. *J Neurosci* **13,** 5393-5401.

Scanziani M, Malenka RC & Nicoll RA. (1996). Role of intercellular interactions in heterosynaptic long-term depression. *Nature* **380,** 446-450.

Scheinin M, Lomasney JW, Hayden-Hixson DM, Schambra UB, Caron MG, Lefkowitz RJ & Fremeau RT, Jr. (1994). Distribution of α_2-adrenergic receptor subtype gene expression in rat brain. *Brain Res Mol Brain Res* **21,** 133-149.

Schellekens H, De Francesco PN, Kandil D, Theeuwes WF, McCarthy T, van Oeffelen WE, Perello M, Giblin L, Dinan TG & Cryan JF. (2015). Ghrelin's orexigenic effect is modulated via a serotonin 2C receptor interaction. *ACS Chem Neurosci* **6,** 1186-1197.

Schellekens H, van Oeffelen WE, Dinan TG & Cryan JF. (2013). Promiscuous dimerization of the growth hormone secretagogue receptor (GHS-R1a) attenuates ghrelin-mediated signaling. *J Biol Chem* **288,** 181-191.

Schinder AF, Berninger B & Poo M. (2000). Postsynaptic target specificity of neurotrophin-induced presynaptic potentiation. *Neuron* **25,** 151-163.

Schmitz D, Gloveli T, Empson RM, Draguhn A & Heinemann U. (1998). Serotonin reduces synaptic excitation in the superficial medial entorhinal cortex of the rat via a presynaptic mechanism. *J Physiol* **508 (Pt 1),** 119-129.

Schoch S, Deak F, Konigstorfer A, Mozhayeva M, Sara Y, Sudhof TC & Kavalali ET. (2001). SNARE function analyzed in synaptobrevin/VAMP knockout mice. *Science* **294,** 1117-1122.

Schroeder BC, Hechenberger M, Weinreich F, Kubisch C & Jentsch TJ. (2000). KCNQ5, a novel potassium channel broadly expressed in brain, mediates M-type currents. *J Biol Chem* **275,** 24089-24095.

Schwartz EJ, Blackmer T, Gerachshenko T & Alford S. (2007). Presynaptic G-protein-coupled receptors regulate synaptic cleft glutamate via transient vesicle fusion. *J Neurosci* **27,** 5857-5868.

Schwendt M & McGinty JF. (2010). Amphetamine up-regulates activator of G-protein signaling 1 mRNA and protein levels in rat frontal cortex: the role of dopamine and glucocorticoid receptors. *Neuroscience* **168,** 96-107.

Segal M. (1980). The action of serotonin in the rat hippocampal slice preparation. *J Physiol* **303,** 423-439.

Shapiro MS & Gamper N. (2009). Regulation of Neuronal Ion Channels by G-Protein-Coupled Receptors in Sympathetic Neurons. In *Structure, Function, and Modulation of Neuronal Voltage-Gated Ion Channels*, ed. Gribkoff VK & Kaczmarek LK, pp. 291 – 316. Wiley & Sons, Inc., Hoboken, New Jersey.

Sharp T & Hjorth S. (1990). Application of brain microdialysis to study the pharmacology of the 5-HT_{1A} autoreceptor. *J Neurosci Methods* **34,** 83-90.

Sheffler DJ, Kroeze WK, Garcia BG, Deutch AY, Hufeisen SJ, Leahy P, Bruning JC & Roth BL. (2006). p90 ribosomal S6 kinase 2 exerts a tonic brake on G protein-coupled receptor signaling. *Proc Natl Acad Sci U S A* **103,** 4717-4722.

Shen K. (2004). Molecular mechanisms of target specificity during synapse formation. *Curr Opin Neurobiol* **14,** 83-88.

Shen KZ & Johnson SW. (2003). Group II metabotropic glutamate receptor modulation of excitatory transmission in rat subthalamic nucleus. *J Physiol* **553,** 489-496.

Shen Y, Monsma FJ, Jr., Metcalf MA, Jose PA, Hamblin MW & Sibley DR. (1993). Molecular cloning and expression of a 5-hydroxytryptamine$_7$ serotonin receptor subtype. *J Biol Chem* **268,** 18200-18204.

Shi J, Zemaitaitis B & Muma NA. (2007). Phosphorylation of $G_{\alpha 11}$ protein contributes to agonist-induced desensitization of 5-HT_{2A} receptor signaling. *Mol Pharmacol* **71,** 303-313.

Shih JC. (1991). Molecular basis of human MAO A and B. *Neuropsychopharmacology* **4,** 1-7.

Shih JC & Chen K. (1999). MAO-A and -B gene knock-out mice exhibit distinctly different behavior. *Neurobiology (Bp)* **7,** 235-246.

Shih JC, Chen K & Ridd MJ. (1999a). Monoamine oxidase: from genes to behavior. *Annu Rev Neurosci* **22,** 197-217.

Shih JC, Chen K & Ridd MJ. (1999b). Role of MAO A and B in neurotransmitter metabolism and behavior. *Pol J Pharmacol* **51,** 25-29.

Shimohama S, Sumida Y, Fujimoto S, Matsuoka Y, Taniguchi T, Takenawa T & Kimura J. (1998). Differential expression of rat brain phospholipase C isozymes in development and aging. *Biochem Biophys Res Commun* **243,** 210-216.

Simkus CR & Stricker C. (2002a). The contribution of intracellular calcium stores to mEPSCs recorded in layer II neurones of rat barrel cortex. *J Physiol* **545,** 521-535.

Simkus CR & Stricker C. (2002b). Properties of mEPSCs recorded in layer II neurones of rat barrel cortex. *J Physiol* **545,** 509-520.

Simons DJ & Woolsey TA. (1984). Morphology of Golgi-Cox-impregnated barrel neurons in rat SmI cortex. *J Comp Neurol* **230,** 119-132.

Singer JH, Bellingham MC & Berger AJ. (1996). Presynaptic inhibition of glutamatergic synaptic transmission to rat motoneurons by serotonin. *J Neurophysiol* **76,** 799-807.

Spruston N, Jaffe DB, Williams SH & Johnston D. (1993). Voltage- and space-clamp errors associated with the measurement of electrotonically remote synaptic events. *J Neurophysiol* **70,** 781-802.

Steinbusch HW. (1981). Distribution of serotonin-immunoreactivity in the central nervous system of the rat-cell bodies and terminals. *Neuroscience* **6,** 557-618.

Stephens EK, Avesar D & Gulledge AT. (2014). Activity-dependent serotonergic excitation of callosal projection neurons in the mouse prefrontal cortex. *Front Neural Circuits* **8,** 97.

Stephens L, Smrcka A, Cooke FT, Jackson TR, Sternweis PC & Hawkins PT. (1994). A novel phosphoinositide 3 kinase activity in myeloid-derived cells is activated by G protein βγ subunits. *Cell* **77,** 83-93.

Sternweis PC & Smrcka AV. (1992). Regulation of phospholipase C by G proteins. *Trends Biochem Sci* **17,** 502-506.

Stott JB, Povstyan OV, Carr G, Barrese V & Greenwood IA. (2015). G-protein βγ subunits are positive regulators of Kv7.4 and native vascular Kv7 channel activity. *Proc Natl Acad Sci U S A* **112,** 6497-6502.

Stout BD, Clarke WP & Berg KA. (2002). Rapid desensitization of the serotonin$_{2C}$ receptor system: effector pathway and agonist dependence. *J Pharmacol Exp Ther* **302,** 957-962.

Strachan RT, Allen JA, Sheffler DJ & Roth BL. (2010). p90 Ribosomal S6 kinase 2, a novel GPCR kinase, is required for growth factor-mediated attenuation of GPCR signaling. *Biochemistry* **49,** 2657-2671.

Strachan RT, Sheffler DJ, Willard B, Kinter M, Kiselar JG & Roth BL. (2009). Ribosomal S6 kinase 2 directly phosphorylates the 5-hydroxytryptamine 2A (5-HT$_{2A}$) serotonin receptor, thereby modulating 5-HT$_{2A}$ signaling. *J Biol Chem* **284,** 5557-5573.

Strassheim D, Law PY & Loh HH. (1998). Contribution of phospholipase C-*β*3 phosphorylation to the rapid attenuation of opioid-activated phosphoinositide response. *Mol Pharmacol* **53,** 1047-1053.

Strassheim D & Williams CL. (2000). P2Y$_2$ purinergic and M$_3$ muscarinic acetylcholine receptors activate different phospholipase C-*β* isoforms that are uniquely susceptible to protein kinase C-dependent phosphorylation and inactivation. *J Biol Chem* **275,** 39767-39772.

Streb H, Irvine RF, Berridge MJ & Schulz I. (1983). Release of Ca^{2+} from a nonmitochondrial intracellular store in pancreatic acinar cells by inositol-1,4,5-trisphosphate. *Nature* **306,** 67-69.

Stricker C, Cowan AI, Field AC & Redman SJ. (1999). Analysis of NMDA-independent long-term potentiation induced at CA3-CA1 synapses in rat hippocampus *in vitro*. *J Physiol* **520 Pt 2,** 513-525.

Stricker C, Field AC & Redman SJ. (1996a). Changes in quantal parameters of EPSCs in rat CA1 neurones *in vitro* after the induction of long-term potentiation. *J Physiol* **490 (Pt 2),** 443-454.

Stricker C, Field AC & Redman SJ. (1996b). Statistical analysis of amplitude fluctuations in EPSCs evoked in rat CA1 pyramidal neurones in vitro. *J Physiol* **490 (Pt 2),** 419-441.

Stricker C & Redman S. (1994). Statistical models of synaptic transmission evaluated using the expectation-maximization algorithm. *Biophys J* **67,** 656-670.

Stricker C, Redman S & Daley D. (1994). Statistical analysis of synaptic transmission: model discrimination and confidence limits. *Biophys J* **67,** 532-547.

Strowbridge BW, Buckmaster PS & Schwartzkroin PA. (1992). Potentiation of spontaneous synaptic activity in rat mossy cells. *Neurosci Lett* **142,** 205-210.

Stuart GJ, Dodt HU & Sakmann B. (1993). Patch-clamp recordings from the soma and dendrites of neurons in brain slices using infrared video microscopy. *Pflugers Arch* **423,** 511-518.

Sudhof TC. (2012). Calcium control of neurotransmitter release. *Cold Spring Harb Perspect Biol* **4,** a011353.

Sudhof TC. (2013). Neurotransmitter release: the last millisecond in the life of a synaptic vesicle. *Neuron* **80,** 675-690.

Sudhof TC & Rizo J. (2011). Synaptic vesicle exocytosis. *Cold Spring Harb Perspect Biol* **3**.

Sugita S, Hata Y & Sudhof TC. (1996). Distinct Ca^{2+}-dependent properties of the first and second C_2-domains of synaptotagmin I. *J Biol Chem* **271,** 1262-1265.

Sutor B & Hagerty T. (2005). Involvement of gap junctions in the development of the neocortex. *Biochim Biophys Acta* **1719,** 59-68.

Sutton RB, Davletov BA, Berghuis AM, Sudhof TC & Sprang SR. (1995). Structure of the first C_2 domain of synaptotagmin I: a novel Ca^{2+}/phospholipid-binding fold. *Cell* **80,** 929-938.

Swann JW, Smith KL & Brady RJ. (1990). Neural networks and synaptic transmission in immature hippocampus. *Adv Exp Med Biol* **268,** 161-171.

Taber E, Brodal A & Walberg F. (1960). The raphe nuclei of the brain stem in the cat. I. Normal topography and cytoarchitecture and general discussion. *J Comp Neurol* **114,** 161-187.

Takahashi M, Freed R, Blackmer T & Alford S. (2001). Calcium influx-independent depression of transmitter release by 5-HT at lamprey spinal cord synapses. *J Physiol* **532,** 323-336.

Takahashi T & Berger AJ. (1990). Direct excitation of rat spinal motoneurones by serotonin. *J Physiol* **423,** 63-76.

Tanaka E & North RA. (1993). Actions of 5-hydroxytryptamine on neurons of the rat cingulate cortex. *J Neurophysiol* **69,** 1749-1757.

Tang J, Maximov A, Shin OH, Dai H, Rizo J & Sudhof TC. (2006). A complexin/synaptotagmin 1 switch controls fast synaptic vesicle exocytosis. *Cell* **126,** 1175-1187.

Tang WJ & Gilman AG. (1991). Type-specific regulation of adenylyl cyclase by G protein βγ subunits. *Science* **254,** 1500-1503.

Taylor SJ, Chae HZ, Rhee SG & Exton JH. (1991). Activation of the *β*1 isozyme of phospholipase C by *α* subunits of the G_q class of G proteins. *Nature* **350,** 516-518.

Tecott LH, Sun LM, Akana SF, Strack AM, Lowenstein DH, Dallman MF & Julius D. (1995). Eating disorder and epilepsy in mice lacking 5-HT_{2C} serotonin receptors. *Nature* **374,** 542-546.

Tedford HW & Zamponi GW. (2006). Direct G protein modulation of Ca_V2 calcium channels. *Pharmacol Rev* **58,** 837-862.

Thompson W & Dawson RM. (1964). The hydrolysis of triphosphoinositide by extracts of ox brain. *Biochem J* **91,** 233-236.

Timmons SD, Geisert E, Stewart AE, Lorenzon NM & Foehring RC. (2004). α_2-Adrenergic receptor-mediated modulation of calcium current in neocortical pyramidal neurons. *Brain Res* **1014,** 184-196.

Törk I. (1990). Anatomy of the serotonergic system. *Ann N Y Acad Sci* **600,** 9-34; discussion 34-35.

Torres-Escalante JL, Barral JA, Ibarra-Villa MD, Perez-Burgos A, Gongora-Alfaro JL & Pineda JC. (2004). 5-HT_{1A}, 5-HT_2, and $GABA_B$ receptors interact to modulate neurotransmitter release probability in layer 2/3 somatosensory rat cortex as evaluated by the paired pulse protocol. *J Neurosci Res* **78,** 268-278.

Torvik A. (1956). Afferent connections to the sensory trigeminal nuclei, the nucleus of the solitary tract and adjacent structures; an experimental study in the rat. *J Comp Neurol* **106,** 51-141.

Toth K & McBain CJ. (2000). Target-specific expression of pre- and postsynaptic mechanisms. *J Physiol* **525 Pt 1,** 41-51.

Trombley PQ. (1994). Noradrenergic modulation of synaptic transmission between olfactory bulb neurons in culture: implications to olfactory learning. *Brain Res Bull* **35,** 473-484.

Tsintsadze T, Williams CL, Weingarten DJ, von Gersdorff H & Smith SM. (2017). Distinct actions of voltage-activated Ca^{2+} channel block on spontaneous release at excitatory and inhibitory central synapses. *J Neurosci* **37,** 4301-4310.

Tsuchioka M, Takebayashi M, Hisaoka K, Maeda N & Nakata Y. (2008). Serotonin (5-HT) induces glial cell line-derived neurotrophic factor (GDNF) mRNA expression via the transactivation of fibroblast growth factor receptor 2 (FGFR2) in rat C6 glioma cells. *J Neurochem* **106,** 244-257.

Tsumoto T, Kimura F & Nishigori A. (1990). A role of NMDA receptors and Ca^{2+} influx in synaptic plasticity in the developing visual cortex. *Adv Exp Med Biol* **268,** 173-180.

Turrigiano GG, Leslie KR, Desai NS, Rutherford LC & Nelson SB. (1998). Activity-dependent scaling of quantal amplitude in neocortical neurons. *Nature* **391,** 892-896.

Twarog BM & Page IH. (1953). Serotonin content of some mammalian tissues and urine and a method for its determination. *Am J Physiol* **175,** 157-161.

Tyler WJ & Pozzo-Miller L. (2003). Miniature synaptic transmission and BDNF modulate dendritic spine growth and form in rat CA1 neurones. *J Physiol* **553,** 497-509.

Ubach J, Lao Y, Fernandez I, Arac D, Sudhof TC & Rizo J. (2001). The C_2B domain of synaptotagmin I is a Ca^{2+}-binding module. *Biochemistry* **40,** 5854-5860.

Uematsu M, Hirai Y, Karube F, Ebihara S, Kato M, Abe K, Obata K, Yoshida S, Hirabayashi M, Yanagawa Y & Kawaguchi Y. (2008). Quantitative chemical composition of cortical GABAergic neurons revealed in transgenic venus-expressing rats. *Cereb Cortex* **18,** 315-330.

Umemiya M & Berger AJ. (1995). Presynaptic inhibition by serotonin of glycinergic inhibitory synaptic currents in the rat brain stem. *J Neurophysiol* **73,** 1192-1201.

Urban DJ & Roth BL. (2015). DREADDs (designer receptors exclusively activated by designer drugs): chemogenetic tools with therapeutic utility. *Annu Rev Pharmacol Toxicol* **55,** 399-417.

Vaidya VA, Marek GJ, Aghajanian GK & Duman RS. (1997). 5-HT_{2A} receptor-mediated regulation of brain-derived neurotrophic factor mRNA in the hippocampus and the neocortex. *J Neurosci* **17,** 2785-2795.

Valenti O, Conn PJ & Marino MJ. (2002). Distinct physiological roles of the Gq-coupled metabotropic glutamate receptors Co-expressed in the same neuronal populations. *J Cell Physiol* **191,** 125-137.

van Brederode JF, Foehring RC & Spain WJ. (2000). Morphological and electrophysiological properties of atypically oriented layer 2 pyramidal cells of the juvenile rat neocortex. *Neuroscience* **101,** 851-861.

van den Pol AN, Gao XB, Patrylo PR, Ghosh PK & Obrietan K. (1998). Glutamate inhibits GABA excitatory activity in developing neurons. *J Neurosci* **18,** 10749-10761.

Vardar G, Chang S, Arancillo M, Wu YJ, Trimbuch T & Rosenmund C. (2016). Distinct Functions of Syntaxin-1 in Neuronal Maintenance, Synaptic Vesicle Docking, and Fusion in Mouse Neurons. *J Neurosci* **36,** 7911-7924.

Varnäs K, Hall H, Bonaventure P & Sedvall G. (2001). Autoradiographic mapping of 5-HT_{1B} and 5-HT_{1D} receptors in the post mortem human brain using [^{3}H]GR 125743. *Brain Res* **915,** 47-57.

Vertes RP, Fortin WJ & Crane AM. (1999). Projections of the median raphe nucleus in the rat. *J Comp Neurol* **407,** 555-582.

Vervaeke K, Lorincz A, Gleeson P, Farinella M, Nusser Z & Silver RA. (2010). Rapid desynchronization of an electrically coupled interneuron network with sparse excitatory synaptic input. *Neuron* **67,** 435-451.

Vyleta NP & Smith SM. (2011). Spontaneous glutamate release is independent of calcium influx and tonically activated by the calcium-sensing receptor. *J Neurosci* **31,** 4593-4606.

Wadenberg ML, Hertel P, Fernholm R, Hygge Blakeman K, Ahlenius S & Svensson TH. (2000). Enhancement of antipsychotic-like effects by combined treatment with the α_1-adrenoceptor antagonist prazosin and the dopamine D_2 receptor antagonist raclopride in rats. *J Neural Transm (Vienna)* **107,** 1229-1238.

Waeber C, Grailhe R, Yu XJ, Hen R & Moskowitz MA. (1998). Putative 5-ht_5 receptors: localization in the mouse CNS and lack of effect in the inhibition of dural protein extravasation. *Ann N Y Acad Sci* **861,** 85-90.

Walling SG, Milway JS, Ingram M, Lau C, Morrison G & Martin GM. (2016). The effects of prolonged administration of norepinephrine reuptake inhibitors on long-term potentiation in dentate gyrus, and on tests of spatial and object recognition memory in rats. *Neurobiol Learn Mem* **128,** 92-102.

Walther DJ, Peter JU, Bashammakh S, Hortnagl H, Voits M, Fink H & Bader M. (2003). Synthesis of serotonin by a second tryptophan hydroxylase isoform. *Science* **299,** 76.

Wang LY & Kaczmarek LK. (1998). High-frequency firing helps replenish the readily releasable pool of synaptic vesicles. *Nature* **394,** 384-388.

Wang RY & Aghajanian GK. (1977). Inhibiton of neurons in the amygdala by dorsal raphe stimulation: mediation through a direct serotonergic pathway. *Brain Res* **120,** 85-102.

Wang W, Li Q, Zou F, Yu Z, Wang Y, Lu T, Hu T & Cui G. (2013). Increased expression of AGS3 in rat brain cortex after traumatic brain injury. *J Neurosci Res* **91,** 726-736.

Watanabe M, Nakamura M, Sato K, Kano M, Simon MI & Inoue Y. (1998). Patterns of expression for the mRNA corresponding to the four isoforms of phospholipase Cβ in mouse brain. *Eur J Neurosci* **10,** 2016-2025.

Watanabe S & Creutzfeldt OD. (1966). Spontaneous post-synaptic potentials of the nerve cells of the motor cortex of the cat. *Exp Brain Res* **1,** 48-64.

Watts SW. (1996). Serotonin activates the mitogen-activated protein kinase pathway in vascular smooth muscle: use of the mitogen-activated protein kinase kinase inhibitor PD098059. *J Pharmacol Exp Ther* **279,** 1541-1550.

Watts SW, Gackenheimer SL, Gehlert DR & Cohen ML. (1994). Autoradiographic comparison of [^{125}I]LSD-labeled 5-HT_{2A} receptor distribution in rat and guinea pig brain. *Neurochem Int* **24,** 565-574.

Weihe E, Schafer MK, Erickson JD & Eiden LE. (1994). Localization of vesicular monoamine transporter isoforms (VMAT1 and VMAT2) to endocrine cells and neurons in rat. *J Mol Neurosci* **5,** 149-164.

Welker C & Woolsey TA. (1974). Structure of layer IV in the somatosensory neocortex of the rat: description and comparison with the mouse. *J Comp Neurol* **158,** 437-453.

Wells CA, Zurawski Z, Betke KM, Yim YY, Hyde K, Rodriguez S, Alford S & Hamm HE. (2012). G$\beta\gamma$ inhibits exocytosis via interaction with critical residues on soluble N-ethylmaleimide-sensitive factor attachment protein-25. *Mol Pharmacol* **82,** 1136-1149.

Wesolowska A, Nikiforuk A, Stachowicz K & Tatarczynska E. (2006). Effect of the selective 5-HT_7 receptor antagonist SB 269970 in animal models of anxiety and depression. *Neuropharmacology* **51,** 578-586.

Westphal RS, Backstrom JR & Sanders-Bush E. (1995). Increased basal phosphorylation of the constitutively active serotonin 2C receptor accompanies agonist-mediated desensitization. *Mol Pharmacol* **48,** 200-205.

White EL. (1978). Identified neurons in mouse Sml cortex which are postsynaptic to thalamocortical axon terminals: a combined Golgi-electron microscopic and degeneration study. *J Comp Neurol* **181,** 627-661.

Wilhelm BG, Mandad S, Truckenbrodt S, Krohnert K, Schafer C, Rammner B, Koo SJ, Classen GA, Krauss M, Haucke V, Urlaub H & Rizzoli SO. (2014). Composition of isolated synaptic boutons reveals the amounts of vesicle trafficking proteins. *Science* **344,** 1023-1028.

Williams GV, Rao SG & Goldman-Rakic PS. (2002). The physiological role of 5-HT_{2A} receptors in working memory. *J Neurosci* **22,** 2843-2854.

Williams JT, Henderson G & North RA. (1985). Characterization of α_2-adrenoceptors which increase potassium conductance in rat locus coeruleus neurones. *Neuroscience* **14,** 95-101.

Williams SR & Mitchell SJ. (2008). Direct measurement of somatic voltage clamp errors in central neurons. *Nat Neurosci* **11,** 790-798.

Willins DL, Deutch AY & Roth BL. (1997). Serotonin 5-HT_{2A} receptors are expressed on pyramidal cells and interneurons in the rat cortex. *Synapse* **27,** 79-82.

Woolsey TA & Van der Loos H. (1970). The structural organization of layer IV in the somatosensory region (SI) of mouse cerebral cortex. The description of a cortical field composed of discrete cytoarchitectonic units. *Brain Res* **17,** 205-242.

Wu LG & Saggau P. (1994). Presynaptic calcium is increased during normal synaptic transmission and paired-pulse facilitation, but not in long-term potentiation in area CA1 of hippocampus. *J Neurosci* **14,** 645-654.

Xiang Z & Prince DA. (2003). Heterogeneous actions of serotonin on interneurons in rat visual cortex. *J Neurophysiol* **89,** 1278-1287.

Xiao Z, Deng PY, Rojanathammanee L, Yang C, Grisanti L, Permpoonputtana K, Weinshenker D, Doze VA, Porter JE & Lei S. (2009). Noradrenergic depression of neuronal excitability in the entorhinal cortex via activation of TREK-2 K^+ channels. *J Biol Chem* **284,** 10980-10991.

Xu A, Wang Y, Xu LY & Gilmour RS. (2001). Protein kinase C alpha -mediated negative feedback regulation is responsible for the termination of insulin-

like growth factor I-induced activation of nuclear phospholipase C beta1 in Swiss 3T3 cells. *J Biol Chem* **276,** 14980-14986.

Xu J & Chuang DM. (1987). Serotonergic, adrenergic and histaminergic receptors coupled to phospholipase C in cultured cerebellar granule cells of rats. *Biochem Pharmacol* **36,** 2353-2358.

Xu T & Pandey SC. (2000). Cellular localization of serotonin$_{2A}$ ($5HT_{2A}$) receptors in the rat brain. *Brain Res Bull* **51,** 499-505.

Yadav VK, Oury F, Suda N, Liu ZW, Gao XB, Confavreux C, Klemenhagen KC, Tanaka KF, Gingrich JA, Guo XE, Tecott LH, Mann JJ, Hen R, Horvath TL & Karsenty G. (2009). A serotonin-dependent mechanism explains the leptin regulation of bone mass, appetite, and energy expenditure. *Cell* **138,** 976-989.

Yamada M, Mizuguchi M, Rhee SG & Kim SU. (1991). Developmental changes of three phosphoinositide-specific phospholipase C isozymes in the rat nervous system. *Brain Res Dev Brain Res* **59,** 7-16.

Yamamoto R, Hatano N, Sugai T & Kato N. (2014). Serotonin induces depolarization in lateral amygdala neurons by activation of TRPC-like current and inhibition of GIRK current depending on 5-HT_{2C} receptor. *Neuropharmacology* **82,** 49-58.

Yao XH, Wang M, He XN, He F, Zhang SQ, Lu W, Qiu ZL & Yu YC. (2016). Electrical coupling regulates layer 1 interneuron microcircuit formation in the neocortex. *Nat Commun* **7,** 12229.

Yoon EJ, Gerachshenko T, Spiegelberg BD, Alford S & Hamm HE. (2007). G*βγ* interferes with Ca^{2+}-dependent binding of synaptotagmin to the soluble N-ethylmaleimide-sensitive factor attachment protein receptor (SNARE) complex. *Mol Pharmacol* **72,** 1210-1219.

Yoshida H, Kanamaru C, Ohtani A, Li F, Senzaki K & Shiga T. (2011). Subtype specific roles of serotonin receptors in the spine formation of cortical neurons in vitro. *Neurosci Res* **71,** 311-314.

Yu Y, Maureira C, Liu X & McCormick D. (2010). P/Q and N channels control baseline and spike-triggered calcium levels in neocortical axons and synaptic boutons. *J Neurosci* **30,** 11858-11869.

Yue C, Ku CY, Liu M, Simon MI & Sanborn BM. (2000). Molecular mechanism of the inhibition of phospholipase C β_3 by protein kinase C. *J Biol Chem* **275,** 30220-30225.

Yuste R & Bonhoeffer T. (2001). Morphological changes in dendritic spines associated with long-term synaptic plasticity. *Annu Rev Neurosci* **24,** 1071-1089.

Zeng W, Mak DO, Li Q, Shin DM, Foskett JK & Muallem S. (2003). A new mode of Ca^{2+} signaling by G protein-coupled receptors: gating of IP_3 receptor Ca^{2+} release channels by Gβγ. *Curr Biol* **13,** 872-876.

Zhang W, Schmelzeisen S, Parthier D, Frings S & Mohrlen F. (2015). Anoctamin Calcium-Activated Chloride Channels May Modulate Inhibitory Transmission in the Cerebellar Cortex. *PLoS One* **10,** e0142160.

Zhang X, Rizo J & Sudhof TC. (1998). Mechanism of phospholipid binding by the C_2A-domain of synaptotagmin I. *Biochemistry* **37,** 12395-12403.

Zhang XL, Upreti C & Stanton PK. (2011). Gβγ and the C terminus of SNAP-25 are necessary for long-term depression of transmitter release. *PLoS One* **6,** e20500.

Zhang Y, Smolen P, Baxter DA & Byrne JH. (2017). Biphasic Regulation of p38 MAPK by Serotonin Contributes to the Efficacy of Stimulus Protocols That Induce Long-Term Synaptic Facilitation. *eNeuro* **4**.

Zhang Z, Cordeiro Matos S, Jego S, Adamantidis A & Seguela P. (2013). Norepinephrine drives persistent activity in prefrontal cortex via synergistic α1 and α2 adrenoceptors. *PLoS One* **8,** e66122.

Zhang ZW. (2003). Serotonin induces tonic firing in layer V pyramidal neurons of rat prefrontal cortex during postnatal development. *J Neurosci* **23,** 3373-3384.

Zhou FM & Hablitz JJ. (1999). Activation of serotonin receptors modulates synaptic transmission in rat cerebral cortex. *J Neurophysiol* **82,** 2989-2999.

Zilles K, Gross G, Schleicher A, Schildgen S, Bauer A, Bahro M, Schwendemann G, Zech K & Kolassa N. (1991). Regional and laminar distributions of α_1-adrenoceptors and their subtypes in human and rat hippocampus. *Neuroscience* **40,** 307-320.

Zurawski Z, Rodriguez S, Hyde K, Alford S & Hamm HE. (2016). G*βγ* binds to the extreme C terminus of SNAP25 to mediate the action of $G_{i/o}$-coupled G protein-coupled receptors. *Mol Pharmacol* **89,** 75-83.